

## **INFORMATION TO USERS**

**This manuscript has been reproduced from the microfilm master. UMI films the text directly from the original or copy submitted. Thus, some thesis and dissertation copies are in typewriter face, while others may be from any type of computer printer.**

**The quality of this reproduction is dependent upon the quality of the copy submitted. Broken or indistinct print, colored or poor quality illustrations and photographs, print bleedthrough, substandard margins, and improper alignment can adversely affect reproduction.**

**In the unlikely event that the author did not send UMI a complete manuscript and there are missing pages, these will be noted. Also, if unauthorized copyright material had to be removed, a note will indicate the deletion.**

**Oversize materials (e.g., maps, drawings, charts) are reproduced by sectioning the original, beginning at the upper left-hand corner and continuing from left to right in equal sections with small overlaps.**

**Photographs included in the original manuscript have been reproduced xerographically in this copy. Higher quality 6" x 9" black and white photographic prints are available for any photographs or illustrations appearing in this copy for an additional charge. Contact UMI directly to order.**

**Bell & Howell Information and Learning  
300 North Zeeb Road, Ann Arbor, MI 48106-1346 USA**

**UMI<sup>®</sup>**  
**800-521-0600**



**Systematic Kinetics**  
**of Reactions of Metal Carbonyl Clusters**  
 **$\text{Ru}_3(\text{CO})_{11}\text{etpb}$ ,  $\text{Ru}_3(\text{CO})_{11}\text{PMe}_3$ , and  $\text{Os}_6(\text{CO})_{18}$**

**By**

**Rongjuan Fei**

**Department of Chemistry**

**A thesis submitted in conformity with the requirements  
for the Degree of Master of Science in the University of Toronto**

**© Rongjuan Fei**

**1996**



**National Library  
of Canada**

**Acquisitions and  
Bibliographic Services**

**395 Wellington Street  
Ottawa ON K1A 0N4  
Canada**

**Bibliothèque nationale  
du Canada**

**Acquisitions et  
services bibliographiques**

**395, rue Wellington  
Ottawa ON K1A 0N4  
Canada**

*Your file Votre référence*

*Our file Notre référence*

**The author has granted a non-exclusive licence allowing the National Library of Canada to reproduce, loan, distribute or sell copies of this thesis in microform, paper or electronic formats.**

**The author retains ownership of the copyright in this thesis. Neither the thesis nor substantial extracts from it may be printed or otherwise reproduced without the author's permission.**

**L'auteur a accordé une licence non exclusive permettant à la Bibliothèque nationale du Canada de reproduire, prêter, distribuer ou vendre des copies de cette thèse sous la forme de microfiche/film, de reproduction sur papier ou sur format électronique.**

**L'auteur conserve la propriété du droit d'auteur qui protège cette thèse. Ni la thèse ni des extraits substantiels de celle-ci ne doivent être imprimés ou autrement reproduits sans son autorisation.**

**0-612-45464-9**

**Canada**

## **ACKNOWLEDGMENT**

**I am sincerely grateful to my supervisor, Professor Anthony J. Poë, for his enthusiastic and outstanding supervising. It has been great pleasure and luck to me to work under his guidance.**

**I am also very grateful to Professor David H. Farrar for his help in the synthesis of  $\text{Os}_6(\text{CO})_{18}$  and the very useful excellent lectures on X-Ray Crystallography he has given.**

## CONTENTS

<b>Symbols and Abbreviations .....</b>	<b>6</b>
<b>Abstract .....</b>	<b>8</b>
<b>Chapter 1 Introduction</b>	
1.1 Importance of Kinetic Studies .....	9
1.2 Associative Reactions of Metal Carbonyl Clusters .....	10
1.3 Dissociative Reactions of Metal Carbonyl Clusters .....	18
<b>References for Chapter 1 .....</b>	<b>20</b>
<b>Chapter 2 Kinetics of Reactions of Metal Carbonyl Clusters <math>\text{Ru}_3(\text{CO})_{11}\text{etpb}</math> and <math>\text{Ru}_3(\text{CO})_{11}\text{PMe}_3</math> with a Variety of P- and As-donor Ligands L'</b>	
2.1 Experimental .....	24
2.1.1 Instruments .....	24
2.1.2 Chemicals .....	24
2.1.3 Synthesis of $\text{Ru}_3(\text{CO})_{11}\text{etpb}$ .....	25
2.1.4 Synthesis of $\text{Ru}_3(\text{CO})_{11}\text{PMe}_3$ .....	30
2.1.5 Kinetic Experiments .....	31
2.1.5.1 Preparation of Solutions .....	32

2.1.5.2	<b>Kinetic Monitoring by UV-Vis Technique</b>	
	.....	35
2.1.5.3	<b>Kinetic Monitoring by FTIR Technique</b>	
	.....	37
2.2	<b>Results of Kinetic Studies</b>	41
2.2.1	<b>The Course of the Reactions of <math>\text{Ru}_3(\text{CO})_{11}\text{PMe}_3</math> with Nucleophiles L'</b>	42
2.2.2	<b>The Course of the Reactions of <math>\text{Ru}_3(\text{CO})_{11}\text{etpb}</math> with Nucleophiles L'</b>	45
2.2.3	<b>Data Treatment</b>	47
2.2.4	<b>Reaction Pathways</b>	50
2.3	<b>Kinetic Data Analyses and Discussion</b>	57
2.3.1	<b>Activation Parameters for CO Dissociation from Ten Clusters <math>\text{Ru}_3(\text{CO})_{11}\text{L}</math></b>	59
2.3.2	<b>Isokinetic Temperature for CO Dissociation from Ten Clusters <math>\text{Ru}_3(\text{CO})_{11}\text{L}</math></b>	67
2.3.3	<b>Derivation of Electronic and Steric Profiles for CO Dissociation from Ten Clusters <math>\text{Ru}_3(\text{CO})_{11}\text{L}</math></b>	70
2.3.4	<b>Derivation of Electronic and Steric Profiles for Associative Substitution Reactions of <math>\text{Ru}_3(\text{CO})_{11}\text{PMe}_3</math> and <math>\text{Ru}_3(\text{CO})_{11}\text{etpb}</math></b>	81
2.3.4.1	<b>Introduction</b>	81
2.3.4.2	<b>Electronic and Steric Profiles</b>	96
2.3.4.3	<b>Stereoelectronic Analyses and Comparison of Data</b>	102

2.3.4.4 Use of an Alternative Steric Parameter $\theta'$	106
2.3.5 Interrelationships of Parameters $\alpha$ , $\beta$ , $\gamma$ , and $\theta_{th}$ for Associative Substitution Reactions of $Ru_3(CO)_{11}L$	107
2.3.6 Intimate Mechanism	110
2.3.7 Conclusion	118
<b>References for Chapter 2</b>	<b>121</b>
<b>Figures for Chapter 2</b>	<b>125</b>
<b>Chapter 3 Kinetics of Reactions of High-Nuclearity Carbonyl Cluster <math>Os_6(CO)_{18}</math> with P-donor Nucleophiles <math>L'</math></b>	
3.1 Introduction	163
3.2 Experimental	168
3.2.1 Synthesis of $Os_6(CO)_{18}$	168
3.2.2 Kinetic Monitoring	173
3.3 Results of kinetic Studies	175
3.3.1 Reactions with P-donor Nucleophiles $L'$	175
3.3.2 Data Treatment	179
3.3.3 Dependence of $k_{obs}$ on $[L']$	179
3.3.4 Activation Parameters $\Delta H_2^\ddagger$ and $\Delta S_2^\ddagger$	186
3.4 Analyses of Kinetic Results	188
3.4.1 Quantitative Separation of Electronic and Steric Effects	188
3.4.1.1 Characteristic Kinetic Parameters	188

3.4.1.2 Temperature Dependence of Electronic Profiles .....	199
3.4.1.2.1 A Novel IKR — $\log k_2$ vs $pK_a'$ for Nucleophiles with Different $\sigma$ -Basicity and Size at the IKT .....	199
3.4.1.2.2 Unique IKRs, $\log k_2$ vs $pK_a'$ for almost Isosteric Nucleophiles or Small Ones with $\theta < \theta_{th}$ at Various Temperatures — Breakthroughs between IKR and LFER .....	200
3.4.1.2.3 A Unique LFER Isoparameter $\xi_{iso}$ — Isokinetic $pK_a'$ — for a Series of Reactions at Various Temperatures .....	201
3.4.1.3 Temperature Dependence of Steric Profiles .....	203
3.4.1.3.1 A Unique LFER Isoparameter $\xi_{iso}$ — Isokinetic $\theta'$ — for a Series of Reactions at Various Temperatures .....	203
3.4.1.3.2 Derivation of Isokinetic $\theta$ for a Series of Reactions at Various Temperatures .....	204
3.4.2 Isokinetic Relationships for the Second Order Substitution Reactions of $Os_6(CO)_{18}$ with L' .....	205

3.4.3 Implications of Derived Kinetic Parameters .....	215
3.5 Intimate Mechanism .....	218
3.6 Discussion of the IKRs .....	221
3.7 Conclusion .....	225
<b>References for Chapter 3 .....</b>	<b>229</b>
<b>Figures for Chapter 3 .....</b>	<b>232</b>
<b>Chapter 4 Summary .....</b>	<b>258</b>
<b>References for Chapter 4 .....</b>	<b>264</b>
<b>Chapter 5 Appendices</b>	
5.1 Electronic and Steric Parameters for some P-donor Ligands .....	265
5.2 <sup>31</sup> P NMR Data for some P-donor Ligands .....	269
5.3 Pseudo-First-Order Rate Constants for Reactions of Ru <sub>3</sub> (CO) <sub>11</sub> PMe <sub>3</sub> with Nucleophiles L' in Heptane .....	271
5.4 Pseudo-First-Order Rate Constants for Reactions of Ru <sub>3</sub> (CO) <sub>11</sub> etpb with Nucleophiles L' in Heptane .....	282
5.5 Pseudo-First-Order Rate Constants for Reactions of Os <sub>6</sub> (CO) <sub>18</sub> with Nucleophiles L' in Toluene .....	293
5.6 Eyring Data for Reactions of Os <sub>6</sub> (CO) <sub>18</sub> with Nucleophiles L' in Toluene .....	305
<b>References for Chapter 5 .....</b>	<b>307</b>

## SYMBOLS AND ABBREVIATIONS

Å	Angstrom unit, $10^{-10}$ m
$A_{\infty}$	absorbance after completion of reaction
Bu	butyl ( <i>-n-</i> , <i>-i-</i> or <i>-t-</i> ; normal, iso or tertiary)
$\text{cm}^{-1}$	wavenumber
CVEs	cluster valence electrons
CVMOs	cluster valence molecular orbitals
Cy	cyclohexyl ( $\text{C}_6\text{H}_{11}$ )
$\Delta(\text{hnp})$	half-neutralization potential
$\epsilon$	molar extinction coefficient
Et	ethyl
etpb	$\text{P}(\text{OCH}_2)_3\text{CEt}$ 4-ethyl-2, 6,7-trioxa-1-phosphabicyclo-[2,2,2]-octane
FTIR	Fourier transform infrared
GS	ground state
h	Planck's constant $6.6256 \times 10^{-34}$ Js
HLAOs	high lying antibonding orbitals
HNCC	high-nuclearity carbonyl cluster
IKT	isokinetic temperature
IKR	isokinetic relationship
IR	infrared
I.R.	intrinsic reactivity
$k_B$	Boltzmann's constant $1.38054 \times 10^{-23}$ JK <sup>-1</sup>
L'	ligand as nucleophile
L	ligand as substituent

<b>LCAO-MO</b>	<b>linear combination of atomic orbital — molecular orbital</b>
<b>LFER</b>	<b>linear free-energy relationship</b>
<b>LHS</b>	<b>left-hand side</b>
<b>LNCC</b>	<b>low-nuclearity carbonyl cluster</b>
<b>Me</b>	<b>methyl</b>
<b>MO</b>	<b>molecular orbital</b>
<b>NMR</b>	<b>nuclear magnetic resonance</b>
<b>nm</b>	<b>nanometer</b>
<b>P-donor</b>	<b>phosphorus donor ligand</b>
<b>Ph</b>	<b>phenyl</b>
<b>Pr</b>	<b>propyl</b>
<b>R</b>	<b>multiple correlation coefficient or Gas Constant (as appropriate)</b>
<b>RHS</b>	<b>right-hand side</b>
<b>RMSD</b>	<b>root mean square deviation</b>
<b>SR</b>	<b>standard reactivity</b>
<b>THF</b>	<b>tetrahydrofuran</b>
<b>t.l.c.</b>	<b>thin layer chromatography</b>
<b>TMS</b>	<b>tetramethyl silane</b>
<b>t<sub>1/2</sub></b>	<b>half-life</b>
<b>TS</b>	<b>transition state</b>
<b>TSI</b>	<b>transition state isomer</b>
<b>UV</b>	<b>ultraviolet</b>
<b>Vis</b>	<b>visible</b>

## ABSTRACT

The kinetics of substitution reactions of the low-nuclearity carbonyl clusters (LNCCs),  $\text{Ru}_3(\text{CO})_{11}\text{etpb}$  and  $\text{Ru}_3(\text{CO})_{11}\text{PMe}_3$ , and the high-nuclearity carbonyl cluster (HNCC)  $\text{Os}_6(\text{CO})_{18}$ , with a variety of P-donor nucleophiles  $\text{L}'$  with different  $\sigma$ -basicity and size have been studied for the first time. The kinetic data were successfully analyzed by the quantitative separation of electronic and steric effects, and meaningful, excellent and precise results were obtained, including unique IKRs. Not only are the clusters characterizable in this way but also the actual mechanistic paths followed can be probed.

The data obtained for the reactions of  $\text{Os}_6(\text{CO})_{18}$  with  $\text{L}'$  lead to five types of excellent isokinetic relationships (three are unique), all indicating an IKT about  $88^\circ\text{C}$ . The statistical analysis of data on validity of IKR also gave exactly the same result, the IKT of around  $88^\circ\text{C}$  with a high degree of probability, showing very precise IKR.

Unique IKRs, a common point of intersection in the LFER plots at various temperatures, were established for the first time. They also show an excellent temperature dependence of electronic profiles, and they are therefore breakthroughs in providing the first two examples of the theoretical interconnection between an IKR and LFER.

A unique definition of IKR,  $\{[\partial \ln k/T (T, \xi)]/\partial(T)\}_{\xi_{\text{iso}}} = \{[\partial \ln k/T (T, \text{pKa}')]/\partial(T)\}_{\text{pKa}'_{\text{iso}}} = 0$ , was established for the first time. The parameter  $\xi$  is not a simple numbering and it does have physical meaning. The  $\xi$  identifies the individual members of the series — the nucleophiles with different  $\sigma$ -basicity and size in this work. When the size of  $\text{L}'$  is kept constant or  $\theta < \theta_{\text{th}}$ ,  $\xi = \text{pKa}'$ .

The unique LFER isoparameters  $\xi_{\text{iso}}$  — isokinetic  $\text{pKa}'$  and isokinetic  $\theta'$  — for a series of reactions at various temperatures were established from both experimental results and theory for the first time. They are natural outcomes of linear relationships between SR &  $\beta$  and SR &  $\gamma$ , respectively, at various temperatures for the reaction series.

## CHAPTER 1

### INTRODUCTION

#### 1.1 Importance of Kinetic Studies

Systematic kinetic data can provide not only a detailed understanding of synthetic and catalytic processes, but also precise quantitative measurement of the reactivity of metal complexes with respect to their various pathways [1]. Thus the kinetic and mechanistic behavior of metal complexes, which defines the dynamic character of each individual complex, is as important as their crystallographic structures and their spectroscopic and other properties in describing their overall natures.

Systematic studies of the reaction kinetics of metal carbonyl clusters can provide characteristic reactivity profiles [2-5]. Quantification of the standard reactivity of the clusters and their sensitivity toward electronic and steric properties of any substituents involved in dissociative processes, or nucleophiles in associative processes, is of great importance in providing the full dynamic character of each cluster. The parameters obtained from the analyses define the dynamic nature of a particular cluster or a group of clusters in a way which complements, and is of comparable importance to the information provided by structural studies. A given cluster can be quantitatively characterized by its sensitivity to the electronic and steric nature of a series of P-donor nucleophiles [2-5], i.e. by its standard reactivity towards nucleophilic attack, by its steric threshold,  $\theta_{th}$ , shown from a series of reactions with various nucleophiles, and

sometimes by the distribution between substitution and fragmentation products formed as a consequence of nucleophilic attack [6]. Alternatively, the S<sub>N</sub>1 kinetics of a group of related clusters, differing only in the nature of their substituents, can also lead to characteristic electronic and steric profiles. These studies provide a very important way of probing the nature of a large and significant group of organometallic compounds.

The kinetic studies of metal carbonyl clusters have received far less attention in spite of enormous efforts devoted to their syntheses and structures [7]. Kinetic studies in this area would not only be of academic interest but also be of significance in providing a detailed understanding of synthetic and catalytic processes, as mentioned above. In view of the importance of kinetic studies in achieving thorough understanding of LNCC and HNCC chemistry, we have chosen three new clusters, Ru<sub>3</sub>(CO)<sub>11</sub>etpb, Ru<sub>3</sub>(CO)<sub>11</sub>PMe<sub>3</sub> and Os<sub>6</sub>(CO)<sub>18</sub>, for systematic kinetic studies.

## 1.2 Associative Reactions of Metal Carbonyl Clusters

The occurrence of associative substitution reactions of a metal carbonyl was first observed by Heck [8] in 1963. That the rates of substitution reactions of Co(CO)<sub>3</sub>(NO) with PPh<sub>3</sub> were first order in [PPh<sub>3</sub>] was shown. This observation was followed by work in Basolo's laboratory, where they found that (η<sup>5</sup>-C<sub>5</sub>H<sub>5</sub>)Rh(CO)<sub>2</sub> also underwent substitution reactions with a number of P-donor ligands L' at rates proportional to [L'] [9]. In the light of the largely dissociative paths followed by binary metal carbonyls in their substitution reactions, the occurrence of these associative reactions must be driven by some

internal structural causes of molecules which underwent the reactions. It is now believed [10] that the key factor is the ability of the substituents  $\text{NO}^+$  and  $\eta^5\text{-C}_5\text{H}_5$  to withdraw an electron pair from the metal during the approach of a nucleophile. This allows the metal to accept the nucleophile without approaching 20-electrons, i.e. without contravention of the 18-electron rule, which is closely obeyed by most metal carbonyls. While doing so, the substituents  $\text{NO}^+$  and  $\eta^5\text{-C}_5\text{H}_5$  are converted to reasonably stable  $\text{NO}^-$  and  $\eta^3\text{-C}_5\text{H}_5$  forms, respectively. Transition states can therefore be formed, which involve  $\text{M}\cdots\text{L}'$  bond making and no  $\text{M}-\text{CO}$  bond breaking.

Electronic effects in associative substitution reactions of metal carbonyls with P-donor nucleophiles were also discovered by Basolo et al. for the reactions of  $(\eta^5\text{-C}_5\text{H}_5)\text{Rh}(\text{CO})_2$  and  $\text{Co}(\text{CO})_3(\text{NO})$  [11]. In both cases the values of  $\log k_2$  varied linearly with a parameter  $\Delta(\text{hnp})$ , which provided a quantitative measure of the proton basicity of the nucleophiles. The  $\Delta(\text{hnp})$  is the relative half-neutralization potential for titration of the P-donor ligand against perchloric acid  $\text{HClO}_4$  in nitromethane [12], which decreases with increasing basicity of L, i.e. the smaller the  $\Delta(\text{hnp})$ , the greater the basicity of L. The  $\Delta(\text{hnp})$  provides a measure of the free energy of attachment of the ligand to the proton,  $\text{H}^+ + :\text{PR}_3 \rightarrow [\text{H}-\text{PR}_3]^+$ , while  $\log k_2$  is proportional to the free energy  $\Delta G^\ddagger$  of attaching the nucleophile to the metal in the transition state,  $\text{M}^{n+} + :\text{PR}_3 \rightarrow [\text{M}-\text{PR}_3]^{n+}$ . So the linear plots of  $\log k_2$  vs  $\Delta(\text{hnp})$  are a type of linear free-energy relationship (LFER). These studies were quickly extended and a common feature which emerged was the deviations from the LFER defined by the smaller nucleophiles, of data

for the larger nucleophile PCy<sub>3</sub>. This was ascribed to an unfavorable steric effect.

The quantitative separation of electronic and steric effects of nucleophiles was first clearly established by Poë and co-workers in 1973 [13], following a study of associative reactions of the cluster Ru<sub>3</sub>(CO)<sub>12</sub>, which had been detected earlier by Candlin and Shortland [14]. A moderately well-defined LFER was exhibited by smaller nucleophiles, but the larger ones, PPh<sub>3</sub> and PCy<sub>3</sub>, showed clear steric deviations. **Poë suggested that the gradients  $\beta$  of this LFER and of other LFERs, derived by the author from data available in the literature then, could be taken as a quantitative measure of the relative extents of M...L bond making in the transition states, and the deviations,  $\Delta(\text{PCy}_3)$  and/or  $\Delta(\text{PPh}_3)$ , from LFER of the values of  $\log k_2$  for these larger nucleophiles could be taken as a quantitative measure of steric effects for reactions of the various complexes involved. This method of data analysis was continued up to 1984 [15]. Afterward the author and others derived a stereoelectronic equation for such reactions, and applications of this approach in a wide variety of systems have been successful.**

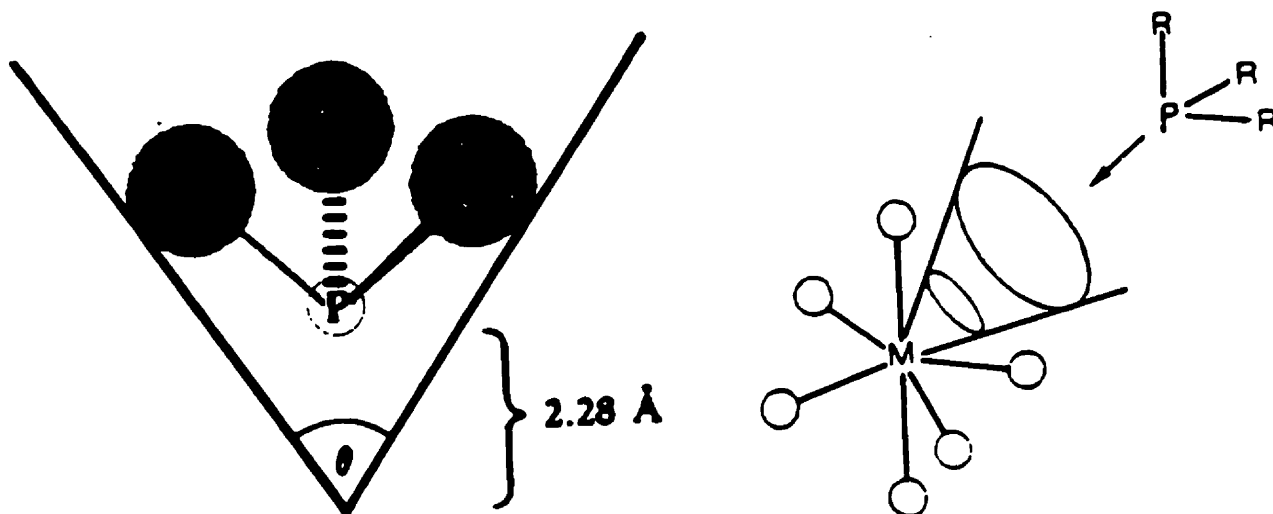
Kochi and co-workers [16] showed that data of associative reactions of  $(\eta^5\text{-C}_5\text{H}_4\text{CH}_3)\text{Mn}(\text{CO})_2(\text{p-NO}_2\text{C}_5\text{H}_4\text{N})^+$  with P-donor nucleophiles gave an excellent fit to Eq.(1.1).

$$\log k_2 = \alpha + \beta \text{pKa} + \gamma \theta \quad (1.1)$$

The steric parameter  $\theta$  is the Tolman cone angle [17] which, as illustrated below [18, 19], is a very useful quantitative measure of the

size of P-donor ligands. The electronic parameter  $pK_a$  is the estimated value for the corresponding phosphonium ion in aqueous solution, a parameter that is linearly related to  $\Delta(hnp)$ .

### Tolman Cone Angle $\theta$ of P-donor Ligand



Acknowledgment is made to the authors of ref. [18, 19] for using of above figures.

The use of  $pK_a$ , rather than  $\Delta(hnp)$ , is to be preferred in the sense that it leads to dimensionless values of  $\beta$ , which bears more direct and clear relation to physical reality, in contrast to  $\beta$  using  $\Delta(hnp)$ , where  $\beta$  is in units of reciprocal volts  $V^{-1}$ , which has no absolute significance although satisfactory for comparative purposes. As Poë pointed out [4, 20], the dimensionless values of  $\beta$  have the virtue that they provide a direct comparison of the strength of the partial  $M\cdots L$  bond in the transition state with the strength of the fully formed  $H^+-L$  bond in the phosphonium ion; while these bonds are not as closely comparable as

would be the  $M\cdots L$  bonds in the transition states and the fully formed  $M-L$  bonds in the products. The strength of the latter is not available and comparison with the fully formed  $H^+-L$  bond is the best that can be done [20]. In addition, a new parameter  $\gamma$  became available to provide a quantitative measure of the steric effect in units of reciprocal degrees (Eq.1.1).

A more general feature was soon found by Poë and co-workers [3] when describing the data for associative reactions of the cluster  $Ir_4(CO)_{12}$ . A downward sloping linear plot of  $\{\log k_2 - \beta\Delta(hnp)\}$  vs  $\theta$  was obtained over a  $70^\circ$  cone angle range. **Poë pointed out that a more general type of behavior must involve a horizontal region for the plot of  $(\log k_2 - \beta pKa)$  vs  $\theta$  at low values of  $\theta$  since values of  $\log k_2$  do often show a linear dependence on  $\Delta(hnp)$  or  $pKa$ , irrespective of the size of nucleophiles,**

$$\log k_2 = \alpha + \beta\Delta(hnp) \quad (1.2)$$

**and then change to a linear downward slope with increasing  $\theta$  when  $\theta$  became large enough.** Examples of this behavior were found to be shown by previously published data.

Almost simultaneously Giering and co-workers [19] had independently come to the same conclusion, and essentially identical exemplary plots, the electronic profile and the steric profile, were shown. They also quantified the change from no steric effect to a finite steric effect by the steric threshold  $\theta_{st}$ , and defined an intrinsic reactivity as being the value of  $\log k_2$  for the quite small nucleophile  $P(OMe)_3$  ( $\theta = 107^\circ$ ). This turns out not to be a good measure of an

intrinsic reactivity of a complex because  $\text{P}(\text{OMe})_3$  is quite a strong base ( $\text{pK}_a = 2.6$ ) and the strength of the  $\text{M}\cdots\text{P}$  bond in the transition state will be relatively large [20]. The stability of the transition state will be determined significantly by the nature of the nucleophile and not solely by the nature of the complex as should be the case when measuring an intrinsic property of the complex [20]. Poë established an alternative way of characterizing the reactivity of a complex, which is to define a standard reactivity [5] as being  $\log k_2^\circ = \log k_2 - \beta(\text{pK}_a + 4)$ , i.e. the value of  $\log k_2$  for a hypothetical nucleophile which is small enough ( $\theta < \theta_{st}$ ) to exhibit no steric effects, and weak enough ( $\text{pK}_a = -4$ , i.e. weaker than any commonly used nucleophiles) that the  $\text{M}\cdots\text{P}$  bond strength in the transition state will be relatively small, and the value of the standard reactivity will be relatively close to the intrinsic reactivity, i.e. to the reactivity of the complex when stabilization of the transition state by bond formation is negligible [20].

Over 50 sets of different systems of metal carbonyl complexes, such as  $\text{Ru}_6\text{C}(\text{CO})_{17}$  — the first HNCC to receive systematic kinetic study [21] and  $\text{Os}_6(\text{CO})_{18}$  (this work), LNCCs  $\text{Ru}_3(\text{CO})_{11}\text{L}$  ( $\text{L} = \text{CO}, \text{P}(\text{OEt})_3, \text{P}(n\text{-Bu})_3, \text{PMe}_3$  etc.) [22, 23, and this work],  $\text{Ru}_3(\text{CO})_{12-n}(\text{PCy}_3)_n$   $n = 1, 2$  [23],  $(\mu\text{-H})_2\text{Os}_3(\text{CO})_{10}$  [24],  $\text{Rh}_4(\text{CO})_{10}(\text{PCy}_3)_2$  [25], and  $\text{Ir}_4(\text{CO})_{12-n}(\text{PPh}_3)_n$   $n = 0, 1$  [26, 27], mononuclear metal carbonyls  $(\eta^5\text{-C}_5\text{H}_5)\text{Rh}(\text{CO})_2$  and  $(\eta^5\text{-Me}_5\text{C}_5)\text{Rh}(\text{CO})_2$  [22], and so on, which are too numerous to mention individually, have been analyzed successfully by Poë's stereoelectronic Eq.(1.3), where  $\text{pK}_a'$  measures the  $\sigma$ -donicity and  $\theta$  the Tolman cone angle of each nucleophile,

$$\log k_2 = \alpha + \beta(\text{pKa}' + 4) + \gamma(\theta - \theta_{\text{th}})\lambda \quad (1.3)$$

thus demonstrating the general validity of Poë's model, and of the electronic and steric parameters used [21, 22, 23]. Tolman [17(c)] suggested that the A1 C-O stretching frequencies in the complexes  $\text{Ni}(\text{CO})_3\text{L}$  provided a good standard measure of the net electron donor capacity of the ligands L, i.e. the combined effects of  $\sigma$  donation of electrons to the metal and withdrawal of  $\pi$  electrons from the metal, which could be expressed by the values  $\chi = \nu_{\text{C-O}}(\text{L}) - \nu_{\text{C-O}}(\text{P-}t\text{-Bu}_3)$  since the ligand P-*t*-Bu<sub>3</sub> is the most effective net electron donor and  $\nu_{\text{C-O}}$  in  $\text{Ni}(\text{CO})_3(\text{P-}t\text{-Bu}_3)$  is the smallest value observed. Giering [28, 29] noted that pKa values are related to  $\chi$  by  $\text{pKa} = (18.9 \pm 1.6) - (0.047 \pm 0.010)\theta - (0.68 \pm 0.03)\chi$ . This equation is only obeyed by  $\sigma$ -donors, and  $\sigma$ -donor/ $\pi$ -acid ligands deviated from the correlation badly [22]. Poë [21] suggested the sterically corrected  $\text{pKa}' \{= \text{pKa} + 0.0464(\theta - 145)\}$ , for  $\sigma$ -donor/ $\pi$ -acid nucleophiles,  $\text{pKa} = \text{pKa}(\text{expt})$ ; for  $\sigma$ -donors,  $\text{pKa} = \text{pKa}(\text{calc}) = 18.93 - 0.0464\theta - 0.673\chi$ , and  $\text{pKa}' = 18.93 - 0.673\chi - 0.0464 \times 145$ . The term  $0.0464(\theta - 145)$  is the correction for the unwanted dependence of pKa on the size of ligands when experimental values of pKa are used, which is ascribed to the fact that the pKa values were derived for the phosphonium ions  $\text{L-H}^+$  in aqueous solution, while the kinetics is followed in the non-aqueous and non-polar organic solvents. The analyses provide important parameters:  $\alpha$  (standard reactivity SR),  $\beta$  (a measure of electronic effects – the susceptibility of a carbonyl to the  $\sigma$ -basicity of nucleophiles),  $\gamma$  (a measure of steric effects – the sensitivity of rates to the cone angle of nucleophiles when  $\theta > \theta_{\text{th}}$ ), and  $\theta_{\text{th}}$  (steric threshold, where steric

effects begin to be apparent), which are characteristic of the dynamic nature of the carbonyl clusters as reflected in their associative reactions with P-donor nucleophiles.

**Poë and co-workers [24] established an alternative steric parameter  $\theta'$**

$$\theta' = 103.8 + 0.553 E_R \quad (1.4)$$

where the values of  $E_R$  are repulsion energies, calculated by Brown et al., that are experienced by L in  $\text{Cr}(\text{CO})_5\text{L}$  [30], for a very wide range of ligands. They found that the values of the Tolman cone angles  $\theta$  and the Brown repulsion energies  $E_R$  correlated quite well [24, 30] for 37 alkyl, aryl and mixed alkyl aryl triphosphines although most phosphites did not fit the correlation at all. Nevertheless it is useful [24] to transform the  $E_R$  values, by what is essentially a scale change, into a cone angle equivalent  $\theta'$  in units of degrees by application of Eq.(1.4). The value of the first term has been chosen so as to make  $\theta = \theta' = 145^\circ$  for the  $\text{P}(\textit{p}\text{-XC}_6\text{H}_4)_3$  ligands and the values of  $\theta'$  for those ligands which fit the  $\theta\text{-}E_R$  correlation are necessarily quite close to their corresponding  $\theta$  values. **The values of  $\theta'$  are directly based on the corresponding values of repulsion energies  $E_R$ , thus it is a more rational parameter to correlate with energetic parameters such as activation free energy  $\Delta G^\ddagger$ , in contrast to the cone angle  $\theta$ , which would not be expected to relate linearly to energetic parameters. The values of  $\theta'$  can be used in stereoelectronic analyses in exactly the same way as the Tolman cone angles. The relationship between  $\theta'$  and  $\theta$  is, therefore, not dissimilar to that between  $\text{pK}_a'$  and  $\chi$  [24].**

The reaction kinetics of metal carbonyls including clusters has been reviewed [31] but little attention was given to systematic studies of associative reactions. Based on the data so far collected (1994–1996), very few kinetic results are available on reactions of HNCCs, except work in Poë's laboratory, where sufficient data for a substantial number of metal carbonyl clusters (LNCCs and HNCCs) are now available for the type of stereoelectronic analysis described by Eq.(1.3).

### 1.3 Dissociative Reactions of Metal Carbonyl Clusters

The studies of effects of different substituents on dissociative reaction kinetics have not enjoyed the extensive exploration that associative reactions have had over the last 30 years. Studies of this type have appeared sporadically throughout the last 20 years.

A study of tetrairidium carbonyl clusters substituted by  $\text{PPh}_3$ ,  $\text{Ir}_4(\text{CO})_{12-n}(\text{PPh}_3)_n$ , represented the first quantitative evidence that such effects did exist for reactions of metal carbonyl clusters [32]. The reaction governed by  $k_1$  is normally assumed to proceed by a simple CO dissociative mechanism [33, 34]. Although other mechanisms are possible [35, 36], there is no positive evidence for them. It seems preferable therefore to regard these reactions as being simply dissociative in nature. Dissociative reactions lead to  $\text{S}_{\text{N}}1$  path substitution.

The dependence of rate constants  $k_1$  on the nature of the substituents, L, can be represented by Eq.(1.5) [23, 37].

$$\log k_1 = \alpha_L + \beta_L \delta(^{13}\text{CO}) + \gamma_L \theta \quad (1.5)$$

where  $\beta_L$  and  $\gamma_L$  represent the dependence of the rates on the electronic parameters,  $\delta(^{13}\text{CO})$  [38], and on the cone angles,  $\theta$ , respectively, which are characteristic of the individual substituents, L. The parameters  $\alpha_L$ ,  $\beta_L$  and  $\gamma_L$  are characteristic of a group of clusters, such as  $\text{Ru}_3(\text{CO})_{11}\text{L}$ , while the parameters  $\alpha(\text{SR})$ ,  $\theta_{\text{th}}$ ,  $\beta$  and  $\gamma$  for associative reactions are characteristic of a single cluster, such as  $\text{Ru}_3(\text{CO})_{11}\text{PMe}_3$ . The electronic parameter  $\delta(^{13}\text{CO})$  measures the  $^{13}\text{C}$  chemical shift of  $\text{Ni}(^{13}\text{CO})_3\text{L}$  relative to that in  $\text{Ni}(^{13}\text{CO})_4$ , and is used to represent the net electron donor capacity of L. This is because  $\pi$ -bonding is likely to be important as well as  $\sigma$ -bonding for these P-donor ligands acting as substituents, and not nucleophiles.

**REFERENCES FOR CHAPTER 1**

- [1] A.J. Poë, *Chemistry in Britain*, 19(1983) 997.
- [2] A.J. Poë, in Metal Clusters, Edited by M. Moskovits, Wiley, New York, 1986, Chapter 4.
- [3] K. Dahlinger, F. Falcone, and A.J. Poë, *Inorg. Chem.*, 25(1986)2654.
- [4] A.J. Poë, *Pure App. Chem.*, 60(1988)1209.
- [5] N.M.J. Brodie, *L. Chem.*, and A.J. Poë, *Int. J. Chem. Kin.*, 20(1988)467.
- [6] N.M.J. Brodie and A.J. Poë, *Inorg. Chem.*, 27(1988)3156.
- [7] (a) B.F.G. Johnson (Ed.), Transition Metal Clusters, Wiley, Chichester, 1980.
- (b) M. Moskovits (Ed.), Metal Clusters, Wiley, New York, 1986.
- (c) B.C. Gates, L. Guzzi, and H. Knözinger (Eds.), Metal Clusters in Catalysis, Elsevier Science Pub.Co., New York, 1986.
- (d) F.A. Cotton and G. Wilkinson, Advanced Inorganic Chemistry, 5th ed., Wiley, New York, 1988, Chapter 22.
- (e) Edited by D.F. Shriver, H.D. Kaesz, and R.D. Adams, The Chemistry of Metal Cluster Complexes, VCH Publishers, Inc., New York, 1990.
- [8] R.F. Heck, *J. Am. Chem. Soc.*, 85(1963)657.
- [9] H.G. Schuster-Woldan and F. Basolo, *J. Am. Chem. Soc.*, 88(1966)1657.
- [10] F. Basolo, *Polyhedron*, 9(1990)1503.

- [11] E.M. Thorsteinson and F. Basolo, *J. Am. Chem. Soc.*, 88(1966)3929.
- [12] (a) C.A. Streuli, *Anal. Chem.*, 31(1959)1652; *Anal. Chem.*, 32(1960)985.  
(b) W.A. Henderson and C.A. Streuli, *J. Am. Chem. Soc.*, 82(1960)5791.  
(c) T. Allman and R.G. Goel, *Can. J. Chem.*, 60(1982)716.
- [13] A.J. Poë and M.V. Twigg, *J. Organomet. Chem.*, 50(1973)C39; *J. Chem. Soc., Dalton Trans.*, (1974)1860; *Inorg. Chem.*, 13(1974)2982.
- [14] J.P. Candlin and A.C. Shortland, *J. Organomet. Chem.* 16(1969)289.
- [15] R.A. Jackson, R. Kanluen and A.J. Poë, *Inorg. Chem.*, 23(1984)523, and references cited therein.
- [16] P.M. Zizelman, C. Amatore and J.K. Kochi, *J. Am. Chem. Soc.*, 106(1984)3771.
- [17] (a) C.A. Tolman, *J. Am. Chem. Soc.*, 92(1970)2953.  
(b) C.A. Tolman, W.C. Seidel, and L.W. Glosser, *J. Am. Chem. Soc.*, 96(1974)53.  
(c) C.A. Tolman, *Chem. Rev.*, 77(1977)313.
- [18] C.M. Lukehart, Fundamental Transition Metal Organometallic Chemistry, Wadsworth, Inc., California, 1985.
- [19] M.N. Golovin, M.M. Rahman, J.E. Belmonte and W.P. Giering, *Organometallics*, 4(1985)1981.
- [20] L. Chen and A.J. Poë, *Coord. Chem. Rev.*, 143(1995)265.
- [21] A.J. Poë, D.H. Farrar, and Y. Zheng, *J. Am. Chem. Soc.*, 114(1992)5146.

- [22] L. Chen, Ph.D. Thesis, University of Toronto, 1991.
- [23] N.M.J. Brodie, Ph.D. Thesis, University of Toronto, 1989.
- [24] R.H.E. Hudson and A.J. Poë, *Organometallics*, 14(1995)3238.
- [25] N.M.J. Brodie and A.J. Poë, *J. Organomet. Chem.*, 383(1990)531.
- [26] K. Dahlinger, F. Falcone, and A.J. Poë, *Inorg. Chem.*, 25(1986)2654.
- [27] R.H.E. Hudson and A.J. Poë, unpublished observations.
- [28] M.M. Rahman, H.Y. Liu, K. Eriks, A. Prock, and W.P. Giering, *Organometallics*, 8(1989)1.
- [29] H.Y. Liu, K. Eriks, A. Prock, and W.P. Giering, *Organometallics*, 9(1990)1758.
- [30] T.L. Brown, *Inorg. Chem.*, 31(1992)1286; T.L. Brown and K.J. Lee, *Coord. Chem. Rev.*, 128(1993)89.
- [31] (a) F.J. Safarowic and J.B. Keister, *Organometallics*, 15(1996)3310.
- (b) L.A.P. Kane-Maguire, M. Manthey, and B. Robinson, *J. Chem. Soc. Dalton Trans.*, (1995)905.
- (c) K.P. Reddy and T.L. Brown, *J. Am. Chem. Soc.*, 117(1995)2845.
- (d) N.E. Leadbeater, *J. Chem. Soc. Dalton Trans.*, (1995)2923.
- (e) O.J. Curnow, J.W. Kampf, M.D. Curtis, J.K. Shen, and F. Basolo, *J. Am. Chem. Soc.*, 116(1994)224.
- (f) A. Tekkaya, C. Kayran, S. Özkar, and C.G. Kreiter, *Inorg. Chem.*, 33(1994)2439.
- (g) S.K. Nayak, G.J. Farrell, and T. J. Burkey, *Inorg. Chem.*, 33(1994)2236.

- (h) J. Wang, Y. Gao, and Q. Shi, *Inorganica Chimica Acta* 240(1995)153.
- [32] K.J. Karel and J.R. Norton, *J. Am. Chem. Soc.*, 96(1974)6812.
- [33] J.A. Howell and P.M. Birkinshaw, *Chem. Rev.* 83(1983)557.
- [34] F. Basolo and R.G. Pearson, Mechanisms of Inorganic Reactions, Wiley, New York, 2nd ed, 1967.
- [35] (a) S. Breitshaft and F. Basolo, *J. Am. Chem. Soc.*, 88(1966)2702.
- (b) L.I.B. Haines and A.J. Poë, *J. Chem. Soc.*, A(1969)2824.
- (c) D. Dewit, J. P. Fawcett, and A.J. Poë, *J. Chem. Soc., Dalton Trans.*, (1976)528.
- (d) D.P. Keeton, S. K. Malik, and A.J. Poë, *J. Chem. Soc., Dalton Trans.* (1977)233.
- (e) D. Taube and P. Ford, *Organometallics*, 5(1986)99.
- (f) A.J. Poë, *Inorg. Chim. Acta*, 129(1987)L17.
- [36] S. Malik and A.J. Poë, *Inorg. Chem.*, 17(1978)1484.
- [37] N.M.J. Brodie and A.J. Poë, *Can. J. Chem.*, 73(1995)1187.
- [38] (a) L. Chen and A.J. Poë, *Inorg. Chem.*, 28(1989)3641.
- (b) G. Bodner, M. May, and L. McKinney, *Inorg. Chem.*, 19(1980)1951.

## CHAPTER 2

### KINETICS OF REACTIONS OF CARBONYL CLUSTERS $\text{Ru}_3(\text{CO})_{11}\text{etpb}$ AND $\text{Ru}_3(\text{CO})_{11}\text{PMe}_3$ WITH A VARIETY OF P- AND As-DONOR LIGANDS

#### 2.1 Experimental

##### 2.1.1 Instruments

Kinetic runs were monitored using a Varian Cary 2200 UV-Vis spectrophotometer equipped with a thermostated water bath, or a Nicolet 10 DX FTIR spectrophotometer.  $^{31}\text{P}$  NMR spectra were recorded with a Varian XL-200 spectrometer.  $^{31}\text{P}$  NMR chemical shifts are referred to  $\text{P}(\text{OMe})_3$  (internal reference), and decoupled from  $^1\text{H}$ .  $^1\text{H}$  NMR chemical shifts are referred to TMS.

##### 2.1.2 Chemicals

$\text{Ru}_3(\text{CO})_{12}$  was used as received from Strem Chemicals. Triphenylphosphine  $\text{PPh}_3$ , and triphenylarsine  $\text{AsPh}_3$  (Aldrich) were recrystallized from absolute alcohol. Etpb (Strem) was sublimed at  $50^\circ\text{C}$  and 0.12 mmHg immediately before use. Trimethylphosphine  $\text{PMe}_3$  (Strem) was transferred from an ampoule into a Schlenk tube filled with argon before use, and then stored in a cool room at about  $-5^\circ\text{C}$  until needed. Tri-*n*-butylphosphine  $\text{P}(n\text{-Bu})_3$  (Aldrich) was distilled over sodium and stored under argon in a Schlenk tube with an air-tight stopper. Triethyl phosphite  $\text{P}(\text{OEt})_3$ , triphenyl phosphite  $\text{P}(\text{OPh})_3$ , tri-*i*-propyl phosphite  $\text{P}(\text{O-}i\text{-Pr})_3$ , and ethyldiphenylphosphine  $\text{PPh}_2\text{Et}$

(Strem) were purified by distillation under low pressures of argon or nitrogen before use. Diethylphenylphosphine PPhEt<sub>2</sub> (Digital) was used as received. Tetrahydrofuran THF (Aldrich) was distilled over sodium-benzophenone (C<sub>6</sub>H<sub>5</sub>)<sub>2</sub>CO. All solvents (Aldrich reagent grade) were dried over activated molecular sieves (4A, BDH), and were allowed to stand for 24 hours before use. The molecular sieves were activated by washing with methanol, followed by drying in an oven at ca. 90°C for 1-2 hours, then in another oven at ca. 600°C for 4-6 hours, with subsequent cooling in a vacuum desiccator. For air sensitive ligands and clusters, such as PMe<sub>3</sub> and Ru<sub>3</sub>(CO)<sub>11</sub>PMe<sub>3</sub>, the solvents were purged with a stream of argon or nitrogen for ca. 20 minutes at least. The purity of air sensitive ligands was checked by measurement of their <sup>31</sup>P NMR spectra to make sure of absence of resonance due to <sup>31</sup>P=O. All gases, obtained from Matheson or Canox Ltd., were research grade. All manipulations were carried out by using standard Schlenk techniques under an atmosphere of oxygen-free N<sub>2</sub> or Ar.

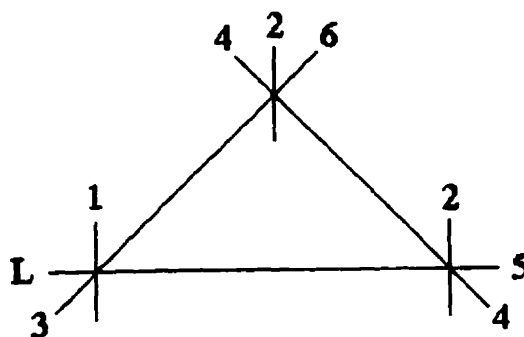
### 2.1.3 Synthesis of Ru<sub>3</sub>(CO)<sub>11</sub>etpb

Ru<sub>3</sub>(CO)<sub>12</sub> (100 mg, 0.156 mmol) was dissolved in THF (ca. 10 ml) under argon with constant stirring and warming (at ca. 40°C). The complex solution was purged with argon for about 20 seconds at least 3 times. The ligand etpb (ca. 29 mg, 0.178 mmol) was dissolved in a little THF. Once dissolution of Ru<sub>3</sub>(CO)<sub>12</sub> was completed, that is when a clear solution was obtained, the etpb solution was introduced with a syringe. Immediately following the etpb addition, the catalyst ketyl radical solution (for preparation see p.28-29) was added dropwise through a bent two-ended stainless steel needle. Addition of the

catalyst was arrested once a brown-red colour appeared in the solution. The brown-red solution was warmed under argon at 40-45°C for 3 hours or so. Completion of the reactions was determined by removing a small amount of solution with a syringe and recording its IR spectrum. The reaction had gone to completion once the peak at 2060  $\text{cm}^{-1}$  corresponding to  $\text{Ru}_3(\text{CO})_{12}$  was no longer visible. Upon completion of the reaction, the brown-red solution was filtered through a small glass pipette with glass wool or chips of soft tissue, leaving a clear orange solution. Then most of the THF was removed by vacuum, leaving a small amount of solution. 10 ml of hexane was added to the remaining solution and orange or yellow crystals of  $\text{Ru}_3(\text{CO})_{11}\text{etpb}$  isolated. The cluster was purified by recrystallization. The procedure is as follows: the cluster is dissolved in a small amount of THF, in which the  $\text{Ru}_3(\text{CO})_{11}\text{etpb}$  has higher solubility than impurities, then 10 ml of hexane is added, where the former has lower solubility than the latter, so pure crystals of  $\text{Ru}_3(\text{CO})_{11}\text{etpb}$  are isolated. By recrystallization twice, the very pure cluster was obtained. The colour is orange for large crystals or yellow for small crystals. The yield was 85 %. Its FTIR spectrum is as given in Figure 2.1. Its purity was identified by comparison with IR data (Table 2.1) in the literature [1], where the product had been purified by chromatography. The C-O stretching frequencies for the parent cluster  $\text{Ru}_3(\text{CO})_{12}$  are 2060  $\text{cm}^{-1}$ (100), 2029  $\text{cm}^{-1}$ (66), and 2010  $\text{cm}^{-1}$ (32). In general, there are eight C-O stretching bands for the mono-substituted cluster  $\text{Ru}_3(\text{CO})_{11}\text{L}$ , three due to 6 trans axial C-Os and five due to 4 cis equatorial C-Os and one unique equatorial CO cis to the equatorial ligand. Because 4 axial C-Os have almost the same position relative to

L and so do 2 equatorial C-Os, six bands usually occur with  $\text{Ru}_3(\text{CO})_{11}\text{etpb}$ , as shown below.

### Six C-O Stretching Bands of $\text{Ru}_3(\text{CO})_{11}\text{L}$



### Eight C-O Stretching Bands of $\text{Ru}_3(\text{CO})_{11}\text{L}$

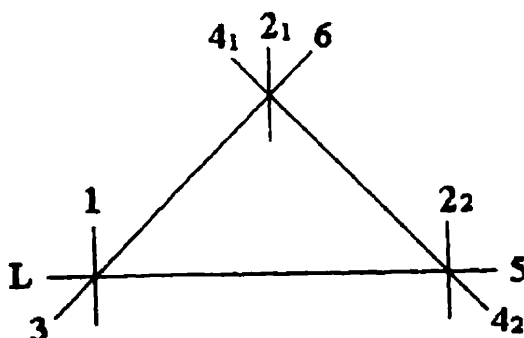


**Table 2.1 FTIR Spectra of Ru<sub>3</sub>(CO)<sub>11</sub>etpb in C-O Stretching Region<sup>a</sup>**

Purification Method	$\nu_{\text{C-O}}$ (cm <sup>-1</sup> ) <sup>b</sup>			Reference
Chromatography	2105(10) <sup>c</sup>	2061(43)	2049(94)	1
	2041(71)	2032(44)	2022(100)	
	2000(41)	1987(17)		
Recrystallization	2105(7) <sup>d</sup>	2061(0) <sup>e</sup>	2049(90)	this work
	2041(67)	2032(0) <sup>e</sup>	2022(100)	
	2000(39)	1987(15)		

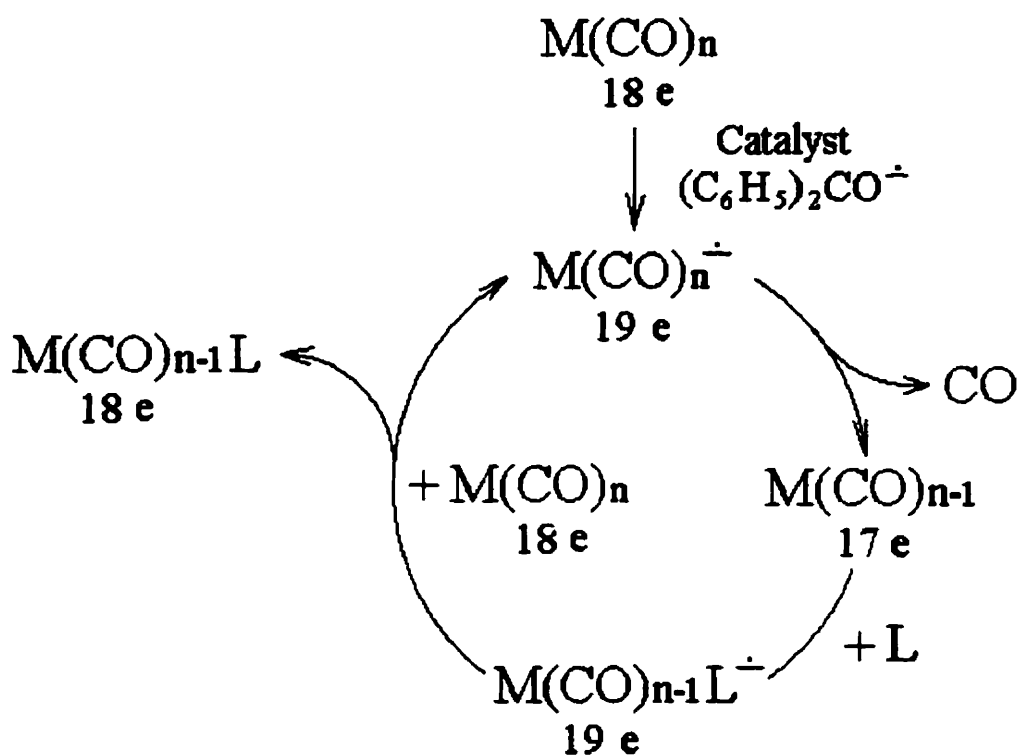
- Spectra were recorded at room temperature.
- Numbers in brackets represent the absorbance measurements relative to the largest absorbance measurement corresponding to (100).
- Dodecane was used as a solvent.
- Hexane was used as a solvent.
- These bands were not seen with carefully recrystallized samples.

Preparation of the ketyl radical (C<sub>6</sub>H<sub>5</sub>)<sub>2</sub>CO<sup>-</sup> is as follows: in order to maintain oxygen-free conditions, the preparation of this solution was carried out on a vacuum line under argon atmosphere. A solution of benzophenone (C<sub>6</sub>H<sub>5</sub>)<sub>2</sub>CO (ca. 45 mg) in THF (ca. 10 ml) was stirred over sodium under argon until a dark purple solution was observed. The colour change of the solution was green → blue → blue-purple → dark-purple during the reaction. The flask, which then

contains the ketyl radical solution, was sealed under argon until needed.

The ketyl radical  $(\text{C}_6\text{H}_5)_2\text{CO}^\cdot$  is a good reducing agent with the unpaired  $\pi$ -electron in a delocalized orbital. The syntheses of clusters  $\text{Ru}_3(\text{CO})_{11}\text{etpb}$  and  $\text{Ru}_3(\text{CO})_{11}\text{PMe}_3$  were carried out by the charge transfer catalysis from the ketyl radical, as shown below:

### Charge Transfer Catalysis



### 2.1.4 Synthesis of $\text{Ru}_3(\text{CO})_{11}\text{PMe}_3$

The cluster  $\text{Ru}_3(\text{CO})_{11}\text{PMe}_3$  was prepared by a similar method to  $\text{Ru}_3(\text{CO})_{11}\text{etpb}$ , but this was more difficult because of air sensitivity of  $\text{Ru}_3(\text{CO})_{11}\text{PMe}_3$  and  $\text{PMe}_3$ .  $\text{Ru}_3(\text{CO})_{12}$  (100 mg, 0.156 mmol) in THF (10 ml) was reacted with  $\text{PMe}_3$  (0.0181 ml, 0.178 mmol), which was transferred under argon, in the presence of a few drops of sodium ketyl in THF at 35°C until the IR band at 2060  $\text{cm}^{-1}$  due to  $\text{Ru}_3(\text{CO})_{12}$  was no longer detectable. It took about 10-15 minutes for the reaction to go to completion. Under argon, the solution of reacted mixture was filtered, leaving the clear orange-red solution. Part of the solvent was removed under vacuum. The major product in the solution was  $\text{Ru}_3(\text{CO})_{11}\text{PMe}_3$ . The cluster was purified by chromatography on a foil-wrapped 60-100 mesh florisil column. The complex  $\text{Ru}_3(\text{CO})_{11}\text{PMe}_3$  was eluted first with a mixture of hexane and dichloromethane  $\text{CH}_2\text{Cl}_2$  (ca. 3:1 by volume), followed by the  $\text{Ru}_3(\text{CO})_{10}(\text{PMe}_3)_2$  compound, as indicated by its IR spectrum. Mononuclear products remained on the column.  $\text{Ru}_3(\text{CO})_{11}\text{PMe}_3$  was isolated as orange-red crystals by removal of solvents, hexane and dichloromethane, under vacuum. The pure cluster was also obtained by recrystallization from changing solvents (for details please see Section 2.1.3). Its FTIR frequencies in the C-O stretching region can be found in Table 2.2, and Figure 2.2.

**Table 2.2 FTIR Spectra of Ru<sub>3</sub>(CO)<sub>11</sub>PMe<sub>3</sub> and Ru<sub>3</sub>(CO)<sub>11</sub>P(*n*-Bu)<sub>3</sub> in C-O Stretching Region<sup>a</sup>**

Cluster	$\nu_{\text{C-O}}$ (cm <sup>-1</sup> )			Reference
Ru <sub>3</sub> (CO) <sub>11</sub> PMe <sub>3</sub>	2097(13)	2043(75)	2028(70)	this work
	2014(100)	2001(27)	1996(25)	
	1984(28)	1976(17)		
Ru <sub>3</sub> (CO) <sub>11</sub> P( <i>n</i> -Bu) <sub>3</sub>	2097(15)	2044(66)	2026(49)	1
	2014(100)	1999(14)	1993(12)	
	1983(21)	1970(10)		

a. Refer to the footnote of Table 2.1.

Ru<sub>3</sub>(CO)<sub>11</sub>PMe<sub>3</sub> is unstable and easily decomposes in air. Thus, a solution of Ru<sub>3</sub>(CO)<sub>11</sub>PMe<sub>3</sub> becomes cloudy after ca. 18 minutes in air and it has to be stored cold under argon. It is better to store the solution of Ru<sub>3</sub>(CO)<sub>11</sub>PMe<sub>3</sub>, rather than the solid, since it seems that the solid is less stable than the solution. The solubility of Ru<sub>3</sub>(CO)<sub>11</sub>PMe<sub>3</sub> in hexane is higher than that of Ru<sub>3</sub>(CO)<sub>11</sub>etpb.

### 2.1.5. Kinetic Experiments

All kinetic runs were carried out in the absence of O<sub>2</sub> and under pseudo-first-order conditions by using at least a 280-fold molar excess of nucleophiles for reactions of Ru<sub>3</sub>(CO)<sub>11</sub>PMe<sub>3</sub>, and a 160-fold for reactions of Ru<sub>3</sub>(CO)<sub>11</sub>etpb. The progress of a given reaction was initially investigated by UV-Vis monitoring (the repetitive scan mode).

The reaction was monitored by scanning a region of UV-Vis spectra, where both the reactants and products absorbed, usually between 600 and 300 nm. The half-life,  $t_{1/2}$ , of a reaction or sometimes even the rate constants can be estimated in the light of changing of UV-Vis spectra against time. Based on the information obtained, a kinetic run can be planned to be carried out under suitable conditions by employing FTIR or UV-Vis monitoring techniques. Reactions were followed for 5 half-lives at least for both monitoring techniques, in order to obtain accurate  $A_{\infty}$  values. All kinetics were monitored in heptane solvent because it is a non-polar paraffin solvent with a relatively high boiling point (98°C) and gives well resolved FTIR absorption peaks.

#### 2.1.5.1 Preparation of Solutions

All solvents were dried over activated molecular sieves for 24 hours at least before use. When  $\text{Ru}_3(\text{CO})_{11}\text{PMe}_3$  or air-sensitive ligands were to be used, and the FTIR monitoring technique was to be employed, solvents were degassed by bubbling with argon for ca. 10 minutes before reactant solutions were made.

All complexes were prepared as saturated solutions due to their quite low solubility. Manipulations with  $\text{Ru}_3(\text{CO})_{11}\text{PMe}_3$  were conducted under argon. Initial concentrations of stock solutions of reacting complexes were generally ca.  $(2-3) \times 10^{-4}$  M.

Ligand solutions were prepared in different ways depending on the nature of the particular ligand used. When a solution of an air-sensitive ligand, such as  $\text{P}(n\text{-Bu})_3$ , was prepared, in order to keep the ligand as little exposed to the air as possible some solvent was first transferred to a volumetric flask and weighed on an analytical balance

under argon. The appropriate amount of ligand was then withdrawn from the ligand container while back-filling with argon, and added to the volumetric flask containing the solvent. The flask was finally reweighed to determine the amount of ligand used. Solutions of air-stable ligands were prepared in normal ways. Initial concentrations of stock solutions of reacting ligands were as follows:

0.1 M AsPh <sub>3</sub>	0.1 M PPh <sub>3</sub>	0.2 M etpb
0.5 M P(OEt) <sub>3</sub>	0.5 M P(O- <i>i</i> -Pr) <sub>3</sub>	0.3 M P(OPh) <sub>3</sub>
0.3 M PPh <sub>2</sub> Et	0.3 M PPhEt	0.5 M P( <i>n</i> -Bu) <sub>3</sub>

The stock solutions were stored in a cool room at about -5°C until needed. The solutions of air-stable ligands could be kept for a few months and those of air-sensitive ligands for a few weeks provided that the volumetric flask above the solution was filled with argon and stoppered securely with specially fitted stopper (Teflon or rubber). The purity of the ligands was checked by <sup>31</sup>P NMR before use.

Because Ru<sub>3</sub>(CO)<sub>11</sub>L complexes are light-sensitive, and some of them, such as Ru<sub>3</sub>(CO)<sub>11</sub>PMe<sub>3</sub>, are air-sensitive, the procedure for mixing complex and ligand had better be that a ligand solution, if air-stable, was added first, then a complex solution (usual 0.15-0.20 ml) added next. When UV-Vis monitoring technique was employed, the total volume of a reacting solution in each cell was kept constant at 3.00 ml. The relative amounts of complex and ligand solutions which combined to make up the total volume of 3.00 ml varied depending on the particular reaction conditions. The ligand solutions (0.50-2.70 ml) and appropriate amount of solvents were pipetted into quartz cells with one centimeter path length, which were then sealed tightly with a Teflon stopper, placed in the thermostated cell holders, and allowed to

warm or cool to the chosen reaction temperature. Once the ligand solution had reached the required temperature (usually 10 minutes), the complex solution was added. The cell was removed from the cell holder and shaken after complex addition. Following replacement of the cell into the cell holder, the automatic timed scanner was started. For air sensitive ligands, the solutions were transferred to cells under an inert gas atmosphere. When a reaction temperature exceeded 30°C, no more than 0.30 ml of complex solution was added. This ensured rapid re-equilibration of the reacting solution to the cell holder temperature after a small portion of complex solution was added. The temperatures of reacting solutions were determined by inserting a thermometer with a reading accurate to  $\pm 0.01^\circ\text{C}$  into another cell filled with water in the same cell holder, through a cover matched with the compartment, before and after the runs were conducted. Alternatively, the temperatures were directly determined by a digital temperature meter with which the Lauda Constant Temperature Bath RCS-6 was equipped in view of the fact that the solutions in cells, the cell holder, and the water bath had almost the same temperature with a difference less than  $0.1^\circ\text{C}$  based on the results of calibration.

Reactions monitored by the FTIR technique were carried out in Schlenk tubes equipped with rubber-septum caps to allow convenient sample removal by using a syringe with a stainless steel needle. The total volume of reacting solutions in each tube was kept constant at 11.00 ml. Ligand solutions (5.00 – 7.00 ml) and appropriate amounts of solvent were pipetted into Schlenk tubes under an inert gas atmosphere, if necessary, stoppered tightly with rubber-septum caps, and then immersed in a water bath. Solutions were purged with a

stream of argon at a speed of 1 bubble every two seconds through two stainless steel needles (one is the entry and the other is the outlet) for ca. 5 minutes, and thermostated to  $\pm 0.1^\circ\text{C}$  by a Lauda Constant Temperature Bath RCS-6, then complex solutions (4.00 ml) were added, and bubbling continued for ca. 1 minute depending on the rates of particular reactions. Every effort was made to keep out as much light as possible. This was achieved by placing the water bath cover on the opening of the water bath only allowing enough room for the Schlenk tube. Samples were withdrawn periodically, transferred to small phials, and the reaction quenched by cooling the phials in liquid  $\text{N}_2$ . FTIR spectra of the quenched liquid samples were recorded in absorbance mode using 1.0 mm path-length solution cells with NaCl windows.

#### **2.1.5.2 Kinetic Monitoring by UV-Vis Technique**

In order to determine whether UV-Vis monitoring may be employed in an individual reaction, first a successive substitution of the reaction was monitored by scanning a region of UV-Vis spectra where both the reactants and products absorbed, usually between 600 and 300 nm (repetitive scan mode). UV-Vis techniques may be employed provided that UV-Vis spectra of reactions of  $\text{Ru}_3(\text{CO})_{11}\text{L}$  with  $\text{L}'$  showed that the initial product  $\text{Ru}_3(\text{CO})_{10}\text{LL}'$  was quite stable under the conditions used and no evidence for the significant further reaction of  $\text{Ru}_3(\text{CO})_{10}\text{LL}'$  with  $\text{L}'$  was observed. Several examples are shown in Figure 2.3. Alternatively, if the second stage reaction was observed, there were sometimes clean isosbestic points in the UV-Vis spectra (Figure 2.4), or it is very clear that the absorbance increased during the

first stage reaction, while that of the second stage reaction decreased (Figure 2.5), and vice versa. Therefore UV-Vis monitoring of these reactions were shown to be satisfactory in providing good values of  $A_{\infty}$  for the first stage reaction,  $\text{Ru}_3(\text{CO})_{11}\text{L}$  with  $\text{L}'$ , to obtain accurate rate constants. UV-Vis spectra of various other reactions are shown in Figures 2.6-2.8 and 2.11-2.13.

To obtain accurate values of rate constants, when a half-life of reaction was less than 30 minutes, just one reaction was monitored by recording absorbance changes at one wavelength (time drive mode). If reactions had half-lives of  $> 30$  minutes, up to five reactions could be monitored (time drive mode) at the same time. Usually the wavelength of the maximum change of absorbance of the reaction (Figure 2.5 at 500nm), other than  $\lambda_{\text{max}}$ , or the wavelength at the isosbestic point occurring during the second stage of reaction (Figure 2.4 at 438 nm) were followed. Reactions were monitored for at least 5 half-lives. Wavelengths in the UV-Vis spectra that were used to monitor various reactions,  $\text{Ru}_3(\text{CO})_{11}\text{L}$  with  $\text{L}'$ , are as follows:

Complex	Entering Ligand (L')	Followed Wavelength (nm)	Isosbestic Point (nm)
Ru <sub>3</sub> (CO) <sub>11</sub> PMe	AsPh <sub>3</sub>	350, 365	
	P(OEt) <sub>3</sub>	438	438
	P(OPh) <sub>3</sub>	458	378
	P(O- <i>i</i> -Pr) <sub>3</sub>	438	438
	PPh <sub>3</sub>	370, 486	414
Ru <sub>3</sub> (CO) <sub>11</sub> etpb	AsPh <sub>3</sub>	315, 435	
	P(OEt) <sub>3</sub>	400	456
	P( <i>n</i> -Bu) <sub>3</sub>	400	470
	PPhEt <sub>2</sub>	440	443
	PPh <sub>3</sub>	360, 500	

### 2.1.5.3 Kinetic Monitoring by FTIR Technique

When a reaction, Ru<sub>3</sub>(CO)<sub>11</sub>L with L', showed that the further reaction of the initial product Ru<sub>3</sub>(CO)<sub>10</sub>LL' with L' was too rapid to allow accurate values of A<sub>∞</sub> of the first stage reaction to be obtained by employing UV-Vis methods, all rate measurements for these kinds of reactions had to be obtained through FTIR monitoring.

The reaction solutions were contained in Schlenk tubes with tight-fitting rubber-septum caps, which were immersed in a thermostated water bath. At accurately timed intervals, a sample was removed from the Schlenk tube by using a syringe fitted with a

stainless steel needle. The CO stretching frequency region between 2200 and 1800  $\text{cm}^{-1}$  was monitored for each sample. Accurate rate constants were usually obtained by monitoring the decreasing absorbances of IR bands of reacting clusters. Reactions were usually followed for at least 5 half-lives. Wavenumbers in the FTIR spectra that were used to monitor various reactions,  $\text{Ru}_3(\text{CO})_{11}\text{L}$  with L', are as follows:

Complex	Entering Ligand (L')	Followed Wavenumber ( $\text{cm}^{-1}$ )	Isosbestic Point ( $\text{cm}^{-1}$ )
$\text{Ru}_3(\text{CO})_{11}\text{PMe}_3$	etpb	2043, 2027	2008
	P(OEt) <sub>3</sub>	2043, 2014	2004
	P(O- <i>i</i> -Pr) <sub>3</sub>	2043, 2013	2003
	PPh <sub>2</sub> Et	2043, 2014	2004, 2057
$\text{Ru}_3(\text{CO})_{11}\text{etpb}$	etpb	2048, 2022	2012, 1991
	P(O- <i>i</i> -Pr) <sub>3</sub>	2049, 2020	2058, 2008
	P( <i>n</i> -Bu) <sub>3</sub>	2047, 2039	2054, 1991
	PPh <sub>2</sub> Et	2048, 2020	2058, 1994
	PPhEt <sub>2</sub>	2048, 2020	2058, 1994

Examples of the FTIR spectroscopic changes are given in Figures 2.9-2.10 and 2.14-2.16 and will be discussed below. The parent clusters and all substituted derivatives were identified by comparing their FTIR spectra in the C-O stretching region with the known ones or analogous

ones in the literature. The spectroscopic data are summarized in Table 2.3. Available literature data [1, 2] are also quoted to show the good agreement with each other.

**Table 2.3 FTIR Spectra for  $\text{Ru}_3(\text{CO})_{11}\text{PMe}_3$ ,  $\text{Ru}_3(\text{CO})_{11}\text{etpb}$ , and their Substituted Derivatives in C-O Stretching Region<sup>a</sup>**

Cluster	$\nu_{\text{C-O}}$ ( $\text{cm}^{-1}$ )
$\text{Ru}_3(\text{CO})_{12}$	2060(s), 2029(m), 2010(w)
$\text{Ru}_3(\text{CO})_{11}\text{PMe}_3^{\text{b}}$	2097(w), 2043(s), 2028(s), 2014(vs) 2001(m), 1984(m), 1976(w)
$\text{Ru}_3(\text{CO})_{11}\text{P}(n\text{-Bu})_3^{\text{c}}$	2097(w), 2044(s), 2026(s), 2014(vs) 1999(w), 1993(w), 1983(m), 1970(w)
$\text{Ru}_3(\text{CO})_{10}(\text{PMe}_3)(\text{P}(\text{OEt})_3)$	2070(m), 1998(s)
$\text{Ru}_3(\text{CO})_{10}(\text{PMe}_3)(\text{PPh}_2\text{Et})$	2074(m), 2062(m), 1997(s), 1985(s)
$\text{Ru}_3(\text{CO})_{10}(\text{PMe}_3)(\text{P}(\text{O-}i\text{-Pr})_3)$	2069(s), 1998(m)
$\text{Ru}_3(\text{CO})_{10}(\text{PMe}_3)(\text{etpb})$	2082(w), 2062(w), 2003(s), 1976(m)
$\text{Ru}_3(\text{CO})_{11}\text{etpb}^{\text{b}}$	2105(w), 2049(vs), 2041(s), 2022(vs) 2000(m), 1987(w)
$\text{Ru}_3(\text{CO})_{11}\text{etpb}^{\text{c}}$	2105(w), 2061(m), 2049(vs), 2041(s) 2032(m), 2022(vs), 2000(m), 1987(w)
$\text{Ru}_3(\text{CO})_{11}\text{P}(\text{OMe})_3^{\text{d}}$	2102(w), 2049(s), 2034(m), 2018(s) 2000(m), 1993(m), 1982(sh) 1970(sh)

Table 2.3 (continued)

Cluster	$\nu_{C-O}$ (cm <sup>-1</sup> )
Ru <sub>3</sub> (CO) <sub>10</sub> (etpb) <sub>2</sub>	2092(w), 2076(w), 2036(m), 2013(s) 1988(w)
Ru <sub>3</sub> (CO) <sub>10</sub> (etpb) <sub>2</sub> <sup>c</sup>	2091(m), 2035(m), 2025(m), 2013(s) 1989(m), 1981(w)
Ru <sub>3</sub> (CO) <sub>10</sub> (P(OMe) <sub>3</sub> ) <sub>2</sub> <sup>d</sup>	2085(w), 2030(m), 2005(s), 1985(sh)
Ru <sub>3</sub> (CO) <sub>10</sub> (P(OEt) <sub>3</sub> ) <sub>2</sub> <sup>e</sup>	2082(w), 2026(m), 2001(s)
Ru <sub>3</sub> (CO) <sub>10</sub> (etpb)(P(O- <i>i</i> -Pr) <sub>3</sub> )	2069(s), 2004(w), 1994(w)
Ru <sub>3</sub> (CO) <sub>10</sub> (etpb)(P( <i>n</i> -Bu) <sub>3</sub> )	2059(w), 2002(s), 1996(m), 1976(s)
Ru <sub>3</sub> (CO) <sub>10</sub> (etpb)(PPh <sub>2</sub> Et)	2075(w), 2061(w), 1976(s)
Ru <sub>3</sub> (CO) <sub>10</sub> (etpb)(PPhEt <sub>2</sub> )	2075(w), 2061(w), 1976(s)
Ru(CO) <sub>4</sub> (P( <i>n</i> -Bu) <sub>3</sub> ) <sup>f</sup>	2059(m), 1983(w), 1944(s)
Ru(CO) <sub>4</sub> (PMe <sub>3</sub> )	2062(m), 1987(w), 1947(s)
Ru(CO) <sub>4</sub> etpb <sup>f</sup>	2077(w), 2007(m), 1976(s)
Ru(CO) <sub>4</sub> etpb	2076(w), 2006(m), 1975(s)

a. This work, and spectra recorded in heptane unless otherwise indicated. Letters in parentheses indicate the relative absorptivities of individual peaks.

b. In hexane, this work.

c. In dodecane, data from ref.[1].

d. In hexane, data from ref.[2].

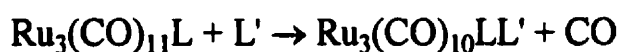
e. In decalin, data from ref.[2].

f. In heptane, data from ref.[2].

## 2.2 Results of Kinetic Studies

A variety of P-donor nucleophiles and AsPh<sub>3</sub> were used to study the reaction kinetics of nucleophilic substitution on Ru<sub>3</sub>(CO)<sub>11</sub>PMe<sub>3</sub> and Ru<sub>3</sub>(CO)<sub>11</sub>etpb. These ligands cover a wide range of pK<sub>a</sub> values (from -2.0 to 8.43 [3-6]), and a fairly large range in size (Tolman cone angle from 101 to 145° [7-8]), and the results of the kinetic studies can be expected to be informative.

Based on FTIR spectra taken during the reactions, the clusters Ru<sub>3</sub>(CO)<sub>11</sub>PMe<sub>3</sub> and Ru<sub>3</sub>(CO)<sub>11</sub>etpb have been shown to react with all ligands and give the trinuclear substituted products, as described by following equations:



In addition, it was clear from the FTIR spectra that fragmentation also occurred as well as successive substitution. The degree of substitution is dependent on the nature of nucleophiles. Multisubstitutions were observed for all but the less basic ligand AsPh<sub>3</sub>. The reactivity of

clusters is dependent on the nature of P-donors, either as substituents or as nucleophiles, in terms of their particular size and basicity, as well as the nature of clusters. The rates of reactions,  $\text{Ru}_3(\text{CO})_{11}\text{etpb}$  with  $\text{L}'$  are smaller than those of corresponding reactions of  $\text{Ru}_3(\text{CO})_{11}\text{PMe}_3$  with  $\text{L}'$ . Most reactions proceeded via a mixture of first and second order paths with the rate equation being given by  $\text{rate} = (k_1 + k_2[\text{L}]) [\text{complex}]$ . Because of the presence of at least a 160-fold molar excess of the ligand concentration, the term,  $(k_1 + k_2[\text{L}])$ , is constant throughout a given reaction, and is equal to  $k_{\text{obs}}$ . The  $k_{\text{obs}}$  is the pseudo first-order rate constant and the rate equation is:  $\text{rate} = k_{\text{obs}} [\text{complex}]$ . Values of  $k_{\text{obs}}$  are obtained from the dependence of absorbance on time as described below.

### 2.2.1 The Course of the Reactions of $\text{Ru}_3(\text{CO})_{11}\text{PMe}_3$ with $\text{L}'$

UV-Vis spectra for the reactions,  $\text{Ru}_3(\text{CO})_{11}\text{PMe}_3$  with  $\text{L}'$  ( $\text{L}' = \text{AsPh}_3$ ) in heptane showed the initial products  $\text{Ru}_3(\text{CO})_{10}(\text{PMe}_3)\text{L}'$  were quite stable and no evidence for the significant further reactions,  $\text{Ru}_3(\text{CO})_{10}(\text{PMe}_3)\text{L}'$  with  $\text{L}'$ , was observed under the conditions used (Figure 2.3). These reactions could thereby be monitored easily by following the UV-Vis spectroscopic changes as a function of time to obtain accurate rate constants, because good values of  $A_\infty$  for the first stage reaction,  $\text{Ru}_3(\text{CO})_{11}\text{PMe}_3$  with  $\text{L}'$ , could be provided by the UV-Vis technique.

The spectroscopic changes in the UV-Vis spectra during reactions with all nucleophiles apart from  $\text{AsPh}_3$  exhibited initial formation of  $\text{Ru}_3(\text{CO})_{10}(\text{PMe}_3)\text{L}'$  followed by further reactions to form  $\text{Ru}_3(\text{CO})_9(\text{PMe}_3)\text{L}'_2$ . UV-Vis spectra of the reaction,  $\text{Ru}_3(\text{CO})_{11}\text{PMe}_3$

with  $\text{P(OPh)}_3$ , showed that the second stage reaction became evident quite soon, because the isosbestic point for the first stage (378 nm) consisted of only 9 spectra (Figure 2.6). But it is very clear that the spectroscopic changes were very small due to the second stage reaction, and quite big due to the first stage reaction when wavelengths were more than 458 nm (Figure 2.6). Good results were therefore obtained by measuring the increase of absorbance at 458 nm. An isosbestic point is indicative of a clean reaction without detectable intermediates.

When the entering ligand was  $\text{P(OEt)}_3$  the UV-Vis spectra of the reaction showed that the second stage reaction was quite slow. The big change in the UV-Vis spectra occurred during the first 10 minutes with a small change during the last 5.5 hours, and an isosbestic region was evident at ca. 438 nm over the last 5.5 hours. The FTIR spectra of the reaction with  $\text{P(OEt)}_3$  also confirmed the second stage reaction was quite slow because the isosbestic point at  $2004\text{ cm}^{-1}$  was quite clean over the whole course of the reaction.

UV-Vis spectra of the reaction with  $\text{PPh}_2\text{Et}$  showed that the second stage reaction affected the spectroscopic changes quite soon because the isosbestic point consisted of only a few spectra (Figure 2.7). The accurate value of  $A_\infty$  for the first stage reaction,  $\text{Ru}_3(\text{CO})_{11}\text{PMe}_3$  with  $\text{PPh}_2\text{Et}$ , could not therefore be provided by the UV-Vis technique. The rate constants for this reaction had to be obtained by the FTIR method. The decreasing bands at 2013 and  $2042.6\text{ cm}^{-1}$  due to  $\text{Ru}_3(\text{CO})_{11}\text{PMe}_3$  were monitored. FTIR spectra of this reaction also confirmed that the second stage reaction was not slow because the isosbestic point at  $2004\text{ cm}^{-1}$  disappeared quite soon

due to the reaction of  $\text{Ru}_3(\text{CO})_{10}(\text{PMe}_3)(\text{PPh}_2\text{Et})$  with  $\text{PPh}_2\text{Et}$ . However, the reaction could be successfully monitored by FTIR spectroscopy when bands with negligible  $A_\infty$  values were used.

When the attacking ligand was  $\text{P}(\text{O}-i\text{-Pr})_3$  the UV-Vis spectrum changes of the reaction were similar to those of the reaction of  $\text{Ru}_3(\text{CO})_{11}\text{PMe}_3$  with  $\text{P}(\text{OEt})_3$ . This showed that the second stage reaction was quite slow, and a good isosbestic point is evident at 438 nm for the second stage of reaction (Figure 2.4). The rate was obtained by measuring the decrease of absorbance at the isosbestic point at 438 nm. FTIR spectra of this reaction also indicated that the further reaction was quite slow because the isosbestic point at  $2003\text{ cm}^{-1}$  was fairly clear over the whole course of the reaction.

UV-Vis spectra of the reaction with etpb showed that the second stage reaction,  $\text{Ru}_3(\text{CO})_{10}(\text{PMe}_3)(\text{etpb})$  with etpb, affected the spectroscopic changes quite soon. A satisfactory value of  $A_\infty$  for the first stage reaction could not be obtained by the UV-Vis technique, so the reaction had to be monitored by the FTIR technique. The rate constants were obtained by measuring the decrease of absorbance at  $2027$  and  $2043\text{ cm}^{-1}$  due to  $\text{Ru}_3(\text{CO})_{11}\text{PMe}_3$  (Figures 2.9-2.10). FTIR spectra of the reactions at  $40.0^\circ\text{C}$  and  $25.0^\circ\text{C}$  showed that the isosbestic point at  $2008\text{ cm}^{-1}$  disappeared faster at the higher temperature. It is a general trend.

### 2.2.2 The Course of the Reactions of $\text{Ru}_3(\text{CO})_{11}\text{etpb}$ with $\text{L}'$

The UV-Vis spectroscopic changes for reactions of  $\text{Ru}_3(\text{CO})_{11}\text{etpb}$  with  $\text{AsPh}_3$  in heptane showed that the first stage reaction product  $\text{Ru}_3(\text{CO})_{10}(\text{etpb})(\text{AsPh}_3)$  is quite stable and no evidence for the significant second stage reaction of  $\text{Ru}_3(\text{CO})_{10}(\text{etpb})(\text{AsPh}_3)$  with  $\text{AsPh}_3$  was observed (Figure 2.3). UV-Vis monitoring of this reaction was thereby shown to be satisfactory in providing good values of  $A_\infty$ , and the growing bands at 315 and 435 nm were followed to obtain rate constants.

When the incoming ligand was  $\text{PPh}_3$  the UV-Vis spectrum changes indicated that the second stage reaction,  $\text{Ru}_3(\text{CO})_{10}(\text{etpb})(\text{PPh}_3)$  with  $\text{PPh}_3$  at  $53.9^\circ\text{C}$  was observed after 2 hrs. But it is very clear that the absorbance decreased during the second stage reaction after an increase during the first stage reaction (Figure 2.5). A good value of  $A_\infty$  for the first stage reaction of  $\text{Ru}_3(\text{CO})_{11}\text{etpb}$  with  $\text{PPh}_3$  could therefore be obtained because the second stage reaction was quite slow and the reaction was followed by measuring the increase of absorbance at 360 and 500 nm (Figure 2.5).

The changes of UV-Vis spectra for the reactions with  $\text{P}(\text{OEt})_3$  showed that the first stage of reaction was essentially complete before the second stage became evident, and the isosbestic region was clear at around 456nm (Figure 2.11). The reaction could therefore be monitored by UV-Vis method. There was a big decrease of absorbance at 400nm and this band was monitored to obtain the rate constants.

When the entering ligand was  $\text{P}(\text{O-}i\text{-Pr})_3$  the UV-Vis spectra showed that the second stage reaction overlapped significantly with the

first stage and the isosbestic point was not very clear. A good value of  $A_{\infty}$  for the first stage reaction,  $\text{Ru}_3(\text{CO})_{11}\text{etpb}$  with  $\text{P}(\text{O-}i\text{-Pr})_3$  could not be obtained by UV-Vis technique. The reaction had to be monitored by FTIR method. The decreasing bands at 2020.0 and 2048.8  $\text{cm}^{-1}$  due to  $\text{Ru}_3(\text{CO})_{11}\text{etpb}$  was followed to obtain rate constants. FTIR spectra of this reaction also indicated the isosbestic point disappeared quite soon, which means the further reaction of  $\text{Ru}_3(\text{CO})_{10}(\text{etpb})(\text{P}(\text{O-}i\text{-Pr})_3)$  with  $\text{P}(\text{O-}i\text{-Pr})_3$  became quite apparent early on.

UV-Vis spectra of the reaction with  $\text{P}(n\text{-Bu})_3$  showed clearly that the second stage reaction occurred but the spectroscopic changes due to the further reaction was quite small. The rate constants could be obtained by UV-Vis technique and following the band at 400 nm. This reaction was also monitored by the FTIR method, and the spectra are given in Figure 2.14.

When the incoming ligand was  $\text{PPh}_2\text{Et}$  the UV-Vis spectra of the reaction showed that the second stage reaction became apparent quite soon and the spectroscopic changes due to the further reaction were quite big in some regions (Figure 2.12). Thus, not only was there no clear isosbestic point at ca. 390 nm but the absorbance at  $>$  ca. 450 nm continued to increase long after the absorbance at 390-430 nm had become essentially constant. A good value of  $A_{\infty}$  for the first stage reaction could therefore not be obtained by UV-Vis method and the reaction was monitored by the FTIR technique. The decreasing bands at 2019.7 and 2048.4  $\text{cm}^{-1}$  due to  $\text{Ru}_3(\text{CO})_{11}\text{etpb}$  were followed to obtain rate constants.

The reaction of  $\text{Ru}_3(\text{CO})_{11}\text{etpb}$  with  $\text{PPhEt}_2$  was monitored by both FTIR and UV-Vis. The UV-Vis spectra are given in Figure 2.13, where the isosbestic point at 443 nm during the second stage of substitution is quite clear. The FTIR spectra are shown in Figure 2.15 and there is quite a sharp isosbestic point at ca.  $1994\text{ cm}^{-1}$ .

The rate constants for the reaction of  $\text{Ru}_3(\text{CO})_{11}\text{etpb}$  with  $\text{etpb}$  were obtained by the FTIR method. The decreasing bands at  $2021.6$  and  $2048.5\text{ cm}^{-1}$  due to  $\text{Ru}_3(\text{CO})_{11}\text{etpb}$  were followed. The FTIR spectra are given in Figure 2.16.

### 2.2.3 Data Treatment

Pseudo-first-order conditions were maintained throughout the kinetic studies by using at least a 160-fold excess of ligand concentration. Pseudo-first-order rate constants  $k_{\text{obs}}$  may be obtained usually in two ways. One is from a unweighted linear least squares analysis of  $\ln(A_t - A_\infty)$  against time for decreasing absorbance readings or  $\ln(A_\infty - A_t)$  against time for increasing absorbance readings (Figure 2.17), where  $A_t$  is the absorbance at time  $t$ , and  $A_\infty$  is the absorbance after completion of a reaction. For this method, the values of  $A_\infty$  need to be inputted. Another is from fitting an exponential curve to the absorbance vs time data by using a non-linear least squares regression program, KORE, which means kinetic analysis using over-relaxation [9]. KORE is especially useful in the cases where  $A_\infty$  is not available. Tables 5.3 and 5.4 (Chapter 5 Appendices) summarize all pseudo-first-order rate constants for reactions of  $\text{Ru}_3(\text{CO})_{11}\text{PMe}_3$  and  $\text{Ru}_3(\text{CO})_{11}\text{etpb}$  respectively with a variety of nucleophiles in heptane. The precision of individual values of  $k_{\text{obs}}$  is excellent as shown by the  $\sigma$

(%) values in Tables 5.3 and 5.4. These are a measure of the goodness of fit of data for that particular run to the exponential change in absorbance with time. The correlation coefficient was generally 0.9999 - 0.999999 for up to 99 % reaction.

The reproducibility of rate constants,  $k_{\text{obs}}$ , obtained by using different techniques, FTIR and UV-Vis, and monitoring different wavenumbers or wavelengths for the same solution is good as shown in Figure 2.18 and Table 2.4. The excellent linearity of the rate plots using both techniques, both wavenumbers, and both wavelengths indicates that no matter what technique was used and which band was monitored, the rate constants agree with one another quite well. In addition, this also indicates that the rate constants obtained from non-linear least squares analyses and linear least squares analyses are in agreement with each other.

**Table 2.4 Comparison of  $k_{\text{obs}}$  Values Obtained by Using Different Techniques and Monitoring Different Wavenumbers or Wavelengths for Substitution Reactions of  $\text{Ru}_3(\text{CO})_{11}\text{PMe}_3$  with  $\text{P}(\text{OEt})_3$  in Heptane at 25.2°C**

[L](M)	<sup>a</sup> $k_{\text{obs}}(\text{s}^{-1})$	$\sigma(\%)$	Monitoring Technique	Monitored Band	<sup>b</sup> Run No
0.366	$(1.86 \pm 0.00) \times 10^{-3}$	0.2	UV-Vis	420 nm	34(a)
0.366	$(1.88 \pm 0.01) \times 10^{-3}$	0.3	UV-Vis	438 nm	36(a)
0.366	$(1.89 \pm 0.00) \times 10^{-3}$	0.3	UV-Vis	438 nm	37(a)
0.731	$(4.00 \pm 0.01) \times 10^{-3}$	0.3	UV-Vis	420 nm	34(b)
0.731	$(3.97 \pm 0.01) \times 10^{-3}$	0.2	UV-Vis	438 nm	36(b)
0.914	$(5.13 \pm 0.02) \times 10^{-3}$	0.4	UV-Vis	420 nm	34(c)
0.914	$(5.25 \pm 0.02) \times 10^{-3}$	0.4	UV-Vis	438 nm	36(c)
0.914	$(5.14 \pm 0.02) \times 10^{-3}$	0.3	UV-Vis	420 nm	35(a)
1.097	$(6.31 \pm 0.02) \times 10^{-3}$	0.4	UV-Vis	420 nm	35(b)
1.097	$(6.46 \pm 0.02) \times 10^{-3}$	0.3	UV-Vis	438 nm	37(b)

Table 2.4 (continued)

[L'](M)	<sup>a</sup> k <sub>obs</sub> (s <sup>-1</sup> )	σ(%)	Monitoring Technique	Monitored Band	<sup>b</sup> Run No
0.0234	(2.00±0.03) × 10 <sup>-4</sup>	1.3	FTIR	2042.9 cm <sup>-1</sup>	38(a)
0.0234	(1.83±0.07) × 10 <sup>-4</sup>	3.7	FTIR	2014.0 cm <sup>-1</sup>	38(b)
0.0936	(5.58±0.16) × 10 <sup>-4</sup>	2.9	FTIR	2042.9 cm <sup>-1</sup>	39(a)
0.0936	(5.55±0.24) × 10 <sup>-4</sup>	4.3	FTIR	2014.0 cm <sup>-1</sup>	39(b)
0.187	9.49 × 10 <sup>-4</sup>		FTIR	2042.9 cm <sup>-1</sup>	40(a)
0.187	(9.34±0.30) × 10 <sup>-4</sup>	3.2	FTIR	2014.0 cm <sup>-1</sup>	40(b)
0.281	(1.53±0.03) × 10 <sup>-3</sup>	2.1	FTIR	2042.9 cm <sup>-1</sup>	41(a)
0.281	(1.49±0.04) × 10 <sup>-3</sup>	2.7	FTIR	2014.0 cm <sup>-1</sup>	41(b)

a. k<sub>obs</sub> with uncertainties were obtained by non-linear least squares regression analyses (KORE) of A<sub>t</sub> vs time. k<sub>obs</sub> without uncertainties were obtained by linear least squares analyses of ln|A<sub>t</sub>-A<sub>∞</sub>| vs time.

b. A multicell equipment was used for the UV-Vis technique and runs with the same number correspond to reactions in different cells carried out at the same time; for the FTIR technique runs with the same number correspond to reactions in the same cell carried out at the same time.

## 2.2.4 Reaction Pathways

The plots of k<sub>obs</sub> vs [L'] for all the kinetic runs show excellent linear relationships (Figures 2.19 and 2.20), and the gradients and intercepts suggest that the nucleophilic substitution reactions of Ru<sub>3</sub>(CO)<sub>11</sub>PMe<sub>3</sub> and Ru<sub>3</sub>(CO)<sub>11</sub>etpb proceeded via a mixture of first

and second order paths. The  $k_1$  path is  $[L']$ -independent, while the  $k_2$  path is  $[L']$ -dependent. A weighted linear least squares analysis of  $k_{\text{obs}}$  against  $[L']$  values showed that the data fit the Eq.(2.1) very well,

$$k_{\text{obs}} = k_1 + k_2 [L'] \quad (2.1)$$

where  $k_1$  is the first-order rate constant, and  $k_2$  is the second-order rate constant. Careful inspection of the plots of  $k_{\text{obs}}$  vs  $[L']$  suggests that the intercepts,  $k_1$ , are independent of the nature of the nucleophiles; that is, for a given cluster, different nucleophiles have the same intercept,  $k_1$ . The gradients of the lines,  $k_2$ , depend strongly on the nature of the nucleophiles and this is a preliminary qualitative indication that there is substantial  $L'-\text{Ru}$  bond making in the transition states.

The values of  $k_1$  and  $k_2$  as well as their probable errors can be obtained by the weighted linear least squares analysis of the dependence of  $k_{\text{obs}}$  values on nucleophile concentrations. It is convenient to analyze the data by assuming the relative weights for each sample point to be  $(1/k_{\text{obs}})^2$ . This is equivalent to assuming that all the values of  $k_{\text{obs}}$  have the same percentage error,  $\sigma(k_{\text{obs}})$ , and this percentage error can be obtained from the scatter of the data about the straight line, i.e.  $\sigma(k_{\text{obs}}) = \{\Sigma(\Delta\%)^2/(N-2)\}^{1/2}$  ( $N$  is the number of values of  $k_{\text{obs}}$ , and 2 is the number of parameters = the number of degrees of freedom). Thus the values of  $\sigma(k_{\text{obs}})$  provide a measure of the experimental error in measuring an individual rate constant for reactions with a given nucleophile at a particular temperature. Tables 2.5 and 2.6 summarize the first- and second-order rate constants for

substitution reactions of  $\text{Ru}_3(\text{CO})_{11}\text{PMe}_3$  and  $\text{Ru}_3(\text{CO})_{11}\text{etpb}$  with a variety of nucleophiles in heptane, respectively. The rate constants are of excellent precision.

**Table 2.5** First- and Second-Order Rate Constants for Reactions of  $\text{Ru}_3(\text{CO})_{11}\text{PMe}_3$  with Nucleophiles  $\text{L}'$  in Heptane,  $[\text{Complex}] = 10 \times 10^{-5}$  and  $3 \times 10^{-5}$  M for FTIR and UV-Vis Monitoring, respectively

T (°C)	N <sup>a</sup>	$10^5 k_1$ (s <sup>-1</sup> )	$10^3 k_2$ (M <sup>-1</sup> s <sup>-1</sup> )	$\sigma(k_{\text{obs}})^b$ (%)	[L'] (M)
<b>L' = AsPh<sub>3</sub></b>					
18.3	8 <sup>c</sup>	$1.52 \pm 0.02^d$		1.5	0.016–0.080
18.5	7	$1.71 \pm 0.03^d$		1.9	0.016–0.080
32.0	14	$15.6 \pm 0.2^d$		1.2	0.016–0.078
41.1	27	$74.4 \pm 0.9^d$		1.2	0.016–0.078
50.4	11	$256 \pm 6^d$		2.6	0.016–0.078
<b>L' = etpb</b>					
25.0	7	$6.74 \pm 1.25^e$	$3.66 \pm 0.30$	10	0.014–0.186
40.0	5	$67.0 \pm 2.7^e$	$10.4 \pm 0.8$	1.3	0.025–0.050
<b>L' = P(OEt)<sub>3</sub></b>					
25.2	13	$7.73 \pm 1.11^{d\&e}$	$4.92 \pm 0.18$	3.2	0.024–0.40

Table 2.5 (continued)

T (°C)	N <sup>a</sup>	10 <sup>5</sup> k <sub>1</sub> (s <sup>-1</sup> )	10 <sup>3</sup> k <sub>2</sub> (M <sup>-1</sup> s <sup>-1</sup> )	σ(k <sub>obs</sub> ) <sup>b</sup> (%)	[L'] (M)
<b>L' = P(OPh)<sub>3</sub></b>					
25.2	8	2.51 ± 0.28 <sup>d</sup>	0.281±0.017	4.3	0.047–0.28
<b>L' = P(O-<i>i</i>-Pr)<sub>3</sub></b>					
25.15	11	5.65 ± 0.57 <sup>d</sup>	1.34 ± 0.04	3.0	0.067–0.40
<b>L' = PPh<sub>2</sub>Et</b>					
25.2	9	6.44 ± 0.65 <sup>e</sup>	0.159±0.048	6.0	0.066–0.26
<b>L' = PPh<sub>3</sub></b>					
25.15	5	5.14 ± 0.06 <sup>d</sup>	0.0165±0.0043	0.5	0.032–0.11

- The number of individual determinations of k<sub>obs</sub>; k<sub>obs</sub> = k<sub>1</sub> + k<sub>2</sub> [L']. N.B. No evidence for any dependence of k<sub>obs</sub> on [AsPh<sub>3</sub>] was observed and the values of k<sub>1</sub> were obtained simply by averaging the values of k<sub>obs</sub> obtained at all concentrations of AsPh<sub>3</sub>.
- Probable error of an individual determination of k<sub>obs</sub> obtained by the data analysis.
- Uncertainties here and elsewhere are estimated standard errors for k<sub>1</sub> and k<sub>2</sub>.
- Studied by using UV-Vis monitoring.
- Studied by using FTIR monitoring.

**Table 2.6 First- and Second-Order Rate Constants for Reactions of  $\text{Ru}_3(\text{CO})_{11}\text{etpb}$  with Nucleophiles  $\text{L}'$  in Heptane,  $[\text{Complex}] = 8 \times 10^{-5}$  and  $2 \times 10^{-5}$  M for FTIR and UV-Vis Monitoring, respectively**

T (°C)	$\text{N}^{\text{a}}$	$10^5 k_1$ ( $\text{s}^{-1}$ )	$10^5 k_2$ ( $\text{M}^{-1}\text{s}^{-1}$ )	$\sigma(k_{\text{obs}})^{\text{b}}$ (%)	$[\text{L}']$ (M)
<b><math>\text{L}' = \text{AsPh}_3</math></b>					
36.2	$10^{\text{c}}$	$2.62 \pm 0.05^{\text{d}}$		1.9	0.014–0.069
44.9	13	$8.88 \pm 0.12^{\text{d}}$		1.3	0.016–0.068
45.4	24	$9.39 \pm 0.06^{\text{d}}$		0.7	0.014–0.069
54.3	24	$34.6 \pm 0.4^{\text{d}}$		1.1	0.008–0.032
60.4	5	$82.0 \pm 0.8^{\text{d}}$		1.0	0.014–0.068
60.5	5	$85.2 \pm 1.4^{\text{d}}$		1.6	0.014–0.069
<b><math>\text{L}' = \text{etpb}</math></b>					
25.1	12	$0.412 \pm 0.033^{\text{e}}$	$12.1 \pm 1.0$	3.0	0.013–0.070
40.0	10	$4.47 \pm 0.40^{\text{e}}$	$35.5 \pm 6.0$	4.5	0.011–0.043
<b><math>\text{L}' = \text{P}(\text{OEt})_3</math></b>					
25.15	5	$0.126 \pm 0.032^{\text{d}}$	$14.8 \pm 0.2$	0.9	0.11–0.41
<b><math>\text{L}' = \text{P}(\text{O-}i\text{-Pr})_3</math></b>					
25.2	20	$0.592 \pm 0.182^{\text{e}}$	$5.82 \pm 0.82$	10	0.12–0.46

Table 2.6 (continued)

T (°C)	N <sup>a</sup>	10 <sup>5</sup> k <sub>1</sub> (s <sup>-1</sup> )	10 <sup>3</sup> k <sub>2</sub> (M <sup>-1</sup> s <sup>-1</sup> )	σ(k <sub>obs</sub> ) <sup>b</sup> (%)	[L'] (M)
<b>L' = P(n-Bu)<sub>3</sub></b>					
25.15	6	-0.013±0.148 <sup>d</sup>	38.7 ± 1.0	2.3	0.074–0.44
<b>L' = PPh<sub>2</sub>Et</b>					
25.1	10	0.769±0.139 <sup>e</sup>	1.29 ± 0.83	11	0.029–0.29

- a. The number of individual determinations of k<sub>obs</sub>; k<sub>obs</sub> = k<sub>1</sub> + k<sub>2</sub> [L']. N.B. No evidence for any dependence of k<sub>obs</sub> on [AsPh<sub>3</sub>] was observed and the values of k<sub>1</sub> were obtained simply by averaging the values of k<sub>obs</sub> obtained at all concentrations of AsPh<sub>3</sub>.
- b. Probable error of an individual determination of k<sub>obs</sub> obtained by the data analysis.
- c. Uncertainties here and elsewhere are estimated standard errors for k<sub>1</sub> and k<sub>2</sub>.
- d. Studied by using UV-Vis monitoring.
- e. Studied by using FTIR monitoring.

The second-order rate constants,  $k_2$ , for the substitution reactions of  $\text{Ru}_3(\text{CO})_{11}\text{PMe}_3$  with  $\text{P}(\text{OEt})_3$  and  $\text{P}(\text{O-}i\text{-Pr})_3$  in heptane at  $25.2^\circ\text{C}$  obtained by different monitoring techniques agree with each other extremely well as shown in Table 2.7. So do the first-order rate constants  $k_1$  (Table 2.9).

**Table 2.7 Comparison of  $k_2$  Values Obtained by Different Monitoring Techniques for Substitution Reactions of  $\text{Ru}_3(\text{CO})_{11}\text{PMe}_3$  in Heptane at  $25.2^\circ\text{C}$**

Attacking Nucleophile	Monitoring Technique	Followed Wavenumber or Wavelength	$k_2$ ( $\text{M}^{-1}\text{s}^{-1}$ )
$\text{P}(\text{OEt})_3$	FTIR	2042.9 $\text{cm}^{-1}$	$4.92 \times 10^{-3}$
	UV-Vis	438 nm	$4.92 \times 10^{-3}$
$\text{P}(\text{O-}i\text{-Pr})_3$	FTIR & UV-Vis	2042.6 $\text{cm}^{-1}$	$1.35 \times 10^{-3}$
		2013.0 $\text{cm}^{-1}$	
		438 nm	
	UV-Vis	438 nm	$1.34 \times 10^{-3}$

### 2.3 Kinetic Data Analyses and Discussion

The substitution reactions of  $\text{Ru}_3(\text{CO})_{11}\text{PMe}_3$  or  $\text{Ru}_3(\text{CO})_{11}\text{etpb}$  with nucleophiles  $\text{L}'$  proceed through both  $[\text{L}']$ -independent and  $[\text{L}']$ -dependent paths, i.e. with the rate equation  $k_{\text{obs}} = k_1 + k_2[\text{L}']$ . The pseudo-first-order rate plots of the reactions show excellent linear relationships (Figures 2.19 and 2.20). Values of  $k_2$  for both clusters were found to depend strongly on the nature of the entering ligands  $\text{L}'$ . The relative reactivities of different entering ligands  $\text{L}'$  with  $\text{Ru}_3(\text{CO})_{11}\text{PMe}_3$  in heptane at 25.0°C are as follows:  $\text{P}(\text{OEt})_3 > \text{etpb} > \text{P}(\text{O-}i\text{Pr})_3 > \text{PPh}_2\text{Et} > \text{PPh}_3 \approx \text{P}(\text{OPh})_3$ , and those with  $\text{Ru}_3(\text{CO})_{11}\text{etpb}$  are  $\text{P}(n\text{-Bu})_3 > \text{etpb} > \text{P}(\text{OEt})_3 > \text{P}(\text{O-}i\text{Pr})_3 > \text{PPh}_2\text{Et}$ . The reactions governed by the rate constants  $k_2$  can therefore be assigned to an associative process. No evidence for any dependence of  $k_1$  on  $[\text{L}']$  was observed and the values of  $k_1$  were reasonably constant with slight deviations for the reactions of a given cluster with different nucleophiles  $\text{L}'$  except that  $\text{P}(n\text{-Bu})_3$ , in the reactions with  $\text{Ru}_3(\text{CO})_{11}\text{etpb}$ , is notorious for giving an unreliable value of  $k_1$  (in this case a negative and meaningless value) as has been shown in previous papers [10] and in work by Darensbourg et al. [11]. So the reactions governed by the rate constants  $k_1$  can be assigned to a dissociative mechanism [10, 12] because the values of  $k_1$  depend only on the nature of the substituents  $\text{L}$ , and are independent of the concentrations and nature of nucleophiles  $\text{L}'$ . The values of  $k_1$  for both clusters are tabulated below :

**Table 2.8 Values of  $k_1$  for Reactions of  $\text{Ru}_3(\text{CO})_{11}\text{L}$  with Nucleophiles  $\text{L}'$  in Heptane;  $[\text{Complex}] = 1.0 \times 10^{-4}$  and  $3.0 \times 10^{-5}$  M for FTIR and UV-Vis Monitoring, Respectively**

Cluster	$\text{L}'$	T(°C)	$10^5 k_1(\text{s}^{-1})$	Average $10^5 k_1(\text{s}^{-1})$
$\text{Ru}_3(\text{CO})_{11}\text{PMe}_3$	$\text{AsPh}_3^{\text{a}}$	25.0	$5.16 \pm 0.10$	$5.62 \pm 0.57$ or $6.31 \pm 0.41^{\text{b}}$
	$\text{PPh}_3$	25.15	$5.14 \pm 0.06$	
	$\text{PPh}_2\text{Et}$	25.2	$6.44 \pm 0.65$	
	$\text{P}(\text{O}-i\text{Pr})_3$	25.15	$5.65 \pm 0.57$	
	$\text{P}(\text{OEt})_3$	25.2	$7.73 \pm 1.11$	
	etpb	25.0	$6.74 \pm 1.25$	
	$\text{P}(\text{OPh})_3$	25.2	$2.51 \pm 0.28$	
$\text{Ru}_3(\text{CO})_{11}\text{etpb}$	$\text{AsPh}_3^{\text{a}}$	25.0	$0.415 \pm 0.014$	$0.463 \pm 0.080^{\text{c}}$
	etpb	25.1	$0.412 \pm 0.033$	
	$\text{P}(\text{OEt})_3$	25.15	$0.127 \pm 0.032$	
	$\text{P}(\text{O}-i\text{Pr})_3$	25.2	$0.592 \pm 0.182$	
	$\text{PPh}_2\text{Et}$	25.1	$0.769 \pm 0.139$	
	$\text{P}(n\text{-Bu})_3$	25.15	$-0.013 \pm 0.148$	

a. Calculated values of  $k_1$  from  $\Delta H_1^\ddagger$  and  $\Delta S_1^\ddagger$  based on the Eyring equation.

b.  $6.31 \pm 0.41 = 6.31 \pm 1.00/6^{1/2}$  if the 2.51 was omitted.

c. The  $k_1$  value for the reactions of  $\text{Ru}_3(\text{CO})_{11}\text{etpb}$  with  $\text{P}(n\text{-Bu})_3$  was omitted in calculating the average.

### 2.3.1 Activation Parameters for CO Dissociation from Ten Clusters $\text{Ru}_3(\text{CO})_{11}\text{L}$

The nucleophile  $\text{AsPh}_3$  was used to obtain precise  $k_1$  values because the values of  $k_{\text{obs}}$  for reactions of  $\text{Ru}_3(\text{CO})_{11}\text{PMe}_3$  or  $\text{Ru}_3(\text{CO})_{11}\text{etpb}$  with  $\text{AsPh}_3$  showed no dependence on  $[\text{L}']$ , that is, the reactions were dominated by the  $k_1$  path, the  $[\text{L}']$ -independent path, and there were no  $k_2[\text{L}']$  terms. This was attributed to its low nucleophilicity and large cone angle ( $142^\circ$ ) [10]. Thus Eq.(2.1) simplifies to  $k_{\text{obs}} = k_1$ , and each individual value of  $\ln(k_{\text{obs}}/T)$  was used in the analysis to obtain activation parameters  $\Delta H_1^\ddagger$  and  $\Delta S_1^\ddagger$  according to the Eyring equation

$$\ln(k_1/T) = 23.76 + \Delta S_1^\ddagger/R - \Delta H_1^\ddagger/RT \quad (2.2)$$

by an unweighted linear least squares analysis of the dependence of  $\ln(k_1/T)$  on  $1/T$ . The activation parameters,  $\Delta H_1^\ddagger$  and  $\Delta S_1^\ddagger$ , for the reactions,  $\text{Ru}_3(\text{CO})_{11}\text{PMe}_3$  with  $\text{AsPh}_3$ , were obtained from 66 experimental values of  $k_{\text{obs}}$  at different temperatures, 18.3-50.4°C. The 66 experimental values of  $k_{\text{obs}}$  fit into the Eyring equation very well (Figure 2.21). For the reactions of  $\text{Ru}_3(\text{CO})_{11}\text{etpb}$  with  $\text{AsPh}_3$ , parameters  $\Delta H_1^\ddagger$  and  $\Delta S_1^\ddagger$  were obtained from 80 experimental values of  $k_{\text{obs}}$  at different temperatures, 36.2-60.5°C. The 80 experimental values of  $k_{\text{obs}}$  also fit into the Eyring equation very well (Figure 2.22). The values of  $\Delta H_1^\ddagger$  and  $\Delta S_1^\ddagger$  are given in Table 2.10.

The experimental values of  $k_1$  at 40.0°C for CO dissociation from  $\text{Ru}_3(\text{CO})_{11}\text{etpb}$  obtained by both different techniques and different entering nucleophiles  $\text{L}'$  were identical as shown in Table 2.9.

**Table 2.9 Comparison of  $k_1$  Values for CO Dissociation from  $\text{Ru}_3(\text{CO})_{11}\text{etpb}$  obtained by Different Techniques and Attacking Nucleophiles  $\text{L}'$**

Attacking $\text{L}'$	$k_1(\text{s}^{-1})$	Monitoring Technique	Involved Formula
<b>T = 40.0 °C</b>			
AsPh <sub>3</sub>	$(4.47 \pm 0.09)10^{-5}$	UV-Vis	$\ln(k_{\text{obs}}/T) = 23.76 + \Delta S_1^\ddagger/R - \Delta H_1^\ddagger/RT$
etpb	$(4.47 \pm 0.40)10^{-5}$	FTIR at 2021.6 cm <sup>-1</sup>	$k_{\text{obs}} = k_1 + k_2[\text{L}']$
etpb	$(4.56 \pm 0.16)10^{-5}$	FTIR at 2048.6 cm <sup>-1</sup>	$k_{\text{obs}} = k_1 + k_2[\text{L}']$
<b>T = 25.0 °C</b>			
AsPh <sub>3</sub>	$(4.14 \pm 0.29)10^{-6}$	UV-Vis	$\ln(k_{\text{obs}}/T) = 23.76 + \Delta S_1^\ddagger/R - \Delta H_1^\ddagger/RT$
etpb	$(4.12 \pm 0.33)10^{-6}$	FTIR	$k_{\text{obs}} = k_1 + k_2[\text{L}']$

The value of  $k_1$  at 40.0°C for the reaction  $\text{Ru}_3(\text{CO})_{11}\text{etpb}$  with AsPh<sub>3</sub>, calculated by  $\Delta H_1^\ddagger$  and  $\Delta S_1^\ddagger$ , which were obtained from the linear dependence of  $\ln(k_{\text{obs}}/T)$  on  $1/T$  based on the Eyring equation, was  $(4.47 \pm 0.09) \times 10^{-5} \text{ s}^{-1}$ . The values of  $k_1$  for the reaction  $\text{Ru}_3(\text{CO})_{11}\text{etpb}$  with etpb at 40.0°C, obtained by FTIR monitoring technique, calculated from the dependence of  $k_{\text{obs}}$  on  $[\text{L}']$  according to the rate equation,  $k_{\text{obs}} = k_1 + k_2[\text{L}']$ , were  $(4.47 \pm 0.40) \times 10^{-5} \text{ s}^{-1}$  and  $(4.56 \pm 0.16) \times 10^{-5} \text{ s}^{-1}$  at the monitored bands 2021.6 and 2048.6 cm<sup>-1</sup> respectively. The experimental values of  $k_1$  at 25.0°C obtained by

different methods and attacking nucleophiles were also in excellent agreement with each other (Table 2.9).

Table 2.10 summarizes the activation parameters,  $\Delta H_1^\ddagger$  and  $\Delta S_1^\ddagger$ , for CO dissociation from  $\text{Ru}_3(\text{CO})_{11}\text{L}$  ( $\text{L} = \text{CO}, \text{P}(\text{OEt})_3, \text{P}(\text{OPh})_3, \text{P}(\text{O-}i\text{-Pr})_3, \text{P}(n\text{-Bu})_3, \text{PPhEt}_2, \text{PPh}_3, \text{PCy}_3, \text{etpb}, \text{and PMe}_3$ ). The results of the two new clusters,  $\text{Ru}_3(\text{CO})_{11}\text{PMe}_3$  and  $\text{Ru}_3(\text{CO})_{11}\text{etpb}$ , are excellent in showing the smallest probable errors among the ten clusters. The large positive values of  $\Delta H_1^\ddagger$  and generally quite large positive values of  $\Delta S_1^\ddagger$  are consistent with a dissociative reaction mechanism.

**Table 2.10 Activation Parameters for CO Dissociation from Ten Clusters  $\text{Ru}_3(\text{CO})_{11}\text{L}$**

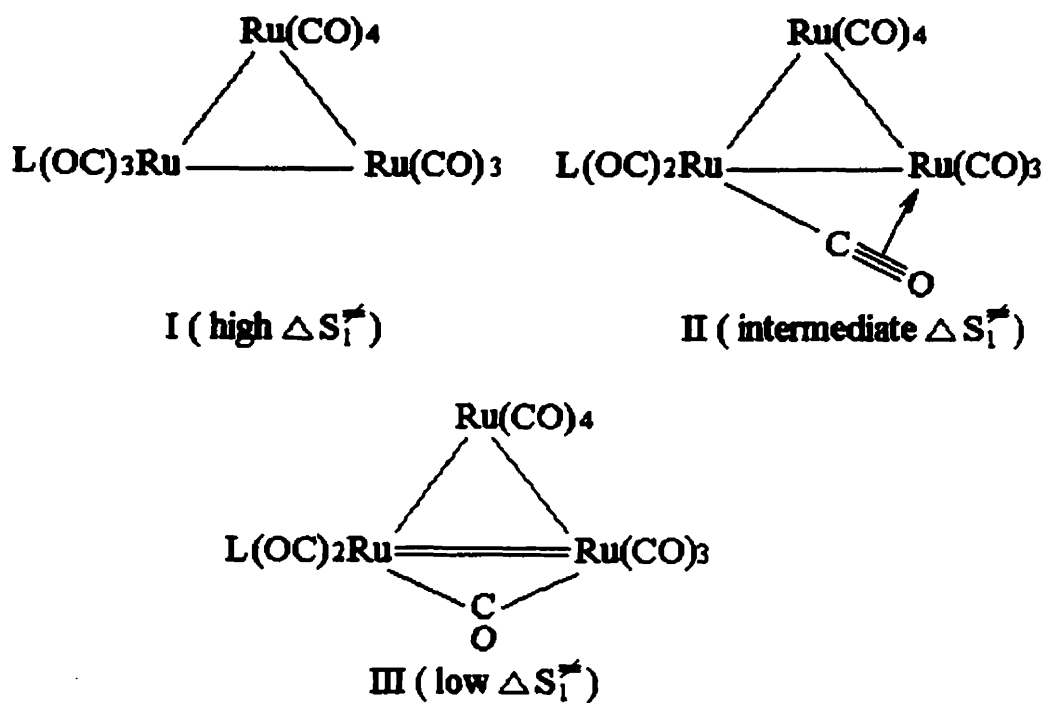
L	$\delta^a$ (ppm)	$\theta$ (deg)	$\Delta H_1^\ddagger$ (kcal mol <sup>-1</sup> )	$\Delta S_1^\ddagger$ (cal K <sup>-1</sup> mol <sup>-1</sup> )	$10^5 k_1(40^\circ\text{C})$ (s <sup>-1</sup> )	$\sigma^b$ (%)	Ref.
CO	0	95	$31.8 \pm 0.2$	$20.2 \pm 0.6$	$1.08 \pm 0.02$	1.9	13
P(OEt) <sub>3</sub>	3.61	109	$29.25 \pm 0.10$	$15.70 \pm 0.23$	$6.8 \pm 0.3$	4.4	10
PPh <sub>3</sub>	4.30	145	$25.6 \pm 0.2$	$9.1 \pm 0.5$	$86 \pm 6$	7.0	14
P( <i>n</i> -Bu) <sub>3</sub>	5.69	132	$22.1 \pm 0.6$	$-1.1 \pm 1.8$	$141 \pm 8$	5.7	15
PCy <sub>3</sub>	6.32	170	$24.94 \pm 0.28$	$11.07 \pm 0.94$	$701 \pm 23$	3.3	16
P(OPh) <sub>3</sub>	1.69	128	$24.67 \pm 0.20$	$2.57 \pm 0.64$	$6.9 \pm 1.0$	15	16
PPhEt <sub>2</sub>	5.36	136	$25.02 \pm 0.15$	$8.54 \pm 0.5$	$165.2 \pm 3.6$	2.2	16
P(O- <i>i</i> -Pr) <sub>3</sub>	3.90	130	$29.30 \pm 0.12$	$18.76 \pm 0.38$	$28.2 \pm 0.5$	1.8	16
PMe <sub>3</sub>	5.05	118	$29.46 \pm 0.28$	$20.66 \pm 0.90$	$59.0 \pm 0.3$	0.5	**c
etpb	2.60	101	$28.81 \pm 0.31$	$13.47 \pm 0.97$	$4.47 \pm 0.09$	2.0	**c

a. The <sup>13</sup>C chemical shift of Ni(<sup>13</sup>CO)<sub>3</sub>L relative to that in Ni(<sup>13</sup>CO)<sub>4</sub> [17].

b. Standard error of  $k_1$  at 40°C.

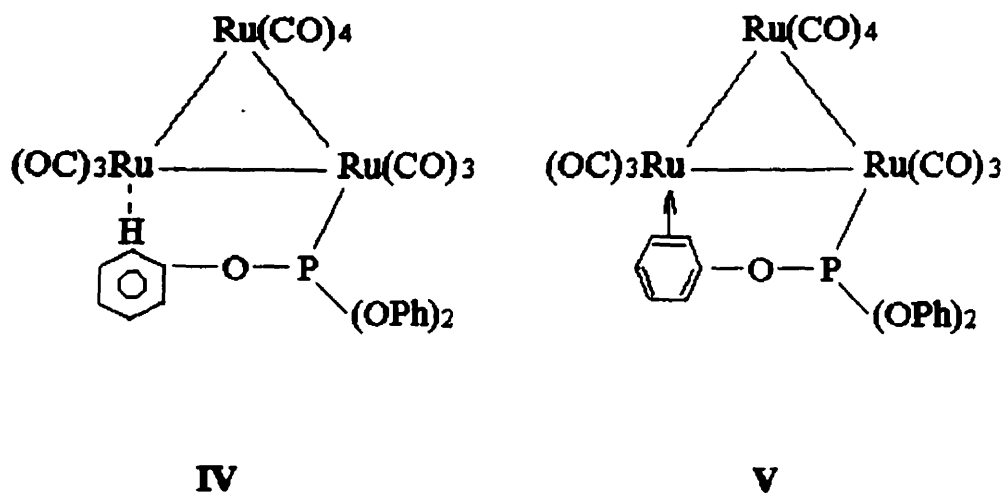
c. This work

However, the values of  $\Delta S_1^\ddagger$  for some clusters are quite low. For example, the values of  $\Delta S_1^\ddagger$  of clusters  $\text{Ru}_3(\text{CO})_{11}\text{P}(\text{OPh})_3$ ,  $\text{Ru}_3(\text{CO})_{11}\text{PPhEt}_2$ , and  $\text{Ru}_3(\text{CO})_{11}\text{PPh}_3$  are less than  $10 \text{ cal K}^{-1} \text{ mol}^{-1}$ . For  $\text{Ru}_3(\text{CO})_{11}\text{P}(n\text{-Bu})_3$ , the value of  $\Delta S_1^\ddagger$  even is negative. The lower values of  $\Delta S_1^\ddagger$  are not typical of those found for simple CO dissociative reactions, especially of mononuclear carbonyls [11, 19]. But low values of this sort have been obtained several times for dissociative reactions of metal carbonyl clusters [10, 11, 18, 19]. They can be ascribed [10, 18, 19] to rearrangements undergone by the residual clusters during the loss of CO ligand. These rearrangements have the effect of maintaining the 18-electron nature of the cluster by recourse to formation of bridging carbonyls and metal-metal double bonds [10]. The intermediates here can be envisaged [10, 18] as being of types varying from I (high  $\Delta S_1^\ddagger$ ), II (intermediate  $\Delta S_1^\ddagger$ ) and III (low  $\Delta S_1^\ddagger$ ). These correspond to increasingly tight bonding, decreasing values of  $\Delta H_1^\ddagger$ , and correspondingly decreased values of  $\Delta S_1^\ddagger$  which result from increased strength of the bonding within the clusters (i.e. higher vibrational frequencies) and increasingly precise atomic movements to form the intermediate clusters [10]. The bridging nature of II would be expected to be encouraged by a more electron donating L, and III might be expected to be a logical extension of this process since this  $\text{Ru}_3$  cluster involves 4 bonding electron pairs rather than the original 3 [10].



The trend in  $\Delta H_1$  with increasing net electronic donating capacity  $\delta(^{13}\text{CO})$  [17] of substituent L among 10 clusters  $\text{Ru}_3(\text{CO})_{11}\text{L}$  is not clear (Figure 2.23). This implies that the steric effect and/or some other reasons are also operative. In general, good electron donors decrease  $\Delta H_1^\ddagger$  by stabilizing the transition state (TS). Strengthening of bonding within a residual cluster moiety leads to lower values of  $\Delta H_1^\ddagger$ . The big substituents correspond to looser TS and higher  $\Delta H_1^\ddagger$ . The value of  $\Delta H_1^\ddagger$  for the substituent  $\text{L} = \text{P}(\text{OPh})_3$  is much lower than expected (Figure 2.23), which suggest a much tighter TS than might be expected by comparison with data for  $\text{L} = \text{CO}$ ,  $\text{etpb}$ ,  $\text{P}(\text{OEt})_3$ ,  $\text{P}(\text{O-}i\text{-Pr})_3$ , and  $\text{PMe}_3$  (Figure 2.23). This was also indicated

for dissociative reaction of  $\text{mer-Ru(CO)}_3\{\text{P(OPh)}_3\}(\text{SiCl}_3)_2$  [20], and might be explained by agostic interaction (IV) of the sort possible for  $\text{Ru-P(OPh)}_3$ , ortho-metallation reactions of such systems being well known [20], or by interaction of a phenyl ring with the vacant coordination site on a neighboring Ru atom (V).



$\text{Ru}_3(\text{CO})_{12}$  undergoes substitution by the [L']-independent path very much faster than  $\text{Os}_3(\text{CO})_{12}$  (Table 2.11) [21]. As Poë and Sekhar have pointed out, the data in Table 2.11 show that this has somewhat more to do with  $\text{Os}_3(\text{CO})_{12}$  having a less positive value of  $\Delta S_1^\ddagger$  than  $\text{Ru}_3(\text{CO})_{12}$  rather than simply a higher value of  $\Delta H_1^\ddagger$  [21]. The clearly dissociative reaction of the second-row-metal carbonyl  $\text{Mo(CO)}_6$  is also much faster than that of the third-row-metal carbonyl  $\text{W(CO)}_6$ , but this is because  $\Delta H_1^\ddagger$  is 9 kcal mol<sup>-1</sup> lower, the value of  $\Delta S_1^\ddagger$  being considerably less favorable [21, 22, 23]. This difference in behavior is not inconsistent with the simple CO dissociative mechanism for the clusters [21]. Clusters can adjust to the loss of a

ligand in a variety of ways not available to mononuclear carbonyls [21, 24]. These can involve [21] strengthening of the bonding within the residual cluster, as mentioned above, thus leading to lower values of  $\Delta H_1^\ddagger$ , and a less positive value of  $\Delta S_1^\ddagger$ . If this happens to a greater extent in the residual moiety  $\text{Os}_3(\text{CO})_{11}$  than in  $\text{Ru}_3(\text{CO})_{11}$ , then the activation parameters can be understood in terms of the CO dissociative mechanism [21]. The activation parameters for the [L']-independent reactions of  $\text{Os}_3(\text{CO})_{11}\text{P}(n\text{-Bu})_3$  can be compared with those for  $\text{Ir}_4(\text{CO})_{11}\text{P}(n\text{-Bu})_3$  (Table 2.11). It may be that the extent of strengthening of bonding within the residual cluster  $\text{Ir}_4(\text{CO})_{10}\text{P}(n\text{-Bu})_3$  is larger than in  $\text{Os}_3(\text{CO})_{10}\text{P}(n\text{-Bu})_3$ . This would be expected in terms of higher nuclearity of the  $\text{Ir}_4$  cluster.

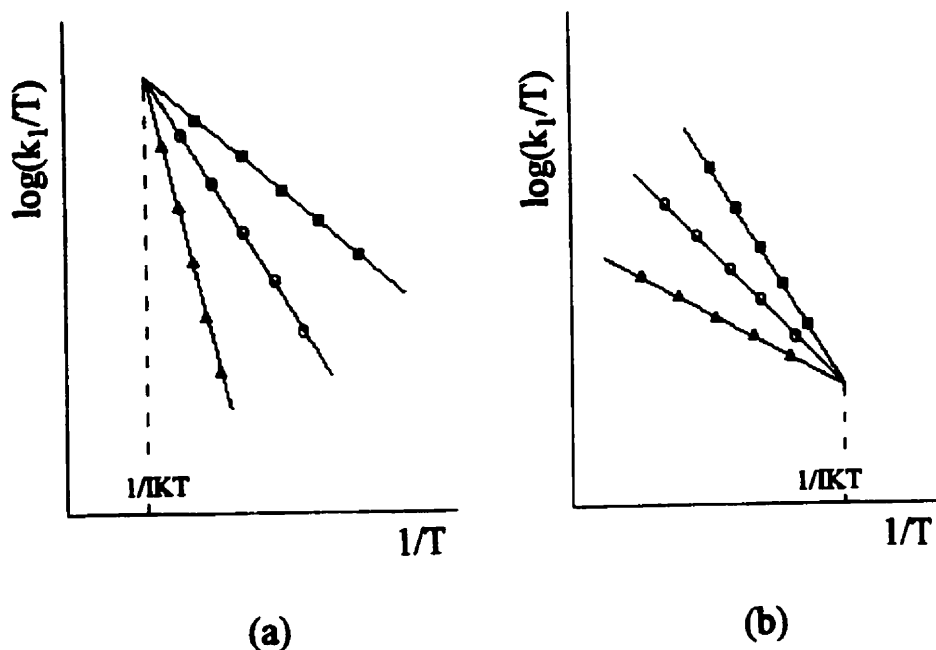
**Table 2.11 Comparison of Activation Parameters for CO Dissociation**

Cluster	$\Delta H_1^\ddagger$ (kcal mol <sup>-1</sup> )	$\Delta S_1^\ddagger$ (cal K <sup>-1</sup> mol <sup>-1</sup> )	$k_1$ (s <sup>-1</sup> )	Ref.
T = 75.0°C				
$\text{Ru}_3(\text{CO})_{12}$	31.8 ± 0.2	20.2 ± 0.6	2.05 × 10 <sup>-3</sup>	13
$\text{Os}_3(\text{CO})_{12}$	33.7 ± 1.5	10.7 ± 4.1	7.15 × 10 <sup>-7</sup>	21
T = 110°C				
$\text{Ir}_4(\text{CO})_{11}\text{P}(n\text{-Bu})_3$	33.0 ± 0.4	18.4 ± 1.1	1.2 × 10 <sup>-2</sup>	25(a)
$\text{Os}_3(\text{CO})_{11}\text{P}(n\text{-Bu})_3$	39.3 ± 1.2	23.1 ± 3.1	3.6 × 10 <sup>-5</sup>	21

### 2.3.2 Isokinetic Temperature (IKT) for CO Dissociation from Ten Clusters $\text{Ru}_3(\text{CO})_{11}\text{L}$

The isokinetic relationship (IKR) has developed rapidly over the past few years, growing from a scientific curiosity into a powerful tool for investigating kinetics and equilibria phenomena within related series of reactions [25(b)]. Linert's review papers on the IKR presented the history, method of performing statistical analyses based on rate or equilibrium constants measured at different temperatures when trying to show the existence of an IKR within a series of reactions, theoretical basis, and applications of IKR [25(b)].

For a series of related reactions, the relative rates can be more dependent on the enthalpy of activation than on the entropy. The faster reactions have lower values of  $\Delta H_1^\ddagger$  (favorable), and lower values of  $\Delta S_1^\ddagger$  (unfavorable) {Figure (a)}, according to the Eyring equation  $\ln(k_1/T) = 23.76 + \Delta S_1^\ddagger/R - \Delta H_1^\ddagger/RT$ . The reactions are faster due to lower values of  $\Delta H_1^\ddagger$  although they are opposed, but not overcome, by lower values of  $\Delta S_1^\ddagger$ . The relative rates of these reactions are controlled by the enthalpies of activation. For other reactions, the relative rates are more dependent on the entropy of activation than on the enthalpy. The faster reactions have higher values of  $\Delta S_1^\ddagger$  (favorable), and higher values of  $\Delta H_1^\ddagger$  (unfavorable) {Figure (b)}. The entropies of activation is therefore the major factor in controlling the relative rates.



At the isokinetic temperature,  $\Delta H_1^\ddagger$  and  $T\Delta S_1^\ddagger$  have parallel changes so that  $\Delta G_1^\ddagger$  has almost no change:

$$\begin{aligned}\Delta G_1^\ddagger &= \Delta H_1^\ddagger - T\Delta S_1^\ddagger \\ \Delta(\Delta G_1^\ddagger) &= 0 \\ \Delta(\Delta H_1^\ddagger) &= T\Delta(\Delta S_1^\ddagger) \\ \text{IKT} &= \frac{\Delta(\Delta H_1^\ddagger)}{\Delta(\Delta S_1^\ddagger)}\end{aligned}$$

All the reactions will occur at the same rate at the isokinetic temperature, that is, the rate constants will become independent of the nature of the reactants. The values of activation parameters,  $\Delta H_1^\ddagger$  and  $\Delta S_1^\ddagger$ , for CO dissociation from  $\text{Ru}_3(\text{CO})_{11}\text{L}$  ( $\text{L}=\text{PCy}_3$ ,  $\text{PPhEt}_2$ ,  $\text{P}(n\text{-Bu})_3$ ,  $\text{PPh}_3$ ,  $\text{PMe}_3$ ,  $\text{P}(\text{O-}i\text{-Pr})_3$ ,  $\text{P}(\text{OPh})_3$ ,  $\text{P}(\text{OEt})_3$ ,  $\text{etpb}$ , and  $\text{CO}$ ) were found to lie on a fairly good isokinetic plot, the gradient of which leads to an isokinetic temperature of about  $116^\circ\text{C}$  (Figure 2.24). At the IKT

all CO dissociation reactions from  $\text{Ru}_3(\text{CO})_{11}\text{L}$  (L as mentioned above) would occur at the same rate,  $k_1 = 2 \text{ s}^{-1}$ , the half-life would be 0.3 seconds, and the value of  $\Delta G_1^\ddagger$  would be  $22 \text{ kcal mol}^{-1}$ , which are values independent of the nature of substituents.

However, the situation is rather more complicated than this. Thus, the clusters fall into two groups (Figure 2.24), one of which {(a) with L =  $\text{PMe}_3$ ,  $\text{P}(\text{O-}i\text{-Pr})_3$ ,  $\text{P}(\text{OEt})_3$ , and  $\text{etpb}$ } shows an average  $\Delta H_1^\ddagger$  of  $29.20 \pm 0.20 \text{ kcal mol}^{-1}$  and  $T\Delta S_1^\ddagger$  values (at 300K) varying from  $4.04\text{--}6.20 \text{ kcal mol}^{-1}$ . The other {(b) with L =  $\text{PCy}_3$ ,  $\text{PPh}_3$ ,  $\text{PPhEt}_2$ , and  $\text{P}(\text{OPh})_3$ } shows an average  $\Delta H_1^\ddagger$  of  $25.06 \pm 0.21 \text{ kcal mol}^{-1}$  and  $T\Delta S_1^\ddagger$  values (at 300K) varying from  $0.77\text{--}3.32 \text{ kcal mol}^{-1}$ . When L =  $\text{P}(n\text{-Bu})_3$ ,  $\Delta H_1^\ddagger$  and  $T\Delta S_1^\ddagger$  are lower, and when L = CO,  $\Delta H_1^\ddagger$  is higher than the other groups (Figure 2.24). The two groups can be roughly distinguished on the basis of size since group (a) involves generally smaller substituents than group (b), apart from  $\text{P}(\text{OPh})_3$ , which is distinct as being the least effective P-donor. The other deviant P-donor is  $\text{P}(n\text{-Bu})_3$  and the reason for this is not obvious. It is obviously unusual in having a negative value of  $\Delta S_1^\ddagger$ .

Dissociative substitution reactions are much more complicated than associative ones because electronic and steric effects of substituents L will act differently on the ground state (GS) and transition state (TS). In general, steric congestion (big  $\theta$ ) is favorable to dissociative reactions because of the relief of steric strain, which would accompany CO loss.

### 2.3.3 Derivation of Electronic and Steric Profiles for CO Dissociation from Ten Clusters $\text{Ru}_3(\text{CO})_{11}\text{L}$

There are similarities in the method used to acquire the electronic and steric effects for the two sets of reactions, the associative and the dissociative. But the implications of the effects determined are different. In associative reactions, the rates are sensitive to the nature of the attacking nucleophiles (of course, also dependent on a particular cluster itself, especially the nature of substituents in the cluster). In dissociative reactions, the rates are independent of the nature of attacking nucleophiles, but are dependent on the nature of ligands which are present in the cluster undergoing reaction, namely substituents. In such cases, the ligand is bound directly to the metal atom in both the GS and the TS, and steric and electronic effects could be important in both states. Further, because of being a substituent and not a nucleophile,  $\pi$ -acidity of L will be important as well as  $\sigma$ -basicity. The electronic effects of substituents have to be quantified by using a parameter which reflects both  $\sigma$ -donor and  $\pi$ -acid properties. The parameter  $\delta(^{13}\text{CO})$  measures the  $^{13}\text{C}$  chemical shift of  $\text{Ni}(^{13}\text{CO})_3\text{L}$  relative to that in  $\text{Ni}(^{13}\text{CO})_4$ , and is chosen to represent the net electron donating capacity of L, including  $\sigma$ - and  $\pi$ - effects, which have been proved useful elsewhere [26, 27]. So the parameter  $\delta(^{13}\text{CO})$  might be the best to use.

The ten tri-ruthenium carbonyl clusters with different substituents were used to study the kinetics of CO dissociation from  $\text{Ru}_3(\text{CO})_{11}\text{L}$ . These substituents cover a wide range of  $\delta(^{13}\text{CO})$  values from 0 to 6.32, and a large range of size from  $95^\circ$  to  $170^\circ$  {Tolman's

cone angle [7, 8]}. Therefore the results of this kinetic study are expected to be informative.

The values of  $\Delta H_1^\ddagger$  and  $\Delta S_1^\ddagger$  of the ten clusters were replaced in the Eyring equation,  $\ln(k_1/T) = 23.76 + \Delta S_1^\ddagger / R - \Delta H_1^\ddagger / RT$ , and the precise  $\log k_1$  values at different temperatures were obtained (Tables 2.12, 2.13, and 2.14)

A plot of  $\log k_1$  vs  $\delta$  defined the dependence of rate constants on the electronic effects induced by substituents. Such a plot does not show a linear relationship because of steric effects and some other reasons. The electronic profile can be assumed to be linear when isosteric substituents are involved, and can be obtained from the data of the clusters containing almost isosteric ligands, such as  $P(\text{OPh})_3$  128°,  $P(\text{O-}i\text{-Pr})_3$  130°, and  $P(\text{n-Bu})_3$  132°. The gradient of this line leads to an initial value of  $\beta_L$ . Values of  $\beta_L$ ,  $\gamma_L$  and  $\alpha_L$  were also obtained by fitting the data for all ten clusters to the stereoelectronic Eq.(2.3) by the multilinear regression program analysis [28],

$$\log k_1 = \alpha_L + \beta_L \delta(^{13}\text{CO}) + \gamma_L \theta \quad (2.3)$$

where  $\beta_L$  and  $\gamma_L$  represent the dependence of the rates of dissociative substitution reactions on the electronic parameter  $\delta(^{13}\text{CO})$  and the cone angles  $\theta$ , respectively, which are characteristic of the individual substituent L. The parameters  $\alpha_L$ ,  $\beta_L$ , and  $\gamma_L$  are characteristic of a group of clusters.

Tables 2.12(a), 2.13(a), and 2.14(a) also include values of  $\log k_1$  (fit) {i.e. the calculated values of  $\log k_1$  that fit exactly to Eq.(2.3)} and the values of the deviations of the calculated values from the

experimental ones. Results of analyses using  $\theta'$  instead of  $\theta$  are given in Tables 2.12(b), 2.13(b), and 2.14(b).

**Table 2.12(a) Values of  $\log k_1$  at 25.0°C for CO Dissociation from Ten Clusters  $\text{Ru}_3(\text{CO})_{11}\text{L}$**

L	$\delta(^{13}\text{CO})$ (ppm)	$\theta$ (deg)	$\log k_1$ (exptl.)	$\log k_1^{\text{a,b}}$ (fit)	Deviation <sup>c</sup>	Ref. <sup>d</sup>
CO	0.00	95	-6.1036	-6.1041	0.0000	13
P(OEt) <sub>3</sub>	3.61	109	-5.2178	-4.9115	-0.3063	10
PPh <sub>3</sub>	4.30	145	-3.9846	-3.9450	-0.0396	14
P( <i>n</i> -Bu) <sub>3</sub>	5.69	132	-3.6482	-3.8934	0.2452	15
PCy <sub>3</sub>	6.32	170	-3.0702	-2.8973	-0.1729	16
P(OPh) <sub>3</sub>	1.69	128	-4.7301	-4.9597	0.2296	16
PPhEt <sub>2</sub>	5.36	136	-3.6818	-3.8854	0.2036	16
P(O- <i>i</i> -Pr) <sub>3</sub>	3.90	130	-4.5856	-4.3752	-0.2104	16
PMe <sub>3</sub>	5.05	118	-4.2851	-4.3601	0.0750	this work
etpb	2.60	101	-5.3826	-5.3578	0.0248	this work

a. Kinetics statistical analysis was carried out by double linear regression & three coefficient computer program.

b.  $\log k_1 = \alpha_L + \beta_L \delta(^{13}\text{CO}) + \gamma_L \theta$

$$\alpha_L = -8.210 \pm 0.477 \quad \beta_L = 0.244 \pm 0.054 \text{ ppm}^{-1} \quad \gamma_L = 0.022 \pm 0.005 \text{ deg}^{-1}$$

$$\text{RMSD} = 0.182 \quad \text{R}^2 = 0.957$$

c. The deviations are differences of  $\log k_1$  (exptl.) from  $\log k_1$ (fit), which are the output of the computer calculation.

d. Source of data for estimation of  $\log k_1$  (exptl.) values.

**Table 2.12(b) Kinetic Data from Stereoelectronic Analysis and  $\theta'$  as a Steric Parameter for CO Dissociation from Ten Clusters  $\text{Ru}_3(\text{CO})_{11}\text{L}$  at 25.0°C**

L	$\delta(^{13}\text{CO})$ (ppm)	$\theta'$ (deg)	$\log k_1$ (exptl.)	$\log k_1^{a,b}$ (fit)	Deviation <sup>c</sup>	Ref. <sup>d</sup>
CO	0.00	108	-6.1036	-6.2303	0.1267	13
P(OEt) <sub>3</sub>	3.61	136	-5.2178	-4.5447	-0.6731	10
PPh <sub>3</sub>	4.30	145	-3.9846	-4.1537	0.1691	14
P( <i>n</i> -Bu) <sub>3</sub>	5.69	139	-3.6482	-3.8212	0.1730	15
PCy <sub>3</sub>	6.32	168	-3.0702	-3.0721	0.0000	16
P(OPh) <sub>3</sub>	1.69	140	-4.7301	-5.0848	0.3547	16
PPhEt <sub>2</sub>	5.36	135	-3.6818	-4.0024	0.3206	16
P(O- <i>i</i> -Pr) <sub>3</sub>	3.90	145	-4.5856	-4.2819	-0.3037	16
PMe <sub>3</sub>	5.05	125	-4.2851	-4.2905	0.0000	this work
etpb	2.60	118	-5.3826	-5.2081	-0.1745	this work

a. Kinetics statistical analysis was carried out by double linear regression & three coefficient computer program.

b.  $\log k_1 = \alpha_L + \beta_L \delta(^{13}\text{CO}) + \gamma_L \theta'$

$$\alpha_L = -8.268 \pm 1.138 \quad \beta_L = 0.321 \pm 0.082 \text{ ppm}^{-1} \quad \gamma_L = 0.019 \pm 0.010 \text{ deg}^{-1}$$

$$\text{RMSD} = 0.296 \quad R^2 = 0.885$$

c. The deviations are differences of  $\log k_1(\text{exptl.})$  from  $\log k_1(\text{fit})$ , which are the output of the computer calculation.

d. Source of data for estimation of  $\log k_1$  (exptl.) values.

**Table 2.13(a) Values of  $\log k_1$  at 50.0°C for CO Dissociation from Ten Clusters  $\text{Ru}_3(\text{CO})_{11}\text{L}$**

L	$\delta(^{13}\text{CO})$ (ppm)	$\theta$ (deg)	$\log k_1$ (exptl.)	$\log k_1^{a,b}$ (fit)	Deviation <sup>c</sup>	Ref. <sup>d</sup>
CO	0.00	95	-4.2651	-4.3393	0.0742	13
P(OEt) <sub>3</sub>	3.61	109	-3.5240	-3.2608	-0.2632	10
PPh <sub>3</sub>	4.30	145	-2.4978	-2.4617	-0.0361	14
P( <i>n</i> -Bu) <sub>3</sub>	5.69	132	-2.3599	-2.3737	0.0138	15
PCy <sub>3</sub>	6.32	170	-1.6208	-1.5528	-6.8000	16
P(OPh) <sub>3</sub>	1.69	128	-3.2960	-3.3638	0.0678	16
PPhEt <sub>2</sub>	5.36	136	-2.2279	-2.3783	0.1504	16
P(O- <i>i</i> -Pr) <sub>3</sub>	3.90	130	-2.8890	-2.8205	-0.0685	16
PMe <sub>3</sub>	5.05	118	-2.5796	-2.7699	0.1903	this work
etpb	2.60	101	-3.7138	-3.6530	-0.0608	this work

a. Kinetics statistical analysis was carried out by double linear regression & 3 coefficient computer program.

b.  $\log k_1 = \alpha_L + \beta_L \delta(^{13}\text{CO}) + \gamma_L \theta$

$$\alpha_L = -6.030 \pm 0.324 \quad \beta_L = 0.230 \pm 0.037 \text{ ppm}^{-1} \quad \gamma_L = 0.0178 \pm 0.0032 \text{ deg}^{-1}$$

$$\text{RMSD} = 0.124 \quad R^2 = 0.973$$

c. The deviations are differences of  $\log k_1(\text{exptl.})$  from  $\log k_1(\text{fit})$ , which are the output of the computer calculation.

d. Source of data for estimation of  $\log k_1$  (exptl.) values.

**Table 2.13(b) Kinetic Data from Stereoelectronic Analysis and  $\theta'$  as a Steric Parameter for CO Dissociation from Ten Clusters  $\text{Ru}_3(\text{CO})_{11}\text{L}$  at 50.0°C**

L	$\delta(^{13}\text{CO})$ (ppm)	$\theta'$ (deg)	$\log k_1$ (exptl.)	$\log k_1^{a,b}$ (fit)	Deviation <sup>c</sup>	Ref. <sup>d</sup>
CO	0.00	108	-4.2651	-4.4378	0.1727	13
P(OEt) <sub>3</sub>	3.61	136	-3.5240	-2.9670	-0.5570	10
PPh <sub>3</sub>	4.30	145	-2.4978	-2.6323	0.1345	14
P( <i>n</i> -Bu) <sub>3</sub>	5.69	139	-2.3599	-2.3122	-0.0477	15
PCy <sub>3</sub>	6.32	168	-1.6208	-1.7018	0.0810	16
P(OPh) <sub>3</sub>	1.69	140	-3.2960	-3.4721	0.1761	16
PPhEt <sub>2</sub>	5.36	135	-2.2279	-2.4678	0.2399	16
P(O- <i>i</i> -Pr) <sub>3</sub>	3.90	145	-2.8890	-2.7498	-0.1392	16
PMe <sub>3</sub>	5.05	125	-2.5796	-2.7055	0.1259	this work
etpb	2.60	118	-3.7138	-3.5276	-0.1862	this work

a. Kinetics statistical analysis was carried out by double linear regression & 3 coefficient computer program.

b.  $\log k_1 = \alpha_L + \beta_L \delta(^{13}\text{CO}) + \gamma_L \theta'$

$$\alpha_L = -6.022 \pm 0.880 \quad \beta_L = 0.294 \pm 0.063 \text{ ppm}^{-1} \quad \gamma_L = 0.0147 \pm 0.0075 \text{ deg}^{-1}$$

$$\text{RMSD} = 0.229 \quad R^2 = 0.908$$

c. The deviations are differences of  $\log k_1(\text{exptl.})$  from  $\log k_1(\text{fit})$ , which are the output of the computer calculation.

d. Source of data for estimation of  $\log k_1(\text{exptl.})$  values.

**Table 2.14(a) Values of  $\log k_1$  at 75.0°C for CO Dissociation from Ten Clusters  $\text{Ru}_3(\text{CO})_{11}\text{L}$**

L	$\delta(^{13}\text{CO})$ (ppm)	$\theta$ (deg)	$\log k_1$ (exptl.)	$\log k_1^{a,b}$ (fit)	Deviation <sup>c</sup>	Ref. <sup>d</sup>
CO	0.00	95	-2.6883	-2.8256	0.1373	13
P(OEt) <sub>3</sub>	3.61	109	-2.0710	-1.8448	-0.2262	10
PPh <sub>3</sub>	4.30	145	-1.2220	-1.1890	-0.0330	14
P( <i>n</i> -Bu) <sub>3</sub>	5.69	132	-1.2542	-1.0698	-0.1844	15
PCy <sub>3</sub>	6.32	170	-0.3771	-0.3989	0.0217	16
P(OPh) <sub>3</sub>	1.69	128	-2.0654	-1.9947	-0.0707	16
PPhEt <sub>2</sub>	5.36	136	-0.9804	-1.0852	0.1048	16
P(O- <i>i</i> -Pr) <sub>3</sub>	3.90	130	-1.4335	-1.4866	0.0531	16
PMe <sub>3</sub>	5.05	118	-1.1166	-1.4055	0.2889	this work
etpb	2.60	101	-2.2821	-2.1906	-0.0915	this work

a. Kinetics statistical analysis was carried out by double linear regression & 3 coefficient computer program.

b.  $\log k_1 = \alpha_L + \beta_L \delta(^{13}\text{CO}) + \gamma_L \theta$

$$\alpha_L = -4.161 \pm 0.386 \quad \beta_L = 0.217 \pm 0.044 \text{ ppm}^{-1} \quad \gamma_L = 0.014 \pm 0.004 \text{ deg}^{-1}$$

$$\text{RMSD} = 0.147 \quad R^2 = 0.951$$

c. The deviations are differences of  $\log k_1(\text{exptl.})$  from  $\log k_1(\text{fit})$ , which are the output of the computer calculation.

d. Source of data for estimation of  $\log k_1$  (exptl.) values.

**Table 2.14(b) Kinetic Data from Stereoelectronic Analysis and  $\theta'$  as a Steric Parameter for CO Dissociation from Ten Clusters  $\text{Ru}_3(\text{CO})_{11}\text{L}$  at 75.0°C**

L	$\delta(^{13}\text{CO})$ (ppm)	$\theta'$ (deg)	$\log k_1$ (exptl.)	$\log k_1^{a,b}$ (fit)	Deviation <sup>c</sup>	Ref. <sup>d</sup>
CO	0.00	108	-2.6883	-2.9003	0.2120	13
P(OEt) <sub>3</sub>	3.61	136	-2.0710	-1.6134	-0.4576	10
PPh <sub>3</sub>	4.30	145	-1.2220	-1.3270	0.1050	14
P( <i>n</i> -Bu) <sub>3</sub>	5.69	139	-1.2542	-1.0175	-0.2367	15
PCy <sub>3</sub>	6.32	168	-0.3771	-0.5257	0.1486	16
P(OPh) <sub>3</sub>	1.69	140	-2.0654	-2.0886	0.0232	16
PPhEt <sub>2</sub>	5.36	135	-0.9804	-1.1510	0.1706	16
P(O- <i>i</i> -Pr) <sub>3</sub>	3.90	145	-1.4335	-1.4353	0.0000	16
PMe <sub>3</sub>	5.05	125	-1.1166	-1.3457	0.2291	this work
etpb	2.60	118	-2.2821	-2.0861	-0.1960	this work

a. Kinetics statistical analysis was carried out by double linear regression & 3 coefficient computer program.

b.  $\log k_1 = \alpha_L + \beta_L \delta(^{13}\text{CO}) + \gamma_L \theta'$

$$\alpha_L = -4.097 \pm 0.827 \quad \beta_L = 0.271 \pm 0.059 \text{ ppm}^{-1} \quad \gamma_L = 0.011 \pm 0.007 \text{ deg}^{-1}$$

$$\text{RMSD} = 0.215 \quad \text{R}^2 = 0.896$$

c. The deviations are differences of  $\log k_1(\text{exptl.})$  from  $\log k_1(\text{fit})$ , which are the output of the computer calculation.

d. Source of data for estimation of  $\log k_1$  (exptl.) values.

Table 2.15 listed two sets of values of parameters  $\alpha_L$ ,  $\beta_L$ , and  $\gamma_L$  at different temperatures for CO dissociation from the ten clusters  $\text{Ru}_3(\text{CO})_{11}\text{L}$ , obtained respectively by using  $\theta$  and  $\theta'$  as a steric parameter. The fit to Eq.(2.3) (with  $\theta$  replaced by  $\theta'$ ) is less good although the values of  $\alpha_L$  and  $\gamma_L$  are unchanged almost.

**Table 2.15 Parameters  $\alpha_L$ ,  $\beta_L$ , and  $\gamma_L$  for CO Dissociation from Ten Clusters  $\text{Ru}_3(\text{CO})_{11}\text{L}$  based on  $\log k_1 = \alpha_L + \beta_L \delta(^{13}\text{CO}) + \gamma_L \theta$**

T (°C)	$\alpha_L$	$\beta_L$ (ppm <sup>-1</sup> )	$\gamma_L$ (deg <sup>-1</sup> )	RMSD <sup>a</sup>	R <sup>2</sup>
Set 1 <sup>b</sup>					
25.0	-8.2 ± 0.5	0.24 ● 0.05	0.022 ± 0.005	0.18	0.96
50.0	-6.0 ± 0.3	0.23 ± 0.04	0.018 ± 0.003	0.12	0.97
75.0	-4.2 ± 0.4	0.22 ± 0.04	0.014 ± 0.004	0.15	0.95
Set 2 <sup>c</sup>					
25.0	-8.3 ● 1.1	0.32 ± 0.08	0.019 ± 0.010	0.30	0.88
50.0	-6.0 ± 0.9	0.29 ● 0.06	0.015 ± 0.008	0.23	0.91
75.0	-4.1 ± 0.8	0.27 ± 0.06	0.011 ± 0.007	0.22	0.90

a. Root mean square deviation =  $[\sum \Delta^2]^{1/2}/N$

b.  $\theta$  was used as a steric parameter.

c.  $\theta'$  was used as a steric parameter.

Compared with the other eight clusters, the rate constants  $k_1$  (25.0°C) of these two new clusters,  $\text{Ru}_3(\text{CO})_{11}\text{etpb}$  and  $\text{Ru}_3(\text{CO})_{11}\text{PMe}_3$ , are of excellent precision, they gave the best fit to the stereoelectronic Eq.(2.3) in terms of the smallest deviations, and the compliance of the data to the equation is almost perfect: the deviations of experimental  $\log k_1$  from fit  $\log k_1$  are just -0.02 and 0.08; 0.00 and -0.17, respectively in terms of  $\theta$  and  $\theta'$  as steric parameters {Tables 2.12(a) and 2.12(b)}.

The values of  $\log k_1^\circ$  can then be calculated according to Eq.(2.4).

$$\log k_1^\circ = \log k_1 - \beta_L \delta(^{13}\text{CO}) \quad (2.4)$$

The plot of  $\log k_1^\circ$  of clusters against  $\theta$  of substituents gives the steric profile. The superimposed data of  $\text{Ru}_3(\text{CO})_{11}\text{etpb}$  and  $\text{Ru}_3(\text{CO})_{11}\text{PMe}_3$  fit the plot extremely well (Figure 2.25). The temperature dependence of steric profiles is shown on Figure 2.26.

The values of  $\beta_L$  and  $\gamma_L$  are all positive, and show a slight decrease with increasing temperature (Table 2.15). A conclusion can therefore be drawn that the rates of dissociative reactions are less dependent on the nature of substituents with increasing temperature. Thus it is easy to be understood that rate constants  $k_1$  will become independent of the nature of substituents at the isokinetic temperature.

Positive values of  $\beta_L$  imply that the stabilizing electron donor effect of substituent L on TS is bigger than that on GS in the clusters  $\text{Ru}_3(\text{CO})_{11}\text{L}$ , and this implies that compensation for CO loss is more effective the higher the basicity of the substituent.

Positive values of  $\gamma_L$  mean that the bigger the size of substituent (the greater the steric effect) the faster the rate because of the release of steric strain which would accompany CO loss. This is much easier to understand. It has been shown that the M–P bond length in metal carbonyl clusters increases linearly with increasing the cone angle of substituent [1, 29]. This implies that steric repulsion could serve to lengthen the M–P bond as well as increase ligand-ligand repulsion energy. So the steric effect will lead to destabilization of the ground state. When the CO ligand leaves, the M–P bond may shorten and increase in strength, which will lead to stabilization of the transition state. In conclusion, the steric effect operates by destabilizing the ground state which results from the L - L repulsion, and by stabilizing the transition state which results from Ru–P bond shortening on CO loss.

### **2.3.4 Derivation of Electronic and Steric Profiles for Associative Substitution Reactions of $\text{Ru}_3(\text{CO})_{11}\text{PMe}_3$ and $\text{Ru}_3(\text{CO})_{11}\text{etpb}$**

#### **2.3.4.1 Introduction**

Associative substitution reactions of metal carbonyl clusters with P-donor nucleophiles have been known for many years to depend systematically on the nature of the entering nucleophiles. It has long been thought that the stereo-electronic properties of P-donor nucleophiles can be parameterized into electronic and steric components. Almost simultaneously Poë and Giering independently came to the same approach — the quantitative separation of electronic and steric effects of P-donor nucleophiles [30, 31], and essentially

identical exemplary plots — the electronic profile and the steric profile. The stereoelectronic equation proposed by Poë et al. [32] is as follows:

$$\log k_2 = \alpha + \beta(\text{pKa}' + 4) + \gamma(\theta - \theta_{\text{th}})\lambda \quad (2.5)$$

which allows for a better definition of the standard reactivity as being  $\log k_2^\circ = \log k_2 - \beta(\text{pKa}' + 4)$  [33, 34].

The electronic parameter  $\text{pKa}'$  was suggested by Poë and co-workers as described below [2, 35(a)]. Following an empirical relationship between  $\text{pKa}$ ,  $\theta$ , and  $\chi$  values derived by Giering et al. [36, 37], Poë et al. obtained a somewhat more precise equation [2, 35(a)], viz. Eq.(2.6), based on a closely similar, but not identical, series of P-donors which had been classified by Giering as  $\sigma$ -donors only.

For  $\sigma$ -donors:

$$\text{pKa} = (18.93 \pm 1.65) - (0.0464 \pm 0.0104)\theta - (0.673 \pm 0.035)\chi \quad (2.6)$$

Since this is an empirical equation, the range of  $\theta$  values over which it is valid can only be the range defined by those P-donors used in the correlation, viz. 118 – ~180°C [35(a)]. The term in  $\theta$  is the correction for the unwanted dependence of  $\text{pKa}$  on the size of ligands, which is ascribed to the fact that the  $\text{pKa}$  values were derived for the phosphonium ions  $\text{L-H}^+$  in aqueous solution. Smaller  $\text{L-H}^+$  ions would be more stabilized by hydration than would the larger ions, and their  $\text{pKa}$  values would be higher as a result. The electronic parameter should not reflect hydration effects because the kinetics is followed in the non-aqueous and non-polar organic solvents. In associative

substitution reactions, it is only the  $\sigma$ -donor capacity of nucleophiles that is important, and any  $\pi$ -acidity, which is characteristic of some P-donor ligands, is not operative in the transition states, possibly because of the greater length of the only partially formed M...P bonds. The  $\pi$ -back bonds cannot be formed, so  $\pi$ -acidity of L' plays a negligible role in the TS. The parameter pKa reflects, of course, only the  $\sigma$ -donor capacity of L' since there are no  $\pi$ -electrons on the proton to be donated back to L'. The  $\chi$  values are obtained in a non-polar solvent, defined by precise  $\nu_{C-O}$  measurements, and are not affected by hydration. Tolman [7] suggested that the A1 C-O stretching frequencies in the complexes  $Ni(CO)_3L$  provided a good standard measure of the net electron donor capacity of L, i.e. the combined effects of  $\sigma$  donation of electrons to the metal and withdrawal of  $\pi$  electrons from the metal, which could be expressed by the values  $\chi = \nu_{C-O}(L) - \nu_{C-O}(P-t-Bu_3)$  since the ligand  $P(t-Bu)_3$  is the most effective net electron donor and  $\nu_{C-O}$  in  $Ni(CO)_3P(t-Bu)_3$  is the smallest value observed. Tolman's values of  $\chi$  have been replaced by a more extensive and precise set obtained by Bartik et al. [35(b)]. In short, the term  $0.0464\theta$  effectively allows for the solvation of the phosphonium ions in relating pKa values in aqueous solution to  $\chi$  values in non-polar solvents, both pKa and  $\chi$  (for  $\sigma$ -donors only) providing a quantitative measure of the  $\sigma$ -donicity of the P-donors [35(a)].

In view of the high precision of the  $\chi$  values [35(b)] (pKa values are almost certainly less precise than  $\chi$  values) and the validity of the steric term dependent on  $\theta$ , the pKa (calc) values can be calculated as follows:

For  $\sigma$ -donors:

$$\text{pKa}(\text{calc}) = 18.93 - 0.0464\theta - 0.673\chi \quad (2.7)$$

which defines the best least squares straight line plot of pKa vs  $(0.0464\theta + 0.673\chi)$  [35(a)]. However, pKa values – even very good ones! – are not a suitable electronic parameter because they are appropriate to the basicity of the P-donors in aqueous solution, and not to the effective basicity in generally non-polar organic solvents such as hydrocarbons. It is in non-polar organic solvents that the kinetics is followed. The pKa (calc) values could therefore be converted to values appropriate to non-polar solvents by taking the term  $-0.0464\theta$  over to the LHS, as shown in Eq.(2.8) [35(a)].

For  $\sigma$ -donors:

$$\text{pKa}(\text{calc}) + 0.0464\theta = 18.93 - 0.673\chi \quad (2.8)$$

However, the solvent adjustment term is very large given that  $\theta$  values range from 118 to  $\sim 180^\circ$ . It is therefore preferable to provide the solvent adjustment relative to the value  $\theta = 145^\circ$ , the cone angle for an important intermediate-sized class of isosteric nucleophiles ( $p\text{-XC}_6\text{H}_4$ )<sub>3</sub>P [35(a)]. The Eq.(2.8) can therefore be changed into Eq.(2.9).

For  $\sigma$ -donors:

$$\text{pKa}(\text{calc}) + 0.0464(\theta - 145) = 18.93 - 0.0464 \times 145 - 0.673\chi \quad (2.9)$$

where the solvent adjustment term is quite small (ca. -0.12 to +0.15) [35(a)], so that the values of the LHS are close to the values of ordinary pKa. The values of LHS can therefore be taken as an accurate value of pKa, designated as pKa', appropriate to non-polar solvents, and it is equal to the RHS, i.e. the values of pKa' are directly derived from the values of  $\chi$  with a simple arithmetical adjustment equivalent to a scale change.

For  $\sigma$ -donors:

$$\text{pKa}' = \text{pKa}(\text{calc}) + 0.0464(\theta - 145) \quad (2.10)$$

$$\text{pKa}' = 18.93 - 0.0464 \times 145 - 0.673\chi \quad (2.11)$$

Eq.(2.10) and (2.11) give different pKa' values, and those from Eq.(2.11) are preferred. These do not have any dependence on the size of the ligands.

Giering and co-workers noted [36, 37] that pKa values are related to  $\chi$  by

$$\text{pKa} = -(0.68 \pm 0.03)\chi - (0.047 \pm 0.010)\theta + (18.9 \pm 1.6) \quad (2.12)$$

which is only obeyed by  $\sigma$ -donors. The  $\sigma$ -donor/ $\pi$ -acid ligands deviated from the equation badly (Figure 2.27) [2]. This suggests that the parameter  $\chi$  would be better to use to define the  $\sigma$  donicity of those ligands which are  $\sigma$ -donors only, and that it should be designated  $\chi_d$ . For ligands which are  $\pi$ -acids as well as  $\sigma$ -donors, the  $\chi$  values measure the combination of  $\pi$ -acidity and  $\sigma$ -donicity effects of the ligands. In these cases Poě et al. [2, 35(a)] proposed that the  $\sigma$

donicity  $\chi_d$  of those ligands which are  $\pi$ -acids as well as  $\sigma$ -donors can be derived directly from experimental pKa values, i.e. from the pKa values appropriate to aqueous solution adjusted for the hydration effects as shown in Eq.(2.13), which reflect only  $\sigma$ -donor part of  $\sigma/\pi$  ligands' nature.

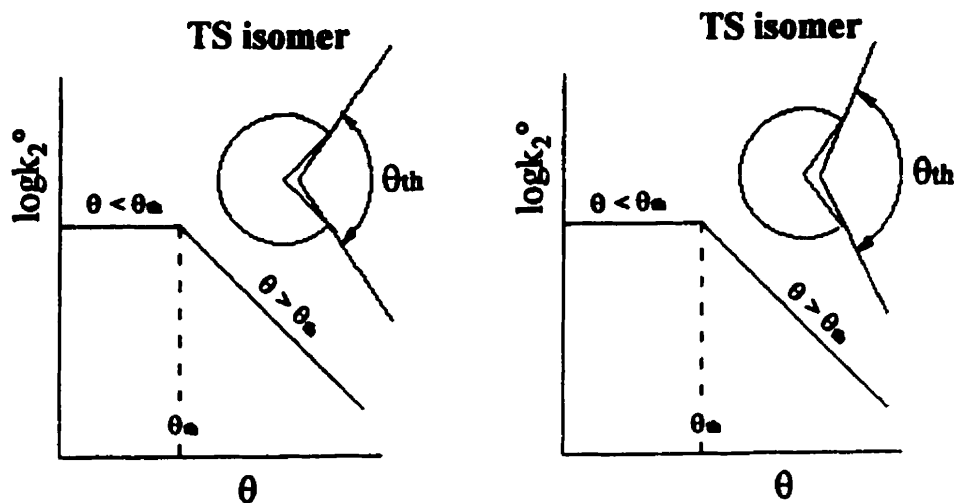
For  $\sigma$ -donor/ $\pi$ -acid nucleophiles:

$$\text{pKa}' = \text{pKa}(\text{expt}) + 0.0464(\theta - 145) \quad (2.13)$$

**It is obvious that Poë's suggestion on pKa' has a lot of virtues:** for  $\sigma$ -donors the values of pKa' still have the virtue of incorporating the precision of measurements of  $\chi$ ; for  $\sigma/\pi$  ligands deviation of  $\chi$  values from the correlation shown by Eq.(2.12) is avoided by using experimental values of pKa; both  $\sigma$ -donors and  $\sigma/\pi$  ligands have the same dependence on the hydration correction {Eq.(2.10) and (2.13)}; values of pKa' are close to ones of normal pKa; pKa', instead of  $\chi$ , can lead to dimensionless values of  $\beta$ , which bear a closer relation to physical reality. In short, pKa' is a measure of  $\sigma$ -donicity or basicity of ligands, corrected for steric effect, and does not reflect its size as pKa itself does, and is directly related to  $\chi$  for  $\sigma$ -donors.

The parameter  $\theta$  in Eq. (2.5) is Tolman cone angle of ligands, and reflects the size of L.  $\theta_{th}$  is the steric threshold. When  $\theta \leq \theta_{th}$  there are no steric effects; when  $\theta > \theta_{th}$  there are certain steric effects. The smaller  $\theta_{th}$  means the earlier onset of steric effect; the bigger  $\theta_{th}$  the later onset.

## Steric Threshold $\theta_{th}$



TSI with a constant amount of bond-making

i.e. a constant M...P distance

- |                                  |                                |
|----------------------------------|--------------------------------|
| (a) • Smaller opening            | (b) • Bigger opening           |
| • Smaller $\theta_{th}$          | • Bigger $\theta_{th}$         |
| • Earlier onset of steric effect | • Later onset of steric effect |

Metal carbonyl complexes exist as closely packed polytopal arrays of CO (and other ) ligands with the metal atom(s) inside the ligand polytope [38]. The packing of carbonyls around the  $M_n$  cluster, in particular, is sufficiently compact that is difficult to see how attack, even by relatively small nucleophiles, could occur without any steric difficulty at all. In view of the existence of the rather sharply defined steric threshold  $\theta_{th}$  and a horizontal region of steric profile, where no

dependence of  $\log k_2^\circ$  on  $\theta$  would occur, it has recently been proposed by Poë et al. [32, 34] that a sudden precise change in the geometry of the carbonyl is induced at some stage during the approach of a nucleophile L', which results in the formation of a relatively high energy isomeric form, the Transition State Isomer (TSI), of the carbonyl. The TSI contains a well-defined roughly conical opening in the ligand polytope. The opening can be made then by breaking one metal-metal bond, which is usually accompanied by a need for an additional pair of electrons for M...L' bond making.

The value of  $\theta_{th}$  is related to the size of this opened space in the TSI. When the size of the open space in the TS is larger than that required by smaller nucleophiles ( $\theta < \theta_{th}$ ), a partial bond M...P can be formed without the occurrence of any steric repulsion. As  $\theta$  of nucleophiles L' increases, there will come a stage where a nucleophile will just fit into the open space ( $\theta = \theta_{th}$ ), so that a partial bond M...P of the same length can just be formed without unfavorable steric interaction. Accommodation of larger nucleophiles ( $\theta > \theta_{th}$ ) must be accompanied by a further opening up of the TSI albeit at some energy cost if the same length of the M...P bond is to be maintained [34]. If the TSI is too inflexible to open up further in this way, then larger nucleophiles of this sort will only be able to form longer and therefore weaker M...P bonds than they would otherwise do, and the TS will be less stabilized as a result [34]. The value of  $\gamma$  found when  $\theta > \theta_{th}$  is a quantitative measure of the energetic difficulty of this process, i.e.  $\gamma$  is a measure of the flexibility of the TSI. The more negative the value of  $\gamma$ , the less flexible the TSI. The situation is illustrated, in sketch form, as shown below [34].

## Transition State Isomer

with a constant size of open space (a, b, and c)  
and a constant amount of M...L' bond-making (b, c, and d)

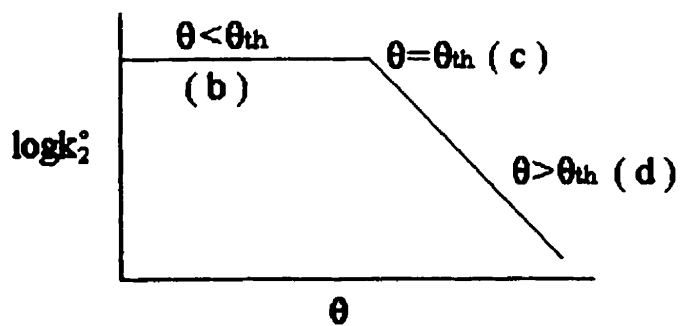
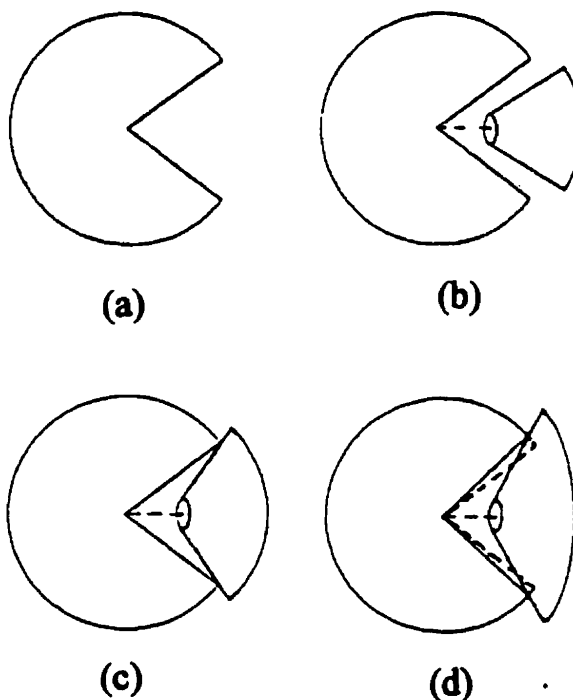
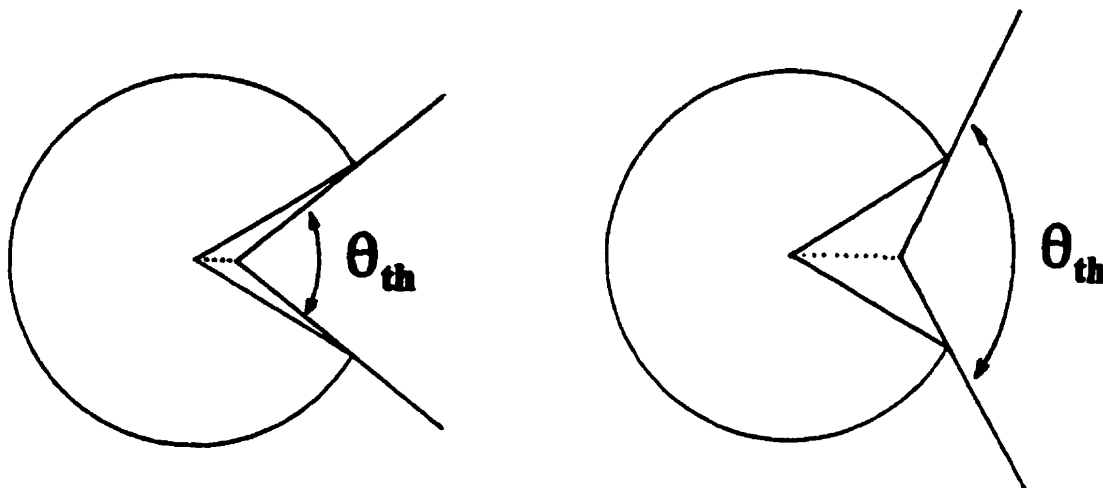


Fig. (a) A TSI with an open space made available for approach of a nucleophile to its electronic electrophilic centre.

- (b) The TSI with a smaller P-donor nucleophile ( $\theta < \theta_{th}$ ) attached to the electrophilic centre. A partial bond  $M\cdots P$  is formed without any steric interaction.
- (c) the TSI with an attached nucleophile ( $\theta = \theta_{th}$ ) such that a partial bond  $M\cdots P$  of the same length as in (b) can just be formed without unfavorable steric interaction.
- (d) The TSI with a large attached nucleophile ( $\theta > \theta_{th}$ ) which has forced the TSI to open up further so that a partial bond  $M\cdots P$  of the same length as in (b) and (c) can be formed, albeit at some energy cost.  
(Taken from ref. 34)

$\lambda$  in Eq.(2.5) is a switching function which is zero when  $\theta \leq \theta_{th}$ , and becomes unity when  $\theta > \theta_{th}$ .  $\beta$  is a electronic discrimination parameter, which indicates the susceptibility of carbonyl clusters to the  $\sigma$ -basicity of nucleophiles, and is a measure of TS stabilization by  $M\cdots P$  bond-making. The higher  $\beta$  means the more  $M\cdots P$  bond-making and the lower  $\beta$  the less  $M\cdots P$  bond-making in TS. For a constant size of opening in the TSI an earlier onset of steric effects might be expected as the degree of bond making becomes more pronounced, as shown below, and vice versa.

## Relationship between $\beta$ and $\theta_{th}$ for Associative Reactions



### TS isomer

with a constant size of open space

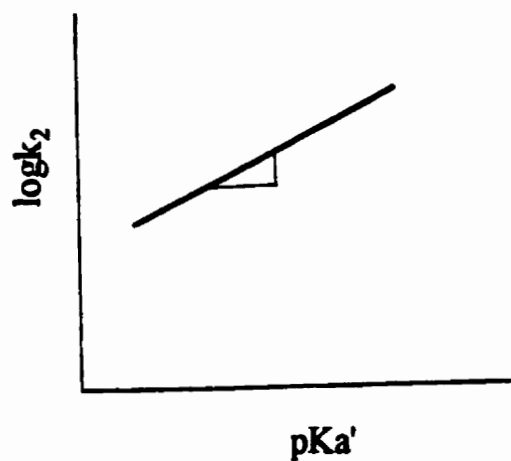
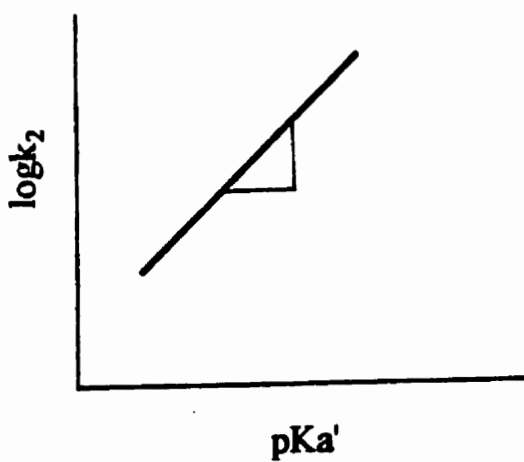
- |  |  |
|--|--|
| <ul style="list-style-type: none"> <li>• More M...P bond-making (higher <math>\beta</math>)</li> <li>• Earlier onset of steric effects (smaller <math>\theta_{th}</math>)</li> </ul> | <ul style="list-style-type: none"> <li>• Less M...P bond-making (lower <math>\beta</math>)</li> <li>• Later onset of steric effects (bigger <math>\theta_{th}</math>)</li> </ul> |
|--|--|

The parameter  $\gamma$  indicates the sensitivity of rates to cone angles of nucleophiles when  $\theta > \theta_{th}$ , and is a measure of the flexibility of the TSI. A high negative value of  $\gamma$  implies a rigid TSI, while a low negative value of  $\gamma$  indicates a flexible TSI. The parameter  $\alpha$  is defined as the standard reactivity SR of carbonyl clusters, proposed by Poë et al. [33] as being  $\log k_2^\circ = \log k_2 - \beta(pK_a' + 4)$ .

These concepts are further illustrated diagrammatically on the following pages.

## Electronic Discrimination Parameter $\beta$

Slope =  $\beta$



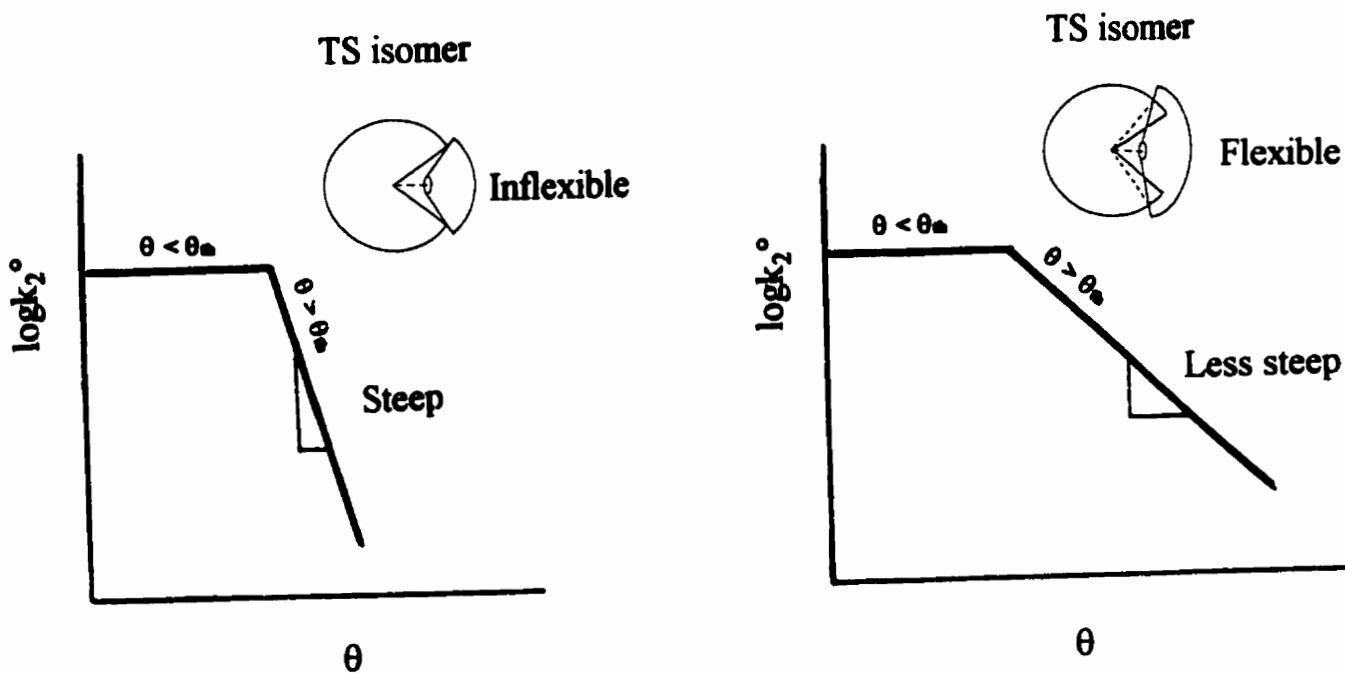
- Higher  $\beta$
- More M ... P  
bond-making  
in TS

- Lower  $\beta$
- Less M ... P  
bond-making  
in TS

$$\log k_2 = \alpha + \beta (pK_a' + 4) + \gamma (\theta - \theta_{th}) \lambda$$

## Steric Sensitivity Parameter $\gamma$

Slope =  $\gamma$

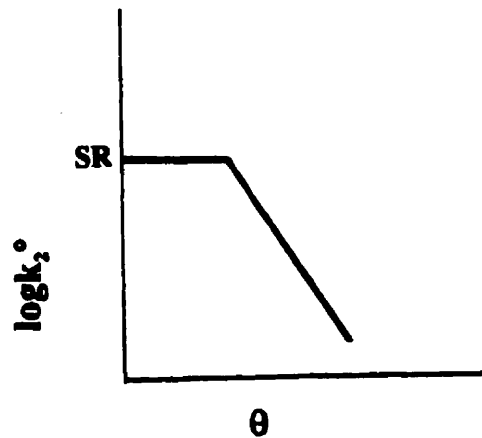
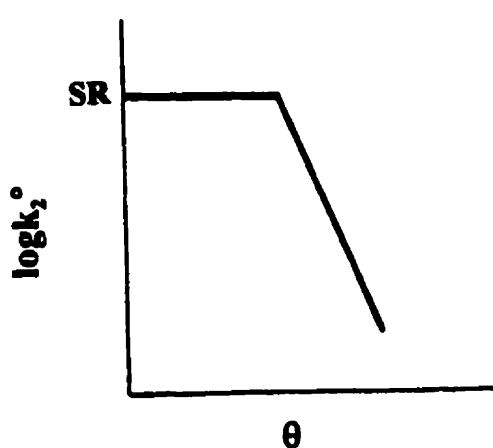


- High negative value of  $\gamma$
- Inflexible TS isomer
- Low negative value of  $\gamma$
- Flexible TS isomer

$$\log k_2^\circ = \log k_2 - \beta (\text{pKa}' + 4) = \alpha + \gamma (\theta - \theta_{th}) \lambda$$

## Standard Reactivity SR

Intercept = SR



- Higher SR
- More reactive

- Lower SR
- Less reactive

$$\log k_2 = \alpha + \beta(\text{pKa}' + 4) + \gamma(\theta - \theta_{\text{th}})\lambda$$

when  $\theta < \theta_{\text{th}}$ ,  $\gamma(\theta - \theta_{\text{th}})\lambda = 0$  ( $\lambda = 0$ )

$$\text{pKa}' = -4, \quad \beta(\text{pKa}' + 4) = 0$$

Thus  $\log k_2 = \log k_2^\circ = \alpha = \text{SR}$

### 2.3.4.2 Electronic and Steric Profiles

Analysis of kinetic data is accomplished through construction of electronic and steric profiles. An electronic profile can be constructed by plotting  $\log k_2$  vs  $pK_a'$ , where values of  $k_2$  are rate constants of associative substitution reactions of a given complex with a series of isosteric or nearly isosteric nucleophiles. Such a plot should give a straight line because the nucleophiles have the same or very similar cone angles and their relative values of  $k_2$  can be taken to be determined mainly by electronic effects. The slope of the line is the parameter  $\beta$ . Three sets of nucleophiles with very different  $\sigma$ -basicity can be chosen to obtain precise values of  $\beta$ : (1) exactly isosteric nucleophiles such as  $P(p\text{-XC}_6\text{H}_4)_3$   $X = \text{H, MeO, Me, Cl, F, etc.}$ , which have a wide range of  $pK_a$  values; (2) nucleophiles small enough ( $\theta \leq \theta_{th}$ ) not to show any steric effects; (3) a series of almost isosteric nucleophiles, such as  $P(\text{OPh})_3$   $\theta = 128^\circ$ ,  $pK_a' = -2.80$ ;  $P(\text{O-}i\text{-Pr})_3$   $\theta = 130^\circ$ ,  $pK_a' = 3.38$ ;  $P(n\text{-Bu})_3$   $\theta = 132^\circ$ ,  $pK_a' = 8.54$ . The set 3 needs to be adjusted to what their  $\log k_2$  would have been if their  $\theta = 130^\circ$  based on steric effects determined later.

Once a value of  $\beta$  is obtained, the steric profile can then be derived by plotting the electronically corrected rate constants,  $\log k_2^\circ$ , against  $\theta$ . The values of  $\log k_2^\circ$  can be calculated according to Eq.(2.14).

$$\log k_2^\circ = \log k_2 - \beta(pK_a' + 4) \quad (2.14)$$

The horizontal part of the plot, (i.e. intercept on y-axis) can be taken as a measure of standard reactivity of the complex towards nucleophilic

attack as described above. A value of  $\theta_{th}$ , originally coined by Giering, can be obtained from the intersection of the horizontal ( $\theta \leq \theta_{th}$ ) and downward sloping ( $\theta > \theta_{th}$ ) parts of the steric profile. After that point, the value of  $\log k_2^\circ$  is affected by the size of the nucleophile, revealed by a drop in reaction rates. A value of  $\gamma$  can be obtained from the slope of the downward sloping line. The data can then be refined by use of Giering's least-squares computer program, which minimizes the squares of the deviations of  $\log k_2(\text{expt})$  from  $\log k_2(\text{calc})$ . The program requires initial input of values of  $\theta_{th}$  and the optimization of the fit by varying  $\theta_{th}$  until a minimum RMS deviation is obtained. This computer analysis provides more accurate values of  $\alpha$ ,  $\beta$ , and  $\gamma$ , together with estimates of their standard deviations, but not of the standard deviation of  $\theta_{th}$ .

The procedure described above for separating the electronic and steric effects of different nucleophiles in associative reactions of metal carbonyl clusters is also entirely successful for reactions of  $\text{Ru}_3(\text{CO})_{11}\text{PMe}_3$  and  $\text{Ru}_3(\text{CO})_{11}\text{etpb}$  clusters. The plot of  $\log k_2$  at 25.1 °C vs  $\text{pKa}'$  for reactions of  $\text{Ru}_3(\text{CO})_{11}\text{PMe}_3$  with P-donor nucleophiles does not show a linear relationship (Figure 2.28), and smaller nucleophiles, *etpb* and  $\text{P}(\text{OEt})_3$ , have positive deviations from the electronic profile, while larger nucleophiles,  $\text{PPh}_2\text{Et}$  and  $\text{PPh}_3$ , have negative deviations. It is obvious that steric effects are significant. However the nucleophiles  $\text{P}(\text{OPh})_3$  (128°, -2.80) and  $\text{P}(\text{O-}i\text{-Pr})_3$  (130° 3.38) have very similar size and very different values of  $\text{pKa}$ , and the electronic profile can be constructed by drawing the straight line between data of  $\text{P}(\text{OPh})_3$  and  $\text{P}(\text{O-}i\text{-Pr})_3$  adjusted according to the steric profile to what they would have been if their cone angles were

both 129°. The gradient of this line gives a electronic discrimination parameter  $\beta$  of 0.16. The plot of  $\log k_2$  (25.1°C) against  $\text{pKa}'$  for reactions of  $\text{Ru}_3(\text{CO})_{11}\text{etpb}$  with attacking nucleophiles is shown in Figure 2.29 where the straight line drawn is corresponding to 2 hypothetical nucleophiles: one with  $\text{pKa}' = 3.38$  and  $\theta = 131^\circ$ , another with  $\text{pKa}' = 8.54$  and  $\theta = 131^\circ$ . This is very close to those of  $\text{P}(\text{O-}i\text{-Pr})_3(3.38, 130^\circ)$  and  $\text{P}(n\text{-Bu})_3(8.54, 132^\circ)$ . The gradient, 0.20 of the straight line can therefore be taken as the value of  $\beta$ . The positive deviations of  $\log k_2$  for smaller nucleophiles,  $\text{etpb}$  and  $\text{P}(\text{OEt})_3$ , or negative deviations for larger nucleophiles,  $\text{PPh}_{3-n}\text{Et}_n$  ( $n = 0,1,2$ ), provided an indication of steric effects (Figure 2.29).

The  $\beta$  values of 0.16 and 0.20 for clusters  $\text{Ru}_3(\text{CO})_{11}\text{PMe}_3$  and  $\text{Ru}_3(\text{CO})_{11}\text{etpb}$ , respectively, were used to calculate the electronically corrected rate constants,  $\log k_2^\circ$ , according to equation  $\log k_2^\circ = \log k_2 - \beta(\text{pKa}' + 4)$ . Each  $\log k_2^\circ$  value for a given cluster corresponds to a particular nucleophile. The steric profiles for both clusters were constructed by plotting  $\log k_2^\circ$  vs  $\theta$ , and the parameters  $\alpha$ ,  $\gamma$ , and  $\theta_{\text{th}}$  were obtained.

The parameters  $\alpha$ ,  $\beta$ ,  $\gamma$ , and  $\theta_{\text{th}}$  derived from electronic and steric profiles can then be refined by use of multi-linear regression program which minimizes the squares of the deviations of  $\log k_2(\text{expt.})$  from  $\log k_2(\text{calc.})$ , according to the stereoelectronic Eq.(2.5),  $\log k_2 = \alpha + \beta(\text{pKa}' + 4) + \gamma(\theta - \theta_{\text{th}})\lambda$  (two independent parameters  $X_1 = \text{pKa}'$ ,  $X_2 = \theta$ , and the dependent parameter  $Y = \log k_2$ ). The optimization of the fit is obtained by varying  $\theta_{\text{th}}$  until the RMSD is minimized, or the R values are maximized. The best fits in the computer output are listed

in Table 2.16. The fitting results around the best fit are also summarized below for comparison.

### **$\text{Ru}_3(\text{CO})_{11}\text{PMe}_3$**

$\theta_{\text{th}}(\text{deg})$	SR	$\beta$	$\gamma(\text{deg}^{-1})$	RMSD	R
121.0	$-3.03 \pm 0.08$	$0.142 \pm 0.026$	$-0.112 \pm 0.007$	0.091718	0.994
122.6	$-3.08 \pm 0.06$	$0.152 \pm 0.021$	$-0.121 \pm 0.006$	0.071245	0.997
<b>122.7</b>	<b><math>-3.08 \pm 0.06</math></b>	<b><math>0.153 \pm 0.021</math></b>	<b><math>-0.122 \pm 0.006</math></b>	<b>0.071164</b>	<b>0.997</b>
122.8	$-3.09 \pm 0.06$	$0.153 \pm 0.021$	$-0.123 \pm 0.006$	0.071278	0.997
124.0	$-3.14 \pm 0.07$	$0.160 \pm 0.026$	$-0.130 \pm 0.008$	0.088101	0.995

### **$\text{Ru}_3(\text{CO})_{11}\text{etpb}$**

$\theta_{\text{th}}(\text{deg})$	SR	$\beta$	$\gamma(\text{deg}^{-1})$	RMSD	R
120.0	$-4.715 \pm 0.098$	$0.180 \pm 0.028$	$-0.0843 \pm 0.0109$	0.086781	0.984
120.7	$-4.718 \pm 0.097$	$0.176 \pm 0.027$	$-0.0869 \pm 0.0111$	0.085863	0.985
<b>120.8</b>	<b><math>-4.718 \pm 0.097</math></b>	<b><math>0.176 \pm 0.027</math></b>	<b><math>-0.0873 \pm 0.0112</math></b>	<b>0.085042</b>	<b>0.986</b>
120.9	$-4.719 \pm 0.097$	$0.175 \pm 0.027$	$-0.0877 \pm 0.0112$	0.085850	0.985
122.0	$-4.724 \pm 0.100$	$0.169 \pm 0.027$	$-0.0920 \pm 0.0121$	0.088126	0.984

**Table 2.16 Parameters  $\alpha$ ,  $\beta$ ,  $\gamma$ , and  $\theta_{th}$  for Associative Reactions of  $Ru_3(CO)_{11}L$  with  $L'$  in Heptane at  $(25.1 \pm 0.1)^\circ C$**

$\theta_{th}(\text{deg})$	SR	$\beta$	$\gamma(\text{deg}^{-1})$	RMSD <sup>a</sup>	R	N <sup>b</sup>
<b><math>Ru_3(CO)_{11}PMe_3</math></b>						
122.7	$-3.08 \pm 0.06$	$0.153 \pm 0.021$	$-0.122 \pm 0.006$	0.071	0.997	6
<b><math>Ru_3(CO)_{11}etpb</math></b>						
120.8	$-4.72 \pm 0.10$	$0.176 \pm 0.027$	$-0.087 \pm 0.011$	0.085	0.986	6

a. Root mean square deviation =  $[\Sigma\Delta^2]^{1/2} / N$

b. Data points, that is, the number of entering ligands.

It is evident from Table 2.16 that the values of  $\log k_2$  for both clusters fit with the stereoelectronic Eq.(2.5) extremely well in view of the values of RMSD and  $R^2$ . Thus, the RMSD is only 0.07 for  $Ru_3(CO)_{11}PMe_3$ , 0.08 for  $Ru_3(CO)_{11}etpb$ . The multiple correlation coefficient squares  $R^2$  are 0.994 and 0.98, respectively. This means that the model used, i.e. Eq.(2.5) and the values of  $pK_a'$  and  $\theta$ , fail to account for only  $100(1 - 0.994) = 0.6\%$  and  $100(1 - 0.98) = 2\%$  of the variations observed in  $k_{obs}$ .

The  $\beta$  values of 0.153 and 0.176 from the computer output for clusters  $Ru_3(CO)_{11}PMe_3$  and  $Ru_3(CO)_{11}etpb$ , respectively, agree with the graphically obtained ones of 0.16 and 0.20 quite well. The accurate electronically corrected rate constants,  $\log k_2^\circ$ , can therefore be calculated with the computer output values of  $\beta$  according to

equation  $\log k_2^\circ = \log k_2 - \beta(\text{pKa}' + 4)$  (Tables 2.17 and 2.18). The steric profiles for both clusters are constructed by plotting  $\log k_2^\circ$  vs  $\theta$ . Excellent plots are obtained (Figure 2.30) as shown by the very small scatter of the data around the steric profiles.

**Table 2.17 Kinetic Data for  $\text{Ru}_3(\text{CO})_{11}\text{PMe}_3$  with P-donor Nucleophiles  $\text{L}'$  in Heptane at  $(25.1 \pm 0.1)^\circ\text{C}$**

$\text{L}'$	$\text{pKa}'$	$\theta$ (deg)	$\log k_2$	$\log k_2 - \beta (\text{pKa}' + 4)$ $\beta = 0.1526$
etpb	-0.33	101	-2.4365	-2.9968
$\text{P}(\text{OEt})_3$	1.62	109	-2.3084	-3.1657
$\text{P}(\text{OPh})_3$	-2.80	128	-3.5506	-3.7339
$\text{P}(\text{O-}i\text{-Pr})_3$	3.38	130	-2.8742	-3.9996
$\text{PPh}_2\text{Et}$	4.46	140	-3.7990	-5.0896
$\text{PPh}_3$	3.14	145	-4.7816	-5.8713

**Table 2.18 Kinetic Data for Ru<sub>3</sub>(CO)<sub>11</sub>etpb with P-donor Nucleophiles L' in Heptane at (25.1 ± 0.1) °C**

L'	pKa'	θ (deg)	logk <sub>2</sub>	logk <sub>2</sub> - β (pKa' + 4) β = 0.1758
etpb	-0.33	101	-3.9168	-4.5623
P(OEt) <sub>3</sub>	1.62	109	-3.8294	-4.8170
P(O- <i>i</i> -Pr) <sub>3</sub>	3.38	130	-4.2350	-5.5315
P( <i>n</i> -Bu) <sub>3</sub>	8.54	132	-3.4124	-5.6171
PPhEt <sub>2</sub>	5.81	136	-4.2922	-6.0164
PPh <sub>2</sub> Et	4.46	140	-4.8891	-6.3759
PPh <sub>3</sub>	3.14	145	-5.5467	-6.8021

### 2.3.4.3 Stereoelectronic Analyses and Comparison of Data

The electronic discrimination parameter  $\beta$  for Ru<sub>3</sub>(CO)<sub>11</sub>PMe<sub>3</sub> is 0.153±0.021, and for Ru<sub>3</sub>(CO)<sub>11</sub>etpb it is 0.176±0.027. This shows that the former is slightly less susceptible to the  $\sigma$  basicity of attacking nucleophiles. The trend in  $\beta$  values implies that the bond-making in TS becomes more important from L = PMe<sub>3</sub> to etpb. A larger  $\beta$  for Ru<sub>3</sub>(CO)<sub>11</sub>etpb suggests that nucleophiles must get quite close to the electrophilic center of the metal for reactions to occur. For this reason, the size of nucleophiles is more important to the reaction rates, that is, the steric effects set in at a slightly smaller cone angle ( $\theta = 121^\circ$ ). On the other hand,  $\beta$  of Ru<sub>3</sub>(CO)<sub>11</sub>PMe<sub>3</sub> is lower, and nucleophiles do not have to get as close to the metal center in order for reactions to occur.

Here the bond-making in TS is less important because a nucleophile is farther from the metal center. For this reason, the size of nucleophiles is less important to reaction rates until they eventually become large enough to be subject to steric effects. Thus steric effect set in at a larger cone angle ( $\theta = 123^\circ$ ).

The steric threshold  $\theta_{th}$  for  $\text{Ru}_3(\text{CO})_{11}\text{PMe}_3$  is  $123^\circ$ , for  $\text{Ru}_3(\text{CO})_{11}\text{etpb}$  is  $121^\circ$ , below which there are no steric effects (Figure 2.30); and above which steric effects become operative, and the rate constants,  $\log k_2^\circ$ , drop linearly with increasing the size of attacking nucleophiles (Figure 2.30). The gradient of the linear sloping region is the parameter  $\gamma$ , which is a quantitative measure of the flexibility of the TSI. The  $\gamma$  value for  $\text{Ru}_3(\text{CO})_{11}\text{PMe}_3$  is  $-0.122 \pm 0.006 \text{ deg}^{-1}$ , for  $\text{Ru}_3(\text{CO})_{11}\text{etpb}$  is  $-0.087 \pm 0.011 \text{ deg}^{-1}$ . It is obvious that the latter is more flexible than the former, revealed by more gradual drop in rate constants  $\log k_2^\circ$  with increasing size of attacking nucleophiles. The values of  $\log k_2^\circ$  of the former drop somewhat more pronouncedly.

The standard reactivity of  $\text{Ru}_3(\text{CO})_{11}\text{L}$  towards nucleophilic attack, indicated by the horizontal portion of steric profiles and approached at low cone angles, decreases from  $\text{L} = \text{PMe}_3$  ( $\text{SR} = -3.08 \pm 0.06$ ,  $\delta(^{13}\text{CO}) = 5.05$ ,  $\theta = 118^\circ$ ) to  $\text{etpb}$  ( $\text{SR} = -4.72 \pm 0.10$ ,  $\delta(^{13}\text{CO}) = 2.60$ ,  $\theta = 101^\circ$ ). Because of being a substituent and not a nucleophile,  $\pi$ -acidity of L will be important as well as  $\sigma$ -basicity. So the parameter  $\delta(^{13}\text{CO})$  would be the best to use. It seems that the standard reactivity increases with increasing net electron donicity  $\delta(^{13}\text{CO})$  and/or with increasing size of substituents. The greater electron donicity of  $\text{PMe}_3$  encourages Ru-Ru bond breaking to a greater extent than it discourages Ru-L' bond making. The greater size of substituent

$\text{PMe}_3$  also encourages the cluster opening to form the TSI as would be expected. The  $\text{Ru}_3(\text{CO})_{11}\text{PMe}_3$  is therefore more reactive due to combination of both effects of the substituent  $\text{PMe}_3$ , as mentioned above. Bond making is relatively less important for more reactive clusters, such as  $\text{Ru}_3(\text{CO})_{11}\text{PMe}_3$  ( $\beta = 0.15$ ), that is, the more reactive a cluster is, the less dependent on electronic property  $\text{pK}_a'$  of nucleophiles  $\text{L}'$  it is.

Other clusters  $\text{Ru}_3(\text{CO})_{11}\text{L}$  also react with nucleophiles via associative paths as well as dissociative paths, and systematic data are available for some of them in Table 2.19 in addition to the ones studied here. This enables one to examine the effect of a series of substituents on the associative reactions of the clusters, just as substituent effects on dissociative reactions can be studied.

**Table 2.19 Kinetic Parameters for Associative Reactions of  $\text{Ru}_3(\text{CO})_{11}\text{L}$  with P-donor Nucleophiles<sup>a</sup>**

L	$\theta_{\text{th}}$ (deg)	Standard Reactivity	$\beta$	$\gamma$ (deg <sup>-1</sup> )	RMS Deviation	Reference
$\text{CO}^c(12)^b$	120	$-3.4 \pm 0.2$	$0.15 \pm 0.02$	$-0.03 \pm 0.01$	0.25	2, 49
$\text{CO}^d(6)$	—	—	$0.35 \pm 0.01$	—	0.06	2, 49
$\text{P}(\text{OEt})_3^e(5)$	123	$-4.2 \pm 0.1$	$0.22 \pm 0.02$	$-0.18 \pm 0.01$	0.07	10
$\text{PMe}_3^f(6)$	123	$-3.1 \pm 0.1$	$0.15 \pm 0.02$	$-0.122 \pm 0.006$	0.07	this work
$\text{P}(\text{OPh})_3^f(6)$	118	$-4.2 \pm 0.2$	$0.25 \pm 0.03$	$-0.107 \pm 0.015$	0.14	16
$\text{P}(n\text{-Bu})_3^g(7)$	129	$-2.4 \pm 0.1$	$0.07 \pm 0.02$	$-0.114 \pm 0.010$	0.09	1
$\text{PCy}_3^g(8)$	123	$-3.2 \pm 0.2$	$0.23 \pm 0.03$	$-0.100 \pm 0.015$	0.22	1
etpb <sup>f</sup> (5)	121	$-4.7 \pm 0.1$	$0.18 \pm 0.03$	$-0.087 \pm 0.011$	0.08	this work

a. Parameters of  $\text{Ru}_3(\text{CO})_{11}\text{PMe}_3$  and  $\text{Ru}_3(\text{CO})_{11}\text{etpb}$  are appropriate to  $(25.1 \pm 0.1)^\circ\text{C}$ , but the others were usually obtained from data at  $50^\circ\text{C}$  or less. Values of  $\beta$  and  $\gamma$  are not appreciably sensitive to temperature [30]. The standard reactivities have been adjusted to  $25^\circ\text{C}$  [1, 2, 10, 16, 49].

b. The number of attacking nucleophiles used.

c. In chlorobenzene with nucleophiles ( $\theta \leq 140^\circ$ )

d. In chlorobenzene with nucleophiles ( $\theta = 145^\circ$ )

e. Decalin as a solvent.

f. Heptane as a solvent.

g. Dodecane as a solvent.

#### 2.3.4.4 Use of an Alternative Steric Parameter $\theta'$

Poë et al. [39] suggested a new set of "cone angles"  $\theta'$ , which fit exactly to Eq.(2.15), established by the 37 phosphine ligands,

$$\theta' = 103.8 + 0.553 E_R \quad (2.15)$$

where values of  $E_R$  are Brown's ligand repulsion energies experienced by the ligands in the complexes  $\text{Cr}(\text{CO})_5\text{L}$  [40]. Analysis of the data according to the stereoelectronic Eq.(2.5) can be carried out exactly as before just with  $\theta$  and  $\theta_{\text{th}}$  replaced by  $\theta'$  and  $\theta'_{\text{th}}$ . The best fits were obtained by varying  $\theta'_{\text{th}}$  to  $134^\circ$  and  $133^\circ$  for  $\text{Ru}_3(\text{CO})_{11}\text{PMe}_3$  and  $\text{Ru}_3(\text{CO})_{11}\text{etpb}$ , respectively, and the values of  $\text{SR}$ ,  $\beta$ , and  $\gamma$  are given in Table 2.20. The fits are much more not as good as when  $\theta$  was used. Nevertheless, the parameters  $\alpha$ ,  $\beta$ , and  $\gamma$  obtained are not significantly different, especially for  $\text{Ru}_3(\text{CO})_{11}\text{PMe}_3$ .

**Table 2.20 Parameters  $\alpha$ ,  $\beta$ , and  $\theta_{th}$  for Associative Reactions of  $Ru_3(CO)_{11}L$  with  $L'$  in Heptane at  $(25.1 \pm 0.1)^\circ C$**

$\theta_{th}$ or $\theta_{th}'$ (deg)	SR	$\beta$	$\gamma$ (deg <sup>-1</sup> )	RMSD	R	Steric Parameter
<b><math>Ru_3(CO)_{11}PMe_3 + L'</math></b>						
123	-3.08±0.06	0.153±0.021	-0.122±0.006	0.07	0.997	$\theta$
134	-2.51±0.64	0.165±0.016	-0.146±0.099	0.63	0.681	$\theta'$
<b><math>Ru_3(CO)_{11}etpb + L'</math></b>						
121	-4.72±0.10	0.176±0.027	-0.087±0.011	0.08	0.986	$\theta$
133	-4.36±0.55	0.121±0.108	-0.127±0.068	0.48	0.741	$\theta'$

### 2.3.5 Interrelationships of Parameters $\alpha$ , $\beta$ , $\gamma$ , and $\theta_{th}$ for Associative Substitution Reactions of $Ru_3(CO)_{11}L$

As is shown in Figure 2.31, there is inverse correlation between the standard reactivity SR and  $\beta$ , which reflects the fact that the more intrinsically susceptible a cluster may be towards nucleophilic attack, the less it will need assistance from  $M \cdots L'$  bond making during its associative reactions, and the less discriminating it will be towards different nucleophiles. The correlation is linear for  $Ru_3(CO)_{11}L$ ,  $L = P(n-Bu)_3$ ,  $PMe_3$ ,  $CO$ ,  $P(OEt)_3$ , and  $P(OPh)_3$ , but  $Ru_3(CO)_{11}PCy_3$  has a higher value of standard reactivity than would be inferred from its  $\beta$  value, and  $Ru_3(CO)_{11}etpb$  has a lower one. There is also a reasonably good inverse correlation between the values of  $\theta_{th}$  and  $\beta$  (Figure 2.32).

An earlier onset of steric effects might be expected as the degree of bond making becomes more pronounced. Figure 2.33 shows the correlation between the values of  $\theta_{th}$  and SR. The values of  $\gamma$  do not appear to correlate with any of the other parameters.

Least-squares analysis shows that the linear relationship between SR and  $\beta$  for clusters  $Ru_3(CO)_{11}L$  { $L = P(n-Bu)_3, PMe_3, CO, P(OEt)_3,$  and  $P(OPh)_3$ } is governed by the equation  $SR = -1.62 - 10.8\beta$  with a correlation coefficient of 0.983 [34]. This has the interesting implication that there is an isokinetic relationship of a novel kind in that a nucleophile with a  $pK_a'$  of 7 will react with all those clusters at the same rate, a fact that is clearly illustrated in Figure 2.34 [34]. The plot also indicates that the standard reactivity and the intrinsic reactivity of these clusters varies as  $L = P(n-Bu)_3 > PMe_3 > CO > P(OPh)_3 > P(OEt)_3$ .

It is obvious from Figure 2.34 there is an " isokinetic  $pK_a'$  " at which all  $\log k_2$  values are the same for a series of clusters  $Ru_3(CO)_{11}L$ ,  $L = P(n-Bu)_3, PMe_3, CO, P(OEt)_3,$  and  $P(OPh)_3$ , where the plots of  $\log k_2$  vs  $pK_a'$  are electronic profiles for these clusters (certainly corrected for steric effects). Such a plot, of course, gives a straight line for each cluster because all relative values of  $\log k_2$  are obtained with nucleophiles for which there is no steric effect, and they are determined by electronic effects as well as standard reactivities. The stereoelectronic Eq.(2.5) can therefore be changed into Eq.(2.15). The " isokinetic  $pK_a'$  " is derived as below.

$$(\log k_2)_1 = \alpha_1 + \beta_1(\text{pKa}' + 4) \quad (2.15)$$

$$\vdots$$

$$(\log k_2)_n = \alpha_n + \beta_n(\text{pKa}' + 4)$$

$$(\log k_2)_n - (\log k_2)_1 = (\alpha_n - \alpha_1) + (\beta_n - \beta_1)(\text{pKa}' + 4)$$

$$(\log k_2)_n - (\log k_2)_2 = (\alpha_n - \alpha_2) + (\beta_n - \beta_2)(\text{pKa}' + 4)$$

$$\vdots$$

$$\text{If } SR_1 = \alpha_1 = a + b\beta_1 \quad (2.16)$$

$$\vdots$$

$$SR_n = \alpha_n = a + b\beta_n$$

$$\text{thus } \frac{(\alpha_1 - \alpha_n)}{(\beta_n - \beta_1)} = \frac{(\alpha_2 - \alpha_n)}{(\beta_n - \beta_2)} = \frac{(\alpha_3 - \alpha_n)}{(\beta_n - \beta_3)} = \dots = -b$$

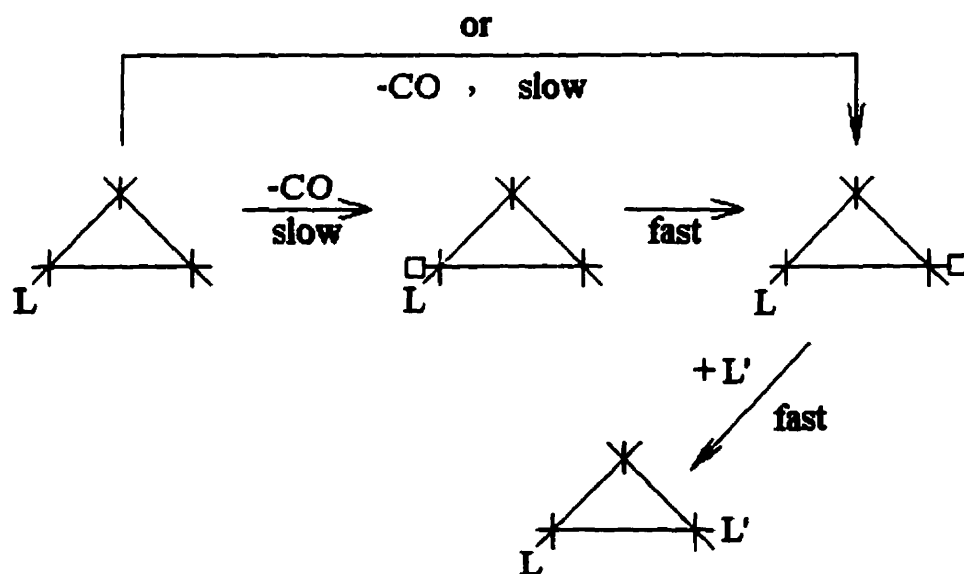
$$\text{If } \text{pKa}' + 4 = -b$$

$$\text{thus } (\log k_2)_n - (\log k_2)_1 = (\log k_2)_n - (\log k_2)_2 = \dots = 0$$

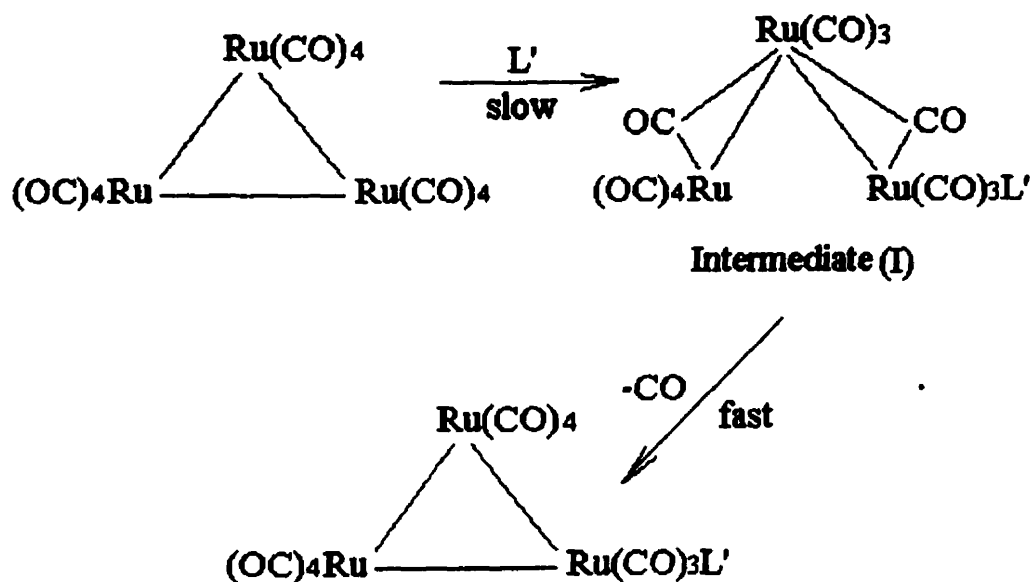
i.e. all  $\log k_2$  values will be the same when  $\text{pKa}' = -(b+4)$ . For a series of clusters  $\text{Ru}_3(\text{CO})_{11}\text{L}$  {L = P(*n*-Bu)<sub>3</sub>, PMe<sub>3</sub>, CO, P(OEt)<sub>3</sub>, and P(OPh)<sub>3</sub>} the isokinetic  $\text{pKa}' = 7 = -(b+4)$ , so  $b = -11$ .

### 2.3.6 Intimate Mechanism

The clusters  $\text{Ru}_3(\text{CO})_{11}\text{L}$  are found to react via a mixture of first and second order paths. For the CO-dissociative path, the rate is independent of the nature of an attacking nucleophile. The intermediate has a reduced coordination number. Atwood [41, 42] suggested that it was always a CO on an already substituted Ru atom that dissociates in the rate determining step. Attack by  $\text{L}'$  at the vacated coordination site cannot occur for steric reasons. The coordinative unsaturation is transferred rapidly to an unsubstituted Ru atom by CO migration after which attack by  $\text{L}'$  can occur [43]. It is hard to distinguish these two structures with a different vacated coordination site. So there is an alternative possibility that cannot be ruled out, i.e. it would be a CO on an unsubstituted Ru atom that dissociates in the rate determining step. A scheme with two possibilities is shown below.

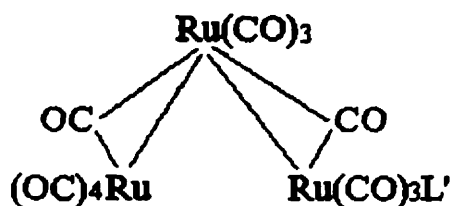


For associative reactions with P-donor nucleophiles, the rate is dependent of the nature of the attacking nucleophile. An intermediate (I) can be formulated as follows [21]:

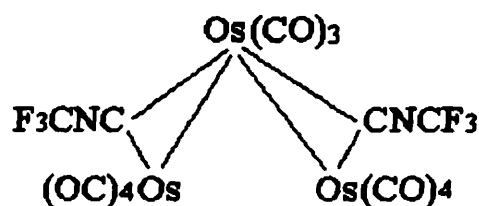


This ensures that the electron count is not increased during the approach of the nucleophile. This is done by breaking a Ru–Ru bond concurrently with making a Ru···L' bond in a way that only clusters can. In the intermediate each Ru atom has still maintained its 18-electron configuration. Subsequent loss of a CO ligand and reformation of the Ru–Ru bond will lead to substitution although an alternative possibility would be fragmentation of the intermediate (I), an outcome which is well known in reactions of several Ru<sub>3</sub> and Os<sub>3</sub> clusters with P-donors which are more nucleophilic[15, 21, 43, 44, 45].

As early as 1974 Poë et al. [46] proposed a structure of this intermediate, and suggested a related one again in 1985 [21]. Almost 20 years later, now the probability of this structure has received strong support through the work of Adams et al. [47] who isolated the compound  $\text{Os}_3(\text{CO})_{11}(\text{CNCF}_3)_2$ , which has the identical structure with Poë's, as shown below.

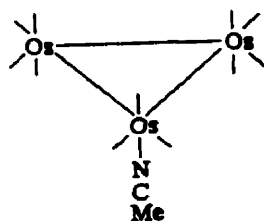
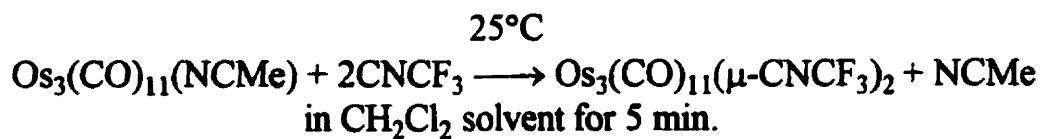


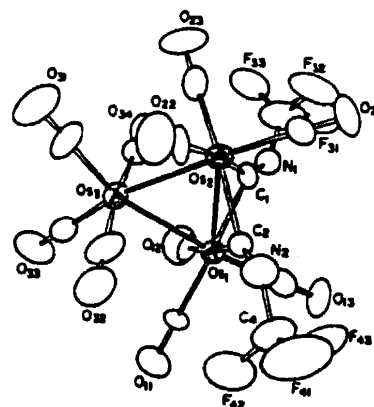
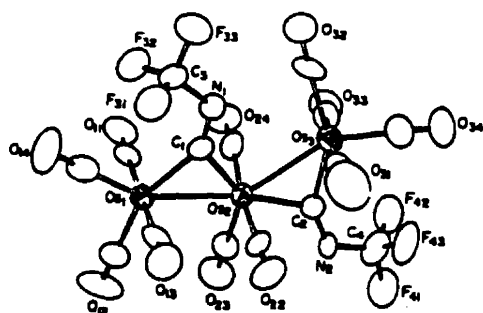
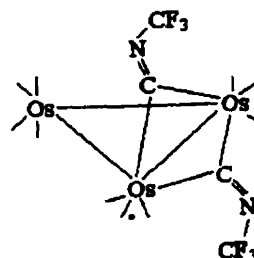
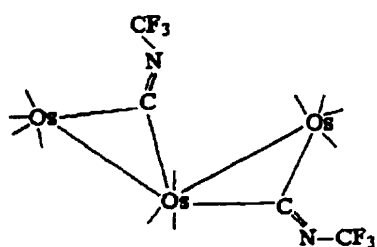
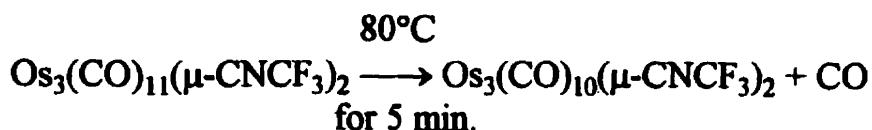
(A.J. Poë 1985)



(R.D. Adams 1992)

The preparation and the crystal structures of Adams compounds are shown below [47].

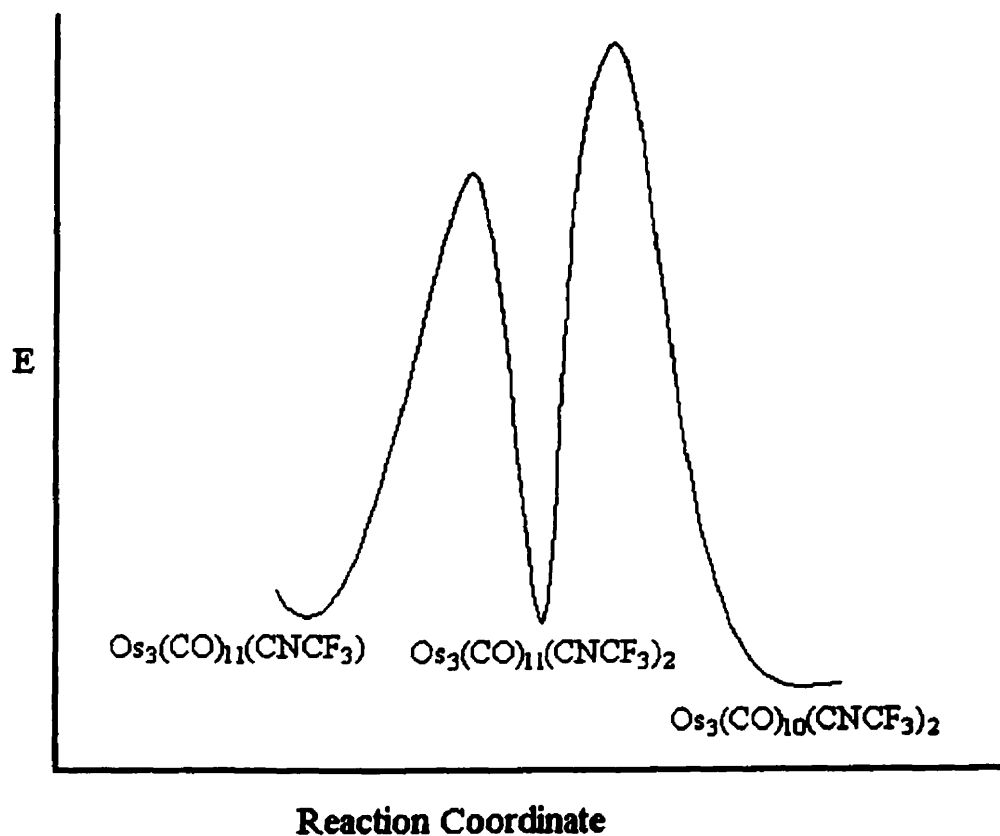




The presence of the two bridging ligands in  $\text{Os}_3(\text{CO})_{10}(\text{CNCF}_3)_2$  makes the structure analogous to that of  $\text{Fe}_3(\text{CO})_{10}(\mu\text{-CO})_2$  and unlike that of  $\text{Os}_3(\text{CO})_{12}$ , which has only terminal ligands.

The most likely mechanism for the formation of  $\text{Os}_3(\text{CO})_{11}(\text{CNCF}_3)_2$  is by initial rapid displacement of the weakly bound NCMe ligand [47] to form  $\text{Os}_3(\text{CO})_{11}(\text{CNCF}_3)$  and this is followed by nucleophilic attack by the second  $\text{CNCF}_3$  to form  $\text{Os}_3(\text{CO})_{11}(\text{CNCF}_3)_2$ . This can subsequently lose CO to form  $\text{Os}_3(\text{CO})_{10}(\text{CNCF}_3)_2$  so that substitution of CO in  $\text{Os}_3(\text{CO})_{11}(\text{CNCF}_3)$  by  $\text{CNCF}_3$  proceeds in two stages via the isolated and fully

crystallographically characterized adduct  $\text{Os}_3(\text{CO})_{11}(\text{CNCF}_3)_2$ . The reaction profile will therefore be as shown.



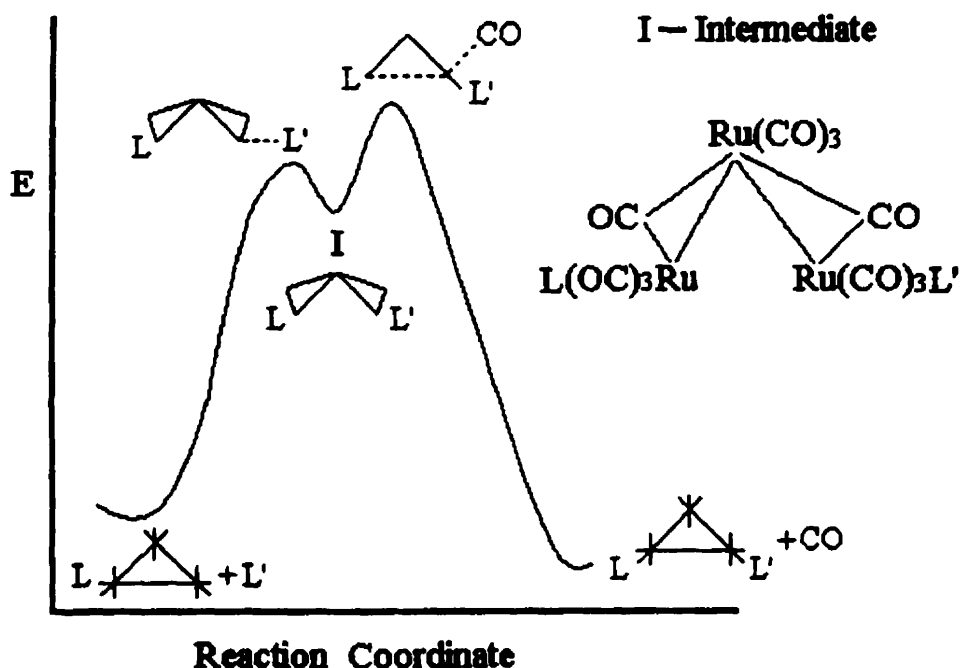
This type of process is also found in substitution reaction of  $\text{Ru}_5\text{C}(\text{CO})_{15}$  with smaller ( $\theta \leq 130^\circ$ ) P-donor nucleophiles and the value of  $\beta$  for the first stage is  $0.214 \pm 0.038$  [48]. With larger nucleophiles ( $\theta \geq 145^\circ$ ), however, no intermediate is detected and a different reaction path is followed with  $\beta = 0.592 \pm 0.024$  [48]. It was proposed that the two reaction paths were distinguished by the occurrence of nucleophilic attack at two different sites on the cluster.

A rather similar situation is observed with  $\text{Ru}_3(\text{CO})_{12}$ , where smaller nucleophiles ( $\theta \leq 130^\circ$ ) react with a  $\beta$  value of  $0.15 \pm 0.02$  and the  $145^\circ$  nucleophiles show  $\beta = 0.35 \pm 0.01$  [49]. In this case,

however, no intermediates are detected for either group of nucleophiles and it is more difficult though not impossible to propose two different sites of nucleophilic attack.

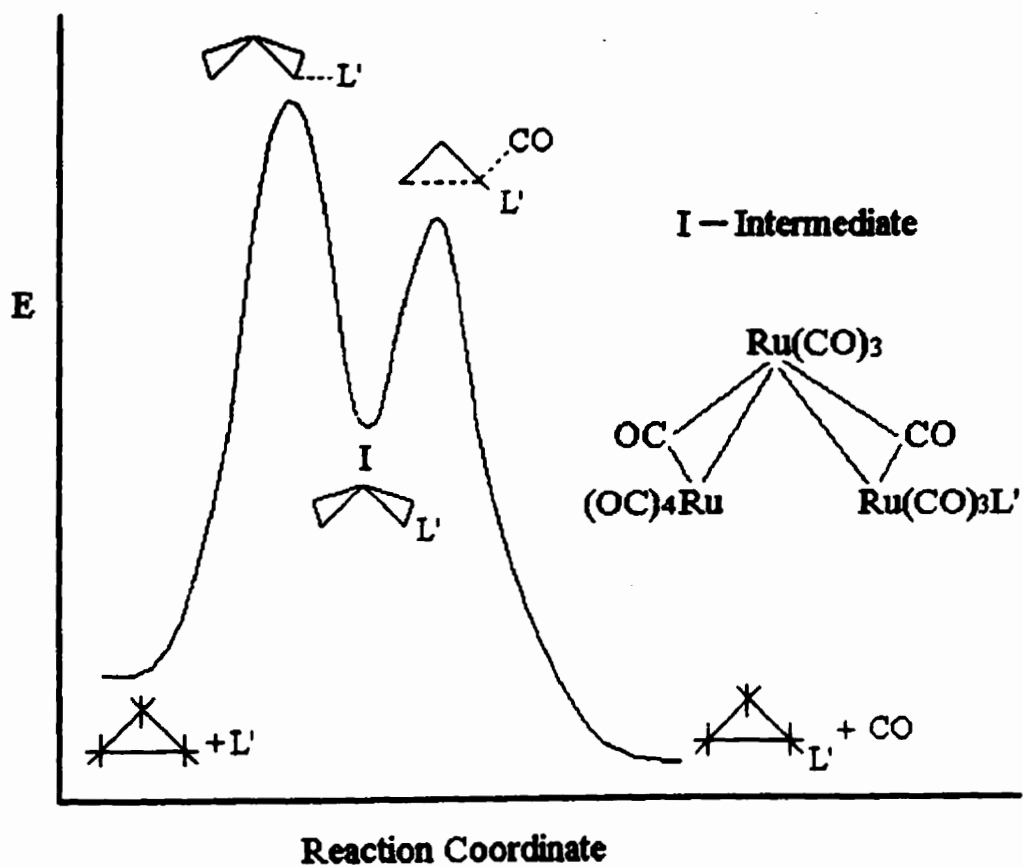
Instead of two different sites of attack one might propose that the relative stabilities of transition states for initial adduct formation and CO dissociation from the adduct could differ for the two paths. The intimate mechanisms are proposed as shown by following reaction profiles.

### Reaction Profile (a)



For reactions of  $\text{Ru}_3(\text{CO})_{11}\text{L}$  with all nucleophiles and  $\text{Ru}_3(\text{CO})_{12}$  with large nucleophiles ( $\theta = 145^\circ$ ), the intermediate would be more reactive and could not be detected.

### Reaction Profile (b)



For reactions of  $\text{Ru}_3(\text{CO})_{12}$  with small nucleophiles  $\text{L}'$  ( $\theta < 145^\circ$ ), the intermediate,  $\text{Ru}_3(\text{CO})_{10}(\mu\text{-CO})_2\text{L}'$ , might be formed in view of the exist of Adams compound  $\text{Os}_3(\text{CO})_{11}(\mu\text{-CNCF}_3)_2$ .

For  $\text{Ru}_3(\text{CO})_{12}$  with the larger ( $\theta = 145^\circ$ ) nucleophiles one could suppose that reaction profile (a) is followed. This would account for the higher value of  $\beta$  because the Ru–L' bonds are fully formed and, in this case (as with the  $\text{Ru}_5\text{C}(\text{CO})_{15}\text{L}$  case [48]), the presence of the larger substituent in the adduct would make CO loss more difficult. With the smaller nucleophiles, Profile (b) could be followed so, in this case, the transition state involves only partial Ru...L' bond formation (and the value of  $\beta$  is lower), and the loss of CO is facilitated because the closing up of the cluster during CO loss is less sterically inhibited by the smaller L's (e.g. the inverse steric effect for loss of CO from  $\text{Ru}_5\text{C}(\text{CO})_{15}\text{L}$  [48]).

For the reactions of the substituted  $\text{Ru}_3(\text{CO})_{11}\text{L}$  clusters there is no evidence for two paths being followed by any one cluster. However, it is noticeable that the  $\beta$  values for all the  $\text{Ru}_3(\text{CO})_{11}\text{L}$  complexes {except when  $\text{L} = \text{P}(n\text{-Bu})_3$ } lie between the values of  $\beta$  for reactions of  $\text{Ru}_3(\text{CO})_{12}$  with smaller and larger nucleophiles. This indicates that the amount of Ru...L' bond-making in associative reactions of the monosubstituted clusters is generally greater than in the case for smaller nucleophiles reacting with the sterically less congested unsubstituted cluster. It can therefore be proposed that the  $\text{Ru}_3(\text{CO})_{11}\text{L}$  clusters { $\text{L} \neq \text{P}(n\text{-Bu})_3$ } probably react via profile (a), loss of CO and reformation of  $\text{Ru}_3$  cluster from  $\text{Ru}_3(\text{CO})_{11}\text{LL}'$  being retarded by the inverse steric effect described above. The fairly low values of  $\beta$  may arise from the fact that loss of CO from  $\text{Ru}_3(\text{CO})_{11}\text{LL}'$  could be retarded by higher basicity of L' (as is the case with  $\text{Ru}_5\text{C}(\text{CO})_{15}\text{L}$ ) so that, we think Ru–L' bond formation is complete in the transition state, there are two opposing effects of increased

basicity. The reason why  $\text{Ru}_3(\text{CO})_{11}\text{P}(n\text{-Bu})_3$  has such a low  $\beta$  value is not clear but its high SR does suggest that for some reasons it requires quite little assistance from  $\text{Ru}\cdots\text{L}'$  bond-making and that reaction profile (b) is followed.

### 2.3.7 Conclusion

Like other monosubstituted  $\text{Ru}_3(\text{CO})_{11}\text{L}$  clusters [1, 2, 16, 49] the clusters  $\text{Ru}_3(\text{CO})_{11}\text{PMe}_3$  and  $\text{Ru}_3(\text{CO})_{11}\text{etpb}$  react with P-donor nucleophiles in heptane via both associative and dissociative pathways. For the  $k_1$  path, the data at 25.0°C of these two new clusters gave the best fit to the stereoelectronic equation,  $\log k_1 = \alpha_L + \beta_L \delta(^{13}\text{CO}) + \gamma_L \theta$ , in terms of their very small deviations, 0.07 and 0.02, respectively, among the ten clusters  $\text{Ru}_3(\text{CO})_{11}\text{L}$ , and the compliance of the data to the equation is excellent, which adds support to the conclusion that the kinetic data for such reactions can be resolved into electronic and steric effects, which can also be expressed graphically by electronic and steric profiles [12]. The activation parameters  $\Delta H_1^\ddagger$  and  $\Delta S_1^\ddagger$  were obtained. The results of these two new clusters are excellent in the light of the very small probable errors among the ten clusters. When combined with activation parameters of  $\text{Ru}_3(\text{CO})_{12}$  and the other seven  $\text{Ru}_3(\text{CO})_{11}\text{L}$  clusters, the values of  $\Delta H_1^\ddagger$  and  $\Delta S_1^\ddagger$  are found to lie on a fairly good isokinetic plot with an isokinetic temperature of about 116°C. The changes in the activation parameters are consistent with major and systematic changes in the nature of the  $\text{Ru}_3(\text{CO})_{10}\text{L}$  moieties left after CO dissociation.

The  $k_2$  path corresponds to associative substitution without detectable intermediate adducts, even though their possible existence

cannot be completely ruled out. It is still possible for such adducts to be formed provided loss of CO from those adducts is faster than their rate of formation. The rate constants,  $k_2$ , for these two clusters,  $\text{Ru}_3(\text{CO})_{11}\text{PMe}_3$  and  $\text{Ru}_3(\text{CO})_{11}\text{etpb}$ , can also be very successfully analyzed according to Poë's stereoelectronic equation  $\log k_2 = \alpha + \beta (\text{pKa}' + 4) + \gamma (\theta - \theta_{\text{th}})\lambda$ , and they gave excellent fits to the equation characterized by RMSD and  $R^2$  values, which are 0.07 and 0.08; 0.994, and 0.98, respectively. Over 50 sets of data of complex systems of different metal carbonyls have been analyzed successfully in this way, thus demonstrating the validity of the model and of the electronic and steric parameters used.

The kinetic parameters SR,  $\beta$ ,  $\gamma$ , and  $\theta_{\text{th}}$ , derived from this analysis, imply that the cluster  $\text{Ru}_3(\text{CO})_{11}\text{PMe}_3$  is much more reactive coupled with a relatively lower degree of M...P bond making, and less flexible in the TS than  $\text{Ru}_3(\text{CO})_{11}\text{etpb}$ . The low flexibility of TSI of  $\text{Ru}_3(\text{CO})_{11}\text{PMe}_3$  indicates that further opening up of the cluster is difficult when the steric threshold is exceeded, which may be related to its congested TSI although its readiness to create a rather well-defined open space during the approach of a nucleophile is relatively a facile process.

The standard reactivity SR, the steric threshold  $\theta_{\text{th}}$ , where steric effects begin to be apparent, the susceptibility  $\beta$  of a carbonyl to the  $\sigma$ -basicity of nucleophiles, and the sensitivity  $\gamma$  of rates to the size of nucleophiles when  $\theta > \theta_{\text{th}}$ , characterize the dynamic nature of each cluster by its responses to the electronic and steric natures of nucleophiles. Associative reactions of clusters may generally be allowed because of their ability to adjust to the approach of a

nucleophile by breaking one of their M–M bonds, so avoiding an excessive electron count. It is also possible to study the effects of P-donor substituents on the susceptibility of the clusters towards the electronic and steric natures of the nucleophiles just as substituent effects on dissociative reactions can be studied. An inverse correlation between standard reactivity and extent of bond making required in the TS is found. An earlier onset of steric effects would be expected as the degree of bond-making become more pronounced for a constant size of opening in the TSI, and vice versa.

## REFERENCES FOR CHAPTER 2

- [1] N.M.J. Brodie Ph.D. Thesis, University of Toronto, 1989.
- [2] L. Chen, Ph.D. Thesis, University of Toronto, 1991.
- [3] C.A. Streuli, *Anal. Chem.* 31(1959)1652; 32(1960)985.
- [4] W.A. Henderson and C.A. Streuli, *J. Am. Chem. Soc.* 82(1960)5791
- [5] T. Allman and R.G. Goel, *Can. J. Chem.*, 60(1982)716.
- [6] M.M. Rahman, H.Y. Liu, K.Eriks, A. Prock, and W.P. Giering, *Organometallics*, 8(1989)1, and references therein.
- [7] C.A. Tolman, *Chem. Rev.*, 77(1977)313.
- [8] C.A. Tolman, *J. Am. Chem. Soc.*, 92(1970)2956.
- [9] C.G. Swain, M.S. Swain, and L.F. Berg, *J. Chem. Inf. Comp. Sci.*, 20(1980)47.
- [10] L. Chen, and A.J. Poë, *Can. J. Chem.*, 67(1989)1924.
- [11] (a) D.J. Darensbourg and B.J. Baldwin-Zuschke, *J. Am. Chem. Soc.*, 104(1982)3906.  
(b) D.J. Darensbourg and M.J. Incorvia, *J. Organomet. Chem.*, 171(1979)89.  
(c) D.J. Darensbourg, *Inorg. Chem.*, 19(1980)2585.  
(d) D.J. Darensbourg, B.S. Peterson, and R.E. Schmidt Jr. *Organometallics*, 1(1982)306.  
(e) D.J. Darensbourg, D.J. Zalewski, and T. Delord, *Organometallics*, 3(1984)1210.  
(f) D.J. Darensbourg, and D.J. Zalewski, *Organometallics*, 4(1985)92.
- [12] N.M.J. Brodie and A.J. Poë, *Can. J. Chem.*, 73(1995)1187.

- [13] A.J. Poë and M.V. Twigg, *J. Chem. Soc., Dalton Trans.*, (1974)1860.
- [14] S. Malik and A.J. Poë, *Inorg. Chem.* 17(1978)1484.
- [15] N.M.J. Brodie, A.J. Poë, and V.C. Sekhar, *J. Chem. Soc. Chem. Commun.*, (1985)1090.
- [16] J. Hao, unpublished work.
- [17] G. Bodner, M. May, and L. McKinney, *Inorg. Chem.* 19(1980)1951.
- [18] S.K. Malik and A.J. Poë, *Inorg. Chem.* 18(1979)1241.
- [19] A.J. Poë, C.N. Sampson, and C.V. Sekhar, *Inorg. Chem.* 26(1986)1057.
- [20] K.L. Chalk and R.K. Pomeroy, *Inorg. Chem.* 23(1984)444.
- [21] A.J. Poë and V.C. Sekhar, *Inorg. Chem.*, 24(1985)4376.
- [22] J.A.S. Howell and P.M. Birkinshaw, *Chem. Rev.* 83(1983)557.
- [23] F. Basolo and R.G. Pearson, Mechanisms of Inorganic Reactions, Wiley, New York, 2nd ed. 1967.
- [24] A.J. Poë in Reactivity of Metal-Metal Bonds, M.H. Chisholm (Ed.), American Chemical Society, Washington, D.C., 1981, ACS Symp. Ser. No. 155, Chapter 7.
- [25] (a) D.C. Sonnenberger and J.D. Atwood, *J. Am. Chem. Soc.*, 104(1982)2113.
- (b) W. Linert and R.F. Jameson, *Chem. Soc. Rev.*, 18(1989)477; W. Linert, *Chem. Soc. Rev.*, (1994)429; W. Linert, *Inorg. Chim. Acta.*, 141(1988)233.
- [26] L.Chen and A.J. Poë, *Inorg. Chem.*, 28(1989)3641.
- [27] J.M. Hanckel, K.W. Lee, P. Rushman, and T.L. Brown, *Inorg. Chem.*, 25(1986)1852, and references therein.

- [28] P.R. Bevington, Data Reduction and Error Analysis for the Physical Sciences, McGraw-Hill, Toronto, (1969) p.172.
- [29] N.M.J. Brodie, L. Chen, A.J. Poë, and J.F. Sawyer, *Acta Cryst.* C45(1989)1314.
- [30] K. Dahlinger, F. Falcone and A.J. Poë, *Inorg. Chem.*, 25(1986)2654.
- [31] M.N. Golovin, M.M. Rahman, J.E. Belmonte and W.P. Giering, *Organometallics*, 4(1985)1981.
- [32] A.J. Poë, D.H. Farrar and Y. Zheng, *J. Am. Chem. Soc.*, 114(1992)5146.
- [33] N.M.J. Brodie, L. Chen, and A.J. Poë, *Int. J. Chem. Kin.*, 20(1988)467
- [34] L. Chen, and A.J. Poë, *Coord. Chem. Rev.*, 143(1995)265.
- [35] (a) Prof. A.J. Poë 's original manuscript of reference [34].  
(b) T. Bartik, T. Himmler, H.G. Schulte, and K. Seevogel, *J. Organomet. Chem.*, 272(1984)29.
- [36] M.M. Rahman, H.Y. Liu, K. Eriks, A. Prock and W.P. Giering, *Organometallics*, 8(1989)1.
- [37] H.Y. Liu, K. Eriks, A. Prock and W.P. Giering, *Organometallics*, 9(1990)1758.
- [38] (a) B.F.G. Johnson, *J. Chem. Soc., Chem. Commu.*, (1976)211.  
(b) R.E. Benfield and B.F.G. Johnson, *J. Chem. Soc; Dalton Trans.*, (1978)1554; in Transition Metal Clusters, B.F.G. Johnson(Ed.), Wiley & Sons, Inc., New York, 1981, p.471.
- [39] R.H.E. Hudson and A.J. Poë, *Organometallics*, 14(1995)3238.
- [40] T.H. Brown, *Inorg. Chem.*, 31(1992)1286; T.H. Brown and K.J. Lee, *Coord. Chem. Rev.*, 128(1993)89.

- [41] D. C. Sonnenberger and J. D. Atwood, *J. Am. Chem. Soc.*, 104(1982)2113.
- [42] D. C. Sonnenberger and J. D. Atwood, *Organometallics*, 1(1982)694.
- [43] A. J. Poë, in Metal Clusters, M. Moskovits (Ed.), John Wiley & Sons, Inc., New York, 1986, Chapter 4.
- [44] D.J. Darensbourg, in The Chemistry of Metal Cluster Complexes, D.H. Shriver, H.D. Kaesz and R.D. Adams (Eds), VCH, New York, 1990, Chapter 4.
- [45] N.M.J. Brodie and A.J. Poë, *Inorg. Chem.*, 27(1988)3156.
- [46] A.J. Poë and M.V. Twigg, *J.C.S. Dalton*, (1974)1860.
- [47] (a) R.D. Adams, Y. Chi, D.D. DesMarteau, D. Lentz, and R. Marschall, *J. Am. Chem. Soc.*, 114(1992)1909.
- (b) R.D. Adams, Y. Chi, D.D. DesMarteau, D. Lentz, R. Marschall, and A. Scherrmann, *J. Am. Chem. Soc.*, 114(1992)10822.
- [48] D.H. Farrar, A.J. Poë and Y. Zheng, *J. Am. Chem. Soc.*, 116(1994)6252.
- [49] H. Chen, L. Chen, and A.J. Poë, unpublished work, 1989.

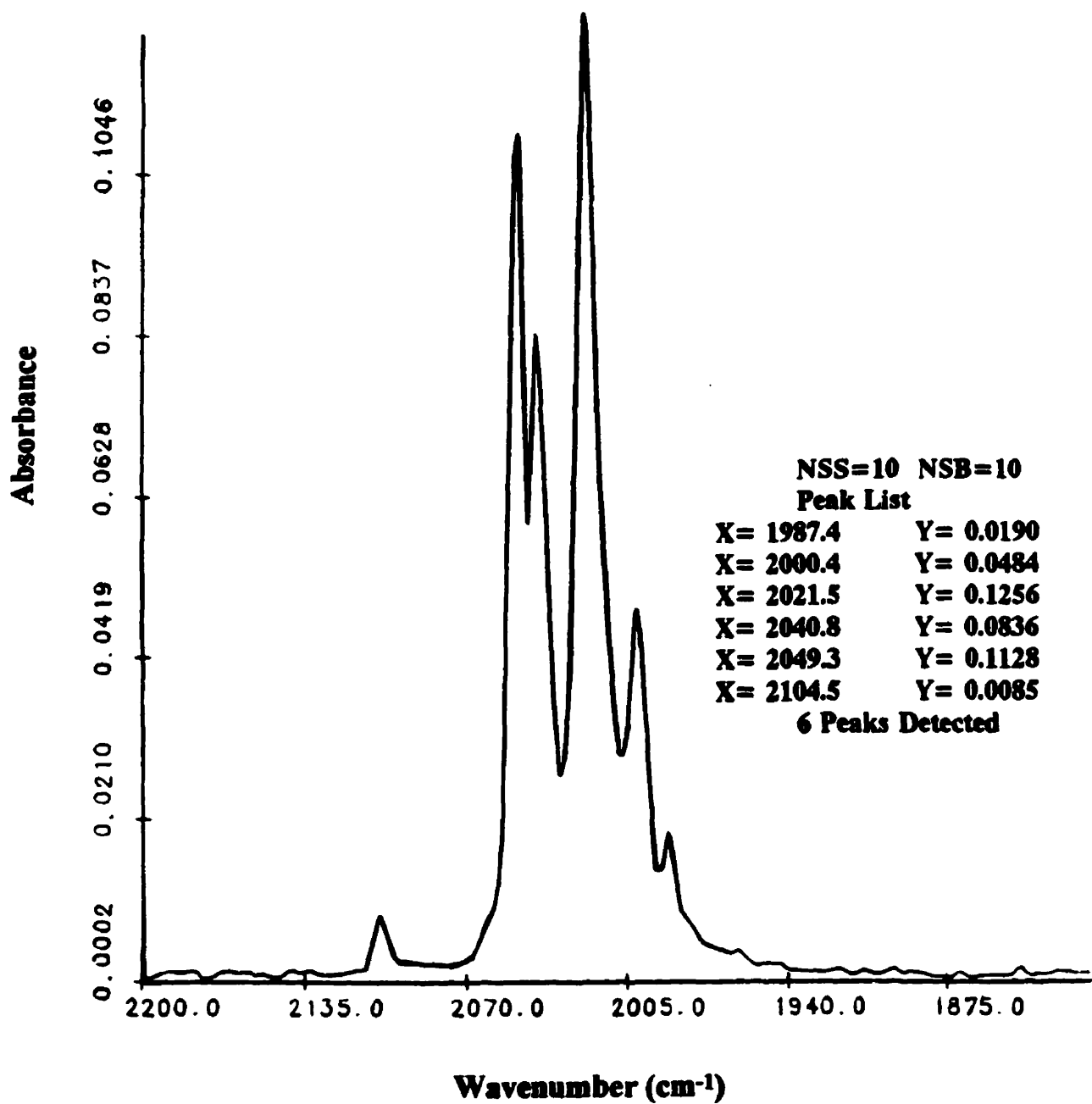


Figure 2.1 FTIR spectrum of pure  $\text{Ru}_3(\text{CO})_{11}\text{etpb}$ .

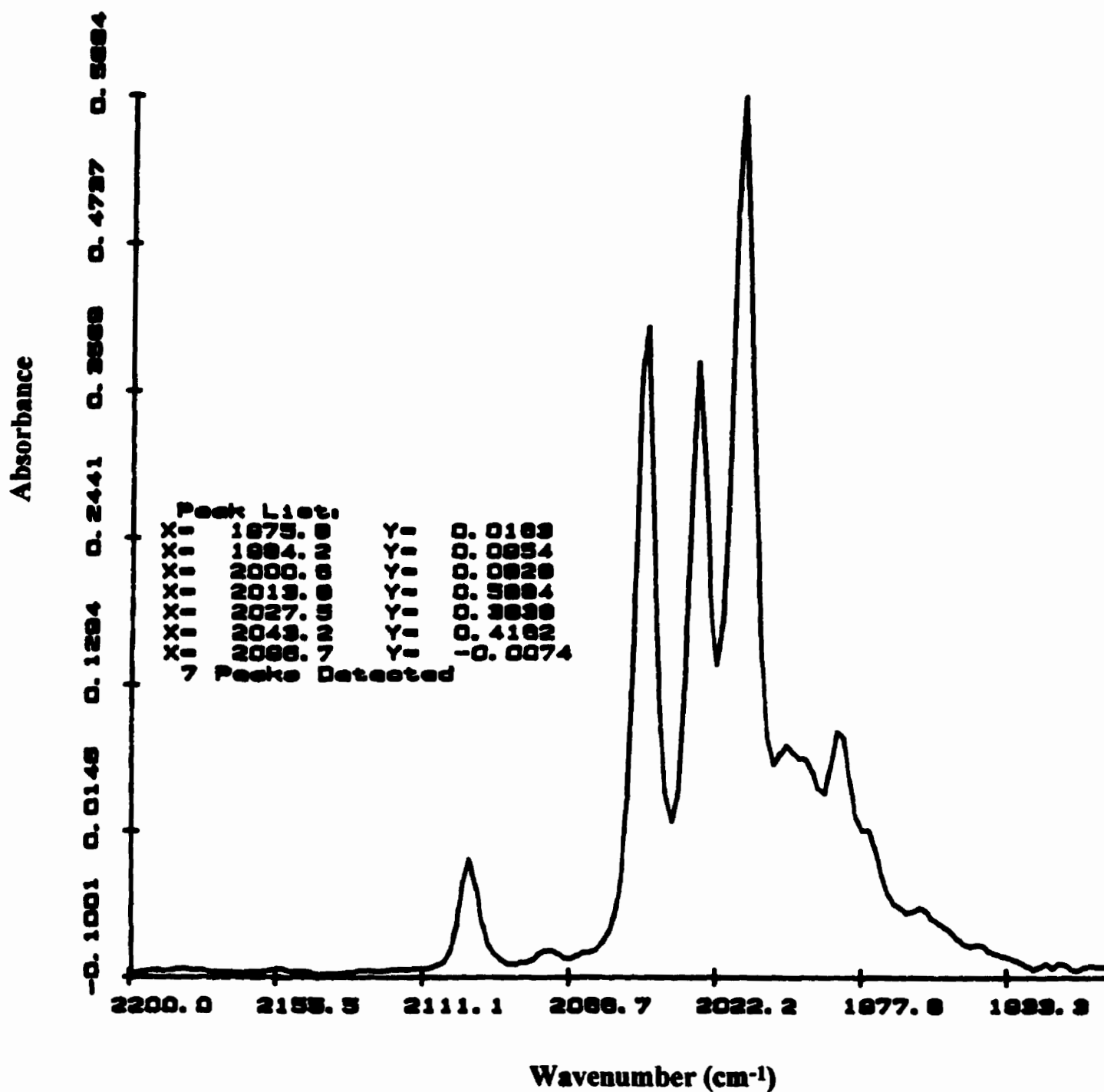


Figure 2.2 FTIR spectrum of pure  $\text{Ru}_3(\text{CO})_{11}\text{PMe}_3$ . Relative intensities are obtained by taking absorbance = -0.1 as the base line.

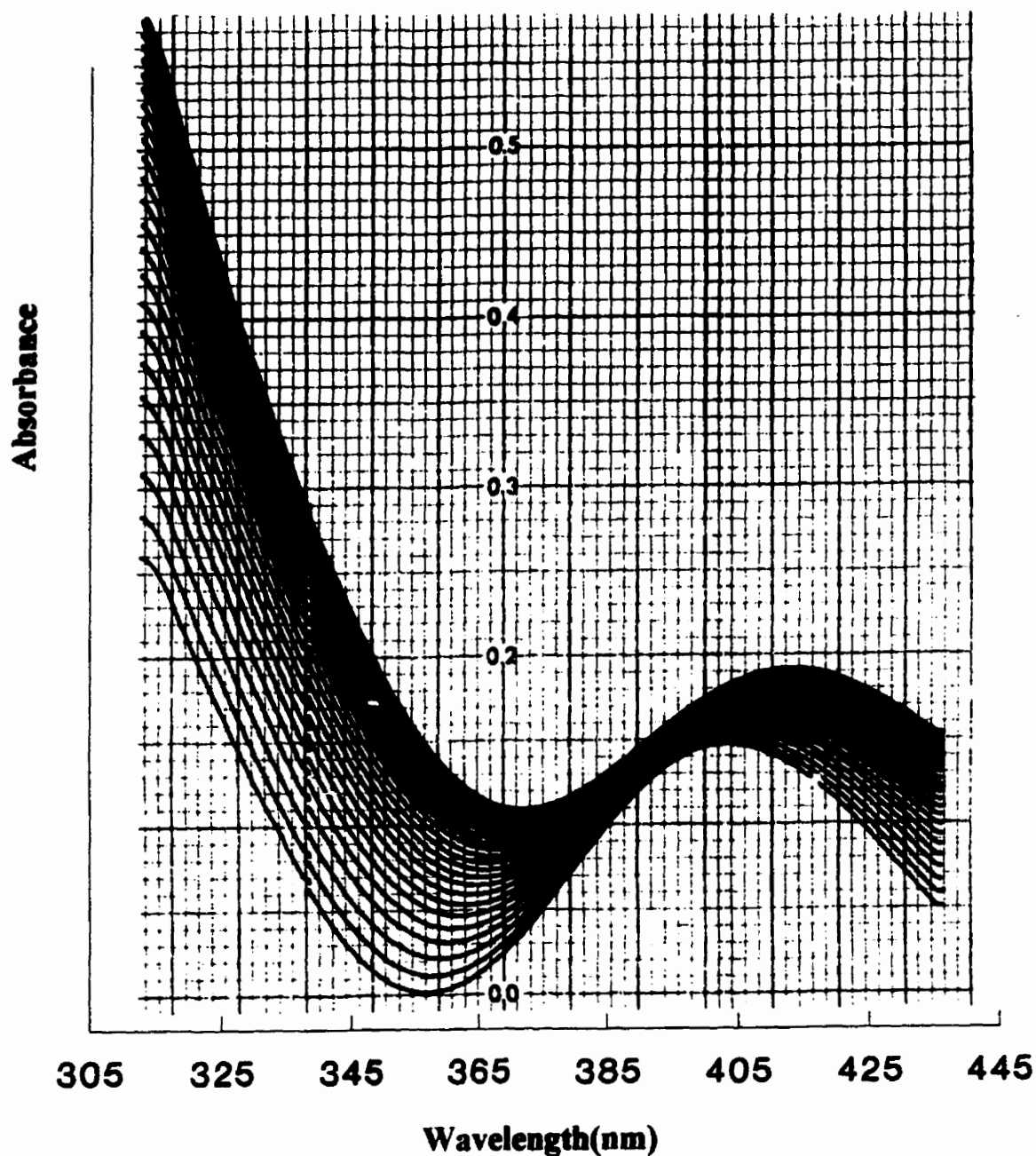


Figure 2.3(a) UV-Vis spectrum changes (Repetitive Scan Mode) during the reaction of  $\text{Ru}_3(\text{CO})_{11}\text{etpb}$  with  $\text{AsPh}_3$  at  $44.8^\circ\text{C}$  in heptane.  $[\text{Complex}] = 2 \times 10^{-5} \text{ M}$ ,  $[\text{L}'] = 0.02423 \text{ M}$ . The product  $\text{Ru}_3(\text{CO})_{10}\text{LL}'$  of the first stage reaction was quite stable under the conditions used, and no evidence for the further reaction of  $\text{Ru}_3(\text{CO})_{10}\text{LL}'$  with  $\text{L}'$  was observed.

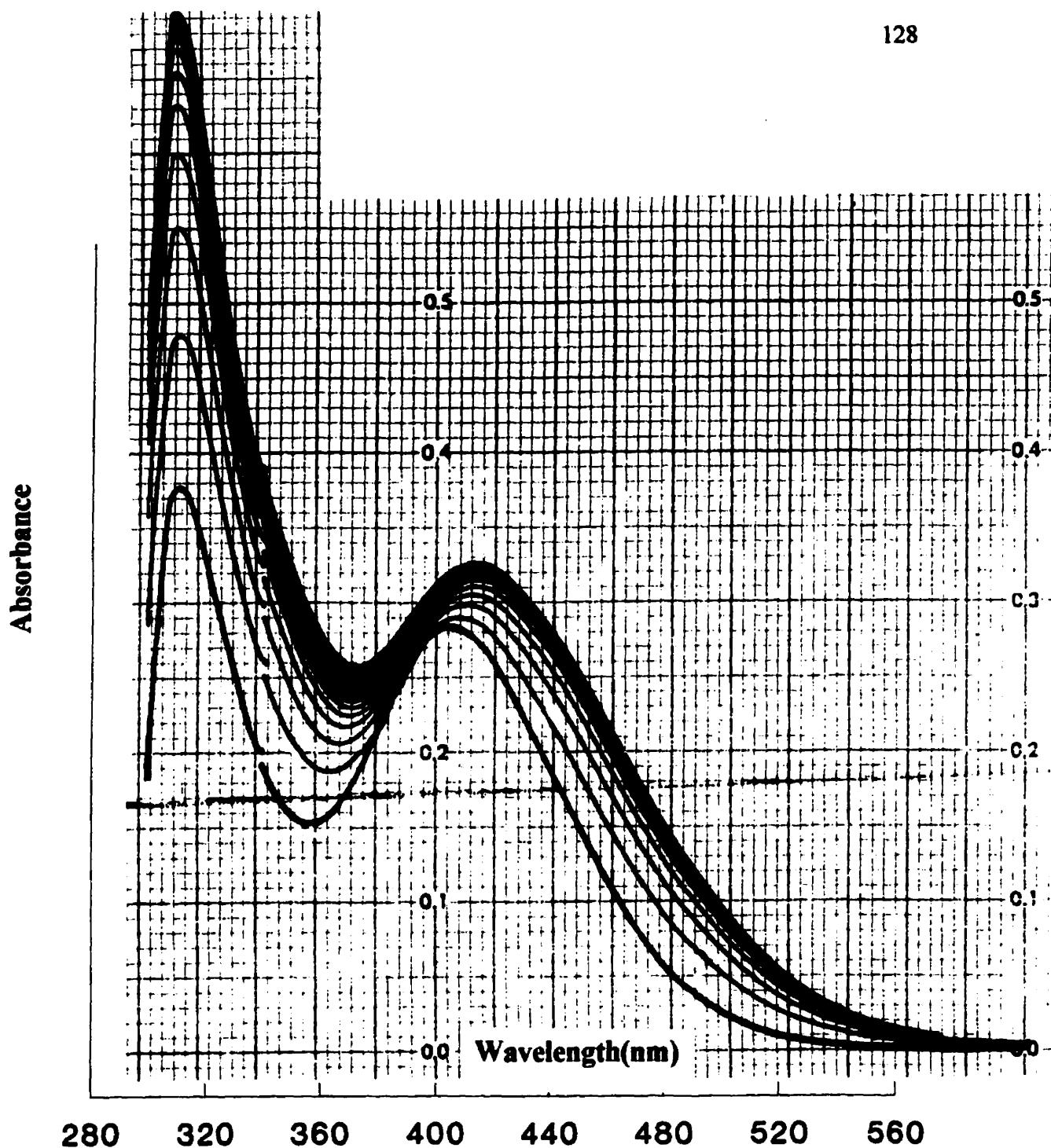


Figure 2.3(b) UV-Vis spectrum changes (Repetitive Scan Mode), over a wider wavelength range than in Figure 2.3(a), during the reaction of  $\text{Ru}_3(\text{CO})_{11}\text{etpb}$  with  $\text{AsPh}_3$  in heptane at  $54.3^\circ\text{C}$ .  $[\text{Complex}] = 2 \times 10^{-5} \text{ M}$ ,  $[\text{L}] = 0.03231 \text{ M}$ . Cycle time = 20 min, cycle number = 32, running for over 10 hrs.

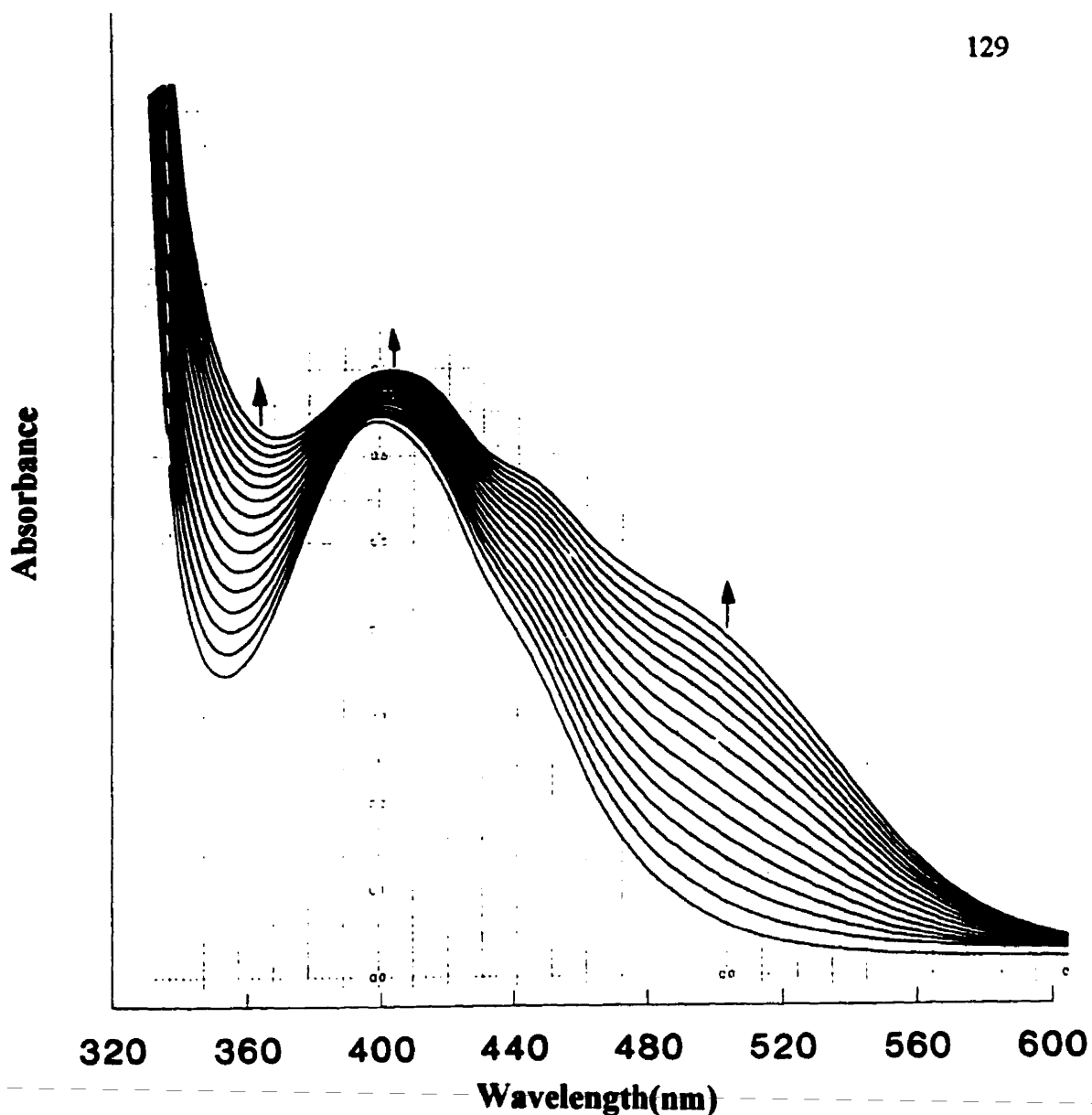


Figure 2.3(c) UV-Vis spectrum changes (Repetitive Scan Mode) during the reaction of  $\text{Ru}_3(\text{CO})_{11}\text{etpb}$  with  $\text{PPh}_3$  at RT in heptane.  $[\text{Complex}] = 2 \times 10^{-5} \text{ M}$ ,  $[\text{L}] = 0.1050 \text{ M}$ . Cycle time = 200 min, cycle number = 16, running for over 50 hrs.

The first stage reaction has not gone to completion although being run for over 50 hrs. Based on monitoring of the reaction at  $53.9^\circ\text{C}$ , it is very clear that the absorbance decreased during the second stage reaction after an increase during the first stage reaction.

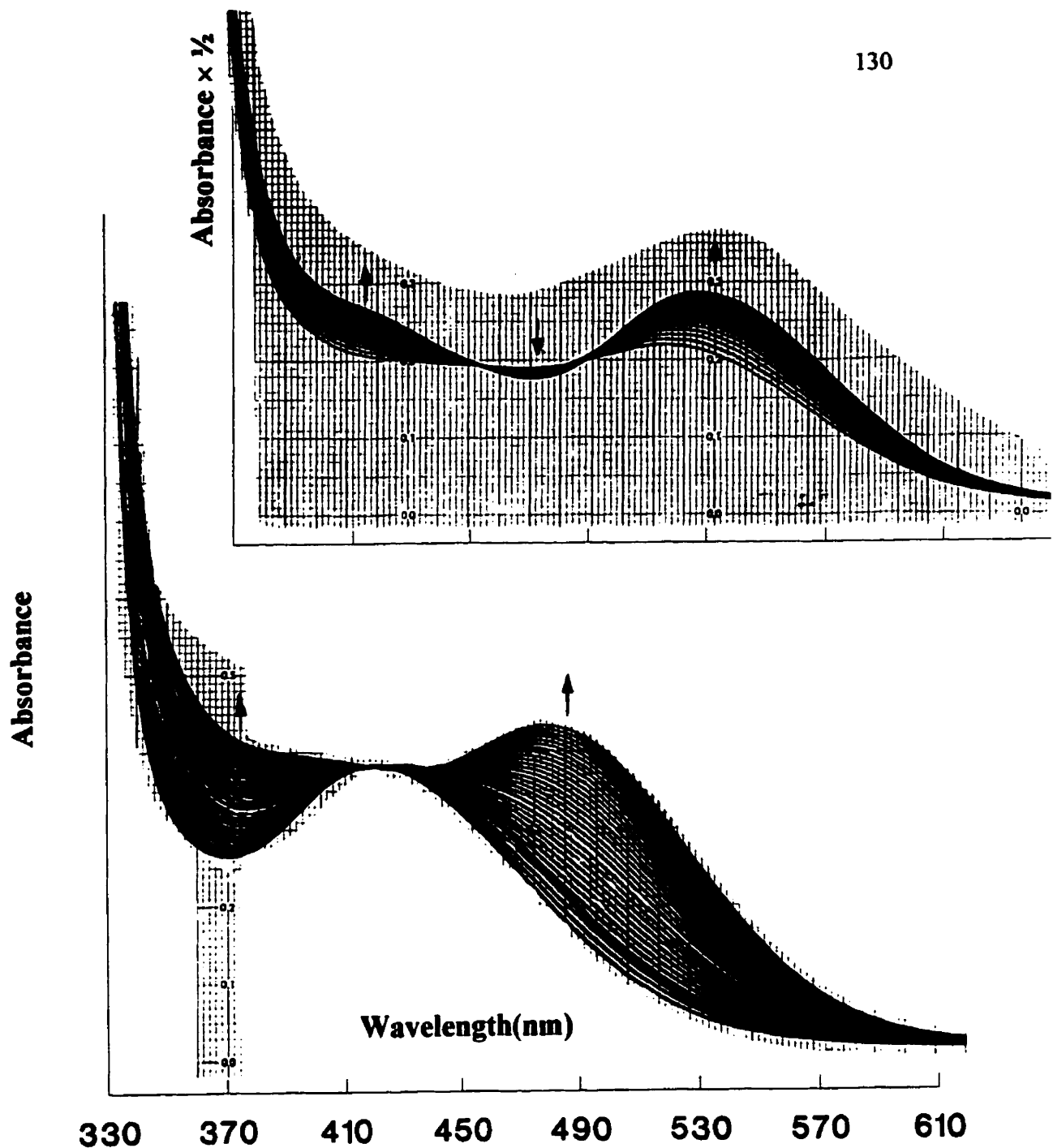
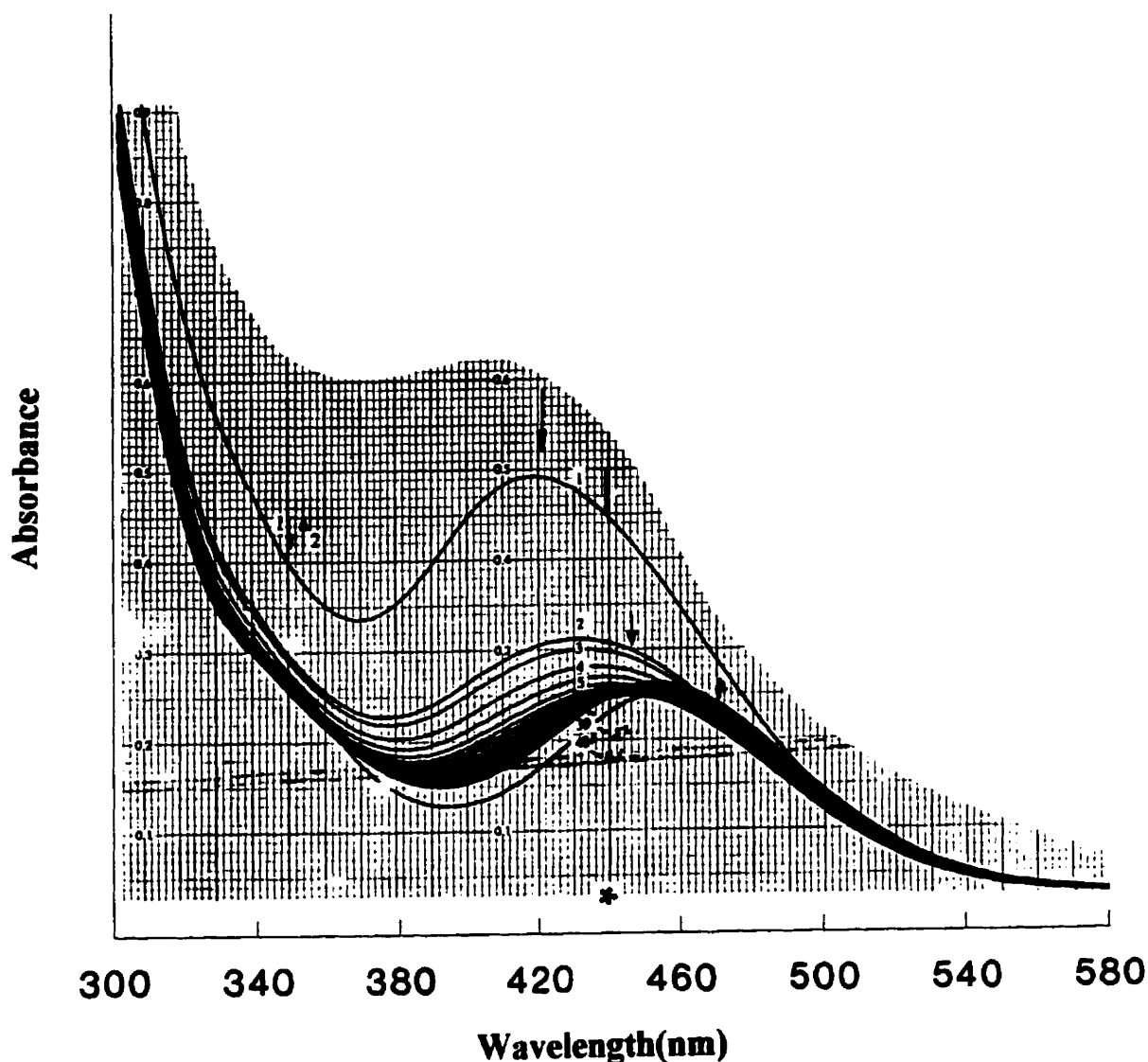


Figure 2.3(d) UV-Vis spectrum changes (Repetitive Scan Mode) during the reaction of  $\text{Ru}_3(\text{CO})_{11}\text{PMe}_3$  with  $\text{PPh}_3$  at  $25.15^\circ\text{C}$  in heptane.  $[\text{Complex}] = 3 \times 10^{-5} \text{ M}$ ,  $[\text{L}'] = 0.06489 \text{ M}$ .

Cycle time = 10 min, cycle number 33, running for the first 5.5 hrs (the bottom figure). Cycle time = 30 min, cycle number 28, running for the last 14 hrs (the upper figure).



**Figure 2.4** UV-Vis spectrum changes (Repetitive Scan Mode) during the reaction of  $\text{Ru}_3(\text{CO})_{11}\text{PMe}_3$  with  $\text{P}(\text{O}-i\text{-Pr})_3$  in heptane at  $25.15^\circ\text{C}$ .  $[\text{Complex}] = 3 \times 10^{-5} \text{ M}$ ,  $[\text{L}'] = 0.4101 \text{ M}$ . Cycle 1-9 = 40 min, cycle 9-40 = 16 hrs. The second stage of reaction, i.e.  $\text{Ru}_3(\text{CO})_{10}\text{LL}'$  with  $\text{L}'$ , was observed, but there was a very clean isosbestic point at 438 nm. A good value of  $A_{\infty}$  for the first stage reaction can still be obtained by following the absorbance change at the isosbestic point.

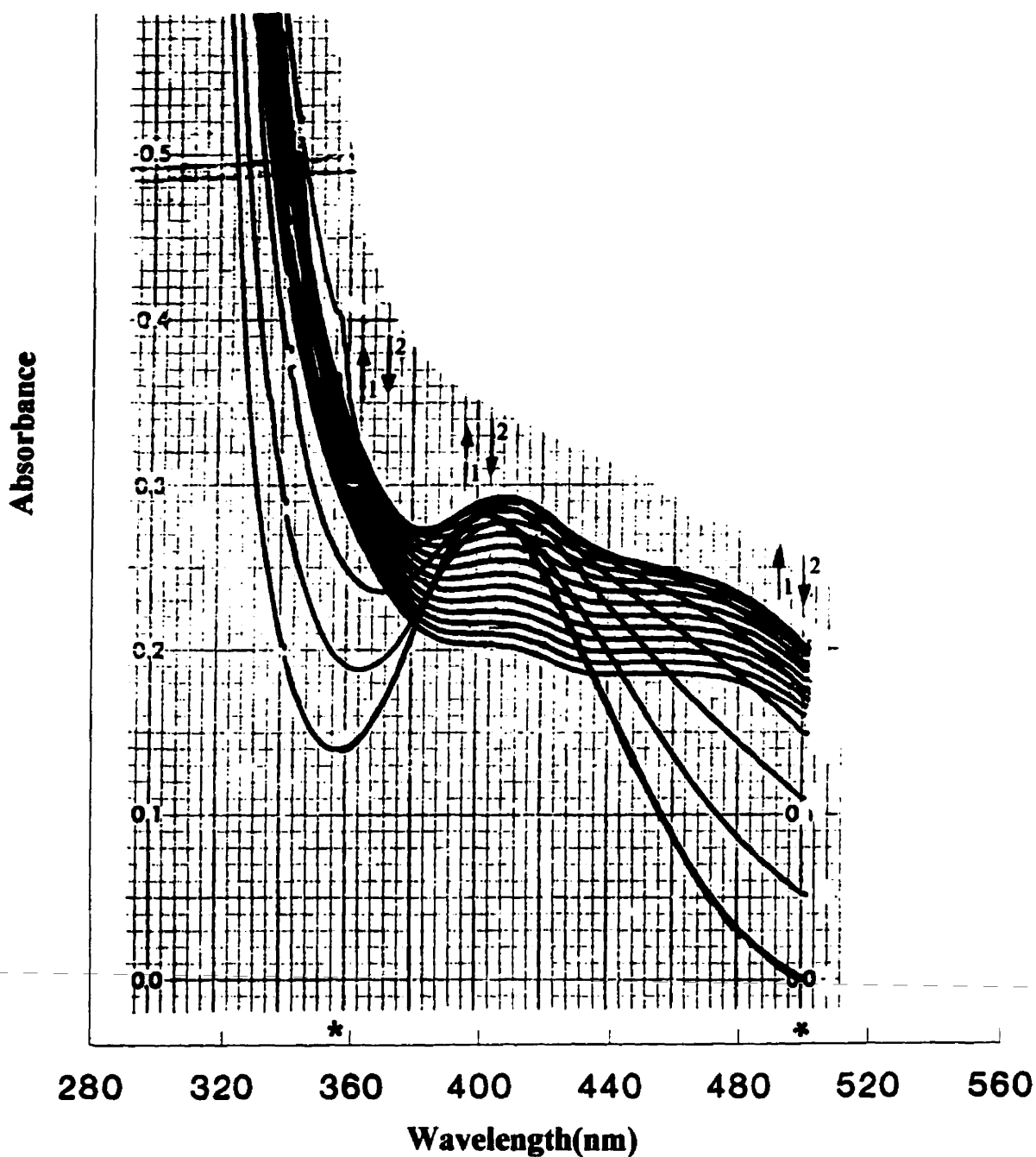


Figure 2.5 UV-Vis spectrum changes (Repetitive Scan Mode) during the reaction of  $\text{Ru}_3(\text{CO})_{11}\text{etpb}$  with  $\text{PPh}_3$  at  $53.9^\circ\text{C}$  in heptane.  $[\text{Complex}] = 2 \times 10^{-5}\text{ M}$ ,  $[\text{L}] = 0.05408\text{ M}$ . Cycle time = 20 min, cycle 1-7 for 2 hrs, cycle 7-18 for 4 hrs.

It is very clear that the absorbance of the first stage reaction increased, and then one of the second stage reaction decreased.

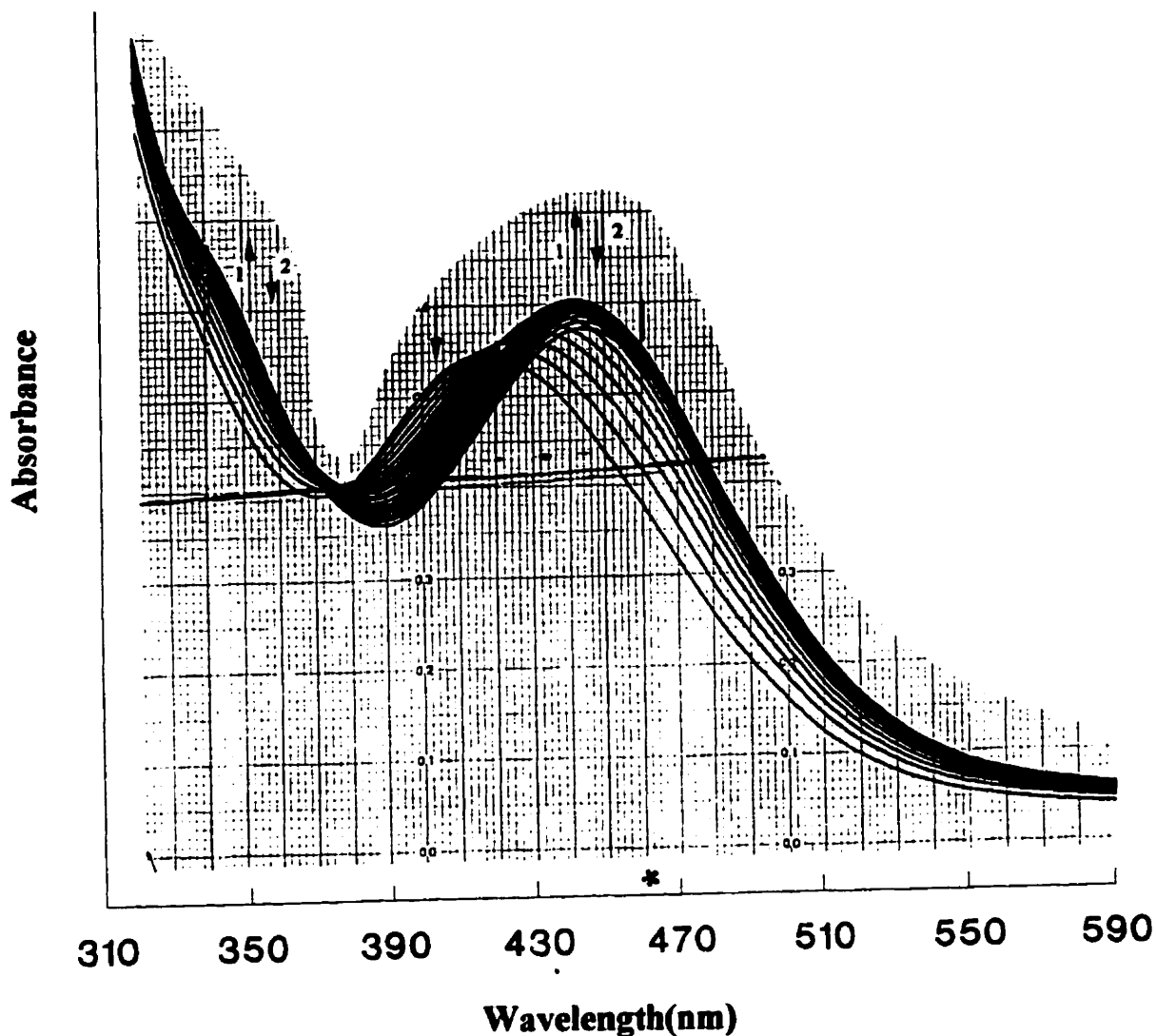
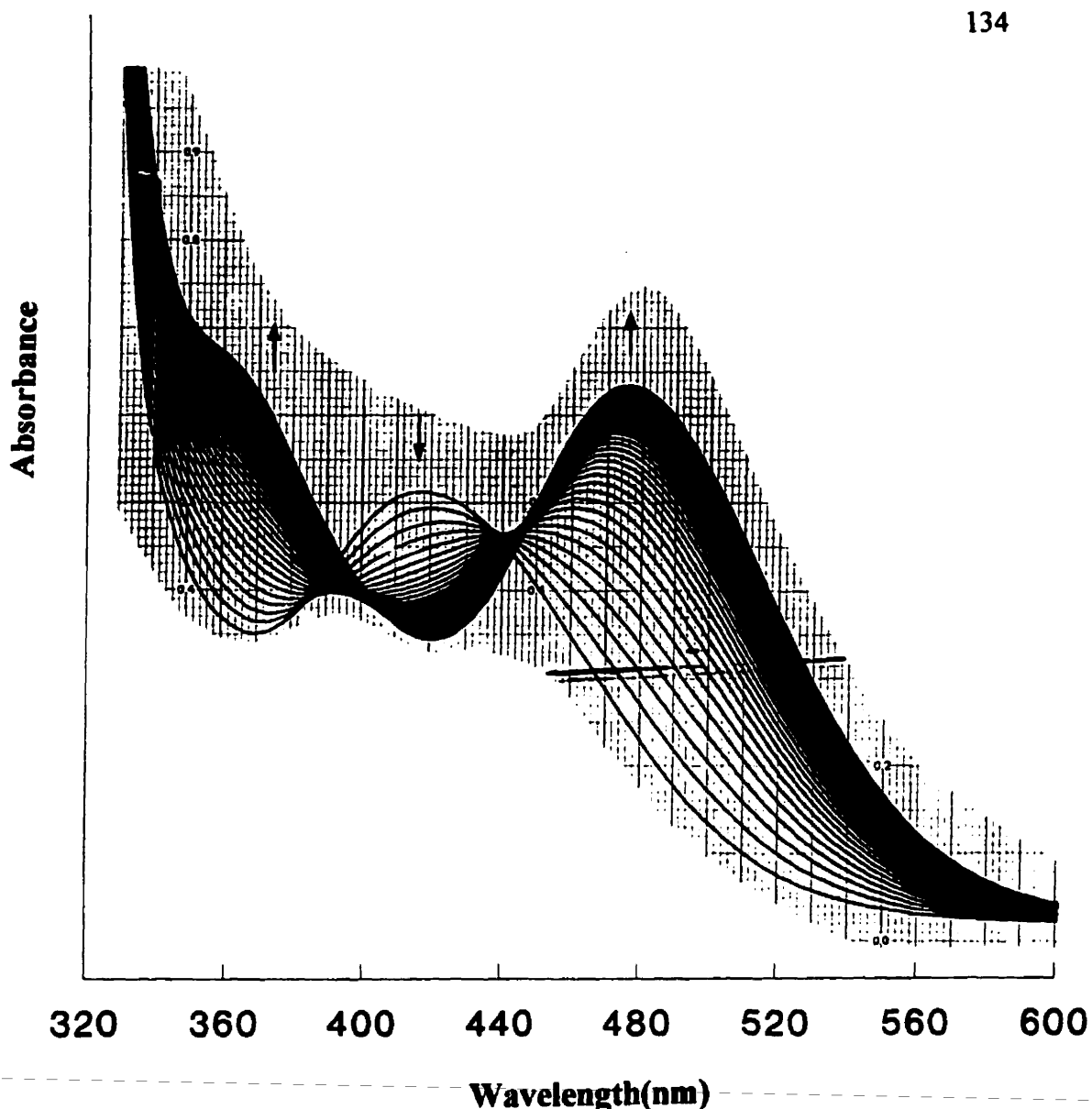
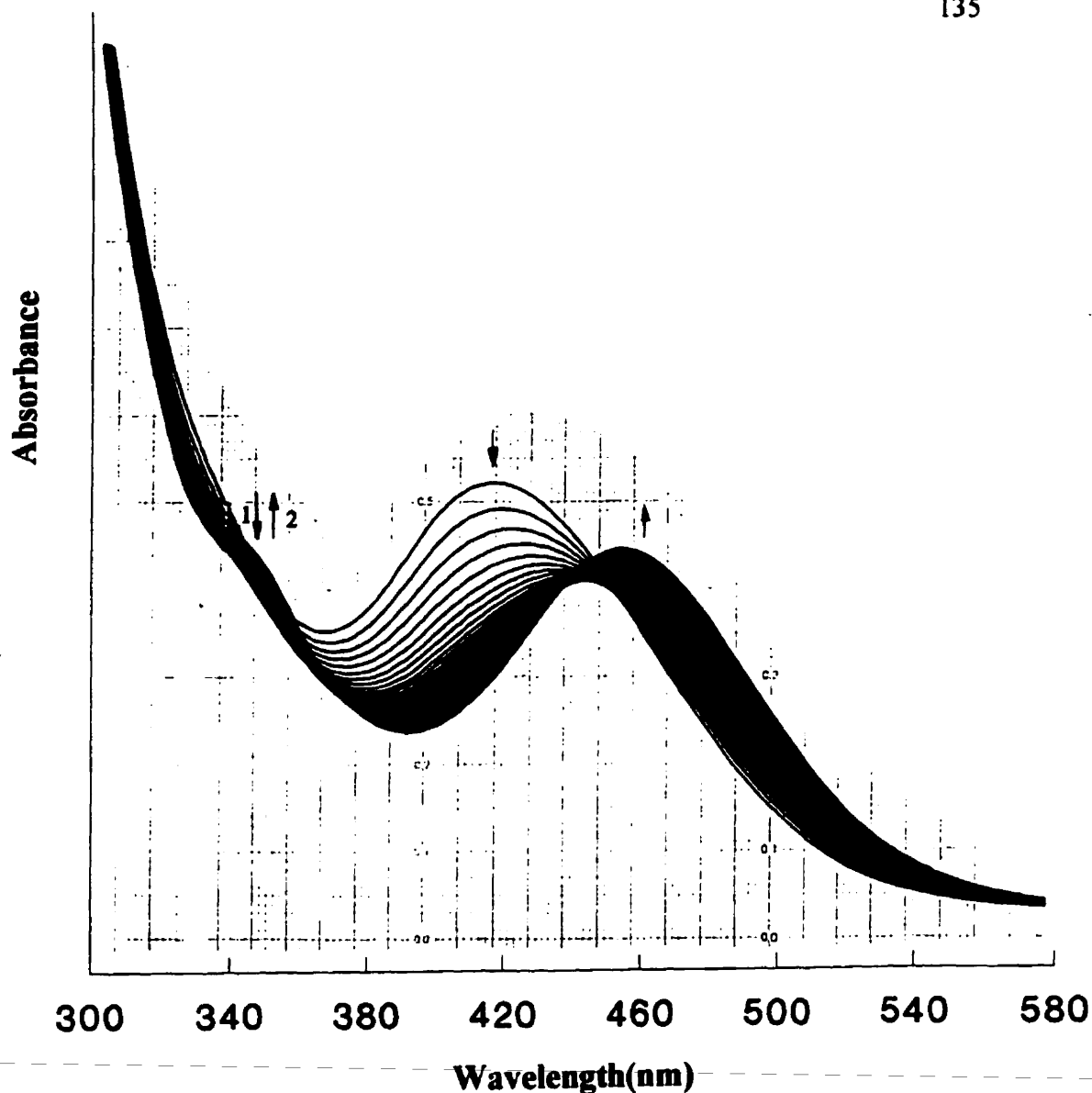


Figure 2.6 UV-Vis spectrum changes (Repetitive Scan Mode) during the reaction of  $\text{Ru}_3(\text{CO})_{11}\text{PMe}_3$  with  $\text{P}(\text{OPh})_3$  at  $25.15^\circ\text{C}$  in heptane.  $[\text{Complex}] = 3 \times 10^{-5} \text{ M}$ ,  $[\text{L}'] = 0.2879 \text{ M}$ . Cycle time = 60 min, cycle number = 18, running for 18 hrs.

The isobestic point at 378 nm consists of only 9 spectra, which means the second stage reaction affected the spectra quite early on. But it is very clear that when  $\lambda \geq 458 \text{ nm}$ , the spectroscopic changes due to the second stage reaction are very small, and quite big due to the first stage reaction. Therefore a good result can be obtained by measuring the increase in absorbance at 458 nm.



**Figure 2.7** UV-Vis spectrum changes (Repetitive Scan Mode) during the reaction of  $\text{Ru}_3(\text{CO})_{11}\text{PMe}_3$  with  $\text{PPh}_2\text{Et}$  at  $25.15^\circ\text{C}$  in heptane.  $[\text{Complex}] = 3 \times 10^{-5} \text{ M}$ ,  $[\text{L}'] = 0.2606 \text{ M}$ . Cycle time = 30 min, running for 20 hrs. It is very clear that a satisfactory value of  $A_\infty$  for the first stage reaction could not be provided by the UV-Vis technique. Although the wavelength at ca. 400 nm is a suitable one to be monitored, the absorbance changes due to the first stage reaction are not big enough (See Text).



**Figure 2.8** UV-Vis spectrum changes (Repetitive Scan Mode) during the reaction of  $\text{Ru}_3(\text{CO})_{11}\text{PMe}_3$  with  $\text{P}(\text{O}-i\text{-Pr})_3$  at  $25.1^\circ\text{C}$  in heptane.  $[\text{Complex}] = 3 \times 10^{-5} \text{ M}$ ,  $[\text{L}'] = 0.06835 \text{ M}$ . Cycle time = 20 min, running for 20 hrs. It is evident that a satisfactory value of  $A_\infty$  for the first stage reaction could not be obtained by the UV-Vis technique. Although the wavelength at ca. 435 nm is a suitable one to be followed, the absorbance changes due to the first stage reaction are too small.

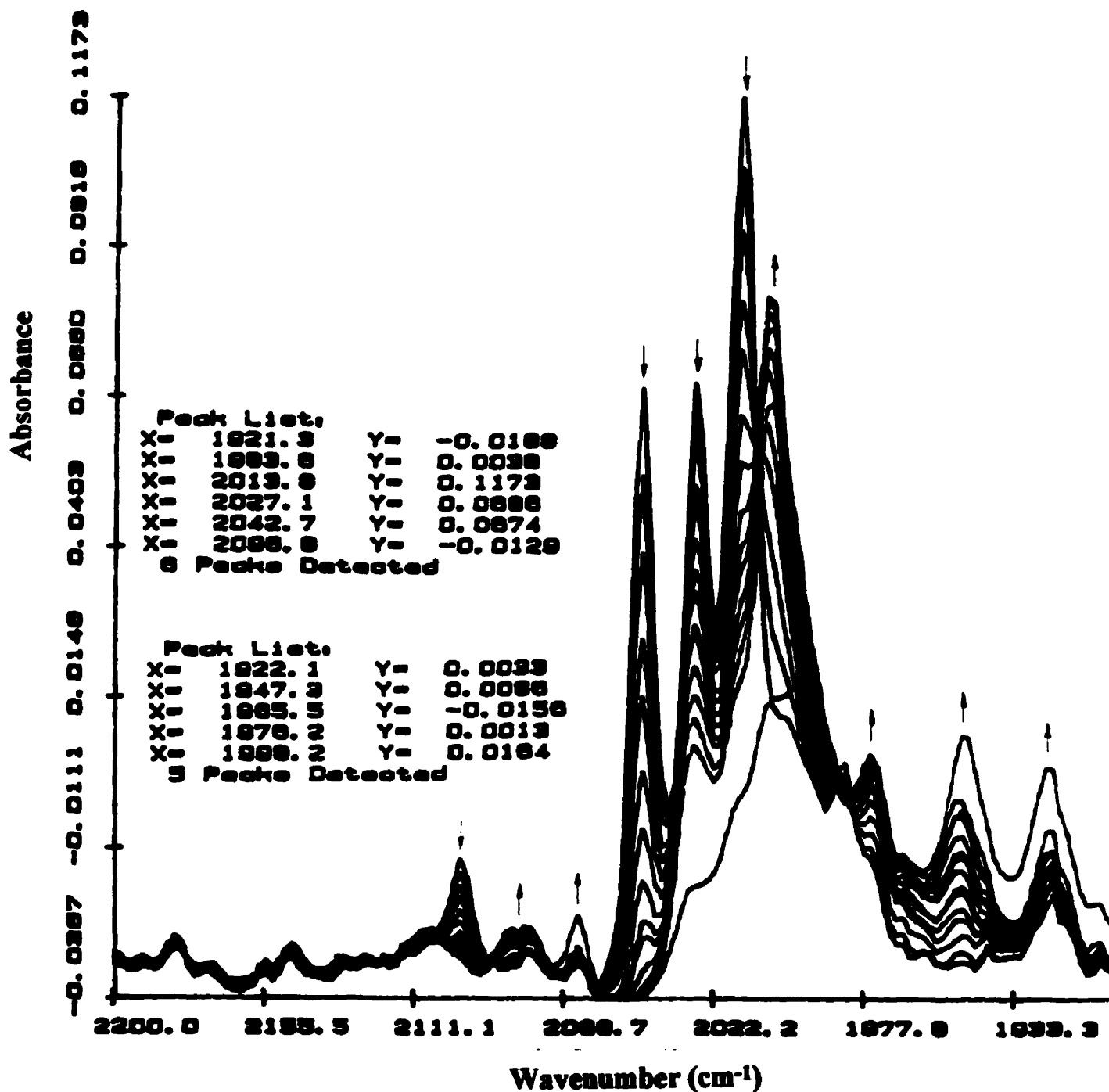


Figure 2.9 FTIR spectrum changes during the reaction of  $\text{Ru}_3(\text{CO})_{11}\text{PMe}_3$  with etpb at  $25.0^\circ\text{C}$  in heptane.  $[\text{Complex}] = 1 \times 10^{-4} \text{ M}$ ,  $[\text{L}'] = 0.02650 \text{ M}$ .

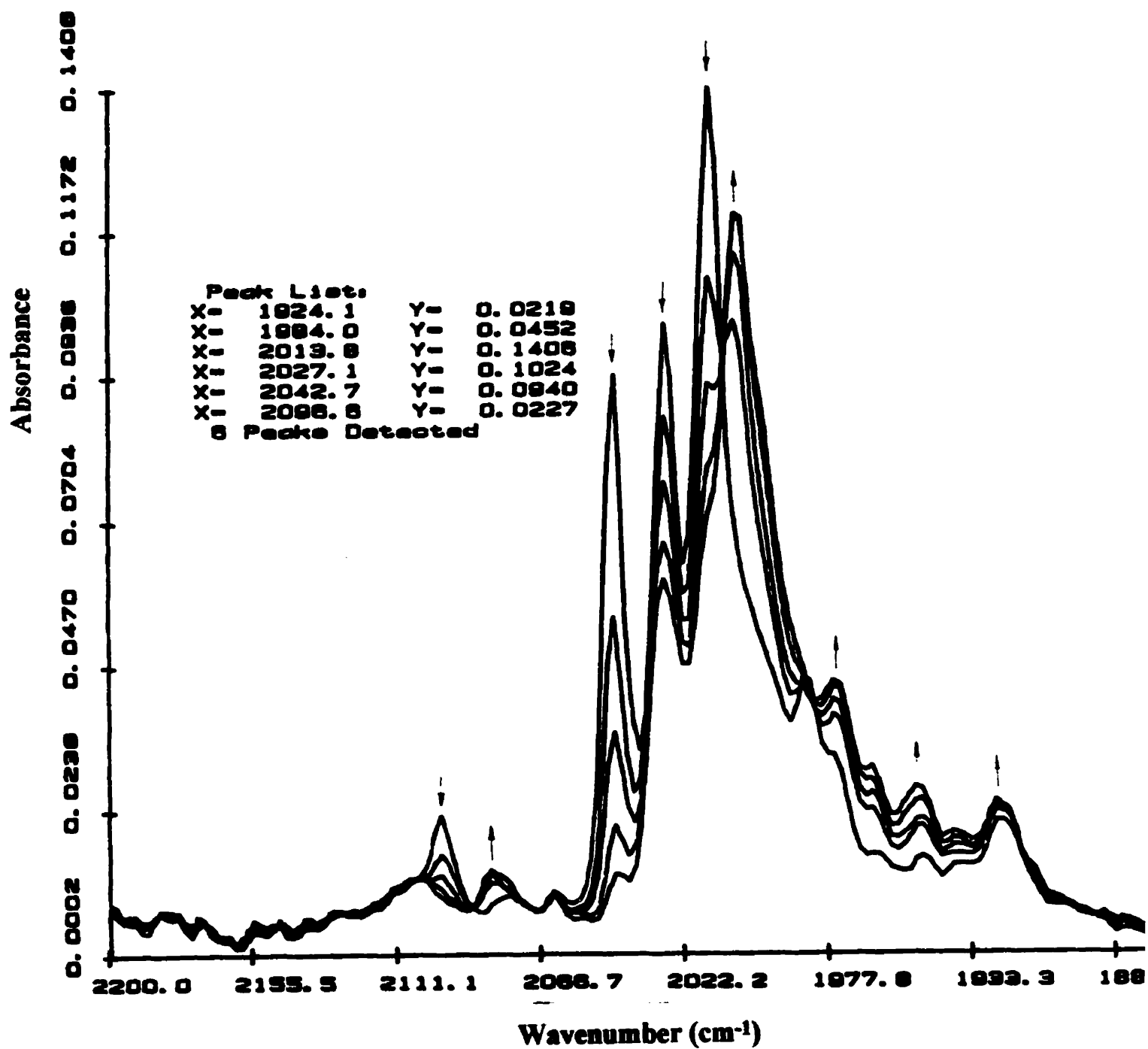


Figure 2.10 FTIR spectrum changes during the reaction of  $\text{Ru}_3(\text{CO})_{11}\text{PMe}_3$  with etpb at  $40.0^\circ\text{C}$  in heptane.  $[\text{Complex}] = 1 \times 10^{-4} \text{ M}$ ,  $[\text{L}'] = 0.03113 \text{ M}$ .

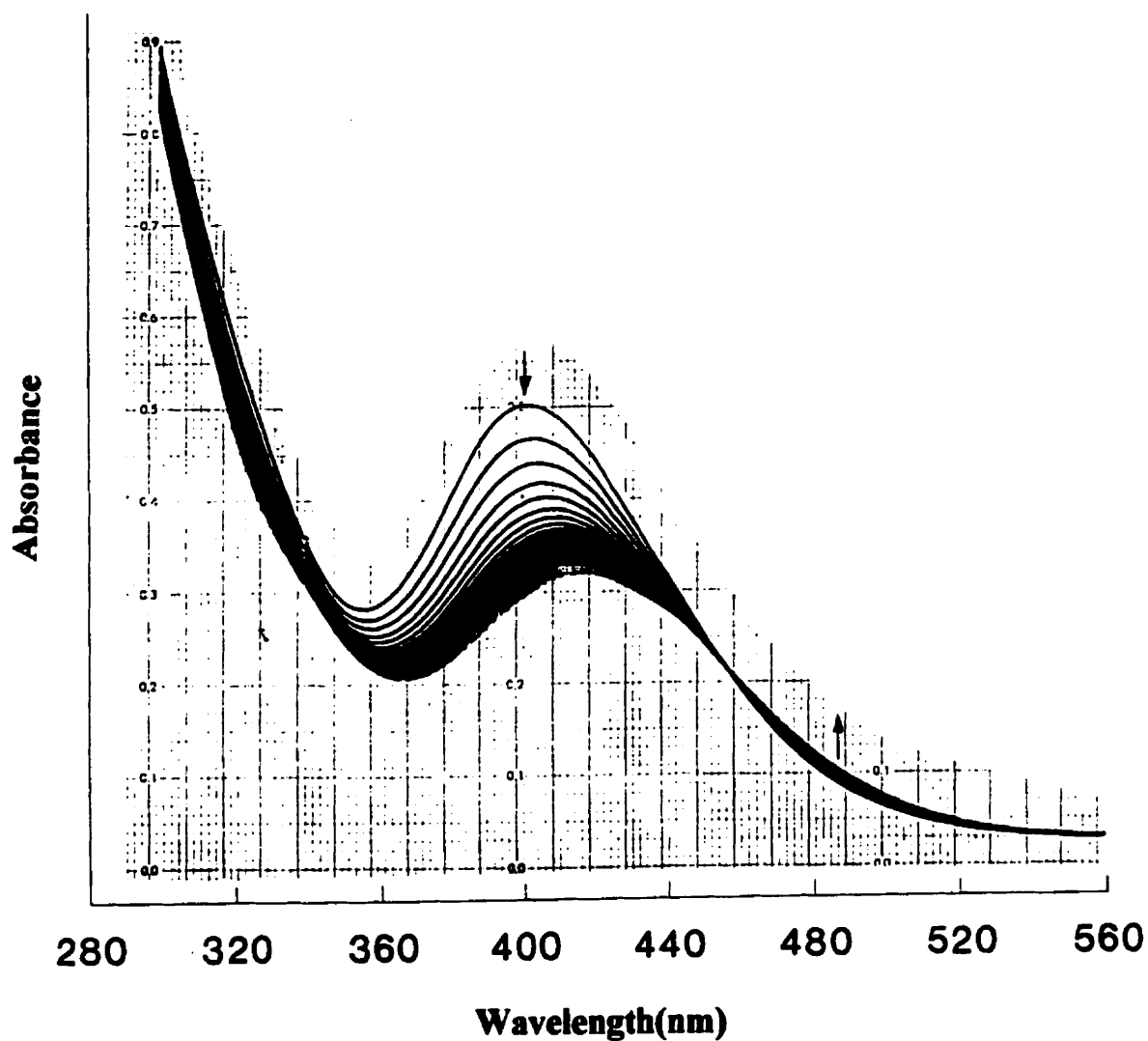
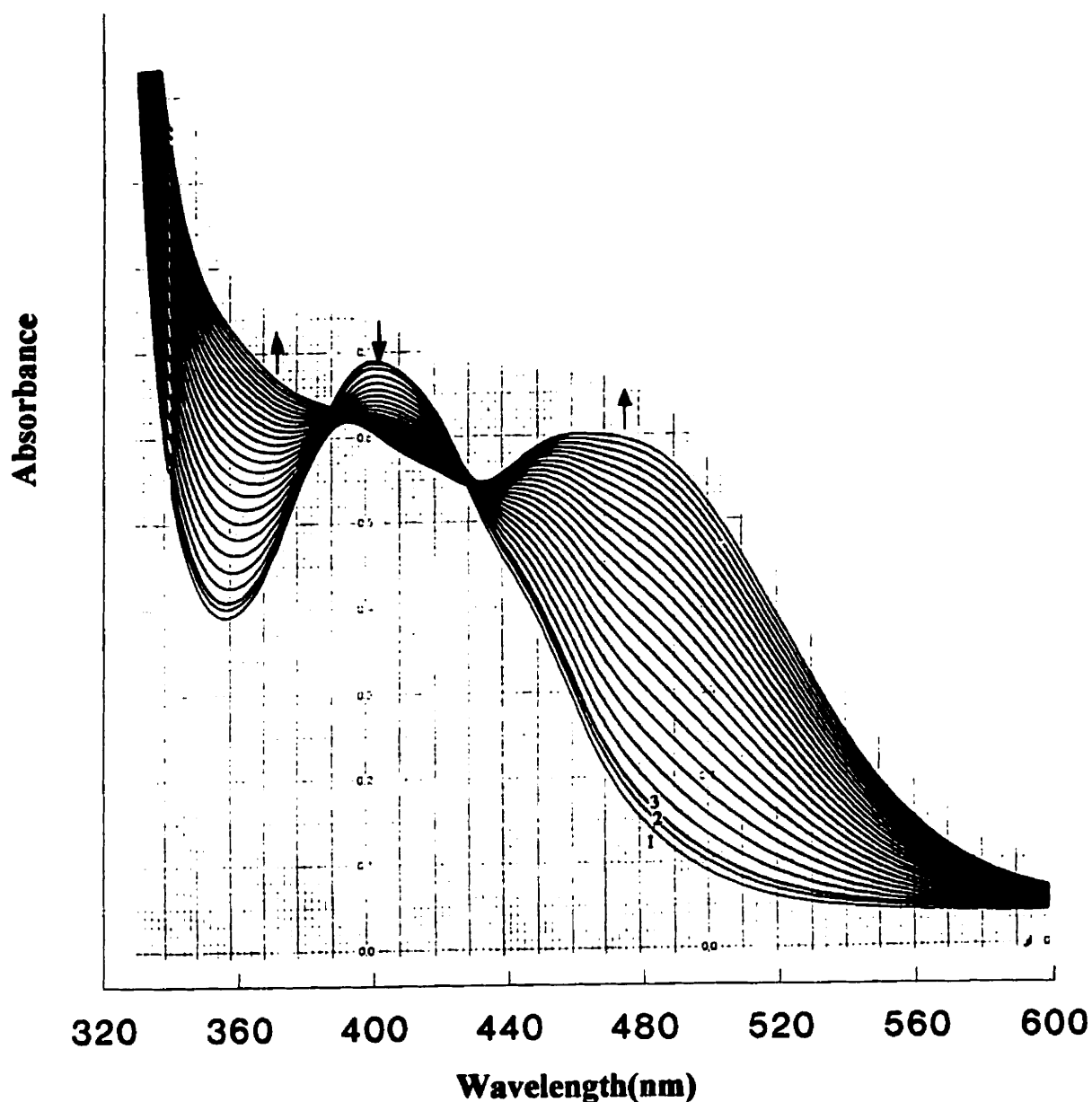
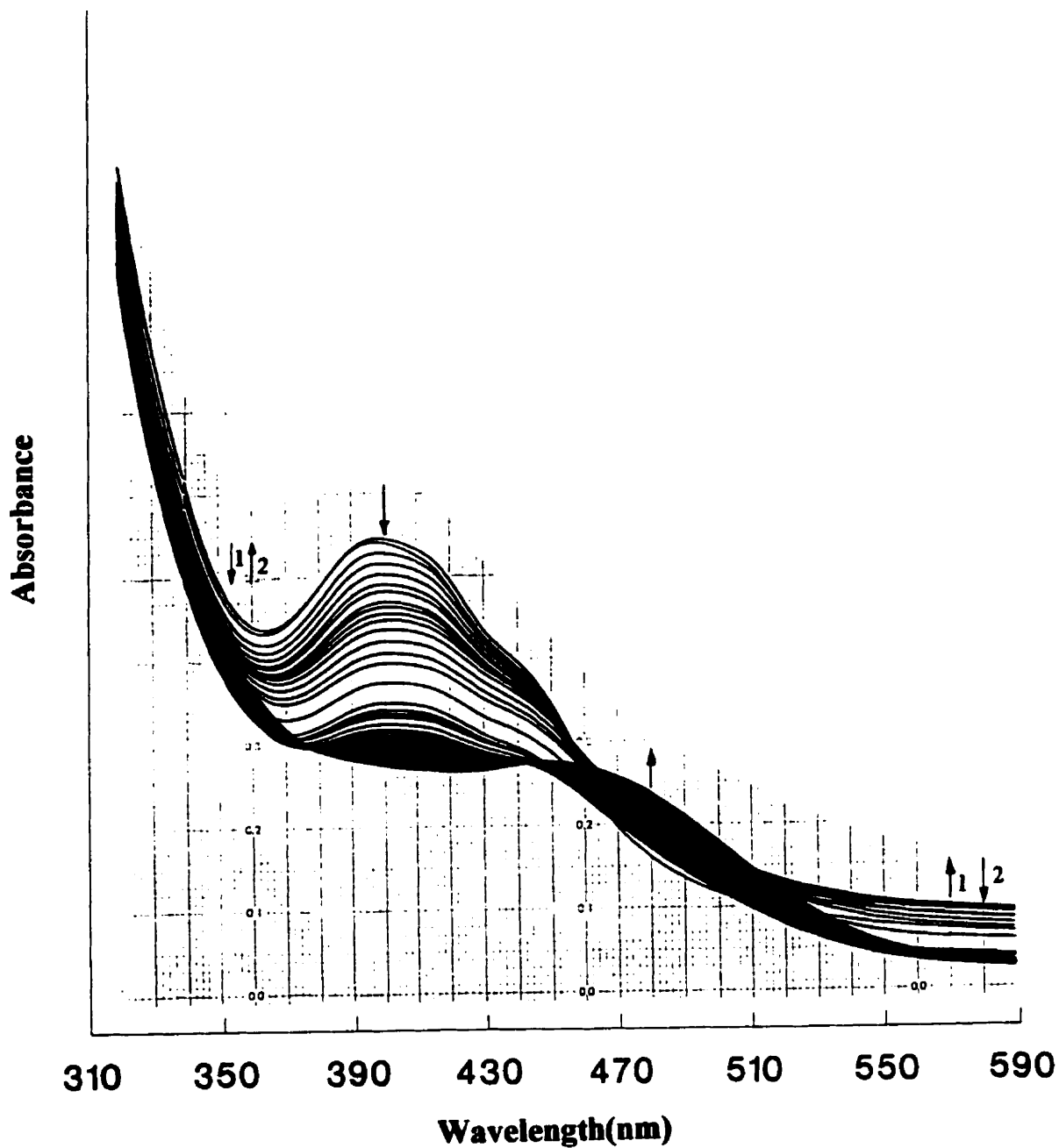


Figure 2.11 UV-Vis spectrum changes (Repetitive Scan Mode) during the reaction of  $\text{Ru}_3(\text{CO})_{11}\text{etpb}$  with  $\text{P}(\text{OEt})_3$  in heptane at  $25.15^\circ\text{C}$ .  $[\text{Complex}] = 2 \times 10^{-5} \text{ M}$ ,  $[\text{L}] = 0.3899 \text{ M}$ . Cycle time = 60 min, running for 53 hrs.



**Figure 2.12** UV-Vis spectrum changes (Repetitive Scan Mode) during the reaction of  $\text{Ru}_3(\text{CO})_{11}\text{etpb}$  with  $\text{PPh}_2\text{Et}$  at  $25.15^\circ\text{C}$  in heptane.  $[\text{Complex}] = 2 \times 10^{-5} \text{ M}$ ,  $[\text{L}] = 0.2895 \text{ M}$ . Cycle (1-3) time = 100 min, cycle (3-25) time = 200 min, running for 77 hrs.

It is clear that a satisfactory value of  $A_{\infty}$  for the first stage reaction could not be obtained by the UV-Vis technique.



**Figure 2.13** UV-Vis spectrum changes (Repetitive Scan Mode) during the reaction of  $\text{Ru}_3(\text{CO})_{11}\text{etpb}$  with  $\text{PPhEt}_2$  at RT in heptane.  $[\text{Complex}] = 2 \times 10^{-5} \text{ M}$ ,  $[\text{L}'] = 0.1388 \text{ M}$ . Cycle time = 40 min, cycle number = 40, running for 26 hrs.

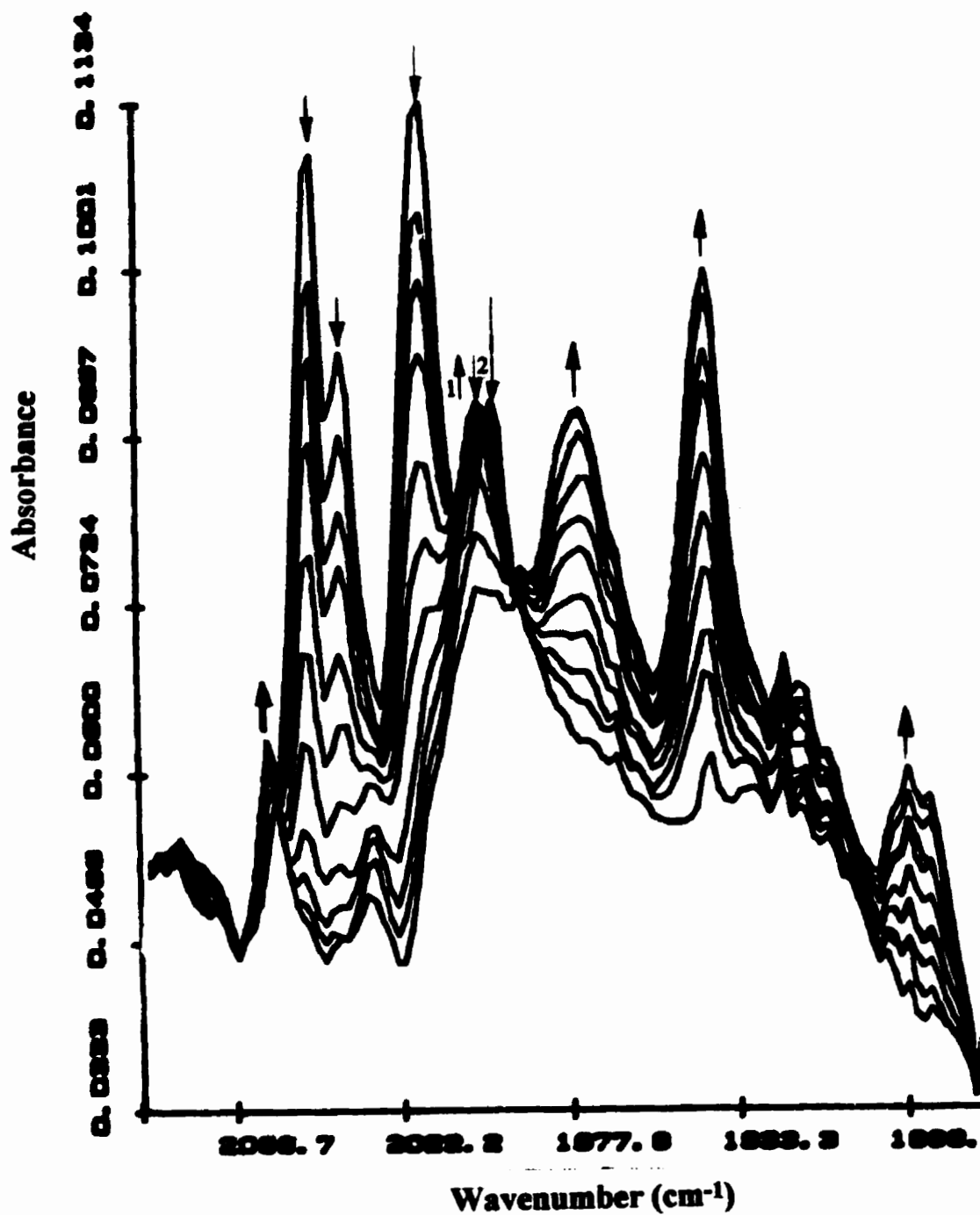


Figure 2.14 FTIR spectrum changes during the reaction of  $\text{Ru}_3(\text{CO})_{11}\text{etpb}$  with  $\text{P}(n\text{-Bu})_3$  at  $25.2^\circ\text{C}$  in heptane.  $[\text{Complex}] = 8 \times 10^{-5} \text{ M}$ ,  $[\text{L}'] = 0.4412 \text{ M}$ .

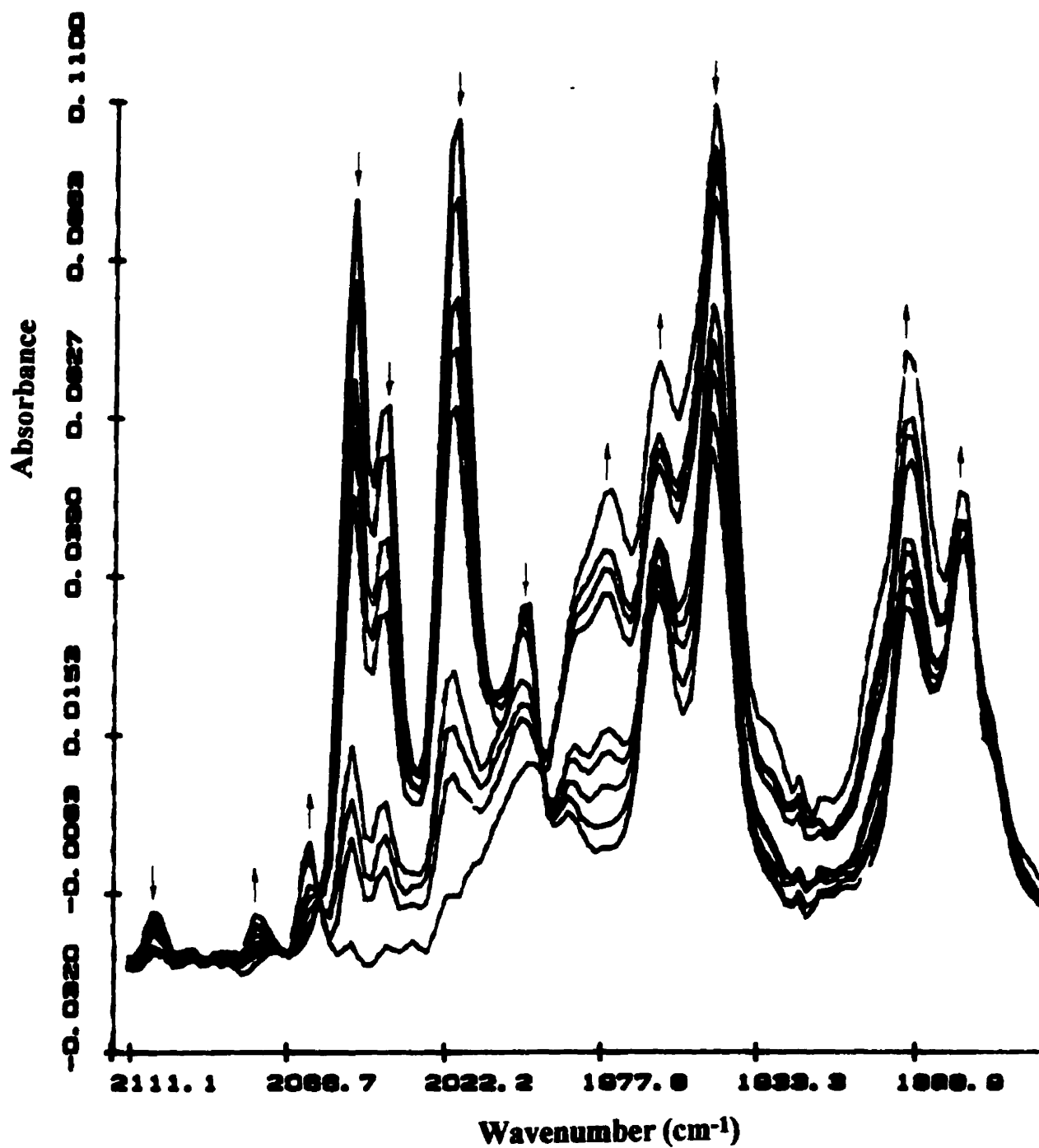


Figure 2.15 FTIR spectrum changes during the reaction of  $\text{Ru}_3(\text{CO})_{11}\text{etpb}$  with  $\text{PPhEt}_2$  at  $25.2^\circ\text{C}$  in heptane.  $[\text{Complex}] = 8 \times 10^{-5} \text{ M}$ ,  $[\text{L}'] = 0.1409 \text{ M}$ .

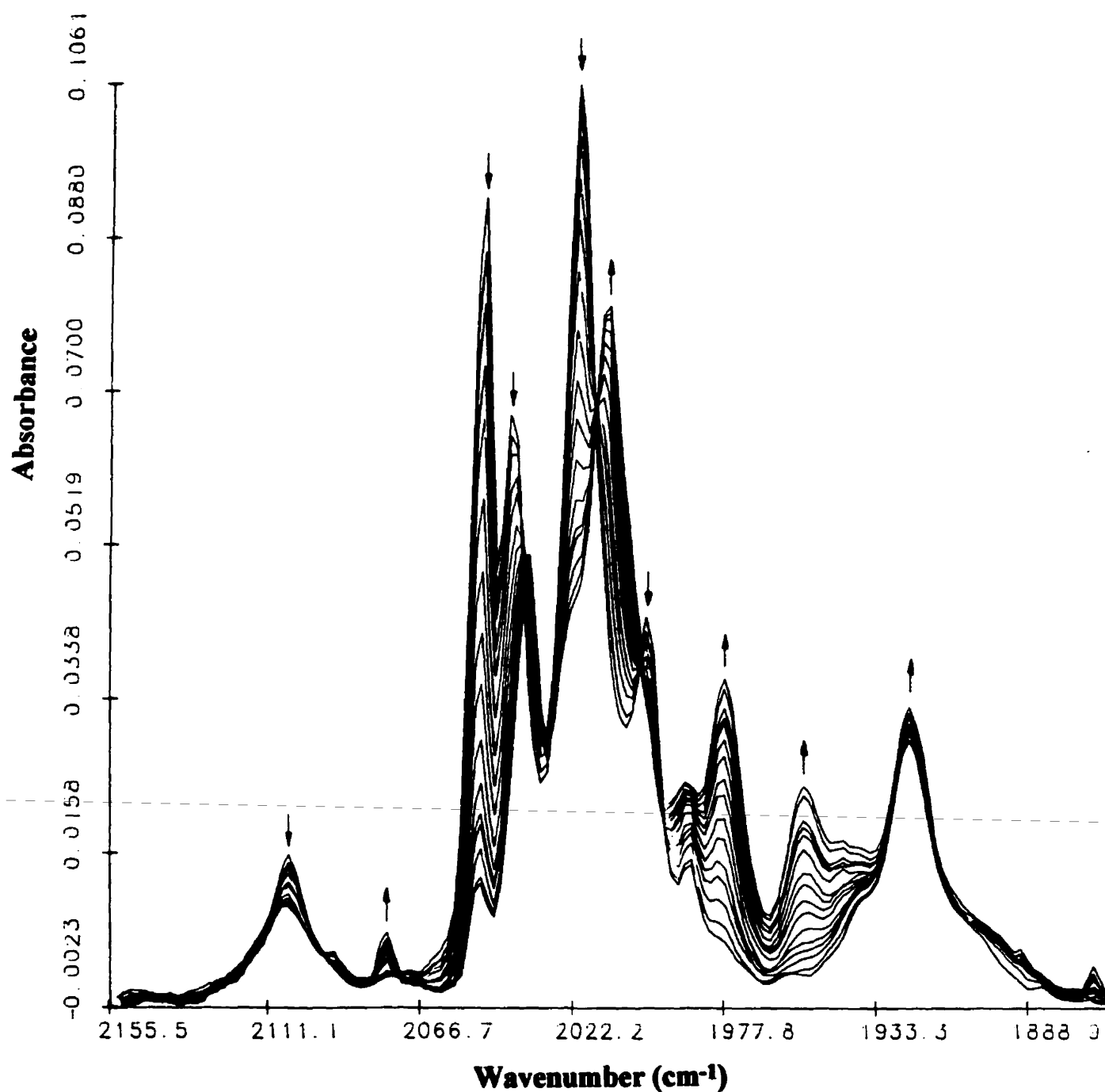


Figure 2.16 FTIR spectrum changes during the reaction of  $\text{Ru}_3(\text{CO})_{11}\text{etpb}$  with  $\text{etpb}$  at  $40.0^\circ\text{C}$  in heptane.  $[\text{Complex}] = 8 \times 10^{-5} \text{ M}$ ,  $[\text{L}'] = 0.04279 \text{ M}$ .

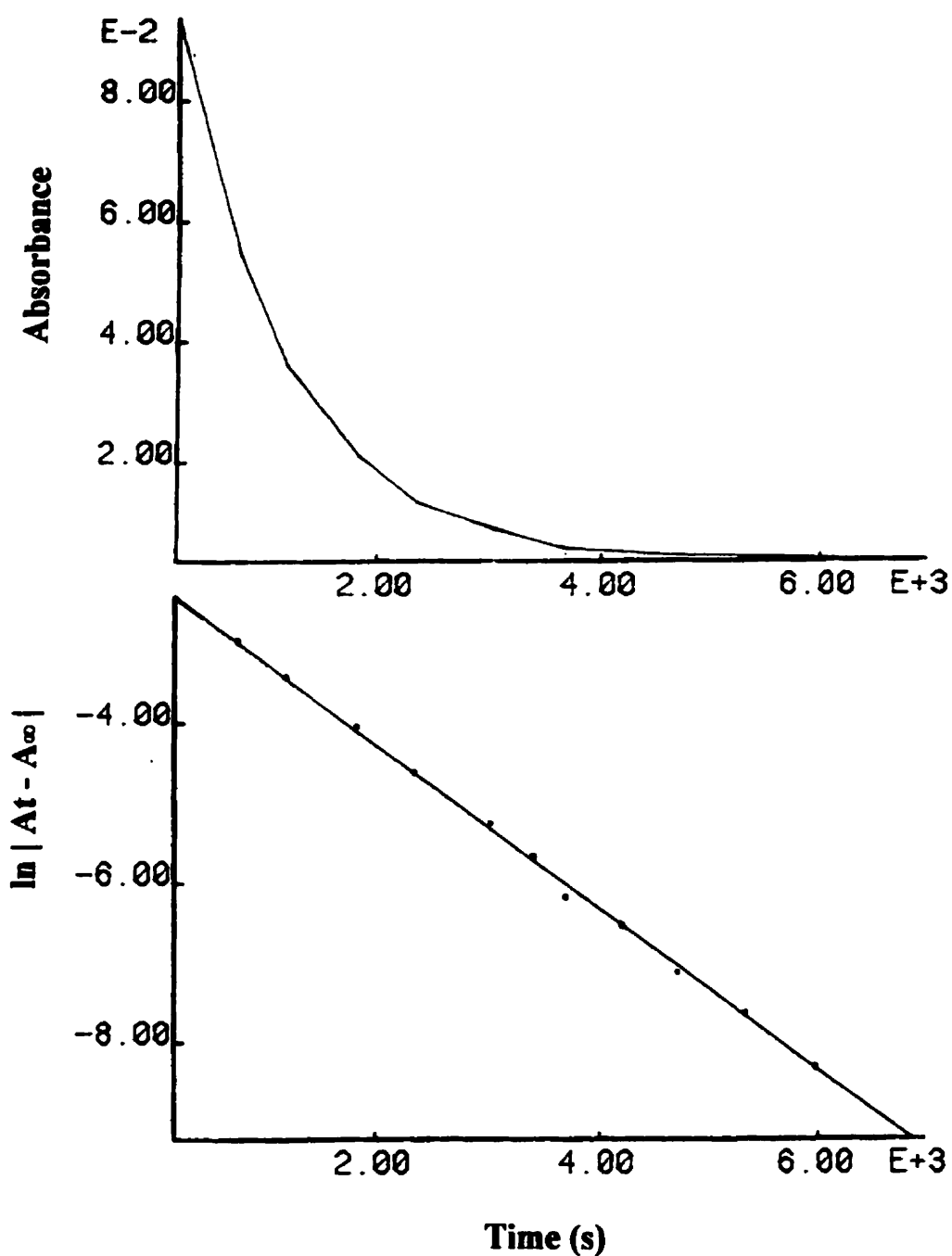


Figure 2.17 Plots of absorbance vs time and  $\ln|A_t - A_\infty|$  vs time, monitored by the FTIR technique, for the reaction of  $\text{Ru}_3(\text{CO})_{11}\text{PMe}_3$  with etpb at  $40.0^\circ\text{C}$  in heptane.  $[\text{Complex}] = 1 \times 10^{-4} \text{ M}$ ,  $[\text{L}'] = 0.03113 \text{ M}$ .

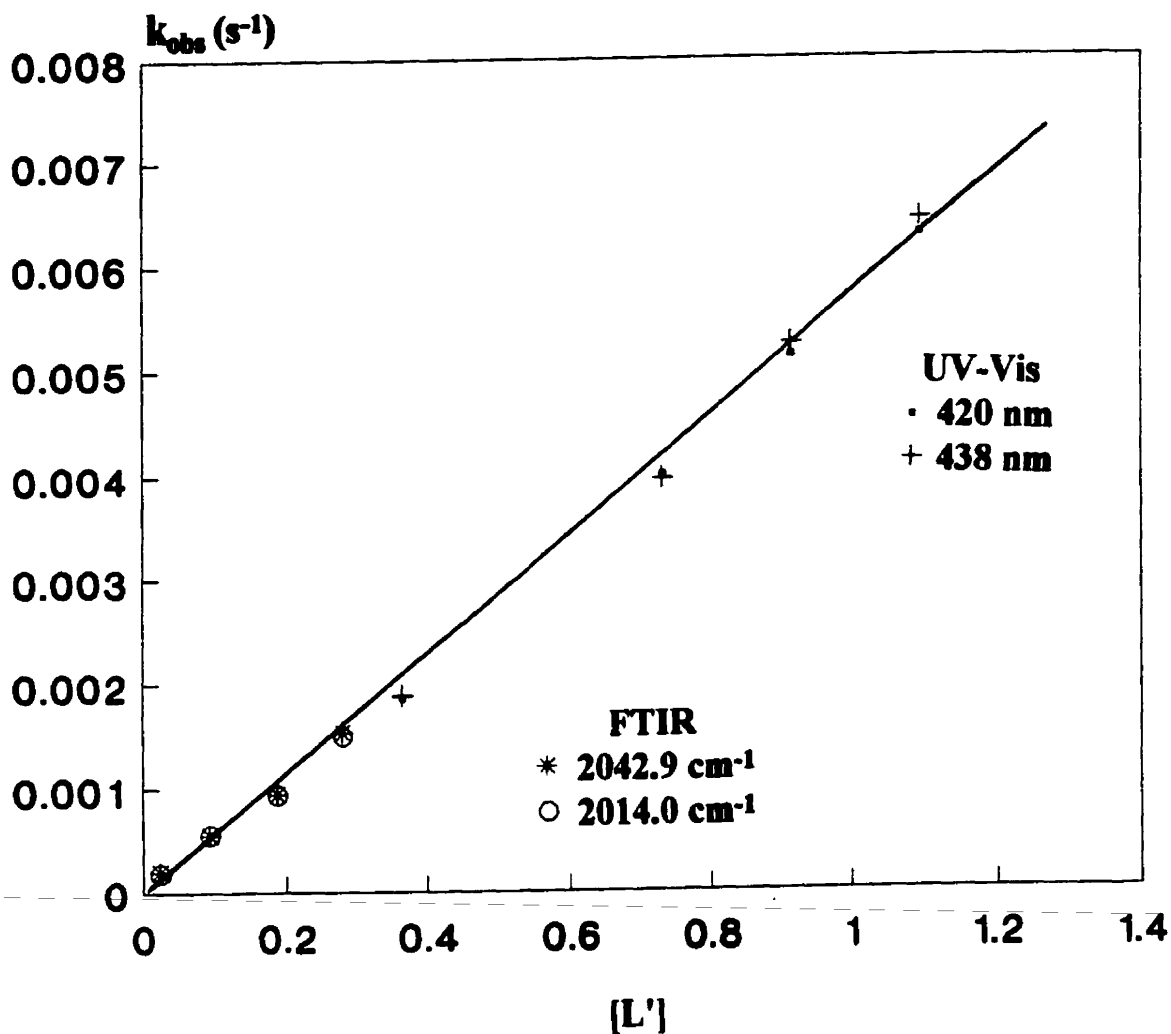


Figure 2.18 Comparison of  $k_{\text{obs}}$  values obtained by using different techniques and monitoring different wavenumbers or wavelengths for the substitution reaction of  $\text{Ru}_3(\text{CO})_{11}\text{PMe}_3$  with  $\text{P}(\text{OEt})_3$  in heptane at 25.2°C.

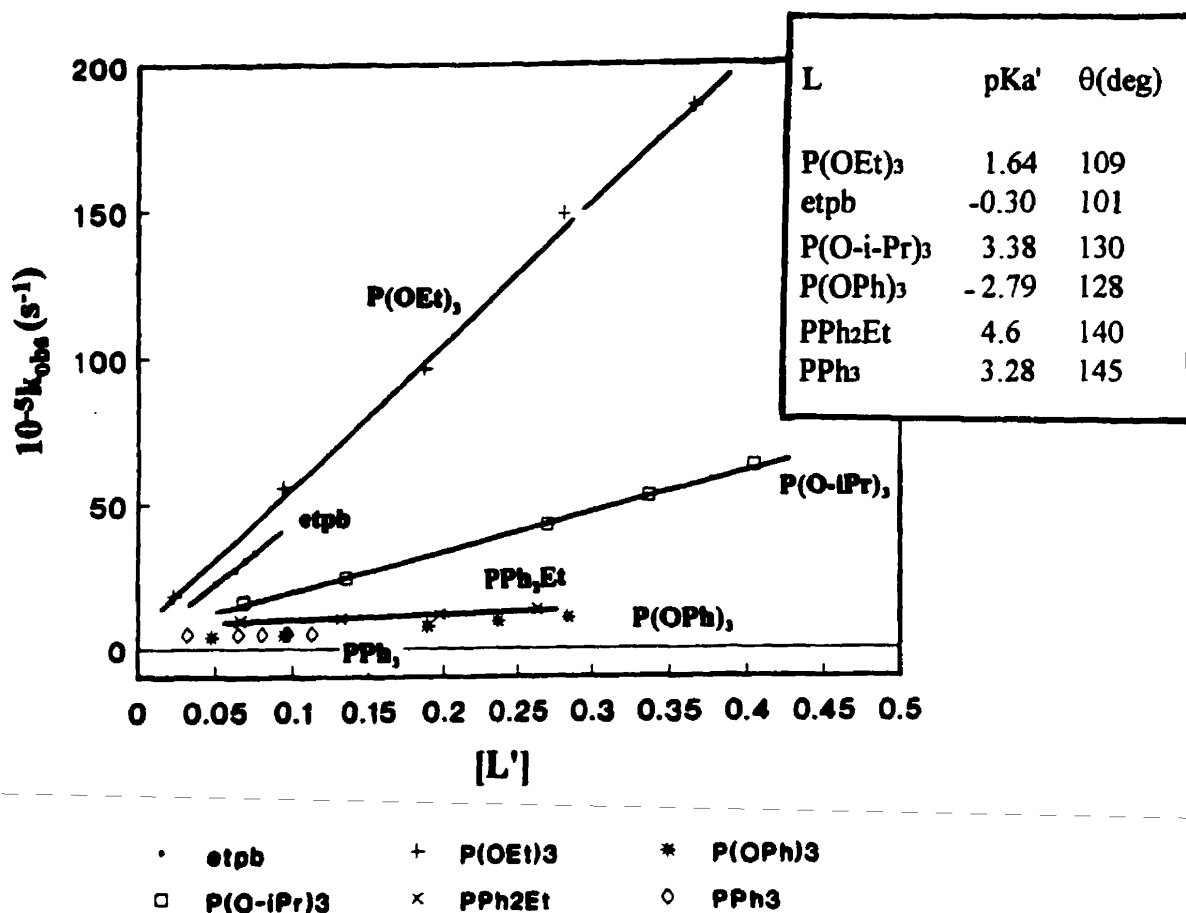


Figure 2.19 Plot of  $k_{\text{obs}}$  vs  $[L']$  for the reaction of  $\text{Ru}_3(\text{CO})_{11}\text{PMe}_3$  with  $L'$  in heptane at  $25.0^\circ\text{C}$ .

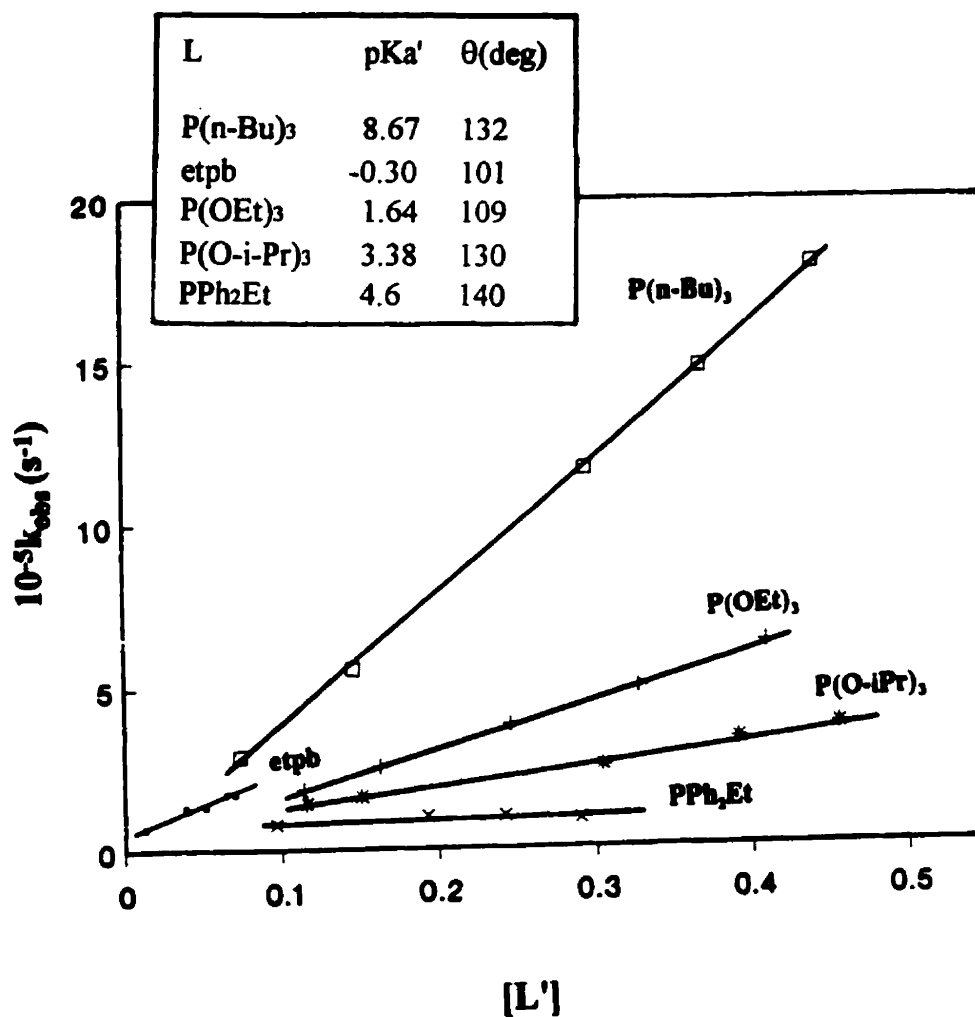


Figure 2.20 Plot of  $k_{\text{obs}}$  vs  $[L']$  for the reaction of  $\text{Ru}_3(\text{CO})_{11}\text{etpb}$  with  $L'$  in heptane at 25.0°C.

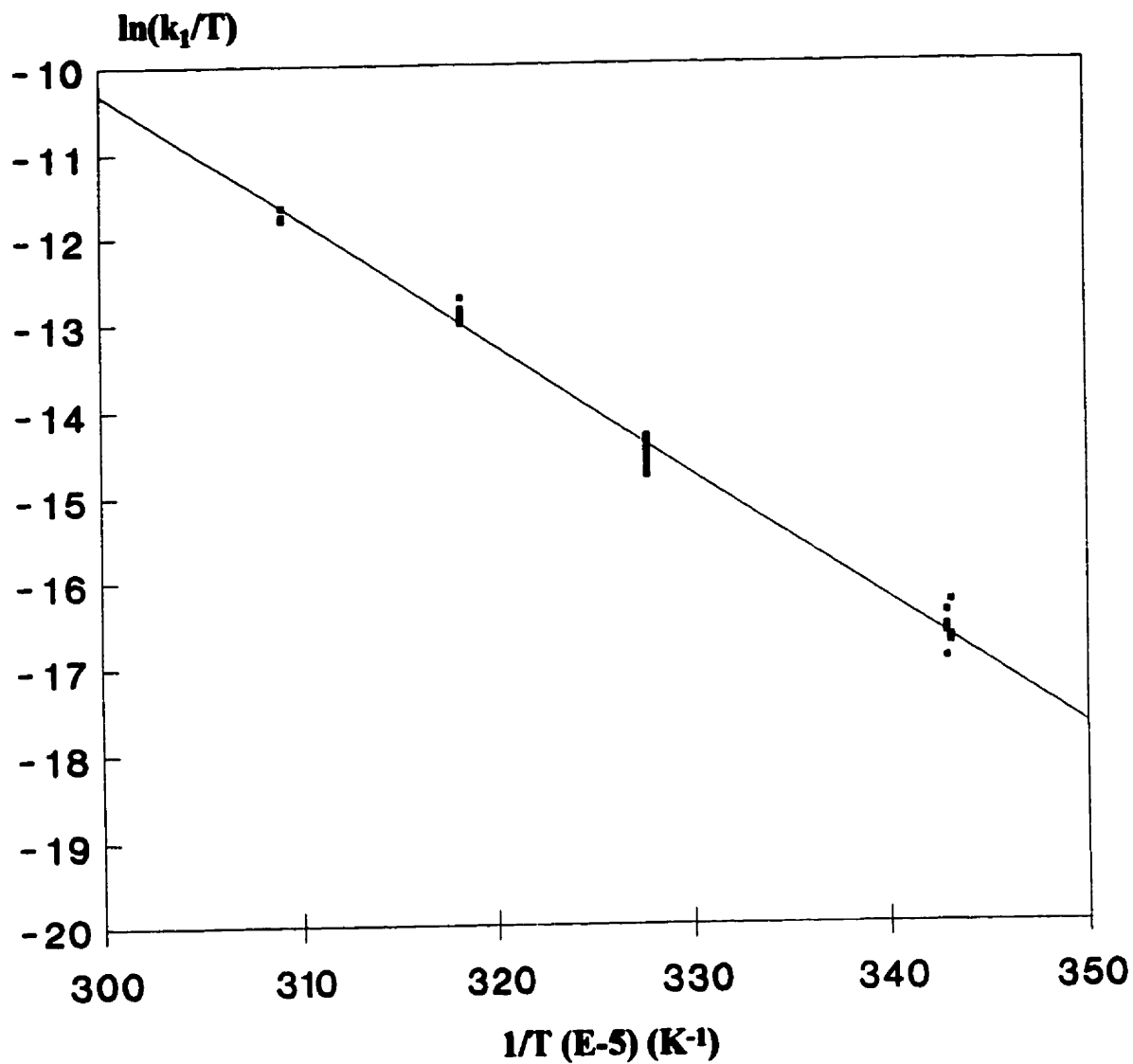


Figure 2.21 Plot of  $\ln(k_1/T)$  vs  $1/T$  for CO dissociation from  $\text{Ru}_3(\text{CO})_{11}\text{PMe}_3$  ( $k_1$  obtained from reactions with  $\text{AsPh}_3$ ).

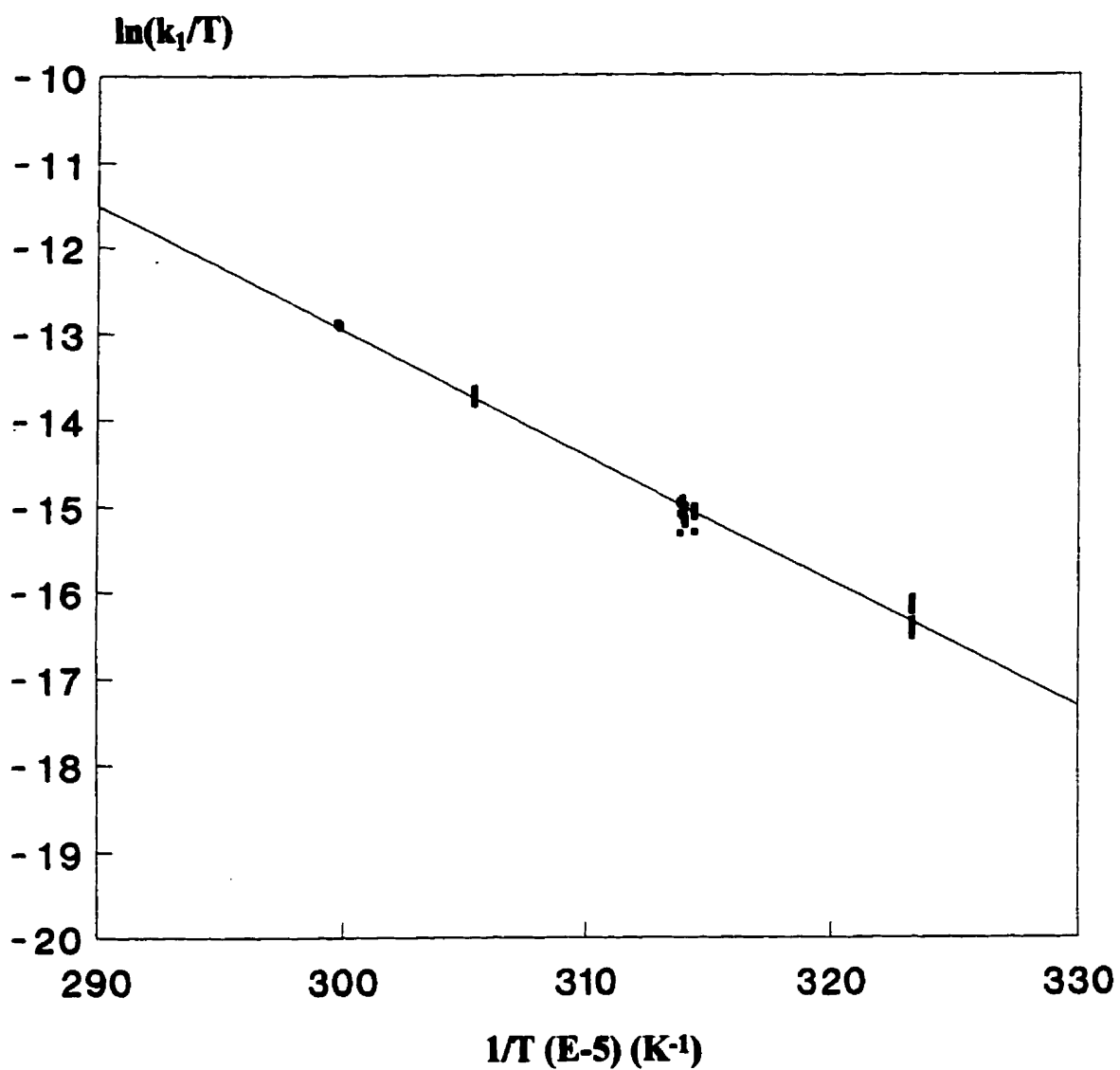


Figure 2.22 Plot of  $\ln(k_1/T)$  vs  $1/T$  for CO dissociation from  $Ru_3(CO)_{11}etpb$  ( $k_1$  obtained from reactions with  $AsPh_3$ ).

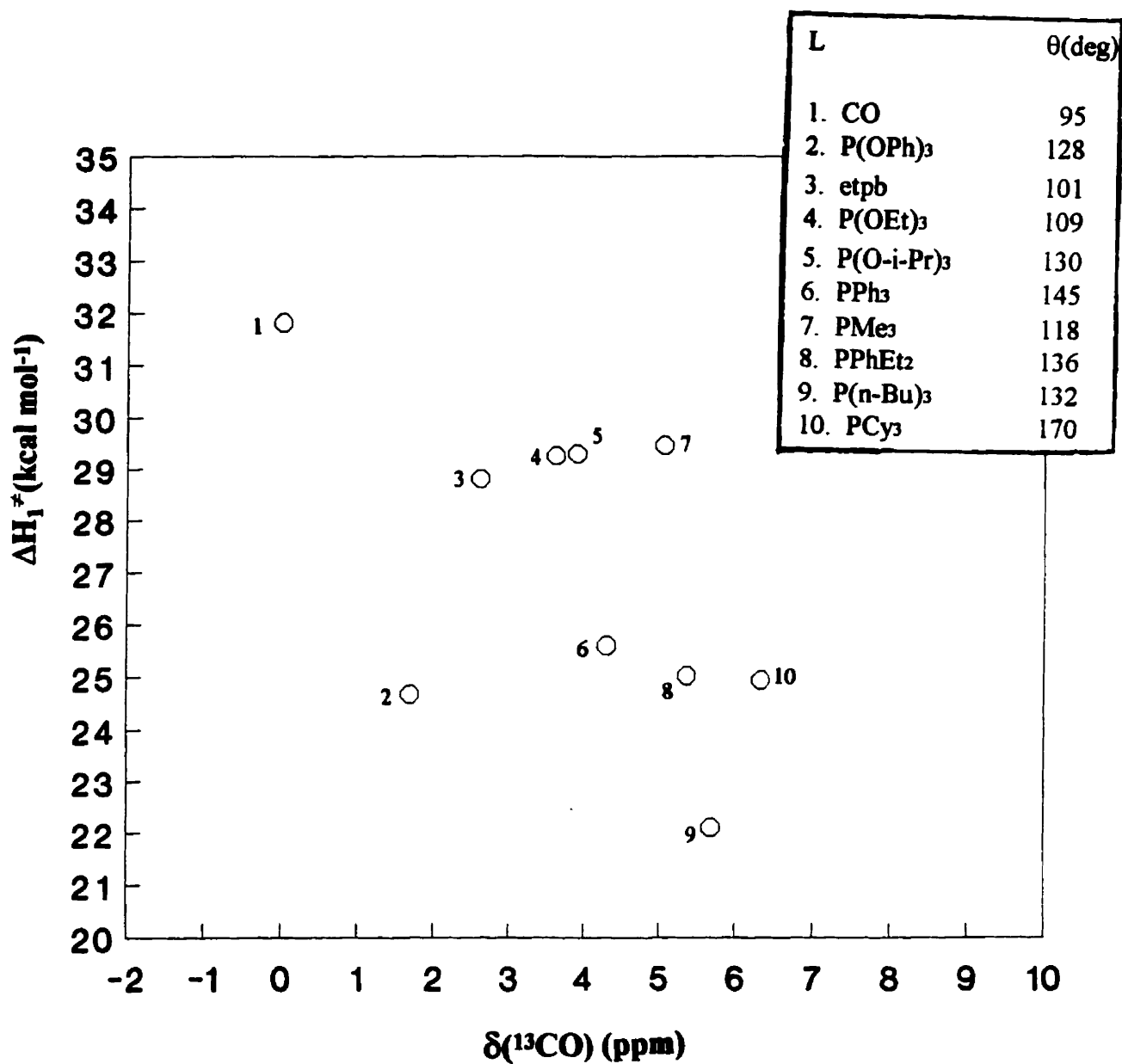


Figure 2.23 Plot of  $\Delta H_1^\ddagger$  vs  $\delta(^{13}\text{CO})$  for CO dissociation from  $\text{Ru}_3(\text{CO})_{11}\text{L}$ . Such a plot does not show linear relationship because of steric effects and some other reasons.

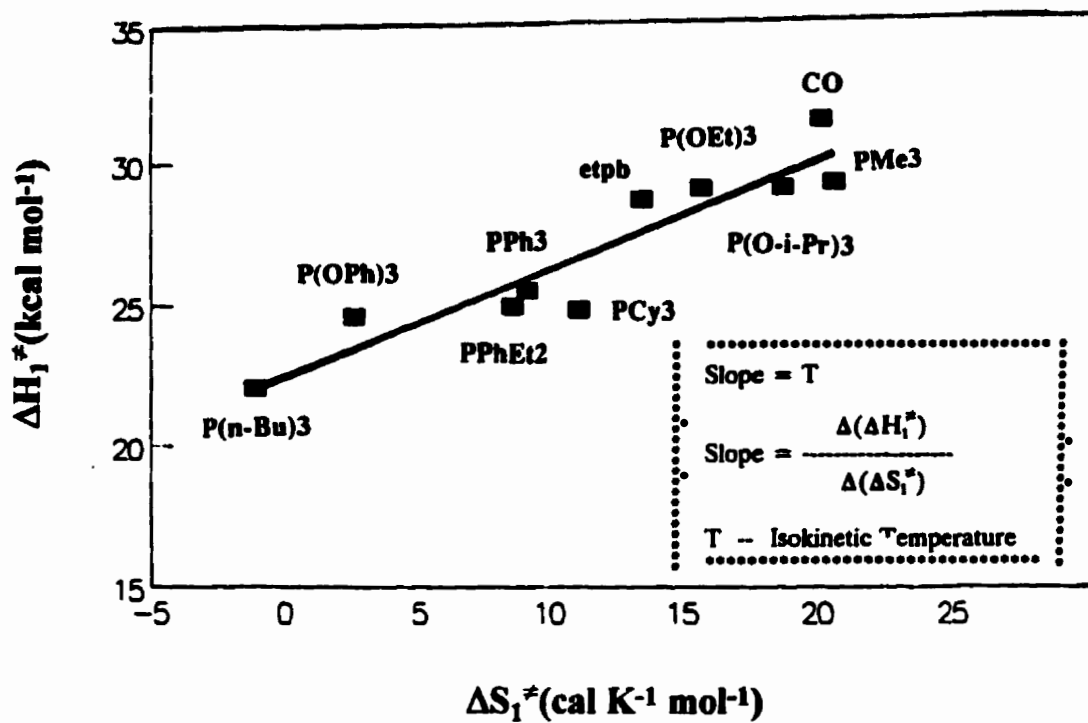


Figure 2.24 Isokinetic plot,  $\Delta H_1^\ddagger$  vs  $\Delta S_1^\ddagger$ , for CO dissociation from  $\text{Ru}_3(\text{CO})_{11}\text{L}$ .

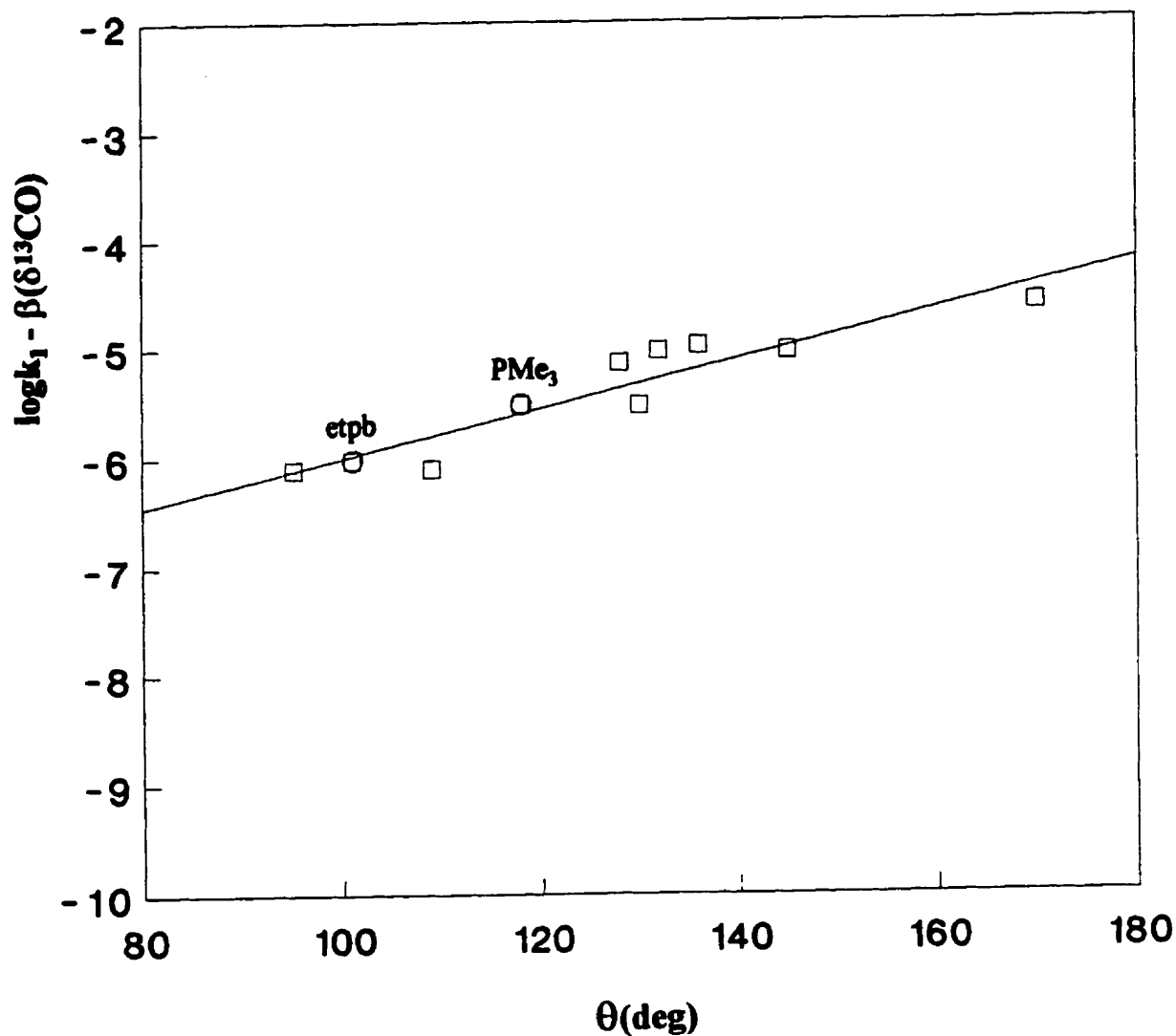


Figure 2.25 Steric profile for CO dissociation from  $\text{Ru}_3(\text{CO})_{11}\text{L}$  at 25.0°C, and  $\theta$  was used as a steric parameter. The clusters  $\text{Ru}_3(\text{CO})_{11}\text{L}$  are listed in order from left to right: L = CO, etpb,  $\text{P}(\text{OEt})_3$ ,  $\text{PMe}_3$ ,  $\text{P}(\text{OPh})_3$ ,  $\text{P}(\text{O-}i\text{-Pr})_3$ ,  $\text{P}(n\text{-Bu})_3$ ,  $\text{PPhEt}_2$ ,  $\text{PPh}_3$ ,  $\text{PCy}_3$  (L = etpb and  $\text{PMe}_3$  this work).

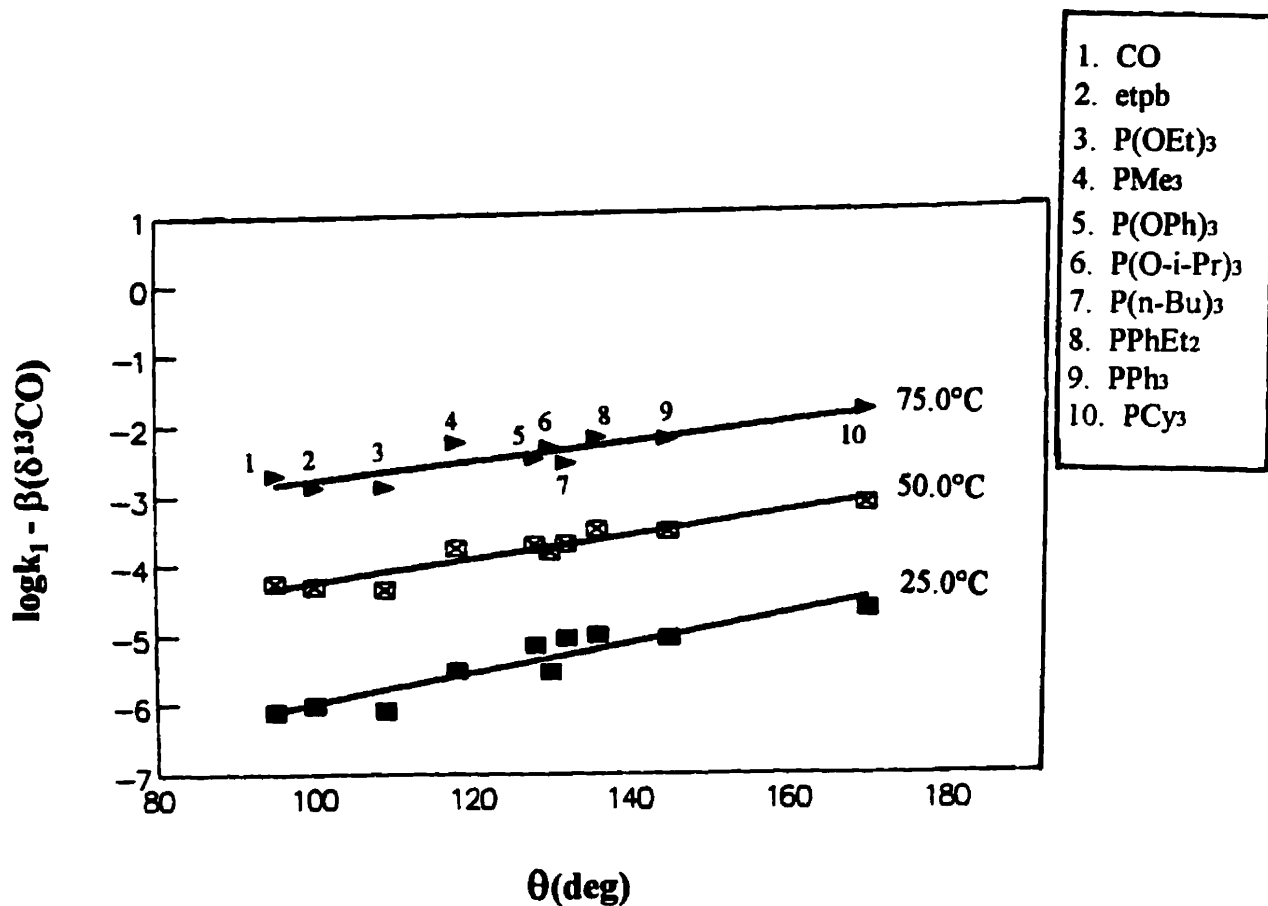


Figure 2.26(a) Temperature dependence of steric profiles for CO dissociation from  $\text{Ru}_3(\text{CO})_{11}\text{L}$ .  $\theta$  was used as a steric parameter.

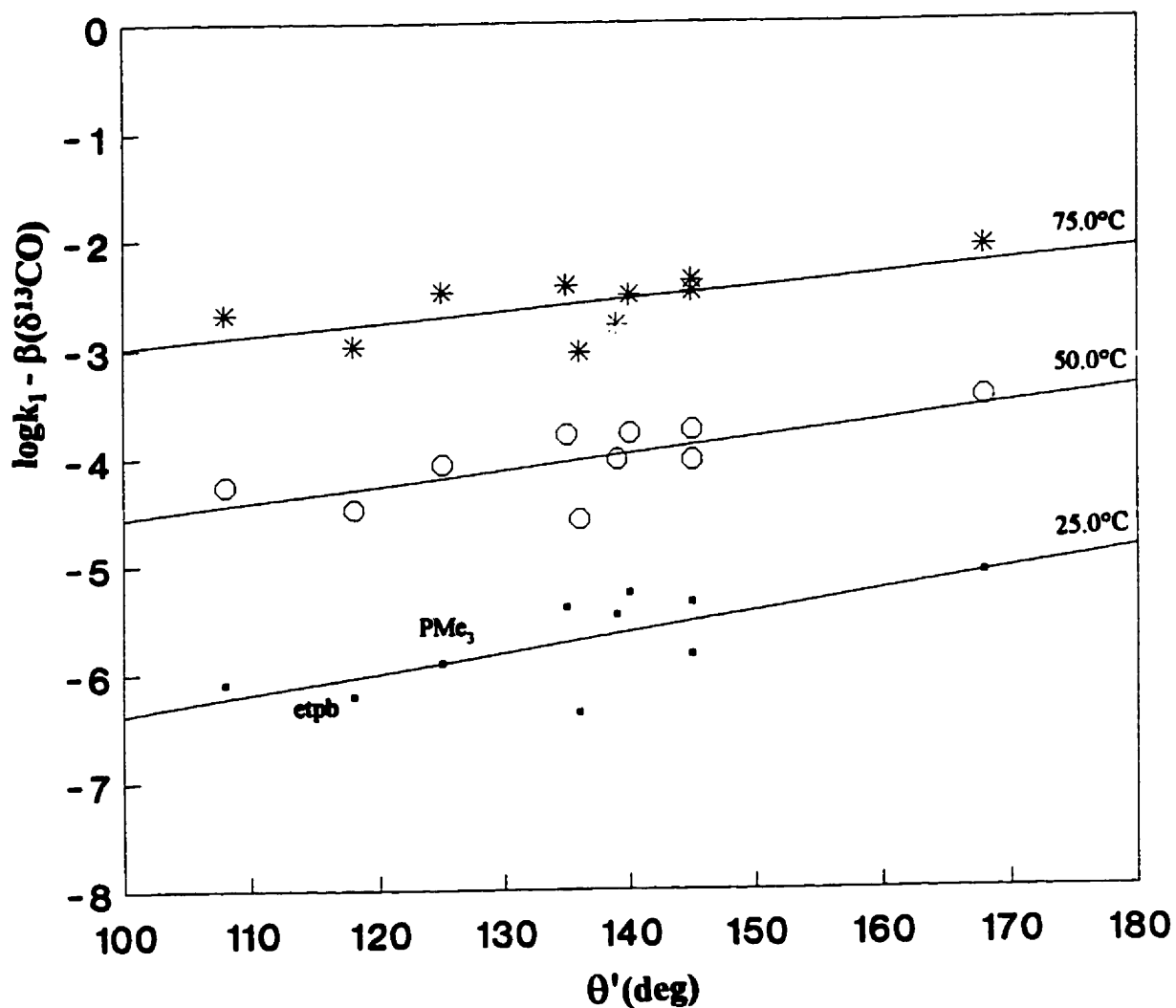


Figure 2.26(b) Temperature dependence of steric profiles for CO dissociation from  $\text{Ru}_3(\text{CO})_{11}\text{L}$ .  $\theta'$  was used as a steric parameter. The clusters  $\text{Ru}_3(\text{CO})_{11}\text{L}$  are listed in order from left to right:  $\text{L} = \text{CO}$ ,  $\text{etpb}$ ,  $\text{PMe}_3$ ,  $\text{PPhEt}_2$ ,  $\text{P}(\text{OEt})_3$ ,  $\text{P}(n\text{-Bu})_3$ ,  $\text{P}(\text{OPh})_3$ ,  $\text{PPh}_3$ ,  $\text{P}(\text{O-}i\text{-Pr})_3$ ,  $\text{PCy}_3$  ( $\text{L} = \text{etpb}$  and  $\text{PMe}_3$  this work).

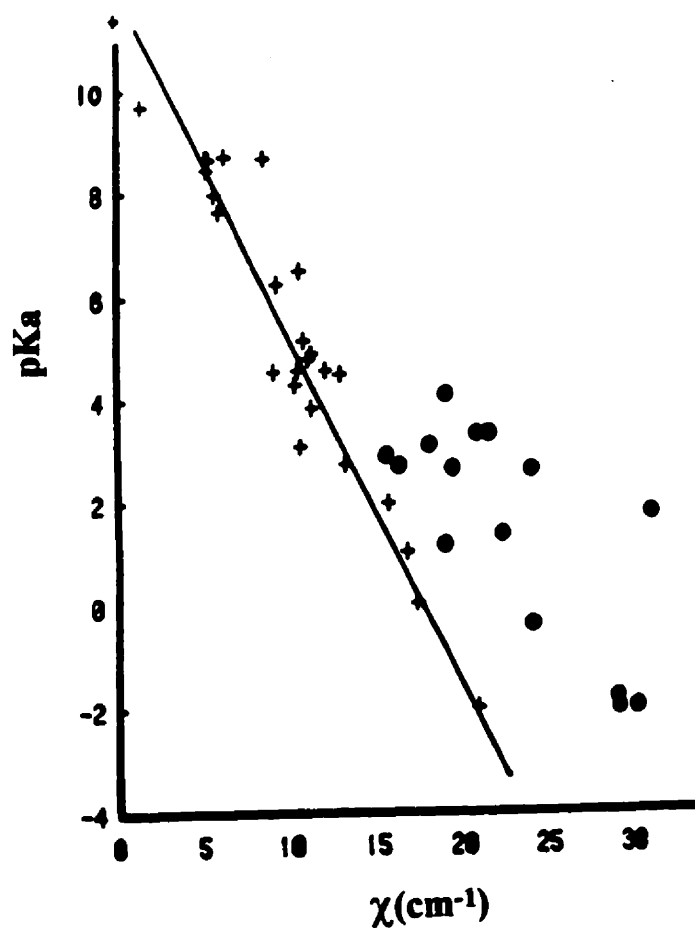


Figure 2.27 Plot of pKa vs  $\chi$  (Bartik's values) for P-donor ligands.

+  $\sigma$ -donors; •  $\sigma$ -donor/ $\pi$ -acid ligands.

$$\chi = \nu_{\text{CO}}(\text{L}) - \nu_{\text{CO}}(\text{P-}t\text{-Bu}_3)$$

for  $\text{Ni}(\text{CO})_3\text{L}$  and  $\text{Ni}(\text{CO})_3\text{P}(t\text{-Bu})_3$ , respectively.

(taken from page 22 of ref. 2)

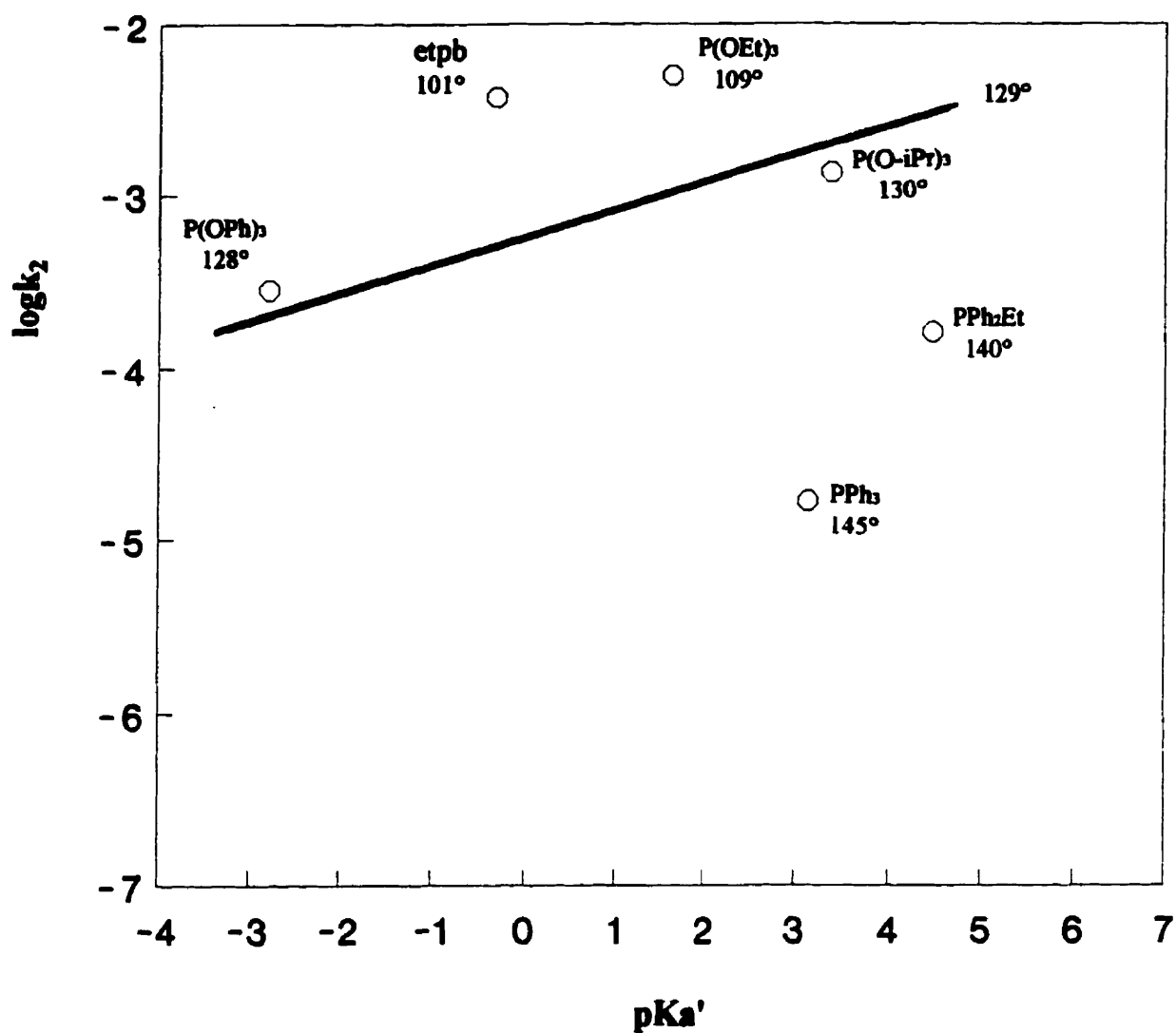


Figure 2.28 Electronic profile: plot of  $\log k_2$  vs  $\text{pK}_a'$ , for the reactions of  $\text{Ru}_3(\text{CO})_{11}\text{PMe}_3$  with  $\text{L}'$  in heptane at  $(25.1 \pm 0.1)^\circ\text{C}$ .

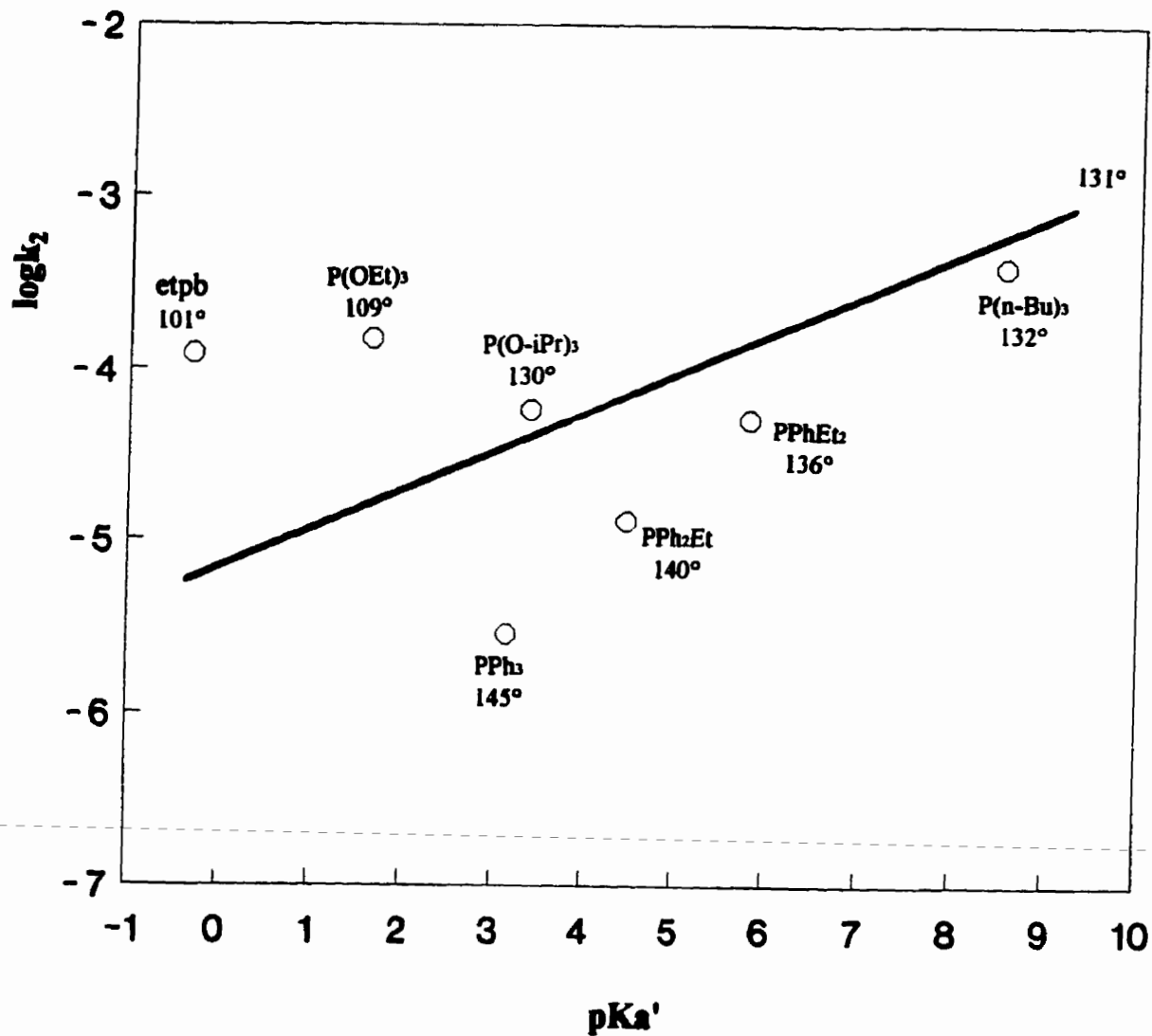


Figure 2.29 Electronic profile: plot of  $\log k_2$  vs  $pK_a'$ , for the reactions of  $Ru_3(CO)_{11}etpb$  with  $L'$  in heptane at  $(25.1 \pm 0.1)^\circ C$ .

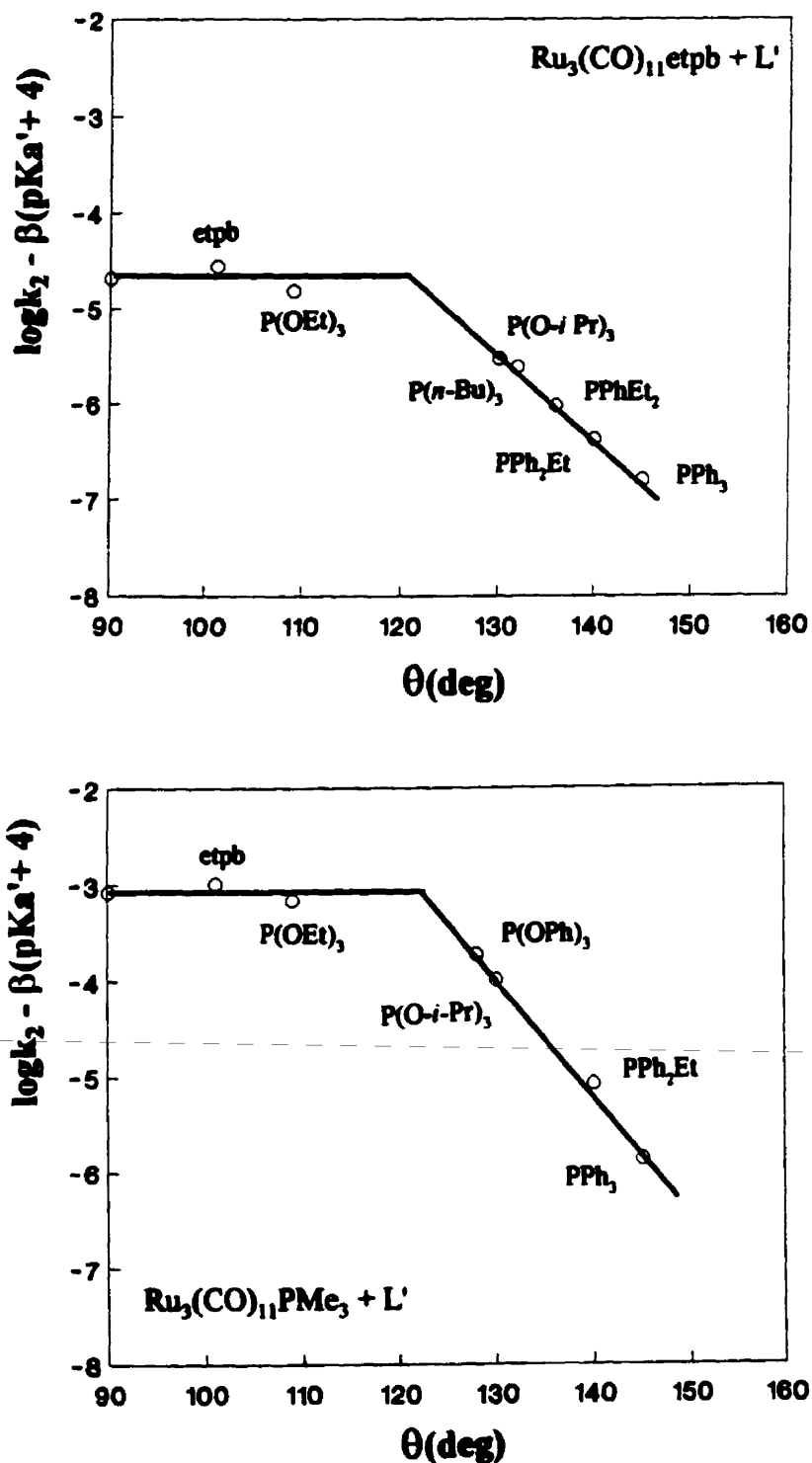


Figure 2.30 Steric profiles for the associative substitution reactions of  $\text{Ru}_3(\text{CO})_{11}\text{L}$  with  $\text{L}'$  in heptane at  $(25.1 \pm 0.1)^\circ\text{C}$  ( $\theta$  used as a steric parameter).

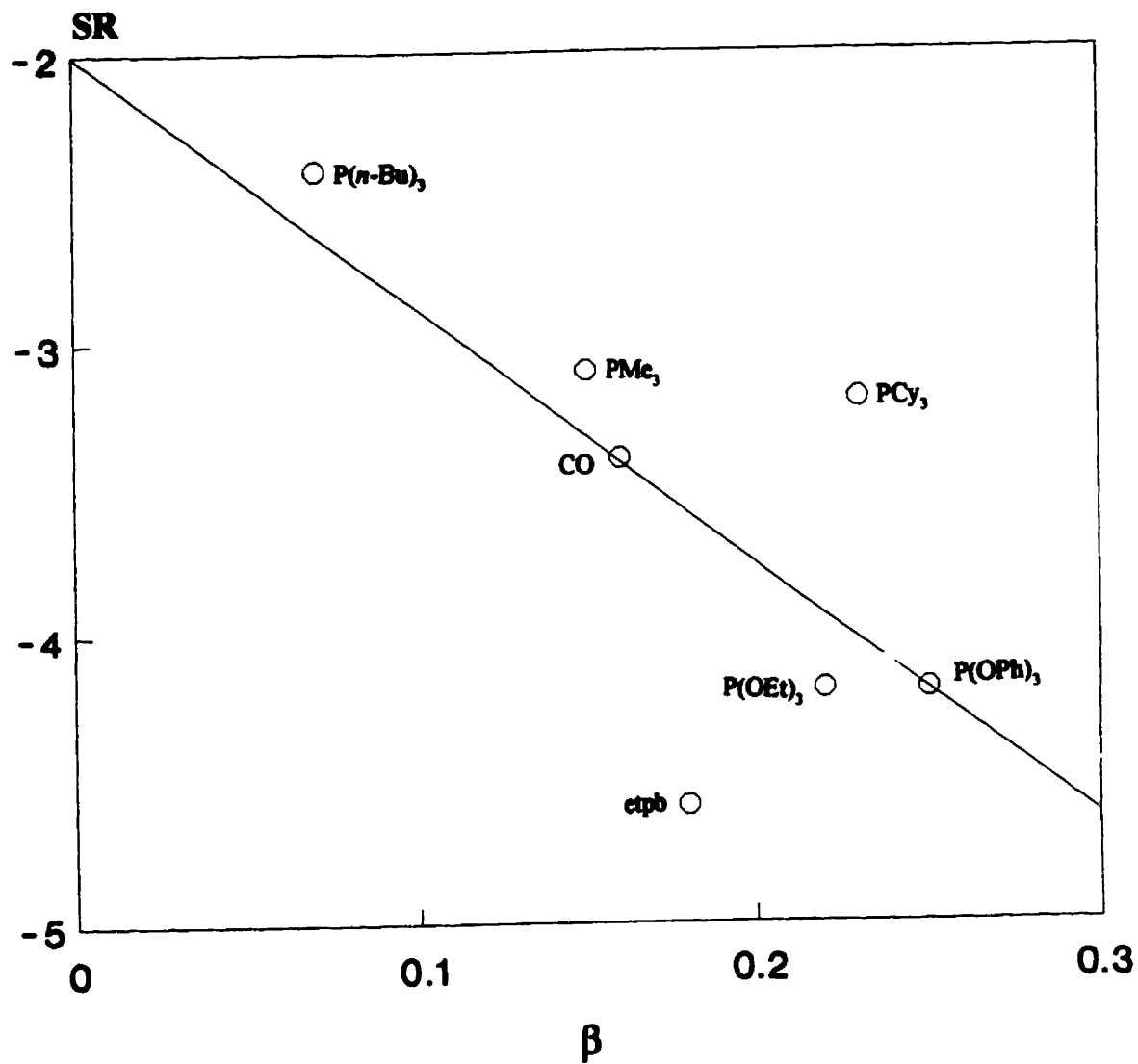


Figure 2.31 The correlation of standard reactivity SR with corresponding value of  $\beta$  for clusters  $\text{Ru}_3(\text{CO})_{11}\text{L}$ .

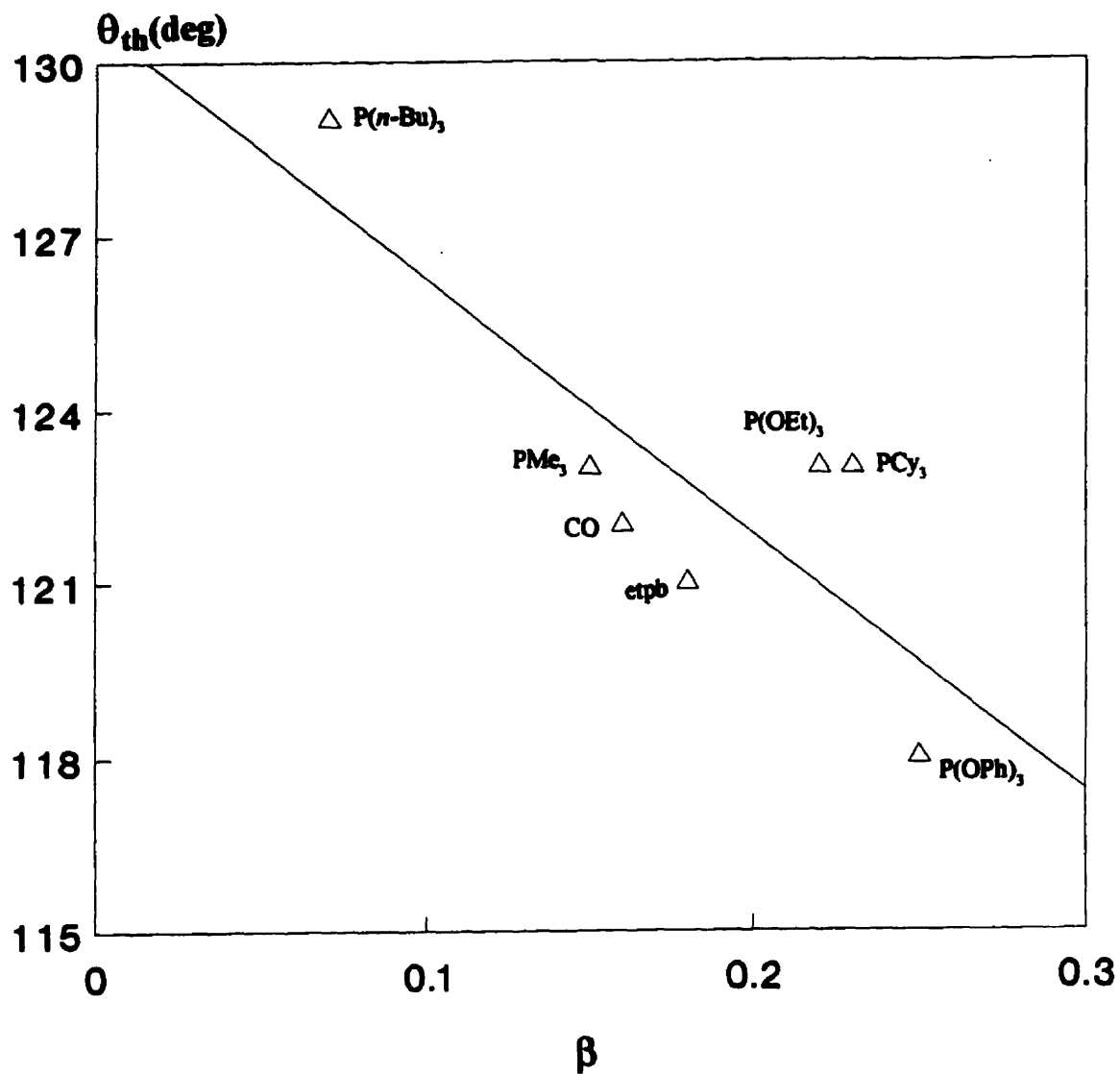


Figure 2.32 The correlation of steric threshold  $\theta_{th}$  with corresponding value of  $\beta$  for clusters  $Ru_3(CO)_{11}L$ .

Such a plot need not show a linear relationship because the size of open space in TSI for each  $Ru_3(CO)_{11}L$  cluster may be different.

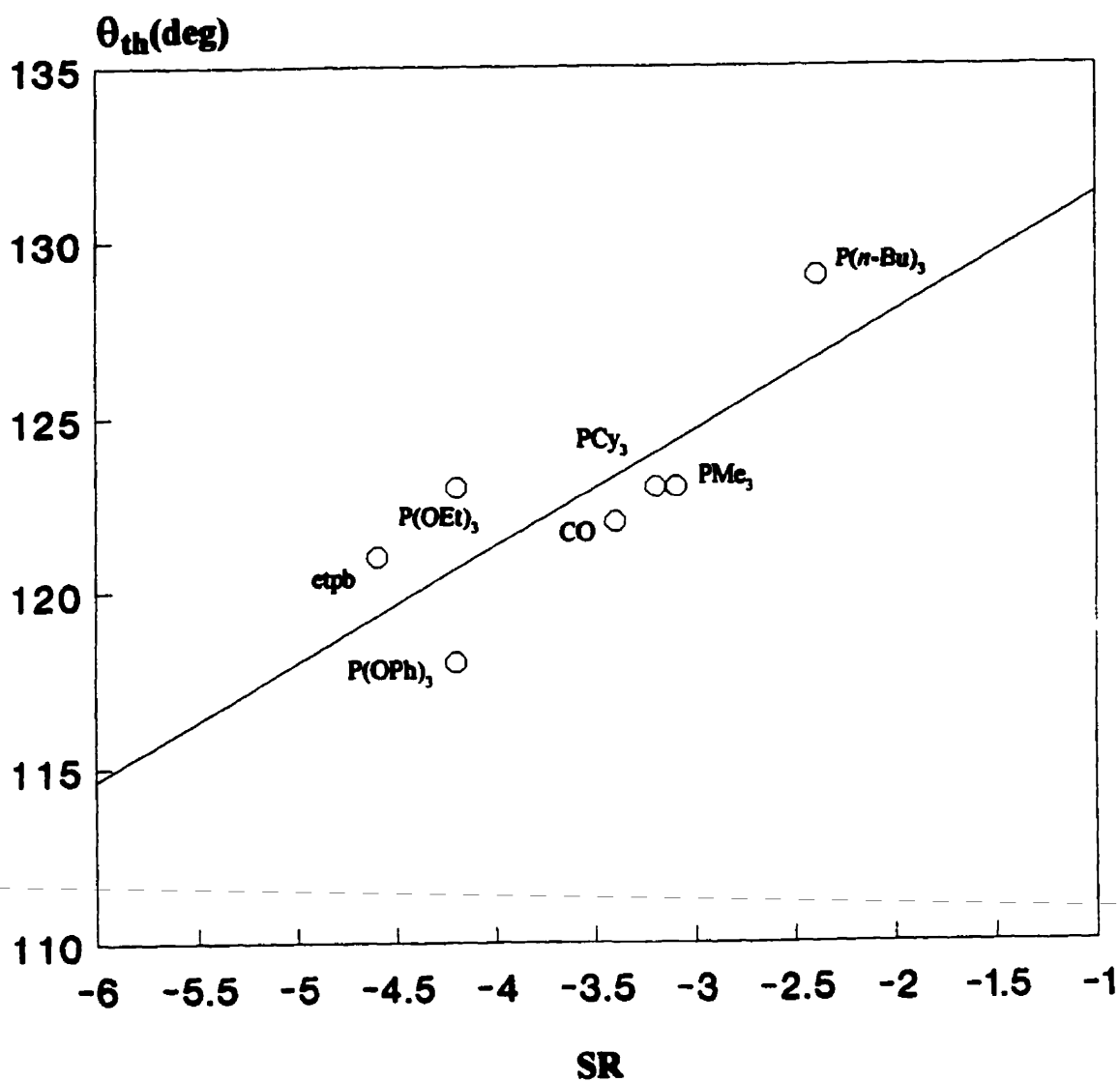
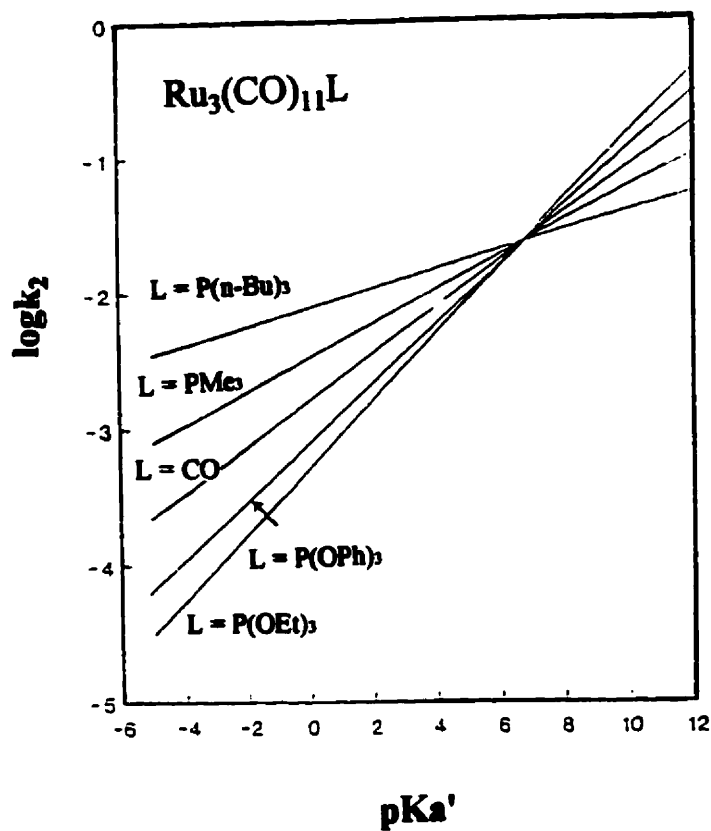


Figure 2.33 The correlation of standard reactivity SR with corresponding value of  $\theta_{th}$  for clusters  $Ru_3(CO)_{11}L$ .



**Figure 2.34** Electronic profiles of associative substitution reactions for a series of clusters  $\text{Ru}_3(\text{CO})_{11}\text{L}$ ,  $\text{L} = \text{P}(n\text{-Bu})_3$ ,  $\text{PMe}_3$ ,  $\text{CO}$ ,  $\text{P}(\text{OEt})_3$ , and  $\text{P}(\text{OPh})_3$ .  
(The experiment data taken from ref. 1, 2, 16, and this work, and the plot from ref. 34)

## CHAPTER 3

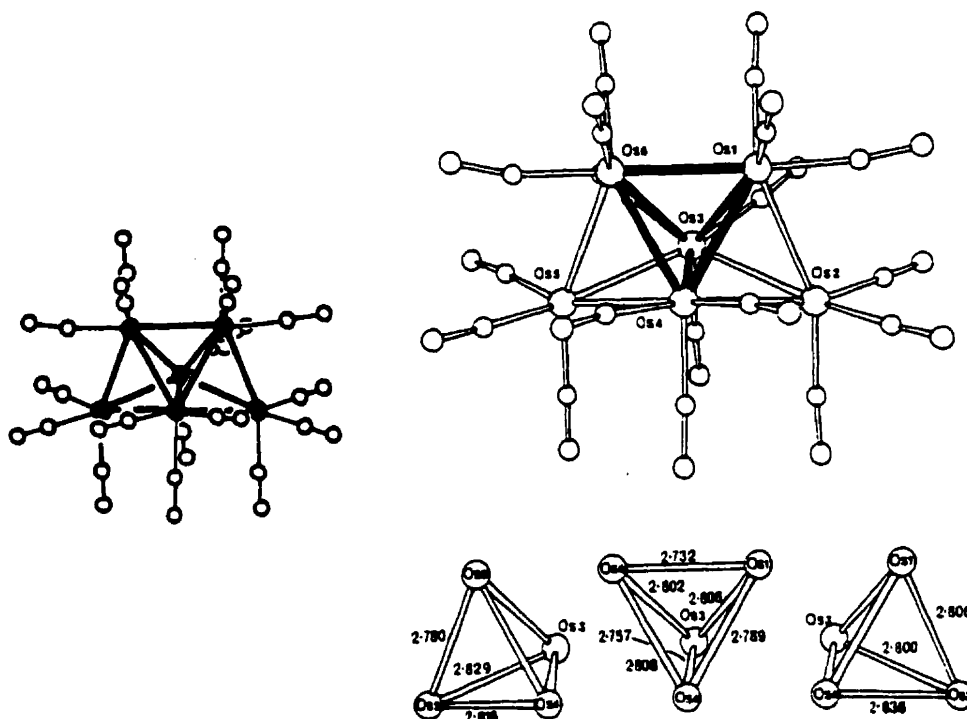
### KINETICS OF REACTIONS OF HIGH-NUCLEARITY CARBONYL CLUSTER $\text{Os}_6(\text{CO})_{18}$ WITH P-DONOR NUCLEOPHILES

#### 3.1 Introduction

There are two types of carbonyl clusters: low-nuclearity carbonyl clusters (LNCCs), which are those with three or four metal atoms, and high-nuclearity carbonyl clusters (HNCCs), which are those with five or more metal atoms, each forming at least one M–M bond [1]. The elements Fe, Ru, and Os, especially osmium, are prolific formers of HNCCs. By far the greatest number of cluster species is formed by osmium; there are numbers of iron and ruthenium analogues of the 5- and 6-atom clusters of osmium [1]. Studies in the chemistry of high nuclearity osmium carbonyl clusters have centered around the hexanuclear species  $\text{Os}_6(\text{CO})_{18}$  and its derivatives. This is likely due to the fact that  $\text{Os}_6(\text{CO})_{18}$  is stable in air, and it is a good starting material for the syntheses of both higher and lower nuclearity clusters.  $\text{Os}_6(\text{CO})_{18}$  has 84 cluster valence electrons (CVEs) ( $8 \times 6 + 2 \times 18$ ). Based on Lauher's semiempirical LCAO-MO treatments [2], among 54 molecular orbitals (MOs) of  $\text{Os}_6(\text{CO})_{18}$ , there are 12 high lying antibonding orbitals (HLAOs) and 42 cluster valence molecular orbitals (CVMOs). Only the CVMOs are suitable energetically for ligand bonding or for containing metal electrons [2]. So its bonding orbitals

are all filled. Like the majority of 84-electron clusters,  $\text{Os}_6(\text{CO})_{18}$  adopts a bicapped tetrahedral geometry [3], as shown below [3, 4].

### Crystal Structure of $\text{Os}_6(\text{CO})_{18}$

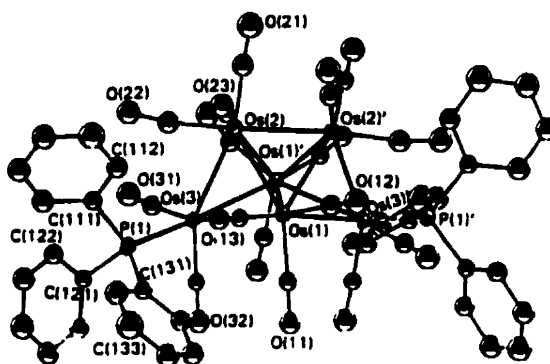
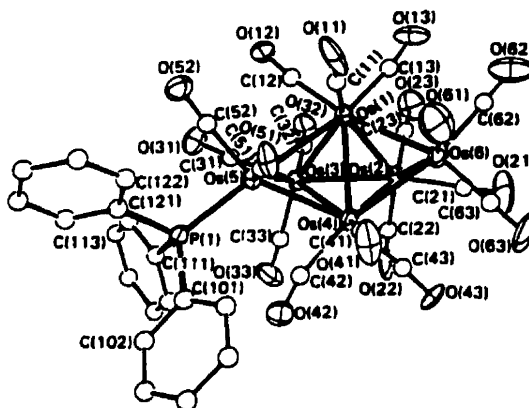


$\text{Os}_6(\text{CO})_{18}$  can be reduced by iodide to form  $[\text{Os}_6(\text{CO})_{18}]^{2-}$  [5]. In the course of reaction the  $\text{Os}_6$  unit changes from the bicapped tetrahedral geometry to that of a regular octahedral arrangement [5, 6].  $[\text{Os}_6(\text{CO})_{18}]^{2-}$  is an 86e species and has 11 HLAOs and 43 CVMOs.

It was found that the introduction of the labile acetonitrile ligand into higher nuclearity osmium clusters, in a similar manner to the trinuclear systems, greatly enhances their reactivity under mild reaction

conditions [7]. The reaction of  $\text{Os}_6(\text{CO})_{18}$  with slight excess of  $(\text{CH}_3)_3\text{NO}$  (1.1 equivalents) in  $\text{CH}_3\text{CN}/\text{CH}_2\text{Cl}_2$  at 195 K affords the complex  $\text{Os}_6(\text{CO})_{17}(\text{NCCH}_3)$  [7]. This product is used *in situ* in the reaction with  $\text{PPh}_3$  (1 equivalent) to give  $\text{Os}_6(\text{CO})_{17}\text{PPh}_3$  as the major product [7]. Synthesis of  $\text{Os}_6(\text{CO})_{16}(\text{PPh}_3)_2$  is similar to that of the mono-substituted complex except that two equivalents of  $(\text{CH}_3)_3\text{NO}$  are used to generate the complex  $\text{Os}_6(\text{CO})_{16}(\text{NCCH}_3)_2$ , which is then reacted with an excess of  $\text{PPh}_3$  to give  $\text{Os}_6(\text{CO})_{16}(\text{PPh}_3)_2$  [7]. The six Os atoms, in both complexes, define a bicapped tetrahedron closely related to that in the parent carbonyl,  $\text{Os}_6(\text{CO})_{18}$  [7]. The  $\text{PPh}_3$  ligands are terminally bound to one, in the mono-substituted cluster, or both, in the di-substituted one, of the capping Os atoms, and in each case the Os–P vector lies approximately *trans* to the longest Os–Os bond [7]. Two terminal carbonyl groups are also bound to these metal atoms, while the other metal atoms are each coordinated to three carbonyl groups. A network of incipient bridging carbonyl ligands is observed in both complexes [7]. The X-ray crystal structures of both clusters are shown below [7].

## Crystal Structures of $\text{Os}_6(\text{CO})_{17}\text{PPh}_3$ and $\text{Os}_6(\text{CO})_{16}(\text{PPh}_3)_2$

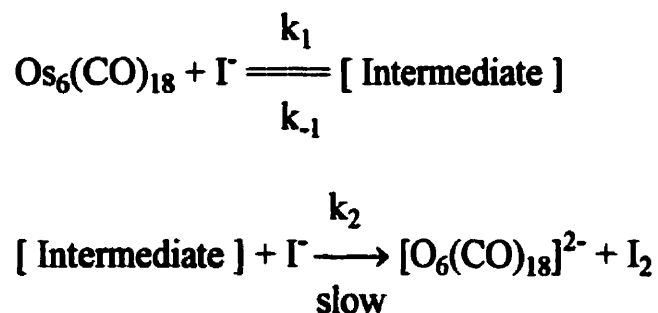


Transition metal carbonyl clusters lie at the focus of two converging lines of study. Synthetic chemists are continually preparing new clusters of increasing nuclearity and complexity, while at the same time chemists concerned with catalysis are devoting more study to the important roles of metal clusters or particles as the active sites in heterogeneous and homogeneous catalysts. The existence of several metal atoms in a cluster provides potential structural and chemical analogs for multisite binding and catalysis of organic substrates or fragments on metal particles [8]. Metal clusters have also been used as

models for bulk metals and metal surfaces in view of the fact that the high nuclearity metal clusters greatly resemble small fragments of bulk metals.

So far, quite a lot of knowledge on the synthesis, characterization, and catalysis of HNCCs has been gained. However, a relative shortage in mechanistic study in HNCC chemistry is obvious. Systematic kinetic studies in this area are of significance in determining reaction mechanisms and providing precise quantitative measurements of the reactivity of these clusters with respect to their various pathways because they provide a sound basis for an understanding of the factors governing the relative importance of these paths and could, in principle, lead to rational tailoring of potential catalysts to suit specific purposes.

Mechanistic studies have been done on the reactions of HNCCs  $\text{Ru}_6\text{C}(\text{CO})_{17}$ ,  $\text{Ru}_5\text{C}(\text{CO})_{15}$ , and their derivatives [9]. Unfortunately, very few kinetic results are available on reactions of HNCCs of osmium. The only reported kinetic study is on two-electron reduction of  $\text{Os}_6(\text{CO})_{18}$  by iodide to form  $[\text{Os}_6(\text{CO})_{18}]^{2-}$  [5]. This may be most easily rationalized in terms of a pre-equilibrium association between  $\text{Os}_6(\text{CO})_{18}$  and  $\text{I}^-$ , followed by rate-determining attack by a second  $\text{I}^-$  ion, as shown below [5].

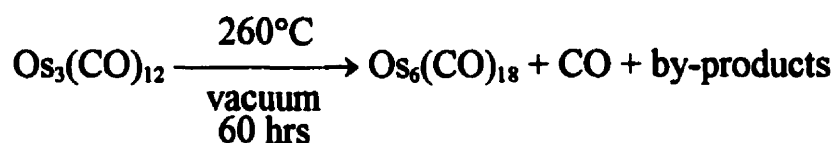


The intermediate may be  $[\text{Os}_6(\text{CO})_{17}(\text{COI})]^-$  (acyl-type) or  $[\text{Os}_6(\text{CO})_{18}\text{I}]^-$  [5]. No matter whatever it may be, it is believed that electron density is withdrawn from the coordinated iodide into the cluster framework [5]. Then a second iodide ion attacks the bound ( $\delta^+$ ) iodide moiety to release free iodine [5]. At one or other stage during the electron transfer process the rearrangement in cluster geometry takes place [5]. Realizing the importance of kinetic study in achieving a thorough understanding of HNCC chemistry, especially that of osmium — the source of the greatest number of HNCC species, we have chosen to investigate systematic kinetics of reactions of  $\text{Os}_6(\text{CO})_{18}$  with some P-donor ligands.

## 3.2 Experimental

### 3.2.1 Synthesis of $\text{Os}_6(\text{CO})_{18}$

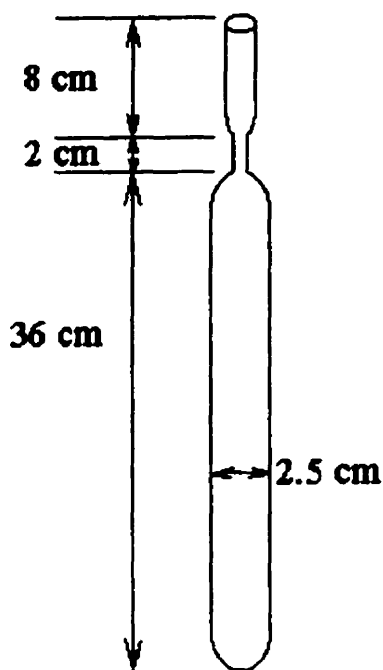
The cluster octadecacarbonylhexaosmium was prepared by the literature method [10] – the pyrolysis of  $\text{Os}_3(\text{CO})_{12}$  to higher nuclearity clusters, the proportions of which are very sensitive to the conditions employed.  $\text{Os}_6(\text{CO})_{18}$  is the major product [10-12].



Separation of the  $\text{Os}_6(\text{CO})_{18}$  from the reaction mixture is effectively achieved by fractional crystallization over a period of weeks.

**Caution.** Because of the toxicity of metal carbonyls, the heating oven used should be located in a well-ventilated hood. The Carius tube should be constructed of thick walled (min. 3.5 mm) Pyrex tubing. In

order to reduce likelihood of explosion, care should be taken when sealing the tube to form a glass seal of uniform thickness.



**Carius tube**

The Carius tube is previously washed with acetone and thoroughly dried for 12 hrs at 130°C. It must be free of water since the pyrolysis of  $\text{Os}_3(\text{CO})_{12}$  in the presence of water gives hydrido clusters instead of the binary carbonyl clusters.

Finely powdered  $\text{Os}_3(\text{CO})_{12}$  (1.2 g, 1.32 mmole) [13] is placed in a Carius tube of 180 ml capacity, through a small glass pipette otherwise the powder sticks on the upper wall of the tube, previously washed with acetone and thoroughly dried as explained above. The charge to volume ratio is 12 g/L (at most) and should be maintained if the scale of the reaction is altered,

otherwise explosion will occur. The tube is then evacuated to 0.015 torr for 2 hrs and sealed under vacuum, making sure that the glass seal is uniform with the thickness of the tube. The tube is then heated in an oven equipped with a fan for approximately 60 hrs at 260 °C.

**Caution.** Opening of the Carius tube after completion of the heating must be carried out with suitable precaution against explosion. The entire assembly should be placed in a well-ventilated hood.

Upon cooling, the tube is removed from the oven using suitable heat-insulating gloves behind an explosion shield in a fume hood. The Carius tube is cooled in air, then placed in a small Dewar flask such that the upper portion is available for opening. Liquid nitrogen is placed in the Dewar flask to cool the lowest portion of the Carius tube to  $-196^{\circ}\text{C}$ , reducing any gas pressure which may have developed in the tube. A scratch is made near the upper-most end of the tube with a standard tungsten-carbide tool or a glass cut-off tool. The Carius tube is then cracked open by applying the heated end of a Pyrex rod to the tip of the scratch, the tip of the Pyrex rod having been heated close to its softening point. After opening, the Carius tube is quickly removed from the liquid nitrogen bath.

The contents of the Carius tube should appear as a brown solid. This is extracted with 10 ml portions of ethyl acetate (boiling range  $77.2\pm 0.1^{\circ}\text{C}$ ), until a deep brown solution is no longer obtained. The unreacted  $\text{Os}_3(\text{CO})_{12}$  (yellow) does not dissolve in ethyl acetate, and metal Os (black) from decomposed  $\text{Os}_3(\text{CO})_{12}$  does not either. The combined fractions are filtered through a small glass pipette packed with kimwipes. If the volume of the solution is more than 15 ml, the extra solvent is removed under vacuum. Then 25–30 ml of hexanes (boiling range  $68\text{--}70^{\circ}\text{C}$ ) is added to the filtrate. The dark brown solution is put in a refrigerator at  $-5^{\circ}\text{C}$ . The first crop of  $\text{Os}_6(\text{CO})_{18}$  crystallized out after about one day. The dark brown crystals were separated by decanting the solution (filtration is not necessary). Then about half of the remaining solvent was removed under vacuum, and 10 ml of hexane were added. The solution was put in the refrigerator at  $-5^{\circ}\text{C}$ . The second crop of  $\text{Os}_6(\text{CO})_{18}$  crystallized out after about one

day, and isolated by decanting the solution. The remaining solution is put in the refrigerator at  $-5^{\circ}\text{C}$  again, and the third crop of  $\text{Os}_6(\text{CO})_{18}$  was isolated by the same way as mentioned above after about one week. The average yield was 71 %. A lot of  $\text{Os}_6(\text{CO})_{18}$  still remained in solution. If this portion was considered, the yield was high. After crystallization of  $\text{Os}_6(\text{CO})_{18}$ , reduction of the solvent volume by small portions can lead to crystallization of clusters in the following order:  $\text{Os}_7(\text{CO})_{21}$  (orange crystals),  $\text{Os}_8(\text{CO})_{23}$  (orange-yellow crystals), and  $\text{Os}_8\text{C}(\text{CO})_{21}$  (deep purple) [10].

The cluster  $\text{Os}_6(\text{CO})_{18}$  is stable indefinitely to air in the solid state. In solution it is stable in non-coordinating solvents. In coordinating solvents adducts are formed [14]. Purity can be checked by t.l.c. (thin layer chromatography) using Baker pre-coated silica gel plates as adsorbent, and 2 % ethyl acetate/hexane as eluent, then by carbonyl absorption in the FTIR (Figure 3.1). Its purity was identified by comparison with IR data (Table 3.1) in the literature [10]. Possible impurities are  $\text{Os}_3(\text{CO})_{12}$ ,  $\text{Os}_5(\text{CO})_{16}$ ,  $\text{Os}_5\text{C}(\text{CO})_{15}$  (yellow crystals),  $\text{Os}_7(\text{CO})_{21}$ ,  $\text{Os}_8(\text{CO})_{23}$ ,  $\text{Os}_8\text{C}(\text{CO})_{21}$ . Mass spectral characterization of these clusters has been described elsewhere [10].

**Table 3.1 Properties of Osmium Cluster Complexes**

Cluster	Colour	$\nu_{\text{C-O}}$ (cm <sup>-1</sup> )		
Os <sub>3</sub> (CO) <sub>12</sub>	yellow	a2066 vs 1997 w	2032 s	2011 w
Os <sub>5</sub> (CO) <sub>16</sub> [10]	pink-red	b2065 vs 2045 s	2060 m (sh) 2039 s (sh)	2052 s 1996 m (br)
Os <sub>6</sub> (CO) <sub>18</sub> [10]	dark brown	b2108 vw 2040 vs	2077 vs 2007 w	2063 vs 1959 w
Os <sub>6</sub> (CO) <sub>18</sub> (this work)	almost black	a2107 vw 2038 vs	2076 vs 2001 w	2062 vs 1955 vw
Os <sub>6</sub> (CO) <sub>18</sub> (this work)	almost black	c2107 vw 2039 vs 1976 vw	2076 vs 2013 w 1972 vw	2062 vs 2005 w 1955 vw
Os <sub>7</sub> (CO) <sub>21</sub> [10]	orange	b2112 vw 2038 w	2076 m 2002 w	2060 vs
Os <sub>8</sub> (CO) <sub>23</sub> [10]	orange-yellow	b2113 vw 2061 vs 2029 w	2083 m 2045 w 2012 vw	2071 s 2038 w 2000 vw
Os <sub>8</sub> C(CO) <sub>21</sub> [10]	deep purple	b2120 w 2039 w	2091 m 2030 m	2073 s 2021 m

a. In toluene

b. In CH<sub>2</sub>Cl<sub>2</sub>

c. In ethyl acetate

### 3.2.2 Kinetic Monitoring

FTIR spectra were obtained by using a Nicolet 10 DX FTIR spectrophotometer with 1.0-mm path-length solution cell with  $\text{CaF}_2$  crystal window. UV-Vis spectra were measured in a Hewlett-Packard 8542A diode array spectrophotometer, an excellent instrument, equipped with a cell holder thermostated by a Lauda Constant Temperature Bath RCS-6 ( $\pm 0.1^\circ\text{C}$ ).  $^{31}\text{P}$  NMR spectra were recorded on a Varian XL-200 spectrometer with  $(\text{CD}_3)_2\text{CO}$  as the insert.  $^{31}\text{P}$  NMR chemical shifts are referred to  $\text{P}(\text{OMe})_3$  (internal reference).

For air-sensitive compounds all manipulations were carried out by using standard Schlenk techniques under an atmosphere of oxygen-free  $\text{N}_2$  or Ar. The nucleophiles  $\text{PMe}_3$  and  $\text{PPhMe}_2$  were used as received (Strem).  $\text{Etpb}$  was sublimed (at ca.  $50^\circ\text{C}$ , under reduced pressure of argon), and could be stored in a desiccator which must be kept in a cool room ( $< -5^\circ\text{C}$ ). Liquid phosphorus ligands  $\text{P}(\text{OPh})_3$ ,  $\text{P}(\text{OEt})_3$ ,  $\text{P}(n\text{-Bu})_3$  and  $\text{P}(\text{O-}i\text{-Pr})_3$  were purified by distillation under reduced pressure of argon, and stored under argon in Schlenk tubes with an air-tight stopper, then kept in the cool room. The purity of nucleophiles was checked by their  $^{31}\text{P}$  NMR. Figure 3.2(a) shows  $^{31}\text{P}$  NMR spectrum of pure  $\text{P}(n\text{-Bu})_3$ . The resonance of  $\text{O}=\text{P}(n\text{-Bu})_3$  would show up at  $> -173.3$  ppm {= the one of  $\text{P}(n\text{-Bu})_3$ }.

All kinetic runs were carried out in the absence of  $\text{O}_2$  and under the pseudo-first-order condition by using at least a 20-fold molar excess of nucleophile. The cluster  $\text{Os}_6(\text{CO})_{18}$  does not dissolve in hexane and heptane solvents, but it does in toluene. Toluene was chosen as a solvent also because the solvent gives well resolved IR absorption peaks, while other solvents, such as  $\text{C}_2\text{H}_2\text{Cl}_4$  and  $\text{C}_2\text{H}_4\text{Cl}_2$ ,

do not give such well resolved IR spectra. The initial concentration of stock solution of reacting complex is generally ca.  $2 \times 10^{-4} \text{M}$ , which is a saturated solution.

The reaction pattern of a given system was preliminarily investigated by the repetitive scan mode of UV-Vis monitoring between 700 and 250 nm {Figure 3.2(b)}. The half-life,  $t_{1/2}$ , of a reaction or sometimes even the rate constants can be estimated. Based on the information obtained, a kinetic run was decided to be done under suitable conditions by employing either FTIR or UV-Vis monitoring techniques. UV-Vis monitoring may be employed provided that accurate values of  $A_{\infty}$  could be obtained, exactly as described in the Chapter 2. Kinetic runs were monitored by using the automatic timed scanner and recording the maximal changes of absorbance at one wavelength, sometimes other than  $\lambda_{\text{max}}$ , because  $\lambda_{\text{max}}$  does not necessarily have the maximal changes of absorbance.

The experiment details for the kinetic monitoring of reactions of  $\text{Os}_6(\text{CO})_{18}$  for both techniques, FTIR and UV-Vis, are exactly the same as for  $\text{Ru}_3(\text{CO})_{11}\text{L}$ . The initial concentration of complex and the total volume of solution in each run were kept constant. FTIR spectral changes are shown in Figures 3.3–3.6. Reactions were monitored for at least 5 half-lives for both techniques. Plots of  $\ln|A_t - A_{\infty}|$  vs time were linear for over 96 % reaction.

### 3.3 Results of Kinetic Studies

#### 3.3.1 Reactions with P-donor Nucleophiles

The seven nucleophiles,  $\text{etpb}$ ,  $\text{P(OEt)}_3$ ,  $\text{PMe}_3$ ,  $\text{PPhMe}_2$ ,  $\text{P(OPh)}_3$ ,  $\text{P(O-}i\text{-Pr)}_3$ , and  $\text{P}(n\text{-Bu)}_3$ , were used to study the substitution reactions of  $\text{Os}_6(\text{CO})_{18}$  in toluene. These ligands cover a wide range of  $\text{pK}_a'$  values from -2.79 to 8.67, and a fairly large range in size from  $101^\circ$  to  $132^\circ$ . Generally speaking,  $\text{Os}_6(\text{CO})_{18}$  reacts with all ligands used to give simple monosubstituted products in the first step. The rates of reaction and the degree of substitution are dependent on the nature of nucleophiles. It was found that rates for most monosubstitution reactions were very slow. It is time-consuming to measure rate constants. For example,  $\text{Os}_6(\text{CO})_{18}$  with  $\text{P(OPh)}_3$   $\{\text{pK}_a' = -2.79, [\text{L}'] = 0.2960 \text{ M}\}$  had no reaction to be observed at ca.  $40^\circ\text{C}$  running for 54 hrs based on both FTIR and UV-Vis monitoring. Even with the strong base  $\text{P}(n\text{-Bu)}_3$  ( $\text{pK}_a' = 8.67$ ) the reaction took about 6.5 hrs to completion at  $25.1^\circ\text{C}$  when  $[\text{P}(n\text{-Bu)}_3] = 0.07459 \text{ M}$ . The estimated half-lives for monosubstitution of  $\text{Os}_6(\text{CO})_{18}$  with nucleophiles are shown below. It can be expected that the reactions with large nucleophiles, such as  $\text{PPh}_3$ , are extremely slow. The introduction of the labile acetonitrile ligand into  $\text{Os}_6(\text{CO})_{18}$  greatly enhances its reactivity under mild reaction conditions [7]. It was reported that the activated complexes  $\text{Os}_6(\text{CO})_{18-n}(\text{NCMe})_n$ ,  $n = 1, 2$ , reacted with  $\text{PPh}_3$  at 195 K to afford the clusters  $\text{Os}_6(\text{CO})_{17}(\text{PPh}_3)$  and  $\text{Os}_6(\text{CO})_{16}(\text{PPh}_3)_2$  [7].

**Table 3.2 Half-lives of Monosubstitution Reactions of  $\text{Os}_6(\text{CO})_{18}$  with  $\text{L}'$  at  $(25.0 \pm 0.1)^\circ\text{C}$ .  $[\text{Complex}] = 8 \times 10^{-5} \text{ M}$  or  $2 \times 10^{-5} \text{ M}$  for FTIR and UV-Vis monitoring, respectively**

$\text{L}'$	Expt.[ $\text{L}'$ ] (M)	$\text{pK}_a'$	$\theta$ (deg)	$\theta'$ (deg)	Half-life (hr)
etpb	0.03550	-0.30	101	118	4.1
$\text{P}(\text{OEt})_3$	0.07650	1.64	109	136	3.4
$\text{PMe}_3$	0.1976	6.45	118	125	0.04
$\text{PPhMe}_2$	0.003000	5.07	122	128	0.7
$\text{P}(\text{OPh})_3$	0.2960	-2.79	128	140	—
$\text{P}(\text{O-}i\text{-Pr})_3$	0.1599	3.38	130	145	6.5
$\text{P}(n\text{-Bu})_3$	0.07459	8.67	132	139	3.2

Figures 3.3 and 3.4 show a series of FTIR spectra recorded during a typical kinetic run. Absorption due to solvent was excluded by 100 % subtraction, using the solvent as a reference. All spectra obtained were leveled to minimize the error due to slight baseline shift. The IR bands in the CO stretching region due to  $\text{Os}_6(\text{CO})_{18}$  and  $\text{Os}_6(\text{CO})_{17}\text{L}$  are well-separated and allow accurate kinetic monitoring of the disappearance of the reactant. As the characteristic IR bands for  $\text{Os}_6(\text{CO})_{18}$  change to the ones assigned to the  $\text{Os}_6(\text{CO})_{17}\text{L}$  species, sharp isosbestic points are usually formed, indicating a clean reaction as shown in Eq.(3.1), without detectable intermediates or disubstituted products (Figures 3.3, 3.4, and 3.5). The FTIR spectroscopic data of

the parent cluster and substituted derivatives, formed *in situ*, are summarized in Table 3.3.



Eventual multisubstitutions were observed for all but the least basic ligand  $\text{P}(\text{OPh})_3$ . The subsequent reactions of the monosubstituted product  $\text{Os}_6(\text{CO})_{17}\text{PMe}_3$  with  $\text{PMe}_3$  (0.001900 M) was followed, and the result shows that the step  $(n + 1)$  is slower than the step  $n$ .

$\text{Os}_6(\text{CO})_{18}$  has a broad absorption band in the ultraviolet region ( $\lambda_{\text{max}} = 356 \text{ nm}$ ), and the monosubstituted products  $\text{Os}_6(\text{CO})_{17}\text{L}$  have much more intense absorption spectra with  $\lambda_{\text{max}} < 300 \text{ nm}$  than the parent cluster. There is a big increasing change of absorption in the region between 320–340 nm during the monosubstitution reactions. Usually some wavelengths between 320–340 nm other than  $\lambda_{\text{max}}$  of  $\text{Os}_6(\text{CO})_{18}$  were chosen to monitor (time drive mode). The rate constants obtained by UV-Vis and FTIR monitoring for the same reaction were found to be in good agreement with each other. Figure 3.7 shows a nice linear plot of  $k_{\text{obs}}$  vs  $[\text{L}']$  from both monitoring techniques.

**Table 3.3 FTIR Data<sup>a</sup> for the Cluster Os<sub>6</sub>(CO)<sub>18</sub> and the Substituted Derivatives, formed *in situ*, in C-O Stretching Region**

Cluster	$\nu_{\text{C-O}}$ (cm <sup>-1</sup> )		
Os <sub>6</sub> (CO) <sub>18</sub>	2107(w)	2076(vs)	2062(vs)
	2038(vs)	2001(w)	1955(w)
Os <sub>6</sub> (CO) <sub>18</sub> <sup>b</sup> [10]	2108(w)	2077(vs)	2063(vs)
	2040(vs)	2007(w)	1959(w)
Os <sub>6</sub> (CO) <sub>17</sub> [P( <i>n</i> -Bu) <sub>3</sub> ]	2090(w)	2055(m)	2043(w)
	2032(s)	2019(vs)	2006(vs)
	1987(w)	1981(w)	
Os <sub>6</sub> (CO) <sub>17</sub> PPh <sub>3</sub> <sup>b</sup> [15a]	2089(m)	2056(s)	2032(s)
	2027(s sh)	1999(w)	1976(w)
	1947(w)		
Os <sub>6</sub> (CO) <sub>17</sub> [PMe <sub>3</sub> ]	2125(vw)	2048(s)	2034(s)
	2006(s)	1996(s)	1992(s)
	1987(s)	1980(m)	1977(m)
	1973(m)	1971(m)	
Os <sub>6</sub> (CO) <sub>17</sub> [P(OEt) <sub>3</sub> ]	2132(m)	2089(m)	2056(s)
	2008(vs)	1986(m)	1973(s)
Os <sub>6</sub> (CO) <sub>17</sub> [P(OMe) <sub>3</sub> ] <sup>b</sup> [15a]	2092(w)	2069(m)	2057(s)
	2036(vs)	2030(vs sh)	1990(w sh)
	1961(w)	1947(w)	1938(w)
Os <sub>6</sub> (CO) <sub>17</sub> [PPhMe <sub>2</sub> ][15b]	2127(w)	2047(s)	2008(s)
	1990(s)		

$\text{Os}_6(\text{CO})_{17}[\text{P}(\text{O}-i\text{-Pr})_3]$	2102(m)	2070(s)	2029(m)
	2003(s)	1977(m)	

---

a. Spectra recorded in toluene unless otherwise indicated. Letters in parentheses indicate relative absorptivities of individual peaks.

b. In  $\text{CH}_2\text{Cl}_2$

### 3.3.2 Data Treatment

Pseudo-first-order rate constants ( $k_{\text{obs}}$ ) were obtained by fitting the exponential dependence of the absorbance vs time and using a nonlinear least-squares regression program, KORE [16], which provides values of  $k_{\text{obs}}$  and  $A_{\infty}$ , the absorbance after completion of the reactions. In all cases the rates of subsequent reactions were slow enough for the values of  $A_{\infty}$  to be well-defined. For some reactions values of  $A_{\infty}$  were also measured after at least 5 half-lives of the reaction, and plots of  $\ln|A_t - A_{\infty}|$  vs time were usually linear for more than 3 half-lives. When KORE was used to obtain the  $k_{\text{obs}}$  values, the correlation coefficient was generally 0.9999 – 0.999999 for up to 99 % reaction. Figures 3.8, 3.9 show absorbance change against time during the reactions. Table 5.5 summarizes all pseudo-first-order rate constants for reactions of  $\text{Os}_6(\text{CO})_{18}$  with nucleophiles in toluene.

### 3.3.3 Dependence of $k_{\text{obs}}$ on $[\text{L}']$

The rate plots for all kinetic runs at all temperatures show excellent linear relationships between  $k_{\text{obs}}$  and  $[\text{L}']$ , as shown in Figures 3.10–3.12. The observed rate constants,  $k_{\text{obs}}$ , are very dependent of concentrations  $[\text{L}']$  of nucleophiles. The usually negligible intercepts

indicate that the nucleophilic substitution reactions of  $\text{Os}_6(\text{CO})_{18}$  in toluene are dominated by an associative mechanism. The gradients, which are the rate constants of the associative substitution reactions, are very sensitive to the nature of nucleophiles along the series  $\text{L}' = \text{PMe}_3$  ( $\text{pK}_a' = 6.45$ ,  $\theta = 118^\circ$ )  $>$   $\text{PPhMe}_2$  (5.07,  $122^\circ$ )  $\gg$   $\text{P}(n\text{-Bu})_3$  (8.67,  $132^\circ$ )  $>$   $\text{etpb}$  (-0.30,  $101^\circ$ )  $>$   $\text{P}(\text{OEt})_3$  (1.64,  $109^\circ$ )  $>$   $\text{P}(\text{O-}i\text{-Pr})_3$  (3.28,  $130^\circ$ ) (Figure 3.10), as expected based on the basicity  $\text{pK}_a'$  and Tolman cone angles  $\theta$  of nucleophiles. The rate constant  $k_2$  at  $25.0^\circ\text{C}$  for the reaction of  $\text{PPhMe}_2$  with  $\text{Os}_6(\text{CO})_{18}$  is 113 times that of  $\text{P}(n\text{-Bu})_3$ .

Linear least-squares analyses of the dependence of  $k_{\text{obs}}$  on  $[\text{L}']$  values show that the data fit closely to Eq.(3.2)

$$k_{\text{obs}} = a + k_2[\text{L}'] \quad (3.2)$$

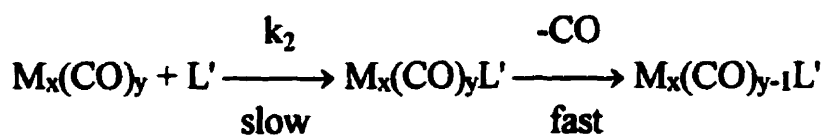
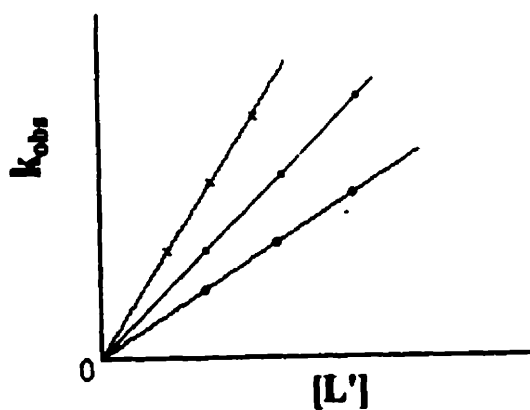
where  $k_2$  is the second-order rate constant, and  $a$  is a constant which in most cases is very close to zero as shown in the rate plots in Figures 3.10–3.12 and by the data in Table 5.5. However, in a few cases  $a$  is not negligible. For instance, when  $\text{L}' = \text{PMe}_3$  at  $35.0^\circ\text{C}$ , and  $\text{etpb}$  at  $35.0^\circ\text{C}$  and  $45.0^\circ\text{C}$ , the straight lines do not pass through the origin. Nevertheless, values of  $a$  are still quite small ( Figure 3.10 and Table 3.4). They are frequently slightly negative. We do not, therefore, regard them as having any mechanistic significance and have to conclude that there are occasional systematic errors or statistical accidents which may lead to the apparently significant values of  $a$ .

The values of  $a$  and  $k_2$  as well as their standard deviations can be obtained by the weighted linear least squares analyses of the

dependence of  $k_{\text{obs}}$  on  $[L']$  values. Each value of  $k_{\text{obs}}$  was weighted according to the assumption of a constant probable error, expressed as a percentage, and these percentage errors are provided by the analyses. Values of  $a$  and  $k_2$  are listed in Table 3.4 together with their standard deviations and the probable errors of each value of  $k_{\text{obs}}$ .

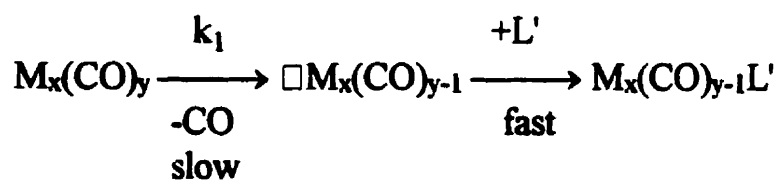
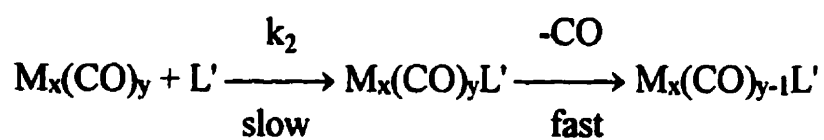
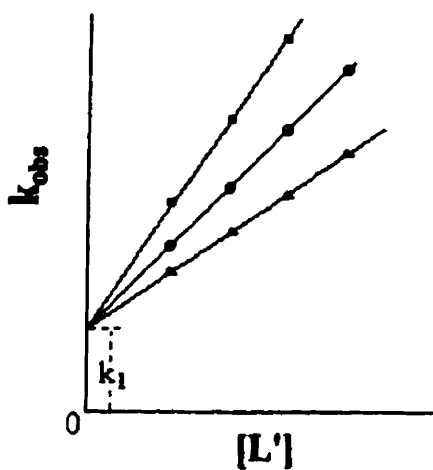
It is obvious that  $a$  does not equal  $k_1$  ( $a \neq k_1$ ) because in most cases  $a$  is close to zero, statistically insignificant, or at least small but very dependent on the nature of  $L'$ , i.e. not the same irrespective of  $L'$ ; while  $k_1$  is a rate constant of dissociative substitution reactions, and it is independent of the nature of  $L'$ , that is, for a given cluster different nucleophiles have the same  $k_1$  value. The  $a$  is not equal to  $k_{-L'}$  either ( $a \neq k_{-L'}$ ) because  $k_{-L'}$  is a backward rate constant of pre-equilibrium association or adduct formation process. The comparison of  $a$ ,  $k_1$ , and  $k_{-L'}$  is shown by following rate equations and plots.

### Associative Process



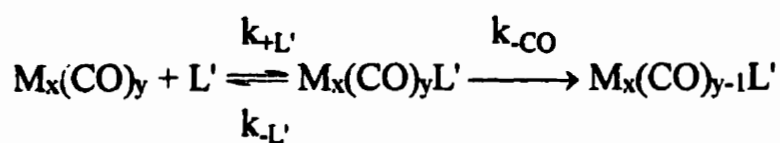
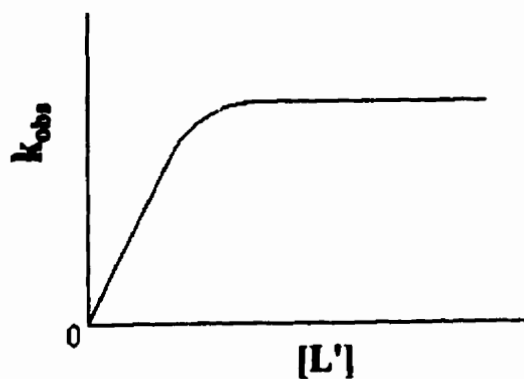
$$k_{\text{obs}} = a + k_2 [L']$$

## Associative and Dissociative Process



$$k_{\text{obs}} = k_1 + k_2 [\text{L}']$$

## Pre-equilibrium Association or Adduct Formation Process



$$k_{\text{obs}} = \frac{k_{-CO} K[\text{L}']}{1 + K[\text{L}']}; \quad K = k_{+L'} / k_{-L'}$$

When  $[\text{L}']$  is very small,  $k_{\text{obs}} = k_{-CO} K[\text{L}']$

When  $[\text{L}']$  is very large,  $k_{\text{obs}} = k_{-CO}$

**Table 3.4 Rate Constants<sup>a</sup> for the Reactions of Os<sub>6</sub>(CO)<sub>18</sub> with Nucleophiles L' in Toluene, [Complex] = 8×10<sup>-5</sup> M and 2×10<sup>-5</sup> M for FTIR and UV-Vis Monitoring, respectively**

T (°C)	N <sup>b</sup>	a (s <sup>-1</sup> )	k <sub>2</sub> (M <sup>-1</sup> s <sup>-1</sup> )	σ(k <sub>obs</sub> ) <sup>c</sup> (%)	[L'] (M)
<b>L' = PMe<sub>3</sub> (pKa' = 6.45, θ = 118°, θ' = 125°)</b>					
15.0	10 <sup>e</sup>	(1.681±0.084)×10 <sup>-3</sup>	(0.7956±0.0197 <sup>d</sup> )	1.8	0.0020–0.0080
25.0	8 <sup>e</sup>	(1.733±0.097)×10 <sup>-3</sup>	(1.712±0.026)	1.2	0.0020–0.0080
35.0	8 <sup>e</sup>	(4.701±0.075)×10 <sup>-3</sup>	(2.343±0.035)	0.6	0.0010–0.0040
<b>L' = PPhMe<sub>2</sub> (pKa' = 5.07, θ = 122°, θ' = 128°) [15(b)]</b>					
25.0	8 <sup>f</sup>	(-2.140±0.720)×10 <sup>-4</sup>	(0.1786±0.0184)	11	0.0030–0.0120
<b>L' = P(n-Bu)<sub>3</sub> (pKa' = 8.67, θ = 132°, θ' = 139°)</b>					
25.1	10 <sup>e</sup> &f	(-3.294±1.663)×10 <sup>-5</sup>	<sup>g</sup> (1.584±0.187)×10 <sup>-3</sup>	9.2	0.067–0.200
35.0	8 <sup>e</sup>	(-1.368±1.752)×10 <sup>-5</sup>	(3.536±0.360)×10 <sup>-3</sup>	10	0.030–0.120
45.0	8 <sup>e</sup>	(1.138±1.170)×10 <sup>-5</sup>	(4.590±0.228)×10 <sup>-3</sup>	4.6	0.030–0.120
<b>L' = etpb (pKa' = -0.30, θ = 101°, θ' = 118°)</b>					
25.1	10 <sup>e</sup>	(1.777±0.353)×10 <sup>-5</sup>	(9.375±0.576)×10 <sup>-4</sup>	4.1	0.036–0.110
35.0	8 <sup>e</sup>	(6.304±0.311)×10 <sup>-5</sup>	(1.848±0.050)×10 <sup>-3</sup>	0.9	0.044–0.088
45.0	8 <sup>e</sup>	(1.970±0.062)×10 <sup>-4</sup>	(3.480±0.098)×10 <sup>-3</sup>	0.8	0.044–0.088

Table 3.4 (continued)

T (°C)	N <sup>b</sup>	a (s <sup>-1</sup> )	k <sub>2</sub> (M <sup>-1</sup> s <sup>-1</sup> )	σ(k <sub>obs</sub> ) <sup>c</sup> (%)	[L'] (M)
<b>L' = P(OEt)<sub>3</sub> (pKa' = 1.64, θ = 109°, θ' = 136°)</b>					
25.0	14 <sup>e&amp;f</sup>	(-0.3991±0.3060)×10 <sup>-5</sup>	(6.654±0.263)×10 <sup>-4</sup>	5.8	0.077–0.340
35.0	8 <sup>e</sup>	(2.810±0.618)×10 <sup>-5</sup>	(9.510±0.498)×10 <sup>-4</sup>	4.7	0.068–0.340
45.0	8 <sup>e</sup>	(4.227±0.664)×10 <sup>-5</sup>	(2.025±0.034)×10 <sup>-3</sup>	1.5	0.112–0.450
55.0	8 <sup>e</sup>	(-5.464±2.298)×10 <sup>-5</sup>	(4.403±0.126)×10 <sup>-3</sup>	2.8	0.068–0.450
<b>L' = P(O-<i>i</i>-Pr)<sub>3</sub> (pKa' = 3.38, θ = 130°, θ' = 145°)</b>					
25.0	10 <sup>e</sup>	(1.768±0.320)×10 <sup>-5</sup>	(2.090±0.117)×10 <sup>-4</sup>	3.7	0.16–0.48
35.0	8 <sup>e</sup>	(2.252±0.338)×10 <sup>-5</sup>	(3.192±0.102)×10 <sup>-4</sup>	1.3	0.24–0.48
45.0	8 <sup>e</sup>	(2.148±1.920)×10 <sup>-5</sup>	(6.749±0.583)×10 <sup>-4</sup>	4.0	0.24–0.48
50.0	8 <sup>e</sup>	(-5.343±2.208)×10 <sup>-5</sup>	(1.205±0.069)×10 <sup>-3</sup>	3.4	0.24–0.48
55.0	8 <sup>e</sup>	(-1.561±0.313)×10 <sup>-4</sup>	(1.681±0.102)×10 <sup>-3</sup>	4.1	0.24–0.48

- a. Values of k<sub>2</sub> are obtained from measurements at different values of [L'] and at two different wavenumbers and/or wavelengths.
- b. The number of individual determinations of k<sub>obs</sub>; k<sub>obs</sub> = a + k<sub>2</sub>[L'].
- c. Probable error of k<sub>obs</sub> obtained from the scatter of the data about the straight line of k<sub>obs</sub> vs [L']; while values of σ(k<sub>obs</sub>) in Table 5.5 were inferred from the scatter of data around the single exponential curve.
- d. Standard deviation.
- e. Studied by using UV-Vis monitoring.
- f. Studied by using FTIR monitoring.

g. The values of  $k_{\text{obs}}$  obtained by monitoring at two different wavenumbers (2076 and 2062  $\text{cm}^{-1}$ ) did not agree well. The true values of  $A_1$  and  $A_\infty$  cannot be obtained for the first stage of reaction by following the band at 2062  $\text{cm}^{-1}$  because the absorbance changes in the region around 2055  $\text{cm}^{-1}$  are quite complicated, increasing first and then decreasing, and this means that the spectral changes of the band 2062  $\text{cm}^{-1}$  are not affected only by decrease of  $[\text{Os}_6(\text{CO})_{18}]$ , as shown in Figures 3.3 and 3.13. Nevertheless, the values of  $k_{\text{obs}}$  obtained from 2076  $\text{cm}^{-1}$  (FTIR), 320 and 324 nm (UV) agree very well one another. A nice linear plot of  $k_{\text{obs}}$  vs  $[L']$  from both monitoring was obtained (Figure 3.7).

### 3.3.4 Activation Parameters $\Delta H_2^\ddagger$ and $\Delta S_2^\ddagger$

The temperature dependence of values of  $k_2$  for the substitution reactions of  $\text{Os}_6(\text{CO})_{18}$  with nucleophiles  $L'$  was also studied. Activation parameters  $\Delta H_2^\ddagger$  and  $\Delta S_2^\ddagger$  were obtained by an unweighted linear least-squares analysis of the dependence of  $\ln(k_2/T)$  on  $1/T$  based on the Eyring equation.

$$\ln(k_2/T) = 23.76 + \Delta S_2^\ddagger/R - \Delta H_2^\ddagger/RT \quad (3.3)$$

The individual Eyring equations derived from the experimental results for the reactions of  $\text{Os}_6(\text{CO})_{18}$  with  $L'$  in toluene are as follows:

$$\begin{array}{ll} Y(i) = (7.306 \pm 0.747) + (-5958 \pm 230)X(i) & L' = \text{etpb} \\ Y(i) = (12.41 \pm 0.55) + (-7750 \pm 171)X(i) & L' = \text{P(OEt)}_3 \\ Y(i) = (9.859 \pm 1.861) + (-4519 \pm 554)X(i) & L' = \text{PMe}_3 \\ Y(i) = (13.32 \pm 1.688) + (-8367 \pm 537)X(i) & L' = \text{P(O-}i\text{-Pr)}_3 \end{array}$$

$$Y(i) = (2.573 \pm 2.204) + (-4339 \pm 678)X(i) \quad L' = P(n\text{-Bu})_3$$

The data fitted linear Eyring plots (Figures 3.14 and 3.15) very well. Table 3.5 lists the activation parameters together with their standard deviations and probable errors in terms of  $k_2$  values obtained from the data analyses. The quite low probable errors indicate the good precision of the rate constants.

**Table 3.5 Activation Parameters for the Second Order Substitution Reactions of  $\text{Os}_6(\text{CO})_{18}$  with P-donor Nucleophiles  $L'$  in Toluene**

$L'$	$pK_a'$	$\theta$	$N^a$	$\Delta H_2^*$ (kcal mol <sup>-1</sup> )	$\Delta S_2^*$ (cal K <sup>-1</sup> mol <sup>-1</sup> )	$k_2(45.0^\circ\text{C})$ (M <sup>-1</sup> s <sup>-1</sup> )	$\sigma^b$ (%)
etpb	-0.30	101	26	11.84±0.46	-32.69±1.48	(3.480±0.098)×10 <sup>-3</sup>	4.9
P(OEt) <sub>3</sub>	1.64	109	32	15.40±0.34	-22.56±1.09	(2.025±0.034)×10 <sup>-3</sup>	5.7
PMe <sub>3</sub>	6.45	118	26	8.98±1.10	-27.62±3.70	4.138 <sup>c</sup>	13.3
P(O- <i>i</i> -Pr) <sub>3</sub>	3.38	130	42	16.62±1.07	-20.74±3.35	(6.748±0.583)×10 <sup>-4</sup>	10.5
P( <i>n</i> -Bu) <sub>3</sub>	8.67	132	24	8.62±1.35	-42.10±4.38	(4.590±0.228)×10 <sup>-3</sup>	15.3

- The number of individual determinations of  $k_{\text{obs}}$  values.
- Standard error in  $k_2$  estimated from the scatter of  $\ln(k_2/T)$  values around the Eyring plot.
- Calculated by  $\Delta H_2^*$  &  $\Delta S_2^*$  for the reactions of  $\text{Os}_6(\text{CO})_{18}$  with  $\text{PMe}_3$  in toluene according to the Eyring equation.

The increases of  $\Delta H_2^\ddagger$ , for the reactions of  $\text{Os}_6(\text{CO})_{18}$  with  $L'$ , are offset by corresponding increases in  $\Delta S_2^\ddagger$ , but not overcome, and the data of  $\Delta H_2^\ddagger$  and  $\Delta S_2^\ddagger$  lie on an excellent isokinetic plot, except those of  $\text{PMe}_3$ , the gradient of which leads to an isokinetic temperature  $89^\circ\text{C}$  (Figure 3.16). The figure shows that the values of  $\Delta H_2^\ddagger$  and  $\Delta S_2^\ddagger$  have parallel changes, and changes in  $\Delta G_2^\ddagger$  are far less pronounced than those of  $\Delta H_2^\ddagger$ . The trends in the rate constants are therefore clearly more dependent on  $\Delta H_2^\ddagger$  than on  $\Delta S_2^\ddagger$ . Thus the values of  $k_2$  decrease along the series  $L' = \text{P}(n\text{-Bu})_3 > \text{etpb} > \text{P}(\text{OEt})_3 > \text{P}(\text{O-}i\text{-Pr})_3$  (Table 3.5).

Figure 3.17 is another excellent example of isokinetic behavior,  $\ln(k_2/T)$  vs  $1/T$ , clearly shows an isokinetic temperature around  $88^\circ\text{C}$ , and implies again that the rates are more dependent on the enthalpy of activation than on the entropy.

### 3.4 Analyses of Kinetic Results

#### 3.4.1 Quantitative Separation of Electronic and Steric Effects

##### 3.4.1.1 Characteristic Kinetic Parameters

Poë's model described in Chapter 2 for separating the electronic and steric effects of various nucleophiles in associative substitution reactions of LNCCs is also entirely successful for the reactions of HNCC  $\text{Os}_6(\text{CO})_{18}$  with nucleophiles  $L'$ , thus demonstrating the general validity of the model and of the electronic and steric parameters used. The kinetic data and parameters at various temperatures, derived by use of double-linear regression and three-coefficient computer program, are listed in Tables 3.6, 3.7, and 3.8.

A plot of  $\log k_2$  values for nucleophiles,  $\text{etpb}$ ,  $\text{P(OEt)}_3$ ,  $\text{PMe}_3$ , and  $\text{PPhMe}_2$ , small enough ( $\theta < \theta_{\text{th}}$ ) not to show any steric effects, against their  $\text{pKa}'$  values provides the electronic profile of associative substitution reactions of  $\text{Os}_6(\text{CO})_{18}$  with nucleophiles  $\text{L}'$  in toluene, as shown in Figure 3.18. The gradient of this straight line gives the electronic discrimination parameter  $\beta$  of 0.470 at 25.0°C. The electronic profile shows a clear LFER for these small nucleophiles ( $\theta \leq 122^\circ$ ). The larger nucleophiles,  $\text{P(O-}i\text{-Pr)}_3$  and  $\text{P}(n\text{-Bu)}_3$ , have negative deviations from the electronic profile.  $\text{P(O-}i\text{-Pr)}_3$  and  $\text{P}(n\text{-Bu)}_3$  are almost isosteric nucleophiles,  $\theta = 130^\circ$  and  $132^\circ$ , with very different  $\sigma$ -basicity,  $\text{pKa}' = 3.38$  and  $8.67$ , respectively. They can also be chosen to obtain precise values of  $\beta$  when adjusted for what their  $\log k_2$  values would have been if their  $\theta = 130^\circ$  based on steric effects. In fact, they give exactly the same values of  $\beta$ , as the small nucleophiles do (Figure 3.18).

The values of  $\beta$  at different temperatures were used to calculate the electronically corrected rate constants,  $\log k_2^\circ = \log k_2 - \beta(\text{pKa}' + 4)$ , at the corresponding temperatures (Table 3.6). The steric profile was constructed by plotting  $\log k_2^\circ$  vs  $\theta$ , as shown in Figure 3.19. The steric profile drawn in terms of  $\theta'$ , namely the plot of  $\log k_2^\circ$  versus  $\theta'$ , is also included in Figure 3.19. The characteristic kinetic parameters,  $\text{SR}$ ,  $\beta$ ,  $\gamma$ , and  $\theta_{\text{th}}$ , derived by use of double-linear regression and three-coefficient computer program and Tolman cone angles  $\theta$  as a steric parameter, are  $-5.35 \pm 0.30$ ,  $0.514 \pm 0.071$ ,  $-0.763 \pm 0.105 \text{ deg}^{-1}$ , and  $127^\circ$  at 25.0°C, respectively (Table 3.8). If the  $\theta$  value of  $\text{P}(n\text{-Bu)}_3$  is  $136^\circ$  as decided by Giering instead of  $132^\circ$ , the kinetic parameters are  $-5.41 \pm 0.30$ ,  $0.527 \pm 0.072$ ,  $-0.277 \pm 0.038 \text{ deg}^{-1}$ , and  $122^\circ$  at 25.0°C,

respectively (Table 3.8). It is obvious that the values of SR and  $\beta$  are precise, the value of  $\theta_{th}$  is between  $122^\circ$  and  $127^\circ$  ( $122^\circ \leq \theta_{th} \leq 127^\circ$ ) as shown in Figure 3.19 clearly, and the value of  $\gamma$  is between  $-0.278$  and  $-0.763 \text{ deg}^{-1}$ . While analyzing with  $\theta'$  values, a better fit was obtained characterized by RMSD and R values of 0.109 and 0.998 at  $25.0^\circ\text{C}$ , respectively, if the data for  $\text{P}(n\text{-Bu})_3$  were omitted. The kinetic parameters, SR,  $\beta$ ,  $\gamma$ , and  $\theta'_{th}$ , derived by use of  $\theta'$  as the steric parameter, are  $-4.79 \pm 0.14$ ,  $0.467 \pm 0.032$ ,  $-0.173 \pm 0.013 \text{ deg}^{-1}$  and  $130^\circ$  at  $25.0^\circ\text{C}$ , respectively. The lower limiting value of  $|\gamma|$  is  $0.173 \text{ deg}^{-1}$ . Except for  $\gamma$ , they are not significantly different from those based on the Tolman cone angles  $\theta$ , viz  $-5.35 \pm 0.30$ ,  $0.514 \pm 0.071$ ,  $-0.763 \pm 0.105 \text{ deg}^{-1}$ , and  $127^\circ$ ;  $-5.07$ ,  $0.470$ ,  $-0.670$ , and  $127^\circ$  at  $25.0^\circ\text{C}$ , respectively derived from least squares analysis and graphical construction of electronic and steric profiles (Table 3.8). If the data for  $\text{P}(n\text{-Bu})_3$  were considered, the value of  $\gamma$  derived with  $\theta'$  as a steric parameter is close to that inferred with  $\theta$  as a steric parameter.

The kinetic parameters  $\alpha$ ,  $\beta$ ,  $\gamma$ , and  $\theta_{th}$  at various temperatures can be used to calculate  $\Delta H_2^\ddagger$  and  $\Delta S_2^\ddagger$  of the reaction for a hypothetical nucleophile with  $\text{Os}_6(\text{CO})_{18}$  based on the Poë's stereoelectronic Eq.(2.5)  $\log k_2 = \alpha + \beta(\text{pKa}' + 4) + \gamma(\theta - \theta_{th})\lambda$  and Eyring equation  $\ln(k_2/T) = 23.76 + \Delta S_2^\ddagger/R - \Delta H_2^\ddagger/RT$ . Because the hypothetical nucleophile is small enough ( $\theta < \theta_{th}$ ) to exhibit no steric effects and weak enough ( $\text{pKa}' = -4$ ) (i.e. weaker than any commonly used nucleophiles) to show no electronic effects, the stereoelectronic Eq.(2.5) can therefore be expressed as below.

For hypothetical nucleophiles

$$(\log k_2)_T = \alpha_T \quad (3.4)$$

The values of  $\log k_2$  at various temperatures can be obtained according to the values of  $\alpha$  at the corresponding temperatures. Then values of  $\Delta H_2^\ddagger$  and  $\Delta S_2^\ddagger$  can be derived by using the linear least-squares analysis of the dependence of  $\ln(k_2/T)$  on  $1/T$  based on the Eyring equation. The data fit the equation quite well with a correlation coefficient of 0.9998 or 0.993 ( $\theta'$  and  $\theta$  as a steric parameter, respectively) as shown in Table 3.9. Two sets of values of  $\Delta H_2^\ddagger$  and  $\Delta S_2^\ddagger$  agree with each other very well.

**Table 3.6 Kinetic Data for Reactions of Os<sub>6</sub>(CO)<sub>18</sub> with Nucleophiles L' in Toluene**

L'	pKa'	θ(deg)	<sup>a</sup> θ'(deg)	logk <sub>2</sub> <sup>b</sup>	logk <sub>2</sub> - β(pKa' + 4)		
(25.0 ± 0.1)°C					<sup>c</sup> β=0.514	<sup>c</sup> β=0.466	
etpb	-0.30	101	118	-3.0314	-4.9332	-4.7556	
P(OEt) <sub>3</sub>	1.64	109	136	-3.4271	-6.3261	-6.0553	
PMe <sub>3</sub>	6.45	118	125	0.1733	-5.1980	-4.6964	
PPhMe <sub>2</sub>	5.07	122	128	-0.7480	-5.4100	-4.9746	
P(O- <i>i</i> -Pr) <sub>3</sub>	3.38	130	145	-3.9236	-7.7169	-7.3627	
P( <i>n</i> -Bu) <sub>3</sub>	8.67	132	139	-2.7276	-9.2400	-8.6318	
35.0°C					<sup>d</sup> β=0.460	<sup>e</sup> β=0.460	
etpb	-0.30	101	118	-2.7354	-4.4374	-4.4374	
P(OEt) <sub>3</sub>	1.64	109	136	-3.0464	-5.6408	-5.6408	
PMe <sub>3</sub>	6.45	118	125	0.4013	-4.4057	-4.4057	
P(O- <i>i</i> -Pr) <sub>3</sub>	3.38	130	145	-3.5139	-6.9087	-6.9087	
P( <i>n</i> -Bu) <sub>3</sub>	8.67	132	139	-2.5082	-8.3364	-8.3364	
45.0°C					<sup>d</sup> β=0.456	<sup>e</sup> β=0.456	
etpb	-0.30	101	118	-2.4575	-4.1447	-4.1447	
P(OEt) <sub>3</sub>	1.64	109	136	-2.6892	-5.2610	-5.2610	
PMe <sub>3</sub>	6.45	118	125	0.6154	-4.1498	-4.1498	
P(O- <i>i</i> -Pr) <sub>3</sub>	3.38	130	145	-3.1295	-6.4948	-6.4948	
P( <i>n</i> -Bu) <sub>3</sub>	8.67	132	139	-2.3021	-8.0797	-8.0797	

Table 3.6 (continued)

L'	pKa'	$\theta$ (deg)	${}^a\theta'$ (deg)	$\log k_2^b$	$\log k_2 - \beta(\text{pKa}' + 4)$	
55.0°C					${}^d\beta=0.447$	${}^e\beta=0.447$
etpb	-0.30	101	118	-2.1962	-3.8501	-3.8501
P(OEt) <sub>3</sub>	1.64	109	136	-2.3533	-4.8744	-4.8744
PMe <sub>3</sub>	6.45	118	125	0.8168	-3.8544	-3.8544
P(O- <i>i</i> -Pr) <sub>3</sub>	3.38	130	145	-2.7681	-6.0670	-6.0670
P( <i>n</i> -Bu) <sub>3</sub>	8.67	132	139	-2.1082	-7.7717	-7.7717
65.0°C					${}^d\beta=0.438$	${}^e\beta=0.438$
etpb	-0.30	101	118	-1.9500	-3.5706	-3.5706
P(OEt) <sub>3</sub>	1.64	109	136	-2.0369	-4.5072	-4.5072
PMe <sub>3</sub>	6.45	118	125	1.0067	-3.5704	-3.5704
P(O- <i>i</i> -Pr) <sub>3</sub>	3.38	130	145	-2.4277	-5.6601	-5.6601
P( <i>n</i> -Bu) <sub>3</sub>	8.67	132	139	-1.9254	-7.4749	-7.4749

- a. Cone angles based on Brown's  $E_r$  values (ligand repulsion energies) [17, 18],  $\theta' = 103.8 + 0.553 E_r$  [19] (see text).
- b. Calculated from the experiment values of  $\Delta H_2^\ddagger$  and  $\Delta S_2^\ddagger$  according to Eyring equation,  $\ln(k_2/T) = 23.76 + \Delta S_2^\ddagger/R - \Delta H_2^\ddagger/RT$ , for the reactions of  $\text{Os}_6(\text{CO})_{18}$  with corresponding nucleophiles L' except  $\text{PPhMe}_2$ .
- c. The results derived by use of linear least-squares computer program and  $\theta$  as the steric parameter.
- d. The results obtained graphically from the electronic profile and  $\theta$  as the steric parameter.

- e. The results derived by use of linear least-squares computer program and  $\theta'$  as the steric parameter.

**Table 3.7 Rate Constants,  $\log k_2^a$ , for Reactions of  $\text{Os}_6(\text{CO})_{18}$  with Nucleophiles  $\text{L}'$  in Toluene at Different Temperatures**

	etpb	P(OEt) <sub>3</sub>	PMe <sub>3</sub>	P(O- <i>i</i> -Pr) <sub>3</sub>	P( <i>n</i> -Bu) <sub>3</sub>	Av. $\Delta(\log k_2)^b$
75.0°C	-1.7175	-1.7384	1.1870	-2.1065	-1.7527	-1.8288 0.2494
78.0°C	-1.6503	-1.6521	1.2393	-2.0136	-1.7028	-1.7547 0.1295
80.0°C	-1.6061	-1.5953	1.2734	-1.9526	-1.6699	-1.7060 0.1233
85.0°C	-1.4977	-1.4561	1.3571	-1.8029	-1.5893	-1.5865 0.1096
90.0°C	-1.3922	-1.3207	1.4385	-1.6572	-1.5109	-1.4702 0.1137
95.0°C	-1.2894	-1.1889	1.5178	-1.5154	-1.4345	-1.3570 0.1179
150.0°C	-0.3176	0.05697	2.2683	-0.1756	-0.7106	
200.0°C	0.3776	0.9466	2.8073	0.7807	-0.1912	
-20.0°C	-4.6453	-5.5049	-1.0679	-6.1594	-3.9219	
-40.0°C	-5.5654	-6.6908	-1.7744	-7.4375	-4.6016	
-60.0°C	-6.6473	-8.0862	-2.6044	-8.9403	-5.3998	
-80.0°C	-7.9491	-9.7666	-3.6021	-10.7505	-6.3593	
-100.0°C	-9.5334	-11.8131	-4.8151	-12.9553	-7.5255	
-162.0°C	-18.0947	-22.8775	-11.3350	-24.8951	-13.8110	

a. Calculated from the experiment values of  $\Delta H_2^\ddagger$  and  $\Delta S_2^\ddagger$  according to the Eyring equation for the reactions of  $\text{Os}_6(\text{CO})_{18}$  with corresponding nucleophiles L'.

b. Mean deviations.

**N.B.** When temperatures are out of the range 75.0 — 95.0°C, the values of  $\log k_2$  have no average taken because data for different ligands are too different for this to be meaningful.

**Table 3.8 Characteristic Kinetic Parameters for Reactions of  $\text{Os}_6(\text{CO})_{18}$  with Nucleophiles L' in Toluene at Various Temperatures**

T (°C)	$\theta_{\text{th}}$ (deg)	SR	$\beta$	$\gamma$ (deg <sup>-1</sup> )	RMSD	R	N <sup>c</sup>
<b>Set 1<sup>a</sup></b>							
25.0	127	-5.07	0.470	-0.670			6
35.0	127	-4.83	0.460	-0.712			5
45.0	127	-4.52	0.456	-0.776			5
55.0	128	-4.19	0.447	-0.818			5
65.0	128	-3.88	0.438	-0.870			5
<b>Set 2<sup>b</sup></b>							
25.0	127	-5.35±0.30	0.514±0.071	-0.763±0.105	0.30071	0.98	6
35.0	128	-5.13±0.47	0.506±0.123	-0.841±0.217	0.41856	0.95	5
45.0	128	-4.81±0.44	0.499±0.117	-0.896±0.218	0.39690	0.96	5
55.0	128	-4.42±0.41	0.484±0.108	-0.924±0.213	0.36327	0.96	5
65.0	128	-4.13±0.37	0.475±0.100	-1.00±0.21	0.33216	0.96	5
<b>Set 3<sup>c</sup></b>							
25.0	122	-5.41±0.30	0.527±0.072	-0.277±0.038	0.30030	0.98	6
<b>Set 4<sup>d</sup></b>							
25.0	130	-4.79±0.14	0.467±0.032	-0.173±0.013	0.10876	0.998	5
35.0	128	-4.44±0.00	0.460±0.000	-0.142±0.000	0.00114	0.9999998	4
45.0	128	-4.15±0.00	0.456±0.000	-0.141±0.001	0.00099	0.9999998	4

55.0	128	-3.85±0.01	0.447±0.000	-0.133±0.000	0.00084	0.9999998	4
65.0	129	-3.57±0.00	0.438±0.005	-0.127±0.000	0.00255	0.999998	4

---

- a. The results obtained graphically from the electronic and steric profiles and  $\theta$  as a steric parameter.
- b. Kinetic parameters derived by use of least-squares computer program and  $\theta$  as a steric parameter.
- c. The same as b except that the  $\theta$  value of  $P(n\text{-Bu})_3$  is  $136^\circ$  in stead of  $132^\circ$ .
- d. Kinetic parameters derived by use of least-squares computer program and  $\theta'$  as a steric parameter.
- e. Data points, that is, the number of nucleophiles.

**Table 3.9 Kinetic Data for the Second Order Substitution Reaction of a Hypothetical Nucleophile with  $\text{Os}_6(\text{CO})_{18}$  in Toluene**

	25.0°C	35.0°C	45.0°C	55.0°C	65.0°C
<b>Set 1</b>					
$\alpha$	-4.791	-4.436	-4.145	-3.850	-3.568
$k_2$	$1.62 \times 10^{-5}$	$3.63 \times 10^{-5}$	$7.08 \times 10^{-5}$	$1.41 \times 10^{-4}$	$2.69 \times 10^{-4}$
$\ln(k_2/T)$	-16.727	-15.954	-15.318	-14.658	-14.044
<b>Set 2</b>					
$\alpha$	-5.35	-5.13	-4.81	-4.42	-4.13
$k_2$	$4.5 \times 10^{-6}$	$7.4 \times 10^{-6}$	$1.5 \times 10^{-5}$	$3.8 \times 10^{-5}$	$7.4 \times 10^{-5}$
$\ln(k_2/T)$	-18.02	-17.54	-16.84	-15.97	-15.33

N.B. 1. Set 1 ( $\theta'$  as a steric parameter)

$$Y(i) = (5.827 \pm 0.222) + (-6721 \pm 70)X(i)$$

$$\Delta S_2^\ddagger = -35.63 \pm 0.44 \text{ cal K}^{-1} \text{ mol}^{-1}$$

$$\Delta H_2^\ddagger = 13.35 \pm 0.14 \text{ kcal mol}^{-1}$$

$$R = 0.9998; \sigma(k_2) = 2.2 \% \text{ (standard deviation)}$$

2. Set 2 ( $\theta$  as a steric parameter)

$$Y(i) = (5.224 \pm 1.519) + (-6974 \pm 482)X(i)$$

$$\Delta S_2^\ddagger = -36.83 \pm 3.02 \text{ cal K}^{-1} \text{ mol}^{-1}$$

$$\Delta H_2^\ddagger = 13.86 \pm 0.96 \text{ kcal mol}^{-1}$$

$$R = 0.993; \sigma(k_2) = 15 \% \text{ (standard deviation)}$$

### **3.4.1.2 Temperature Dependence of Electronic Profiles**

#### **3.4.1.2.1 A Novel IKR — $\log k_2$ vs $pK_a'$ for Nucleophiles with Different $\sigma$ -Basicity and Size at the IKT**

The electronic profiles at various temperatures are shown in Figure 3.20. These plots do not include data for  $L' = PPhMe_2$ , which was only studied at one temperature, or  $L' = PMe_3$ , which does not fit with the isokinetic behavior. It is very clear that the differences of rate constants  $\log k_2$  among various nucleophiles, i.e. the scatter of  $\log k_2$  values around the plot of  $\log k_2$  vs  $pK_a'$ , decrease substantially with increasing temperatures, and eventually the rate constants become the same and the electronic discrimination parameter  $\beta$  is close to zero when the isokinetic temperature is reached (Figure 3.20). It sets a novel isokinetic relationship,  $\log k_2$  vs  $pK_a'$  for nucleophiles with different  $\sigma$ -basicity and size at the IKT, and clearly indicates that all the reactions of  $Os_6(CO)_{18}$  with P-donor nucleophiles in toluene except those with  $PMe_3$ , no matter what size and  $\sigma$ -basicity the nucleophiles have, will occur at the same rate at the IKT about 88°C.

The rate constants in a wide temperature range of -162.0 – 200.0 °C are listed in Table 3.7. It is clear that there is a minimum difference of  $\log k_2$ , i.e. a minimum scatter of  $\log k_2$  values, for reactions of  $Os_6(CO)_{18}$  with various nucleophiles except  $PMe_3$  in a range of 85.0 – 90.0°C. In other words, the IKT is around 85 – 90°C, confirming the IKT about 88°C again.

### 3.4.1.2.2 Unique IKRs — $\log k_2$ vs $pK_a'$ for almost Isosteric Nucleophiles or Small Ones with $\theta < \theta_{th}$ , respectively, at Various Temperatures for a Series of Reactions — Breakthroughs between IKR and LFER

The nucleophiles  $P(O-i-Pr)_3$  and  $P(n-Bu)_3$  have very different  $\sigma$ -basicity,  $pK_a' = 3.38$  and  $8.67$ , and almost the same size,  $\theta = 130^\circ$  and  $132^\circ$ , respectively, which show the same steric effects almost. They can be chosen to obtain precise temperature dependence of electronic profiles, namely LFER, because the rates increase appropriately with varying temperatures. The data obtained for the reactions of  $Os_6(CO)_{18}$  with  $L' \{= P(O-i-Pr)_3 \text{ and } P(n-Bu)_3\}$  lead to a totally new sort of IKR, a common point of intersection in the LFER plots for different temperatures — a unique characteristic LFER isoparameter  $\xi_{iso}$ .

Figure 3.21(a) is a unique example of isokinetic behavior shown by plots of  $\log k_2$  vs  $pK_a'$  for almost isosteric nucleophiles,  $P(O-i-Pr)_3$  and  $P(n-Bu)_3$ , at various temperatures. It also shows an excellent LFER at different temperatures for the reaction series, and it is therefore **a breakthrough in providing the first example of the theoretical interconnection between an IKR and LFER**. Figure 3.21(a) clearly illustrates that a nucleophile with a  $pK_a'$  of 14.3 — isokinetic  $pK_a'$  — will react with the cluster  $Os_6(CO)_{18}$  at the same rate,  $k_2$ , at various temperatures, and that the parallel line to the X axis which passes through the intersection leads to the isokinetic temperature about  $90^\circ C$ . Least-squares analysis shows an excellent linear relationship between SR and  $\beta$  for the reaction series of  $Os_6(CO)_{18}$  with  $L'$  at various temperatures {Figure 3.21(c)}, which is

governed by the equation  $SR_T = 10.9 + (-33.1)\beta_T$  with a correlation coefficient of 0.998. So the isokinetic  $pK_a'$  is a natural outcome of the linear relationship between SR and  $\beta$ .

Figure 3.21(b) illustrates another unique IKR,  $\log k_2$  vs  $pK_a'$  for the small nucleophiles with  $\theta < \theta_{th}$ , etpb and  $P(OEt)_3$ , which exhibit no steric effects, at various temperatures (25.0°C–200.0°C). An extremely nice common point of intersection in the LFER plots within a very wide range of temperature was established. The parallel line to the X axis which passes through the intersection leads to the isokinetic temperature about 86°C. A nucleophile with a  $pK_a'$  of -7.0 – isokinetic  $pK_a'$  – will react with the cluster  $Os_6(CO)_{18}$  at the same rate,  $k_2$ , at various temperatures. It is also a **breakthrough** in providing the first two examples of the theoretical interconnection between an IKR and LFER.

The isokinetic  $pK_a'$  here refers to a series of reactions for an individual cluster with nucleophiles that are isosteric, and show the same steric effects, or small enough to exhibit no steric effects at various temperatures, while the isokinetic  $pK_a'$  obtained for  $Ru_3$  clusters relates with a series of reactions for a group of clusters with nucleophiles isosteric or small enough at the same temperature.

#### **3.4.1.2.3 A Unique LFER Isoparameter $\xi_{iso}$ , Isokinetic $pK_a'$ , for a Series of Reactions at Various Temperatures**

If there is a linear relationship between the standard reactivity SR and electronic discrimination parameter  $\beta$  for a series of reactions at various temperatures,  $SR_T = a + b\beta_T$ , it is obvious there is a common point of intersection, a unique LFER isoparameter  $\xi_{iso}$  —

isokinetic  $pK_a'$ , in the electronic profiles, plots of  $\log k_2$  vs  $pK_a'$ , for this reaction series, a fact that is clearly illustrated in Figures 3.21(a) and 3.21(b). The isokinetic  $pK_a'$  is derived as below.

For a series of reactions at various temperatures

$$\text{if } SR_{T_1} = \alpha_{T_1} = a + b\beta_{T_1} \quad (3.5)$$

$$\vdots$$

$$SR_{T_n} = \alpha_{T_n} = a + b\beta_{T_n}$$

$$\text{thus } \frac{(\alpha_{T_n} - \alpha_{T_1})}{(\beta_{T_n} - \beta_{T_1})} = \frac{(\alpha_{T_n} - \alpha_{T_2})}{(\beta_{T_n} - \beta_{T_2})} = \frac{(\alpha_{T_n} - \alpha_{T_3})}{(\beta_{T_n} - \beta_{T_3})} = \dots = b$$

The plots of  $\log k_2$  vs  $pK_a'$  in Figures 3.21(a) and 3.21(b) are electronic profiles at various temperatures for the reaction series. Such a plot, of course, gives a straight line for each temperature. In other words, the stereoelectronic Eq.(2.5) can be changed into Eq.(3.6).

$$(\log k_2)_{T_1} = \alpha_{T_1} + \beta_{T_1}(pK_a'+4) \quad (3.6)$$

$$\vdots$$

$$(\log k_2)_{T_n} = \alpha_{T_n} + \beta_{T_n}(pK_a'+4)$$

$$(\log k_2)_{T_n} - (\log k_2)_{T_1} = (\alpha_{T_n} - \alpha_{T_1}) + (\beta_{T_n} - \beta_{T_1})(pK_a'+4)$$

$$(\log k_2)_{T_n} - (\log k_2)_{T_2} = (\alpha_{T_n} - \alpha_{T_2}) + (\beta_{T_n} - \beta_{T_2})(pK_a'+4)$$

$$\vdots$$

$$\vdots$$

If  $\text{pKa}' + 4 = -b$

thus  $(\log k_2)_{T_n} - (\log k_2)_{T_1} = (\log k_2)_{T_n} - (\log k_2)_{T_2} = \dots = 0$

In short, if a nucleophile has  $\text{pKa}' = -(4+b)$ , all its values of  $\log k_2$  at various temperatures for the reaction series will be the same. This  $\text{pKa}'$  value is referred to as the isokinetic  $\text{pKa}'$ .

### 3.4.1.3 Temperature Dependence of Steric Profiles

#### 3.4.1.3.1 A Unique LFER Isoparameter $\xi_{\text{iso}}$ , Isokinetic $\theta'$ , for a Series of Reactions at Various Temperatures

The steric profiles at various temperatures (-80.0 – 200.0°C) for the reactions of  $\text{Os}_6(\text{CO})_{18}$  with L', plots of  $\log k_2^\circ$  vs  $\theta'$ , are shown in Figure 3.22(a). It is very clear that there is an isokinetic relationship of a novel kind, an isokinetic  $\theta'$ , in that a nucleophile with a  $\theta'$  of 148° will react with the cluster  $\text{Os}_6(\text{CO})_{18}$  at the same value of  $\log k_2^\circ$  at various temperatures {Figure 3.22(a)}. Although values of  $\log k_2$  of the nucleophile at various temperatures are different, and the  $\beta$  values of the reaction series at various temperatures are varying as well, the difference,  $\log k_2^\circ \{= \log k_2 - \beta(\text{pKa}' + 4)\}$ , at various temperatures is the same. Least squares analysis shows that the linear relationship between SR and  $\gamma$  at various temperatures for the reaction series is governed by the equation  $\text{SR}_T = -13.7 + (-9.7)\gamma_T$  with a correlation coefficient of 0.992 {Figure 3.22(b)}. This implies that there is an isokinetic  $\theta'$ , a fact as shown in Figure 3.22(a).

### 3.4.1.3.2 Derivation of the Isokinetic $\theta$ for a Series of Reactions at Various Temperatures

If there is a linear relationship between the standard reactivity SR and steric sensitivity parameter  $\gamma$  for a series of reactions at various temperatures,  $SR_T = g + h\gamma_T$ , there must be a common point of intersection, a unique LFER isoparameter  $\xi_{iso}$  — isokinetic  $\theta$ , in the steric profiles, plots of  $\log k_2^\circ \{= \log k_2 - \beta(pK_a' + 4)\}$  vs  $\theta$ , for this reaction series, a fact that is clearly illustrated in Figure 3.22(a). The isokinetic  $\theta$  is inferred as follows.

For a series of reactions at various temperatures

$$\text{if } \begin{array}{l} SR_{T1} = \alpha_{T1} = g + h \gamma_{T1} \\ \vdots \\ SR_{Tn} = \alpha_{Tn} = g + h \gamma_{Tn} \end{array} \quad (3.7)$$

$$\text{thus } \frac{(\alpha_{Tn} - \alpha_{T1})}{(\gamma_{Tn} - \gamma_{T1})} = \frac{(\alpha_{Tn} - \alpha_{T2})}{(\gamma_{Tn} - \gamma_{T2})} = \frac{(\alpha_{Tn} - \alpha_{T3})}{(\gamma_{Tn} - \gamma_{T3})} = \dots = h$$

When the electronic effects are corrected, the stereoelectronic Eq.(2.5) can be expressed as below.

$$\begin{array}{l} (\log k_2^\circ)_{T1} = \alpha_{T1} + \gamma_{T1}(\theta - \theta_{th}) \\ \vdots \\ (\log k_2^\circ)_{Tn} = \alpha_{Tn} + \gamma_{Tn}(\theta - \theta_{th}) \end{array} \quad (3.8)$$

If it is assumed that values of  $\theta_{th}$  have no changes with varying temperatures (actually this is true if a range of temperature is "small" such as 20–80°C), the following equations can therefore be obtained.

$$\begin{aligned}(\log k_2^\circ)_{Tn} - (\log k_2^\circ)_{T1} &= (\alpha_{Tn} - \alpha_{T1}) + (\gamma_{Tn} - \gamma_{T1})(\theta - \theta_{th}) \\(\log k_2^\circ)_{Tn} - (\log k_2^\circ)_{T2} &= (\alpha_{Tn} - \alpha_{T2}) + (\gamma_{Tn} - \gamma_{T2})(\theta - \theta_{th}) \\ \vdots & \qquad \qquad \qquad \vdots \\ \vdots & \qquad \qquad \qquad \vdots\end{aligned}$$

If  $\theta - \theta_{th} = -h$

thus  $(\log k_2^\circ)_{Tn} - (\log k_2^\circ)_{T1} = (\log k_2^\circ)_{Tn} - (\log k_2^\circ)_{T2} = \dots = 0$

In conclusion, if a nucleophile has  $\theta = -h + \theta_{th}$ , all its values of  $\log k_2^\circ$  at various temperatures for the reaction series will be the same. The value of  $\theta$  is called the isokinetic  $\theta$ .

### 3.4.2 Isokinetic Relationships for the Second Order Substitution Reactions of $Os_6(CO)_{18}$ with Nucleophiles L'

IKRs were originally revealed by means of linear relationships between  $\Delta H^\ddagger$  and  $\Delta S^\ddagger$ , also commonly referred to as "compensation effects" [20]. The activation parameters are usually calculated from the slopes and intercepts of Eyring plots, and they are statistically dependent parameters, and therefore cannot be treated as statistically independent variables, as required for a linear regression analysis [21]. Similar analyses can be obtained from equilibrium data by consideration of van't Hoff plots. A common point of intersection of Arrhenius or Eyring (or van't Hoff) lines is mathematically equivalent

to a linear relationship between activation energies and pre-exponential factors or between enthalpic and entropic terms [20]. However, this mathematical equivalence does not always hold from a statistical point of view [21] because experimental uncertainties of the derived parameters (for example  $E_a$  and  $\ln A$  or  $\Delta H^\ddagger$  and  $\Delta S^\ddagger$ ) can all-too-often lead to an artificial linear dependence without a significant meaning [20]. The pitfall of such a procedure is illustrated by the data from the isomerization of a series of triphenylformazanes [21]. It is necessary to employ a valid method of statistical analysis before accepting the "effect" as real. However, statistical methods to decide whether a reaction series is isokinetic in character and computer programs are available from Linert [21, 22], who established effective statistical analysis methods (original and simplified ones) based on rate or equilibrium constants measured at different temperatures. These methods are important fundamental tools for investigating the temperature dependence of reaction series.

Thus, for a given set of straight lines in the Eyring plot the common point of intersection is calculated at an arbitrary position along the ordinate (the  $\ln k/T$  axis) and abscissa (the  $1/T$  axis) [21]. For this point the sum,  $S_x$ , of squares of the deviations of the measurement points from the corresponding straight lines, including this point of intersection, is calculated. These are called constrained lines [21]. By varying the common point of intersection along the ordinate and abscissa, the minimum of  $S_x$  is calculated and denoted by  $S_0$  [21]. By means of a F test this value is compared with the sum,  $S_{00}$ , of squares of the deviations of the measurement points from the unconstrained lines. In detail  $S_x$ ,  $S_{00}$ ,  $y$  (equal to  $y_{iso}$  for  $S_x = \text{Min.}$ ) and the F value

to be compared with the corresponding F value from the table are given by following equations[21]:

$$y = \frac{\sum_{ij} y_{ij} - \sum_i \frac{(\sum_j x_{ij} - m_i x)(\sum_j x_{ij} y_{ij} - x \sum_j y_{ij})}{\sum_j x_{ij}^2 - 2x \sum_j x_{ij} + m_i x^2}}{\sum_i m_i - \sum_i \frac{(\sum_j x_{ij} - m_i x)^2}{\sum_j x_{ij}^2 - 2x \sum_j x_{ij} + m_i x^2}} \quad (3.9)$$

$$S_x = \sum_{ij} y_{ij}^2 + ly^2 - \sum_i \frac{1}{m_i + 1} (\sum_i y_{ij} + y)^2$$

$$- \sum_i \frac{[\sum_j x_{ij} y_{ij} + xy - \frac{1}{m_i + 1} (\sum_j x_{ij} + x)(\sum_i y_{ij} + y)]^2}{\sum_j x_{ij}^2 + x^2 - \frac{1}{m_i + 1} (\sum_j x_{ij} + x)^2} \quad (3.10)$$

$$S_{oo} = \sum_j y_{ij}^2 - \sum_i (1/m_i)(\sum_j y_{ij})^2$$

$$- \sum_i \{ \{ \sum_j x_{ij} y_{ij} - (1/m_i) \sum_i x_{ij} \sum_j y_{ij} \}^2 / \{ \sum_j x_{ij}^2 - (1/m_i) (\sum_j x_{ij})^2 \} \} \quad (3.11)$$

$$F = \{(S_o - S_{oo})/f_1\} (f_2/S_{oo}) \quad (3.12)$$

$$S_{\infty} = \sum_{ij} y_{ij}^2 - \sum_i (1/m_i)(\sum_j y_{ij})^2 -$$

$$\left[ \left\{ \sum_{ij} x_{ij} y_{ij} - \sum_i (1/m_i)(\sum_j x_{ij})(\sum_j y_{ij}) \right\}^2 / \left\{ \sum_{ij} x_{ij}^2 - \sum_i (1/m_i)(\sum_j x_{ij})^2 \right\} \right] \quad (3.13)$$

In this expression  $x$  and  $y$  are the coordinate axes ( $x = T^{-1}$ ;  $y = \ln k$ ),  $m_i$  the number of points per straight line  $i$ ;  $l$  the number of such straight lines and  $f$  statistical degrees of freedom,  $f_1 = l - 1$  and  $f_2 = \sum_i m_i - 2l$  [21]. A curved line plot of RMSD vs  $1/T$  represent the function  $s_x = (S_x/f_x)^{1/2}$  with  $f_x = \sum_i m_i - l - 1$ . The  $S_0$  value should be smaller than the residual sum  $S_{\infty}$ , which corresponds to the hypothesis of parallel lines, to ensure that the analysis based on a common point of intersection is generally better than one based on the existence of isoenthalpic reaction series [21].

The existence of an IKR is usually accepted when the hypothesis "there is a common point of intersection" cannot be rejected at a certain significance level, i.e. when  $F$  is smaller than the corresponding table value [21]. For extremely accurate data the reversal hypothesis "there is no common point of intersection" can be rejected by means of a comparison of  $1/F$  value with the corresponding  $1/F$  table value for  $f_2$  and  $f_1$  degrees of freedom. If the  $1/F$  value is greater, one has to accept the existence of this IKR at the given significance level [21]. As can be seen in this work (Table 3.10 and 3.11) the IKRs are very precisely established.

The data obtained for the reaction series of  $Os_6(CO)_{18}$  with  $L'$  lead to **five types of excellent isokinetic relationships (three are unique)**, which all indicate an IKT about  $88^\circ\text{C}$ :

- I)  $\Delta H_2^\ddagger$  vs  $\Delta S_2^\ddagger$  (conventional)
- II)  $\ln(k_2/T)$  vs  $1/T$  (conventional)
- III)  $\log k_2$  vs  $pK_a'$  for nucleophiles with different  $\sigma$ -basicity and size at the IKT (novel)
- IV)  $\log k_2$  vs  $pK_a'$  for almost isosteric nucleophiles, which show the same steric effects, at various temperatures (unique)
- V)  $\log k_2$  vs  $pK_a'$  for small nucleophiles with  $\theta < \theta_{th}$ , which exhibit no steric effects, at various temperatures (unique)

The statistical analysis of data on validity of IKR, i.e. the statistical analysis on a common point of intersection of the Eyring plots, also gave exactly the same result, the IKT around 88°C with a high degree of probability, showing very precise IKR. All the results on IKT, no matter what analysis method was used, are in excellent agreement with one another.

For the IKR (I), the data of  $\Delta H_2^\ddagger$  and  $\Delta S_2^\ddagger$  lie on an excellent isokinetic plot, except those of  $PMe_3$ , the gradient of which leads to an isokinetic temperature 89°C (Figure 3.16). The experimental uncertainties of the activation parameters are quite small, as shown in Table 3.5, so the IKR is not necessarily an artificial linear dependence. The IKR (II) clearly shows a common point of intersection for Eyring lines of various nucleophiles except  $PMe_3$ . The common point of intersection corresponds an IKT at 88°C.

The novel IKR (III) clearly illustrates that the rate constants  $\log k_2$  for the reaction series of  $Os_6(CO)_{18}$  with various nucleophiles except  $PMe_3$ , no matter what size and  $\sigma$ -basicity they have, eventually become the same when the IKT around 88°C is reached.

**Unique IKRs (IV) and (V), a common point of intersection in the LFER plots at various temperatures, were established for the first time.** The parallel lines to the X axis which pass through the intersections lead the IKT about 88°C. The IKRs (IV) and (V) also show an excellent temperature dependence of electronic profiles, and they are therefore **breakthroughs in providing the first two examples of the theoretical interconnection between an IKR and LFER.** The common point of intersection, a unique LFER isoparameter  $\xi_{iso}$  — isokinetic pKa' — was established from both experimental results and theory for the first time. It is a natural outcome of linear relationships between SR and  $\beta$  at various temperatures for the reaction series.

The statistical analysis of the data on validity of IKR, i.e. the statistical analysis on a common point of intersection of Eyring plots,  $\ln(k_2/T)$  against  $1/T$ , also gave exactly the same result, the IKT at 88°C with a high degree of probability in terms of the small critical F value  $4.38 \times 10^{-2}$  (with 3 L') –  $2.00 \times 10^{-1}$  (with 4 L') thus the  $1/F$  value is greater than the corresponding table value ( $\alpha \leq 0.05$ ), i.e. a significance level of  $(1-\alpha) \geq 95\%$  at which the IKR has to be accepted. It exhibits highly precise IKR, showing that this relationship is not necessarily an artifact based on measurement errors. The results of the statistical analysis carried out according to the Linert's method are summarized in Table 3.10. Table 3.11 lists critical  $1/F$  values [23]. A statistical method to decide whether a reaction series is isokinetic in nature is the strongest test for the existence of the IKR of all methods available.

The activation parameters  $\Delta H_2^\ddagger$  and  $\Delta S_2^\ddagger$  for the reaction series,  $\text{Os}_6(\text{CO})_{18}$  with L', obtained from the corresponding Eyring line

including the common point of intersection, i.e. the point  $\{1/T_{\text{iso}}, \ln(k_{\text{iso}}/T_{\text{iso}})\}$ , are summarized in Table 3.12. The excellent linearity of each constrained Eyring line, i.e. each with a correlation coefficient  $R$  larger than 0.99 at least, indicates the highly precise IKR again. Two sets of precise values of  $\Delta H_2^\ddagger$  and  $\Delta S_2^\ddagger$ , derived from both constrained and unconstrained Eyring lines, respectively, agree very well with each other as shown in Table 3.12, confirming the excellent IKR.

**Table 3.10 Results of Statistical Analysis on IKT for Reactions of  $\text{Os}_6(\text{CO})_{18}$  with Nucleophiles  $L'$  in Toluene**

No	t (°C)	1/T	$\ln(k_2/T)$	$S_o^a$
74	88	2.768933E-03	-9.185485	9.804109E-02
$f_1^d$	$f_2^e$	$S_{oo}^b$	$S_{\infty}^c$	$F^f$
3	14	9.400988E-02	0.3721367	0.20011

a.  $S_x$  = sum of squares of the deviations of the measurement points from the corresponding straight line including the common point of intersection. These lines are called constrained ones. The minimum of  $S_x$  is denoted by  $S_o$  [21].

b.  $S_{oo}$  = sum of squares of the deviations of the measurement points from the unconstrained lines [21].

c.  $S_{\infty}$  = sum of squares of the deviations of the measurement points from the hypothetical parallel lines.

d. Statistical degrees of freedom (as numerator).  $f_1 = l - 1$ , where  $l$  is the number of straight lines [21].

e. Statistical degrees of freedom (as denominator).  $f_2 = \sum_i m_i - 2l$ , where  $m_i$  is the number of points per straight line [21].

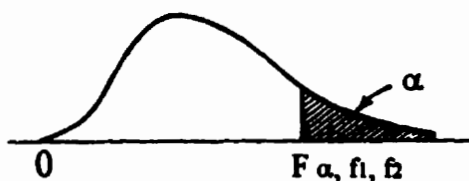
f. Critical value  $F = (S_o - S_{oo})f_2 / S_{oo}f_1$ , i.e.  $1/F = S_{oo}f_1 / (S_o - S_{oo})f_2$ .

N.B. 1) If the  $S_o$  value is smaller than the residual sum  $S_{oo}$ , the found common point of intersection is not an artefact due to the existence of isoenthalpic reaction series [21].

2) This computer program was made by Dr. J. Hao.

**Table 3.11 Critical 1/F Values**

Numerator		Denominator $f_2$				
$f_1$	$\alpha$	14	15	16	17	18
3	0.050	8.715	8.703	8.692	8.683	8.675
	0.025	14.277	14.253	14.232	14.213	14.196
	0.010	26.924	26.872	26.827	26.787	26.751
	0.005	43.172	43.085	43.008	42.941	42.880
	0.001	127.645	127.376	127.136	126.927	126.738



$f_1$  = numerator degrees of freedom

$f_2$  = denominator degrees of freedom

For lower critical F values, use the relationship:

$$F_{1-\alpha, f_1, f_2} = 1/F_{\alpha, f_2, f_1}$$

$$P(F > F_{\alpha, f_1, f_2}) = \alpha$$

**Table 3.12** Activation Parameters  $\Delta H_2^\ddagger$  and  $\Delta S_2^\ddagger$  Derived from a Set of Constrained Eyring Lines for the Reactions of  $\text{Os}_6(\text{CO})_{18}$  with  $L'$  in Toluene

$L'$	$\Delta H_2^\ddagger$ (kcal mol <sup>-1</sup> )		$\Delta S_2^\ddagger$ (kcal K <sup>-1</sup> mol <sup>-1</sup> )		$R^c$	
	Constrained <sup>a</sup>	Unconstrained <sup>b</sup>	Constrained	Unconstrained	Cons.	Uncons.
etpb	11.14±0.23	11.84±0.46	-34.96±0.74	-32.69±1.48	0.999	0.997
P(OEt) <sub>3</sub>	14.47±0.35	15.40±0.34	-25.56±1.10	-22.56±1.09	0.998	0.999
P(O- <i>i</i> -Pr) <sub>3</sub>	18.62±0.60	16.62±1.07	-14.45±1.87	-20.74±3.35	0.996	0.99
P( <i>n</i> -Bu) <sub>3</sub>	8.74±0.52	8.62±1.35	-41.71±1.67	-42.10±4.38	0.991	0.95

- a. Each Eyring line of  $\ln(k_2/T)$  vs  $1/T$  includes the common point of intersection, i.e. the point  $\{1/T_{iso}, \ln(k_{iso}/T_{iso})\}$ .
- b. The unconstrained mean the results obtained from each set of data separately.
- c. Correlation coefficient.

### 3.4.3 Implications of Derived Kinetic Parameters

The characteristic kinetic parameters (Table 3.8) derived for  $\text{Os}_6(\text{CO})_{18}$  imply that the cluster shows significant sensitivity to the electronic and steric properties of the nucleophiles. This would be expected for the extremely low reactivity of the cluster ( $\text{SR} = -5.35 \pm 0.30$  at  $25.0^\circ\text{C}$ ), while values of SR for most LNCCs and HNCCs lie between +2 and -3. The values of  $\beta$  is exceedingly high ( $0.514 \pm 0.071$ , at  $25.0^\circ\text{C}$ ). It is indicated that a remarkably high degree of bond making is involved in the transition state, which can also be understood as a result of the inherently electron-deficient nature of this high nuclearity carbonyl cluster [4, 24]. The high  $\beta$  value is coupled with the low positive  $\Delta H_2^\ddagger$  and the high negative  $\Delta S_2^\ddagger$  (Table 3.5) to confirm the high degree of bond-making in the TSI. Values of  $\beta$  for most clusters including mononuclear metal carbonyls are usually between 0.1 and 0.3. Ones with the top three values of  $\beta$  are  $\text{Ru}_5\text{C}(\text{CO})_{15}$  with large  $L'$  ( $\theta \geq 145^\circ$ ) with  $\beta = 0.59 \pm 0.03$  [9],  $\text{Fe}(\text{CO})_3(\text{N}_4\text{Me}_2)$  with  $\beta = 0.55 \pm 0.08$  [25], and  $\text{Ru}_6\text{C}(\text{CO})_{17}$  with  $\beta = 0.41 \pm 0.04$  [9]. The value of  $\theta_{\text{th}}$  ( $= 127^\circ$  at  $25.0^\circ\text{C}$ ) for  $\text{Os}_6(\text{CO})_{18}$  is quite high so the TSI is quite "open". The very negative value of  $\gamma$  ( $-0.763 \pm 0.105 \text{ deg}^{-1}$  at  $25.0^\circ\text{C}$ ) has not been surpassed by any metal carbonyls {so far the lowest one is  $-0.23 \pm 0.01$  for  $\text{Ru}_5\text{C}(\text{CO})_{15}$  [9]}. The flexibility of the widely opened TSI of  $\text{Os}_6(\text{CO})_{18}$  is therefore extremely low. The further opening up, needed when large nucleophiles above the steric threshold are involved, is exceptionally difficult. For example, the rate constant  $k_2$  for the reaction of  $\text{Os}_6(\text{CO})_{18}$  with the highly nucleophilic ligand  $\text{P}(n\text{-Bu})_3$  ( $\text{pK}_a' = 8.67$ ,  $\theta = 132^\circ$ ) is much slower than that with relatively low one,  $\text{PPhMe}_2$

( $pK_a' = 5.07$ ,  $\theta = 122^\circ$ ). The former is  $1.58 \times 10^{-3} \text{ M}^{-1} \text{ s}^{-1}$  at  $25.0^\circ\text{C}$ , while the latter is  $1.79 \times 10^{-1} \text{ M}^{-1} \text{ s}^{-1}$ . It is very obvious that the flexibility of the TSI is very low so the rate for the reaction with the large  $L'$  ( $\theta > \theta_{th}$ ) dropped very fast. This may be ascribed to the rigid TSI of  $\text{Os}_6(\text{CO})_{18}$ , and the inability of larger nucleophiles to approach as close to the electrophilic center in the TSI. Strictly speaking, the value of  $\theta_{th}$  is between  $122^\circ$  and  $127^\circ$  and the  $\gamma$  value is in the range of  $-0.763$  —  $-0.173 \text{ deg}^{-1}$  at  $25.0^\circ\text{C}$ .

The fact that the cluster  $\text{Os}_6(\text{CO})_{18}$  shows the exceptional low reactivity toward nucleophilic attack, lower than those of any LNCCs and HNCCs so far { $\text{Os}_3(\text{CO})_{12}$  may be less reactive than  $\text{Os}_6(\text{CO})_{18}$  but no data are available}, explains why the rate constants  $k_2$  of this cluster with large and/or weak nucleophiles, such as  $\text{PPh}_3$  ( $pK_a' = 3.28$ ,  $\theta = 145^\circ$ ), and  $\text{P(OPh)}_3$  ( $pK_a' = -2.79$ ,  $\theta = 128^\circ$ ), cannot be obtained conveniently due to extremely low rates. However, they can be calculated based on the stereoelectronic Eq.(2.5) and the characteristic kinetic parameters  $\alpha$ ,  $\beta$ ,  $\gamma$ , and  $\theta_{th}$ . Ones at  $25.0^\circ\text{C}$  are shown below:

$$k_2 = 4.55 \times 10^{-16} \text{ M}^{-1}\text{s}^{-1} \text{ for the reaction with } \text{PPh}_3$$

$$k_2 = 3.23 \times 10^{-6} \text{ M}^{-1}\text{s}^{-1} \text{ for the reaction with } \text{P(OPh)}_3$$

The small positive values of  $\Delta H_2^\ddagger$  and the large negative values of  $\Delta S_2^\ddagger$  are in line with a straightforward associative reaction mechanism involving attack by a nucleophile at a metal atom in the cluster [26]. The values of  $\Delta H_2^\ddagger$  increase substantially in the order  $L' = \text{P}(n\text{-Bu})_3 < \text{etpb} < \text{P(OEt)}_3 < \text{P(O-}i\text{-Pr)}_3$  (Table 3.5 & Figure 3.16). The values of  $\Delta S_2^\ddagger$  increase in the same order. The reactions with nucleophiles  $\text{PMe}_3$  and  $\text{P}(n\text{-Bu})_3$  have almost the same values of  $\Delta H_2^\ddagger$ , 8.98 and 8.62  $\text{kcal}\cdot\text{mol}^{-1}$ , but very different values of  $\Delta S_2^\ddagger$ , -27.62 and

-42.10 cal·K<sup>-1</sup>·mol<sup>-1</sup>, respectively. So the reactions with PMe<sub>3</sub> are much faster than those with P(*n*-Bu)<sub>3</sub>, and PMe<sub>3</sub> is the most reactive ligand.

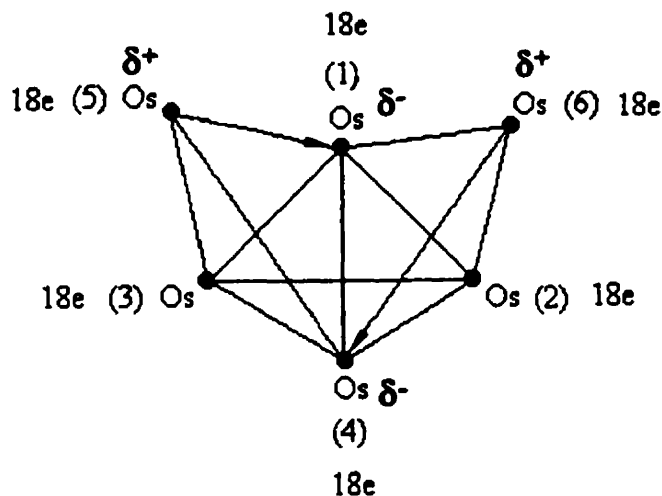
Compared with the known values of  $\Delta H_2^\ddagger$  and  $\Delta S_2^\ddagger$  for the low nuclearity carbonyl clusters (LNCCs) in analogous reactions, those for Os<sub>6</sub>(CO)<sub>18</sub> are generally lower and more negative, respectively. For instance, values of  $\Delta H_2^\ddagger$  and  $\Delta S_2^\ddagger$  for reactions of Os<sub>3</sub>(CO)<sub>12</sub> with P(*n*-Bu)<sub>3</sub> in decalin have been reported to be 20.64±0.16 kcal mol<sup>-1</sup> and -22.7±0.6 cal K<sup>-1</sup> mol<sup>-1</sup> [27], and in this study for the reactions of Os<sub>6</sub>(CO)<sub>18</sub> with P(*n*-Bu)<sub>3</sub> in toluene, they are 8.62±1.35 kcal mol<sup>-1</sup>, and -42.10±4.38 cal K<sup>-1</sup> mol<sup>-1</sup>, respectively (Table 3.5).

Trimetal carbonyl clusters have been observed to have lower values of  $\Delta H_2^\ddagger$  and more negative values of  $\Delta S_2^\ddagger$  than mononuclear binary carbonyls [26, 27]. This decrease in values of  $\Delta H_2^\ddagger$  and increasingly negative values of  $\Delta S_2^\ddagger$  corresponds a general increase in the susceptibility to nucleophilic attack as the nuclearity of metal carbonyls becomes higher [28]. The high nuclearity carbonyl clusters (HNCCs) seem to have much higher reactivity than LNCCs of corresponding metals and even higher than mononuclear ones in reacting with nucleophiles. Further confirmation of this conclusion was provided by the values of the kinetic parameters  $\alpha$ ,  $\beta$ ,  $\gamma$ , and  $\theta_{th}$ , derived from the quantitative separation of electronic and steric effects of this and other work [9].

### 3.5 Intimate Mechanism

Bimolecular reactions of metal carbonyls with P-donor nucleophiles have been ascribed to direct nucleophilic attack at a metal atom [26, 29, 30]. Analogous explanations can be given to the cluster  $\text{Os}_6(\text{CO})_{18}$ . Each of the 6 Os atoms in  $\text{Os}_6(\text{CO})_{18}$  has three COs bonded to it, the number of connections to other metal atoms varies from atom to atom. The electron counts and M–M bonding around each Os atom are shown below.

#### Electron Counts and M–M bonding in $\text{Os}_6(\text{CO})_{18}$

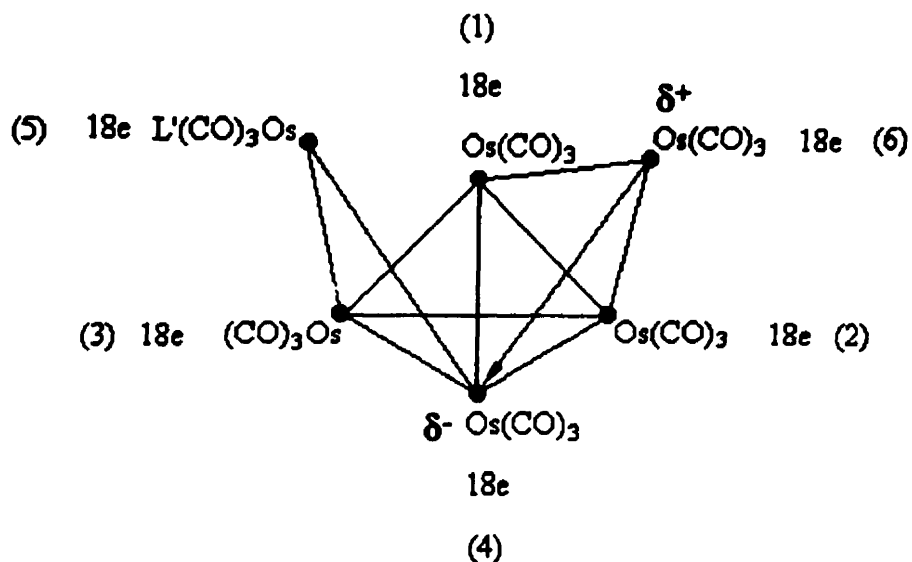


The capping atoms, Os(5) and Os(6), have the lowest electron density and are likely to be the site of nucleophilic attack and the site of attachment of the nucleophile  $\text{L}'$  in the product. This site of replacement reflects the better  $\sigma$ -donor properties of a P-donor  $\text{L}'$  compared to a carbonyl by formally placing greater electron density on

the electron-deficient metal [7]. The position is also the one which would cause the least steric congestion in replacing a CO by a bulkier group [7].

It was reported [7] that a network of incipient bridging carbonyl ligands is observed in the clusters  $\text{Os}_6(\text{CO})_{18-n}(\text{PPh})_n$ ,  $n = 1, 2$ . Incipient carbonyl bridge bonding is usually observed between metal atoms in different formal electron counts [7]. This interaction is characterized by relatively short  $\text{Os}\cdots\text{C}$  contacts and deviations from linearity of the carbonyl group [7]. In view of the facts described above, the intimate mechanism for the reactions of  $\text{Os}_6(\text{CO})_{18}$  with  $\text{L}'$  is suggested as below. When a nucleophile  $\text{L}'$  attacks a capping Os atom, e.g. Os(5), it is proposed that the cluster will open up by breaking one of the Os–Os bonds. The one most likely to be broken is the longest and, therefore, probably the weakest i.e. the Os(5)–Os(1) bond  $\{d[\text{Os}(5)\text{--Os}(1)] = 2.836 \text{ \AA}$ , the next longest Os(6)–Os(4) bond being  $2.829 \text{ \AA}$  [3]}. This opened up cluster can be represented as follows:

### Intermediate $\text{Os}_6(\text{CO})_{18}\text{L}'$



in which all the Os atoms have maintained their 18 electron structures as before in a way that only clusters can. Subsequent loss of a CO ligand and reformation of the Os–Os bond will lead to substitution.

The susceptibility of metal carbonyl clusters to nucleophilic attack has been found to be due to the ability of a cluster to undergo just this sort of M–M bond breaking concurrently with  $\text{M}\cdots\text{L}'$  bond making so as to form an intermediate. The high susceptibility of  $\text{Ir}_4(\text{CO})_{12}$  to nucleophilic attack has been demonstrated and explained in terms of weakening of cluster bonding on forming an  $\text{Ir}\cdots\text{P}$  bond and flexibility of a coordination sphere during approach of a nucleophile [31]. This is especially true if one has in mind that the bonding in HNCCs is more appropriately described by a delocalized cluster bonding scheme (polyhedral skeletal electron pair theory PSEPT) [24]. High reactivity is usually related to facile changes in bonding of other

ligands attached to the metal centre [32, 33]. In view of delocalized bonding, this would mean corresponding changes in the whole cluster bonding system. The cluster  $\text{Os}_6(\text{CO})_{18}$  is an unreactive HNCC. It has 84 CVEs, and its 42 CVMOs are all filled. Thus the extra pair of electrons from an entering ligand can only be accommodated in a low-lying non-bonding or high-lying anti-bonding orbital. The cluster has an exceptionally low standard reactivity, lower than those of any HNCCs and LNCCs {so far the four lowest values of SR are  $-4.7 \pm 0.1$  for  $\text{Ru}_3(\text{CO})_{11}\text{etpb}$  (this work in Chapter 2),  $-4.2 \pm 0.1$  for  $\text{Ru}_3(\text{CO})_{11}\text{P}(\text{OEt})_3$ ,  $-4.2 \pm 0.2$  for  $\text{Ru}_3(\text{CO})_{11}\text{PPh}_3$ ,  $-3.4 \pm 0.2$  for  $\text{Ru}_3(\text{CO})_{12}$  [34] and the value of  $\text{Os}_3(\text{CO})_{12}$  is not available}, coupled with an exceedingly high degree of bond making in the transition state, and shows an extremely low TSI flexibility, lower than those of any LNCCs and HNCCs to data, when the steric threshold is exceeded. The inflexibility of TSI is probably related to the high value of  $\theta_{\text{th}}$  which implies that the TSI is already quite open compared with the sterically congested original cluster. For it to become even more open so as to accommodate nucleophiles with  $\theta > \theta_{\text{th}}$  might therefore be expected to require significant amount of extra energy.

### 3.6 Discussion of the IKRs

The IKR or its equivalent in thermodynamic terms, the isoequilibrium relationship IER, refers to a common point (or small area) of intersection of Eyring lines,  $\ln(k/T)$  vs  $1/T$ , or van't Hoff lines,  $\ln K$  vs  $1/T$ , for a series of reactions. A common point of intersection of straight lines is mathematically equivalent to a proportionality of their intercepts and slopes, such as the activation entropies and

enthalpies in case of Eyring plots. Therefore it has been referred to as the "compensation effect". This is, however, not equivalent from the statistical point of view [21]. The proportionality may be an artifact due to measurement errors [21].

Such common points of intersection are also found when the same data are depicted for different temperatures in the LFER plots. Unique IKRs,  $\log_2 k_2$  vs  $pK_a'$  for almost isosteric nucleophiles or small ones with  $\theta < \theta_{th}$ , respectively, at various temperatures for the reaction series of  $Os_6(CO)_{18}$  with  $L'$  {Figures 3.21(a) and 3.21(b)}, show an excellent LFER at different temperatures for the reaction series and a common point of intersection, a characteristic LFER isoparameter  $\xi_{iso}$  — isokinetic  $pK_a'$ , is established. In short, when an IKR is found (Figure 3.17), a LFER isoparameter  $\xi_{iso}$  — isokinetic  $pK_a'$  in this work {Figures 3.21(a) and 3.21(b)} — appears, and vice versa.

The common points of intersection are defined in different form by means of the abscissa where the net differences in the selectivity have vanished [35], i.e. where there is a minimum of deviations between the different members of the reaction series [20]. For Eyring plots,  $\ln(k/T)$  vs  $1/T$ , the IKR is given by

$$\frac{\partial \ln k/T(\xi, T)}{\partial \xi} \Big|_{1/T_{iso} = 0} = 0 \quad (3.14)$$

For a generalized LFER, the IKR is expressed as below.

$$\frac{\partial \ln k/T(T, \xi)}{\partial(T)} \Big|_{\xi_{iso} = 0} \quad (3.15)$$

Whether this can be accepted as a real IKR or rejected as an artifact for any given experimental case has to be decided upon by careful statistical analysis [20]. Linert pointed out that  $\xi$  might be a simple numbering (i.e. an index  $i$ ) but preferably it represents a continuous parameter having physical meaning [20]. Based on the unique IKRs {Figures 3.21(a) and 3.21(b)} in this work, **the parameter  $\xi$  is not a simple numbering, and it does have physical meaning.**  $\xi$  identifies the individual members of the series — the nucleophiles with different  $\sigma$ -basicity and size in this work. When the size of  $L'$  is kept constant or  $\theta < \theta_{th}$ ,  $\xi = pKa'$ . In terms of these unique IKRs {Figures 3.21(a) and 3.21(b)}, **a definition on IKR** can be also given as follows.

$$\frac{\partial \ln k/T(T, \xi)}{\partial(T)} \Big|_{\xi_{iso}} = \frac{\partial \ln k/T(T, pKa')}{\partial(T)} \Big|_{pKa'_{iso} = 0} \quad (3.16)$$

There can be little doubt that a true IKT exists for the reaction series of  $Os_6(CO)_{18}$  with the four nucleophiles  $etpb$ ,  $P(OEt)_3$ ,  $P(O-i-Pr)_3$ , and  $P(n-Bu)_3$ . Thus, the same isokinetic temperature is found from the  $\Delta H^\ddagger$  vs  $\Delta S^\ddagger$  plot, the Eyring plots, the  $\log k_2$  vs  $pKa'$  plot for almost isosteric nucleophiles at various temperatures, the  $\log k_2$  vs  $pKa'$

plot for small nucleophiles with  $\theta < \theta_{th}$  at various temperatures, and the  $\log k_2$  vs  $pK_a'$  plot for nucleophiles with different  $\sigma$ -basicity and size at the IKT. The existence of the IKT at ca. 88°C is also statistically justified with a high degree of probability by the analyses of the Eyring plots. The occurrence of an invariant point in both Eyring and LFER plots at an IKT corresponds to an interaction between the reactants and the available heat bath (i.e. the molecular surroundings of the reactants, such as solvent) [20]. The IKT is believed to be related to the vibration frequency of the heat bath [20],

$$T_{iso} = h\nu_{heat\ bath} / k_B \quad [3.17]$$

where  $h$  is Planck's constant, and  $k_B$  is Boltzmann's constant. A vibrational–vibrational energy exchange between reactants and their direct molecular surroundings occurs in the case of condensed phase [20] such as in this work. The heat bath — reactant interaction may be taken as being equal (or invariant) with respect to all members of a considered reaction series [21]. In other words, the reactions included in an IKR are similar, forming a series of reactions. From the occurrence of a distinct IKR, it can generally be concluded that only one reaction mechanism is present for all reactions included in this series. In the case where some Eyring lines of the considered reaction series miss the condition of the IKR, or in the case where two or more common points of intersection are found, either a change in the reaction mechanism occurs within the series or the resonance condition between reactants and their molecular surroundings is not fulfilled [36].

It is not clear why the nucleophile  $\text{PMe}_3$  fits into one or other of these categories.

### 3.7 Conclusion

The kinetics of substitution reactions of the HNCC  $\text{Os}_6(\text{CO})_{18}$  with P-donor nucleophiles  $\text{L}'$  in toluene shows that it undergoes reactions solely by an associative path,  $k_{\text{obs}} = a + k_2[\text{L}']$ , where  $a$  is always statistically insignificant or at least small. The site of attachment of a nucleophile  $\text{L}'$  in a mono-substituted product occurs at a formally electron-deficient metal centre, one of capping Os atoms with the longest Os–Os distance and, therefore, probably the weakest bond. Although there is no spectroscopic indication (by FTIR) of formation of intermediate adducts, their possible existence can not be ruled out. An intermediate adduct  $\text{Os}_6(\text{CO})_{18}\text{L}'$ , the structure of which was proposed, may be formed during approach of a nucleophile.

The data obtained for the reaction series of  $\text{Os}_6(\text{CO})_{18}$  with  $\text{L}'$  lead to **five types of excellent isokinetic relationships (three are unique)**, which all indicate an IKT of about  $88^\circ\text{C}$ :

- I)  $\Delta H_2^\ddagger$  vs  $\Delta S_2^\ddagger$  (conventional)
- II)  $\ln(k_2/T)$  vs  $1/T$  (conventional)
- III)  $\log k_2$  vs  $\text{pKa}'$  for nucleophiles with different  $\sigma$ -basicity and size at the IKT (novel)
- IV)  $\log k_2$  vs  $\text{pKa}'$  for almost isosteric nucleophiles, which show the same steric effects, at various temperatures (unique)
- V)  $\log k_2$  vs  $\text{pKa}'$  for small nucleophiles with  $\theta < \theta_{\text{th}}$ , which exhibit no steric effects, at various temperatures (unique)

The statistical analysis of data on validity of IKR, i.e. the statistical analysis on a common point of intersection of the Eyring plots, also gave exactly the same result, the IKT around 88°C with a high degree of probability, showing very precise IKR. All the results on IKT, no matter what analysis method was used, are in excellent agreement with one another.

The **novel IKR (III)** clearly illustrates that the rate constants  $\log k_2$  for the reaction series of  $\text{Os}_6(\text{CO})_{18}$  with various nucleophiles except  $\text{PMe}_3$ , no matter what size and  $\sigma$ -basicity they have, eventually become the same when the IKT around 88°C is reached.

**Unique IKRs (IV) and (V)**, a common point of intersection in the LFER plots at various temperatures, were established for the first time. They also show an excellent temperature dependence of electronic profiles, and they are therefore **breakthroughs** in providing the first two examples of the theoretical interconnection between an IKR and LFER. Based on these unique IKRs {Figures 3.21(a) and 3.21(b)} in this work, a **definition on IKR** can be given as follows.

$$\frac{\partial \ln k/T(T, \xi)}{\partial(T)} \Big|_{\xi_{\text{iso}}} = \frac{\partial \ln k/T(T, \text{pKa}')}{\partial(T)} \Big|_{\text{pKa}'_{\text{iso}} = 0}$$

The **parameter  $\xi$  is not a simple numbering, and it does have physical meaning.** In this work,  $\xi$  identifies the individual members of the series — the nucleophiles with different  $\sigma$ -basicity and size. When the size of  $L'$  is kept constant or  $\theta < \theta_{\text{th}}$ ,  $\xi = \text{pKa}'$ .

When an IKR is found (Figure 3.17), a LFER isoparameter  $\xi_{\text{iso}}$  — isokinetic  $\text{pKa}'$  in this work {Figures 3.21(a) and 3.21(b)} — appears, and vice versa.

The unique LFER isoparameters  $\xi_{\text{iso}}$ , **isokinetic  $\text{pKa}'$**  and **isokinetic  $\theta'$** , for a reaction series at various temperatures were established from both experimental results and theory for the first time. They are natural outcomes of linear relationships between SR &  $\beta$  and SR &  $\gamma$ , respectively, at various temperatures for the reaction series. A nucleophile with a  $\text{pKa}'$  of 14.3 or -7.0, respectively — isokinetic  $\text{pKa}'$  — will react with the cluster  $\text{Os}_6(\text{CO})_{18}$  at the same value of  $\log k_2$  at various temperatures. A nucleophile with a  $\theta'$  of  $148^\circ$  — isokinetic  $\theta'$  — will react with  $\text{Os}_6(\text{CO})_{18}$  at the same value of  $\log k_2^\circ$   $\{= \log k_2 - \beta(\text{pKa}' + 4)\}$  at various temperatures.

The derived kinetic parameters, SR,  $\beta$ ,  $\gamma$  and  $\theta_{\text{th}}$ , imply the exceptional low susceptibility of this HNCC toward nucleophilic attack, lower than those of any HNCCs and LNCCs so far, coupled with an exceedingly high degree of M...P bond making in the TS, and the lowest flexibility of the TSI among HNCCs and LNCCs to date. The very low reactivity suggests that opening up of the cluster is a quite slow process as indicated by the value of SR, in spite of the fact that the open space is quite wide as indicated by the value of  $\theta_{\text{th}}$ , even more difficult for further opening up when the  $\theta_{\text{th}}$  is exceeded as indicated by the value of  $\gamma$ . The use of an alternative steric parameter,  $\theta'$  ( $=103.8+0.553\text{ER}$ ), is shown not to have significant difference on the values of SR,  $\beta$ , and  $\theta_{\text{th}}$  for both models.

Two sets of precise values of  $\Delta H_2^\ddagger$  and  $\Delta S_2^\ddagger$  with very nice linearity were derived from both constrained and unconstrained Eyring

lines, respectively, and they are in excellent agreement with each other, showing the highly precise IKR again. The small positive values of  $\Delta H_2^\ddagger$  and the large negative values of  $\Delta S_2^\ddagger$  are in line with a straightforward associative reaction mechanism.

**REFERENCES FOR CHAPTER 3**

- [1] F.A. Cotton and G. Wilkinson, Advanced Inorganic Chemistry, Chapter 28, 5th ed., John Wiley & Sons, Inc., New York, 1988.
- [2] J.W. Lauher, *J. Am. Chem. Soc.*, 100(1978)5305.
- [3] R. Mason, K.M. Thomas, and D.M.P. Mingos, *J. Am. Chem. Soc.*, 95(1973)3802.
- [4] D. H. Farrar, and R. J. Goudsmit, in Metal Clusters, M. Moskovits (Ed.), John Wiley & Sons, Inc., New York, 1986.
- [5] G.R. John, B.F.G. Johnson, J. Lewis, and A.L. Mann, *J. Organomet. Chem.*, 171(1979)C9-C13.
- [6] M. McPartlin, C.R. Eady, B.F.G. Johnson, and J. Lewis, *J. Chem. Soc. Chem. Commun.*, (1976)883.
- [7] C. Couture and D.H. Farrar, *Acta Cryst.*, C42(1986)163.
- [8] W.L. Gladfelter and K.L. Roessellet in The Chemistry of Metal Cluster Complexes, Chapter 7, D.H. Shriver, H.D. Kaesz, and R.D. Adams (Ed.), VCH Publisher Inc., New York, 1990.
- [9] (a) A.J. Poë, D.H. Farrar, and Y. Zheng, *J. Am. Chem. Soc.*, 114(1992)5147.  
(b) A.J. Poë, D.H. Farrar, and Y. Zheng, *J. Am. Chem. Soc.*, 116(1994)6252.  
(c) J. Hao, unpublished work.
- [10] C.R. Eady, B.F.G. Johnson, and J. Lewis, *J. Chem. Soc. Dalton Trans.*, (1975)2606.
- [11] P.F. Jackson, B.F.G. Johnson, J. Lewis, W.J.H. Nelson, and M. McPartlin, *J. Chem. Soc. Dalton Trans.*, (1982)2099;  
D. Braga, B.F.G. Johnson, J. Lewis, M. McPartlin, W.J.H.

- Nelson, A. Sironi, and M.D. Vargas, *J. Chem. Soc. Chem. Commun.*, (1983)1131.
- [12] R. Mason, K.M. Tomas, and D.M.P. Mingos, *J. Am. Chem. Soc.*, 95(1973)3802
- [13] B.F.G. Johnson and J. Lewis, *Inorg. Synthesis*, 13(1972)93.
- [14] G.R. John, B.F.G. Johnson, and J. Lewis, *J. Organomet. Chem.*, 181(1979)143.
- [15] (a) Christiane Couture, Ph.D. Thesis, University of Toronto, 1986.
- (b) A summer student's work.
- [16] C.G. Swain, M.S. Swain, and L.F. Berg, *J. Chem. Inf. Comp. Sci.* 20(1980)47.
- [17] T.L. Brown, *Inorg. Chem*, 31(1992)1286.
- [18] T.L. Brown and K.J. Lee, *Coord. Chem. Rev.*, 128(1993)89.
- [19] R.H.E. Hudson and A.J. Poë, *Organometallics*, 14(1995)3238.
- [20] W. Linert, *Chem. Soc. Rev.*, (1994)429.
- [21] W. Linert, *Inorg. Chim. Acta.*, 141(1988)233.
- [22] W. Linert and R.F. Jameson, *Chem. Soc. Rev.*, 18(1989)447.
- [23] Shirly Dowdy and Stanley Wearden, Statistics for Research, John Wiley & Sons, Inc., New York, 1991.
- [24] S.M. Owen, *Polyhedron*, 7(1988)253, and references therein.
- [25] C. Chang, C.E. Johnson, T.G. Richmond, Y. Chen, W.C. Trogler, and F. Basolo, *Inorg. Chem.*, 20(1981)3167.
- [26] J. A. S. Howell, and P. M. Burkinshaw, *Chem. Rev.* 83(1983)557.
- [27] A.J. Poë and V.C. Sekhar, *Inorg. Chem*, 24(1985)4376.

- [28] A.J. Poë, in Metal Clusters, Chapter 4, M. Moskovits (Ed.), John Wiley & Sons, Inc., New York, 1986.
- [29] A.J. Poë and M.V. Twigg, *J. Chem. Soc., Dalton Trans.*, (1974)1860.
- [30] D. C. Sonnenberger and J. D. Atwood, *Inorg. Chem.*, 20(1981)3243.
- [31] K. Dahlinger, F. Falcone, and A.J. Poë, *Inorg. Chem.*, 25(1986)2654.
- [32] F. Basolo, *Inorg. Chim. Acta*, 100(1985)33.
- [33] M. Basato and A.J. Poë, *J. Chem. Soc., Dalton Trans.*, (1974)456.
- [34] L. Chen and A.J. Poë, *Coord. Chem. Rev.*, 143(1995)265.
- [35] W. Linert and V.N. Sapunov, *Chemical Physics*, 119(1988)265.
- [36] W. Linert, *J. Chem. Inf. Comput. Sci.*, 32(1992)221.
- [37] C.R. Eady, P.D. Gavens, B.F.G. Johnson, J. Lewis, M.C. Malatesta, M.J. Mays, A.G. Orpen, A.V. Rivera, G.M. sheldrick, and M.B. Hursthouse, *J. Organomet. Chem.*, 149(1978)C43.

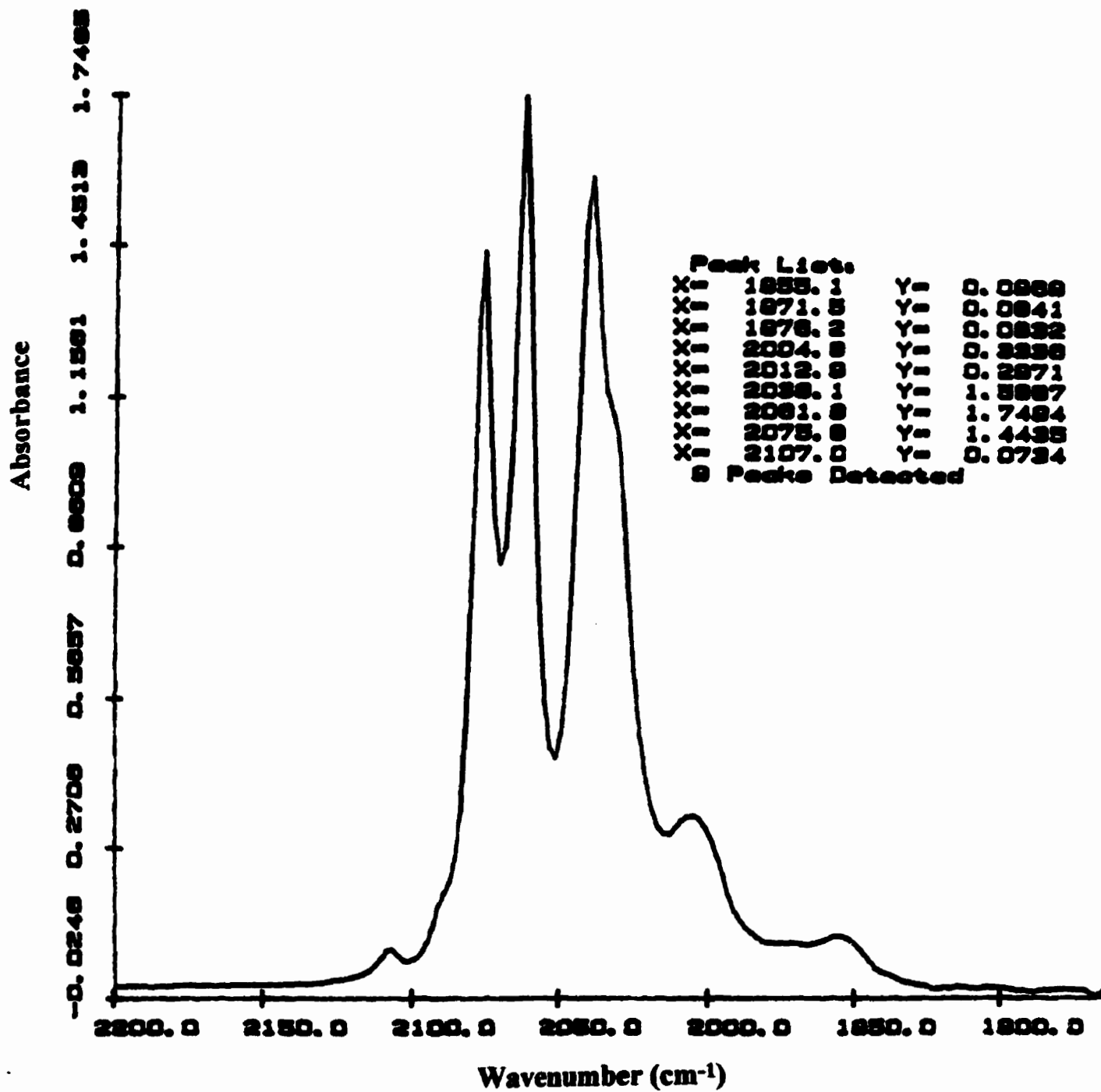


Figure 3.1 FTIR spectrum of pure  $\text{Os}_6(\text{CO})_{18}$  in ethyl acetate.

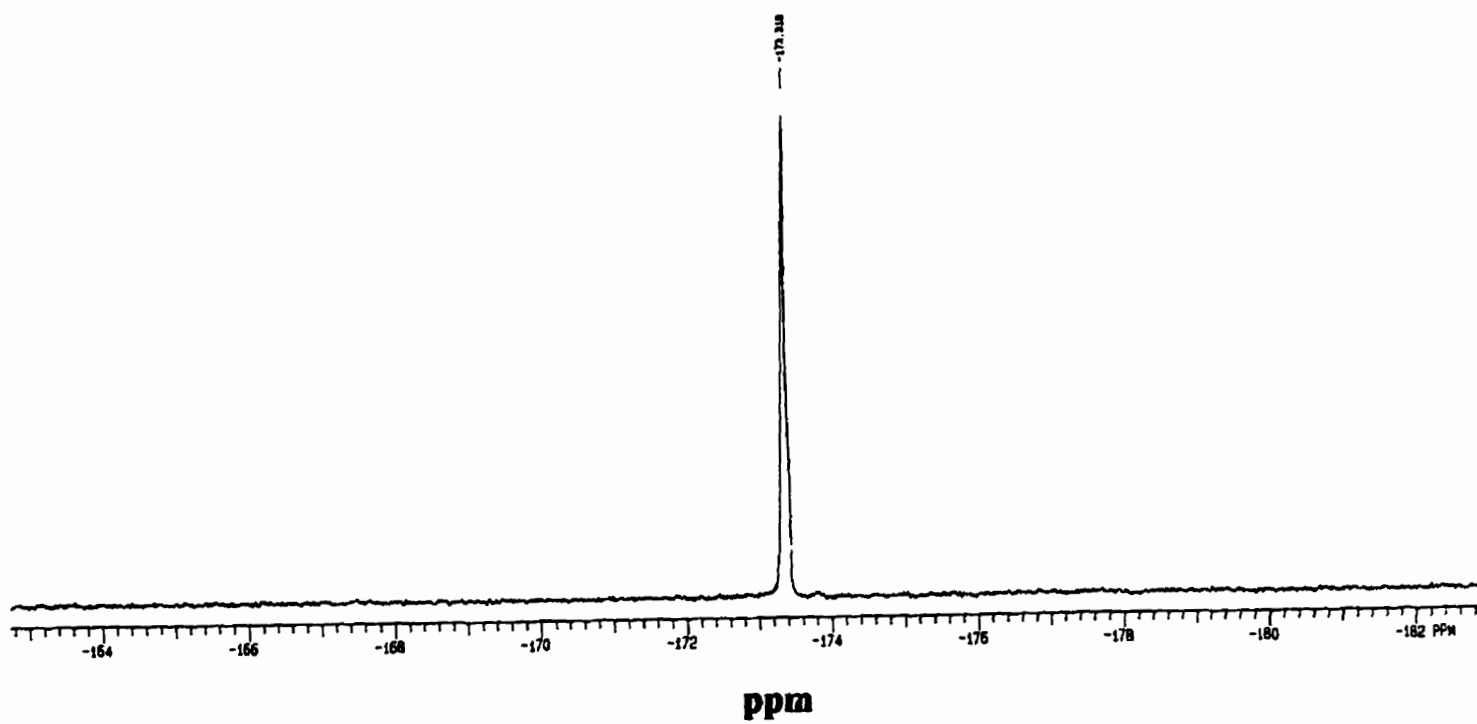


Figure 3.2(a)  $^{31}\text{P}$  NMR spectrum of pure  $\text{P}(n\text{-Bu})_3$ .

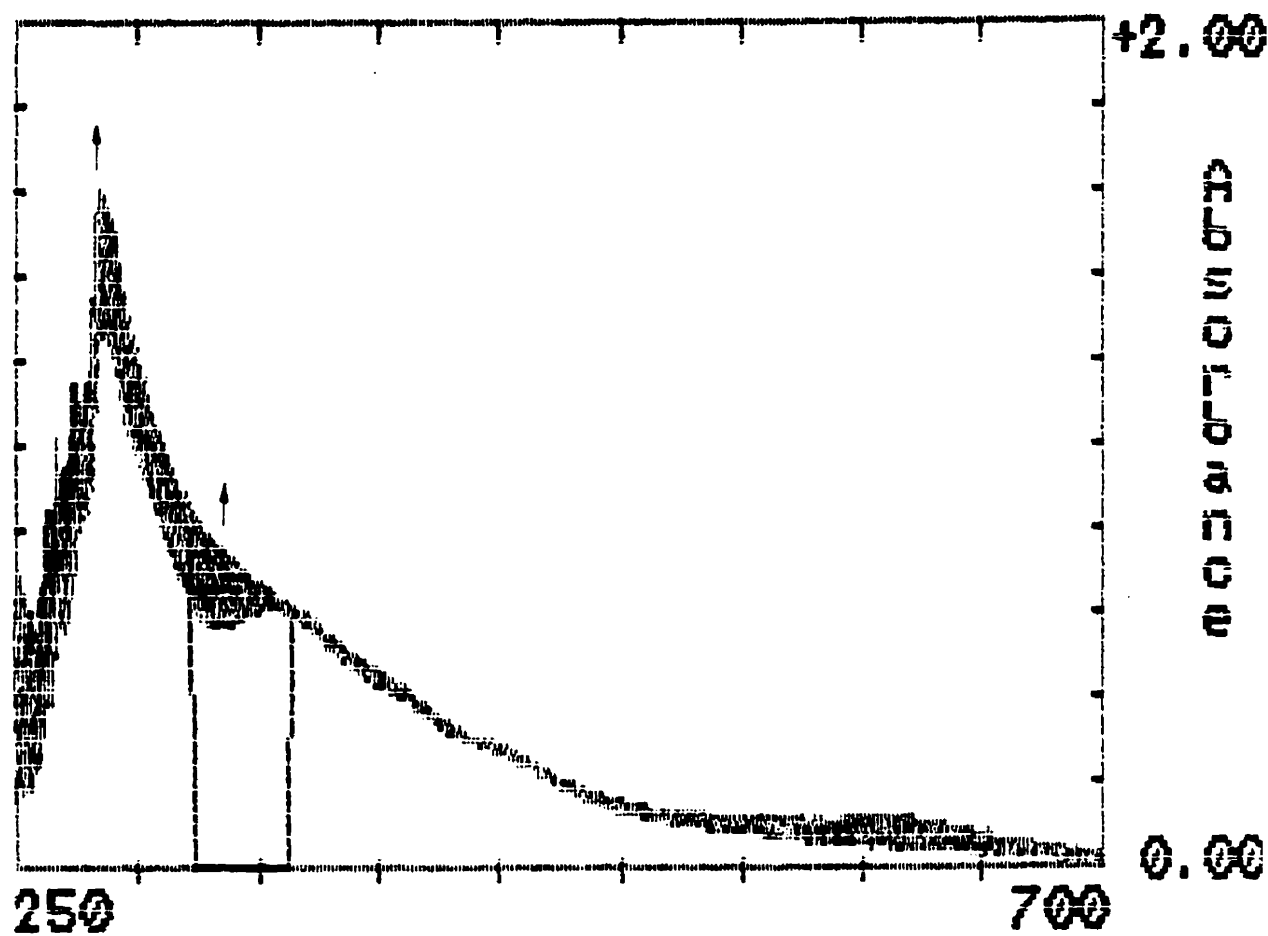


Figure 3.2(b) Successive UV-Vis spectra for the reaction of  $\text{Os}_6(\text{CO})_{18}$  with  $\text{P}(\text{OEt})_3$  in toluene at  $35.0^\circ\text{C}$ .  $[\text{Complex}] = 2 \times 10^{-5} \text{ M}$ ,  $[\text{L}'] = 0.1125 \text{ M}$ , running for 5 hrs.

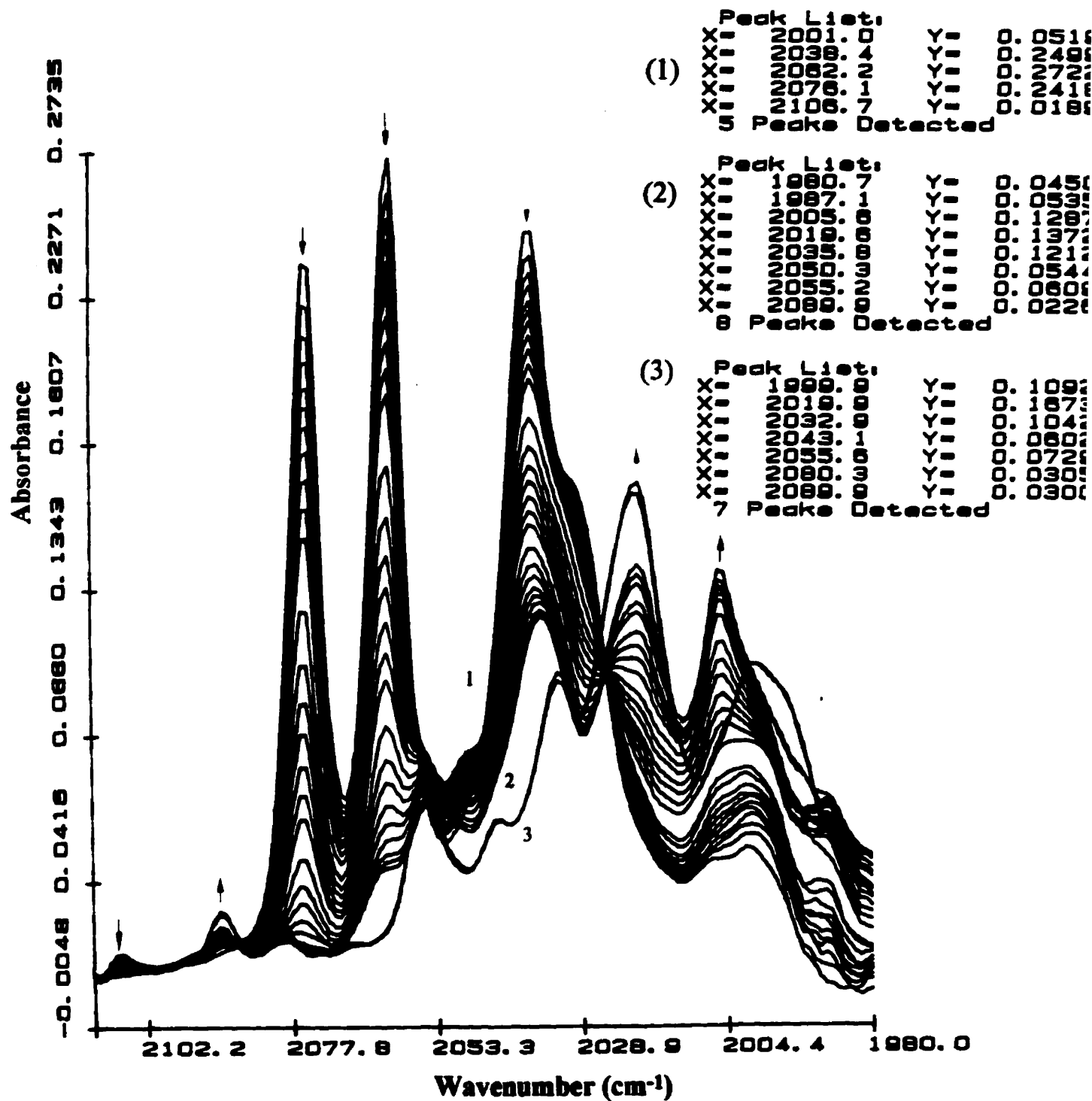


Figure 3.3 Successive FTIR spectra for the reaction of  $\text{Os}_6(\text{CO})_{18}$  with  $\text{P}(n\text{-Bu})_3$  in toluene at  $(23.2 \pm 0.1)^\circ\text{C}$ .  $[\text{Complex}] = 8 \times 10^{-5} \text{ M}$ ,  $[\text{L}] = 0.1187 \text{ M}$ , running for 18.5 hrs.



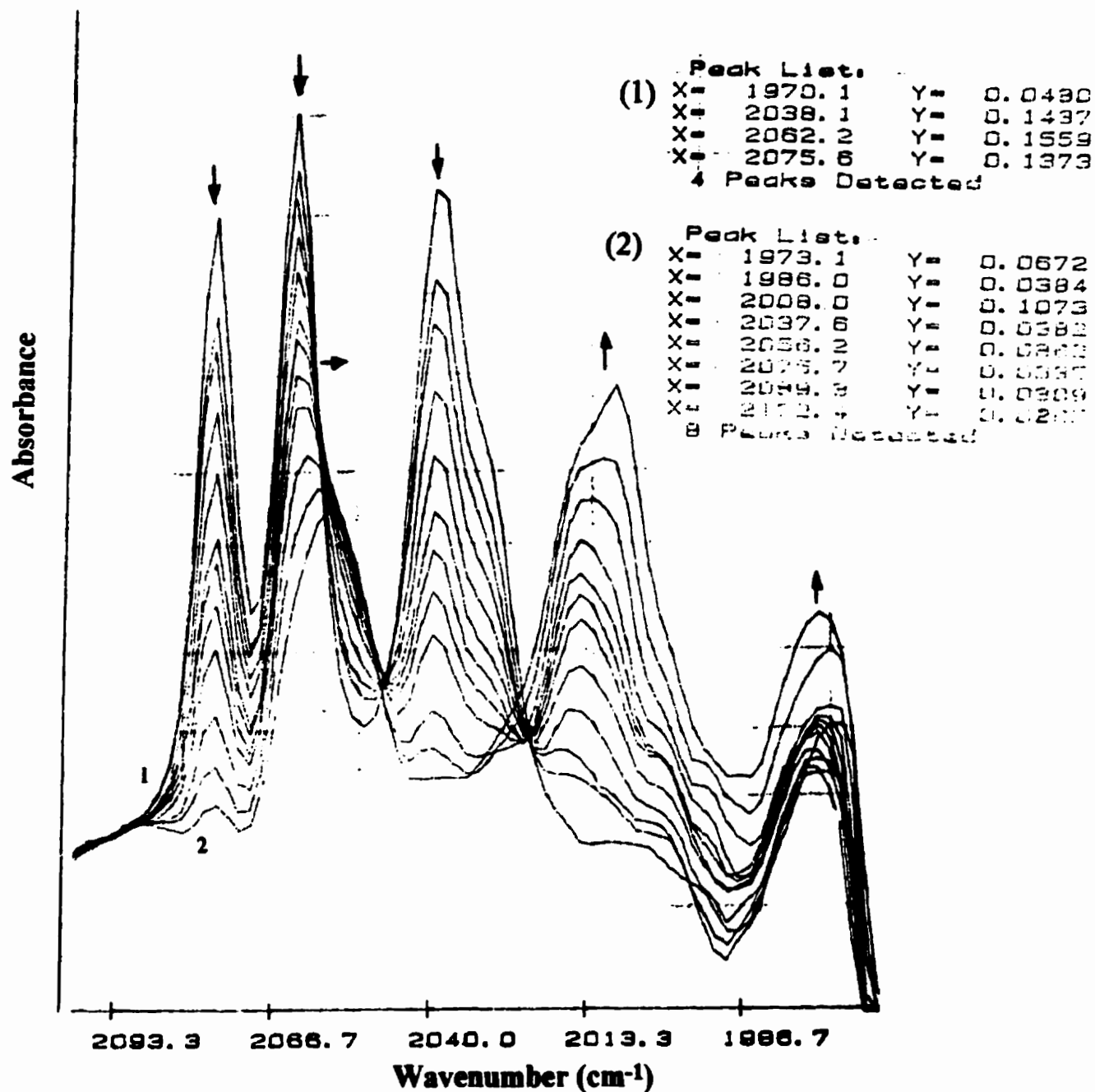


Figure 3.5 FTIR spectra changes during the reaction of  $\text{Os}_6(\text{CO})_{18}$  with  $\text{P}(\text{OEt})_3$  in toluene at  $25.0^\circ\text{C}$ .  $[\text{Complex}] = 8 \times 10^{-5}$  M,  $[\text{L}] = 0.2295$  M.

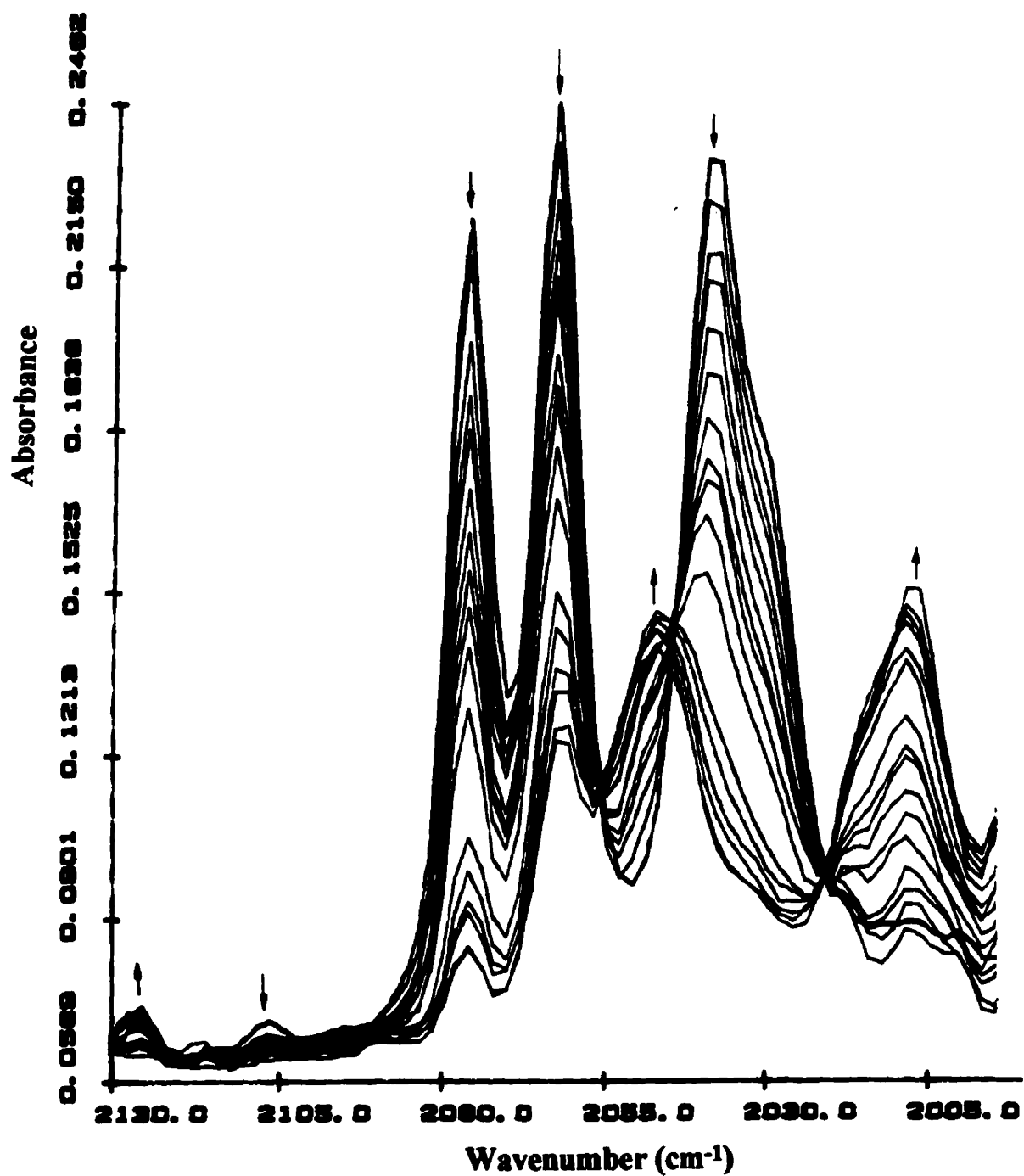


Figure 3.6 FTIR spectra changes during the reaction of  $\text{Os}_6(\text{CO})_{18}$  with  $\text{PPhMe}_2$  in toluene at  $25.0^\circ\text{C}$ .  $[\text{Complex}] = 1.2 \times 10^{-4} \text{ M}$ ,  $[\text{L}] = 0.003000 \text{ M}$  [15(b)].

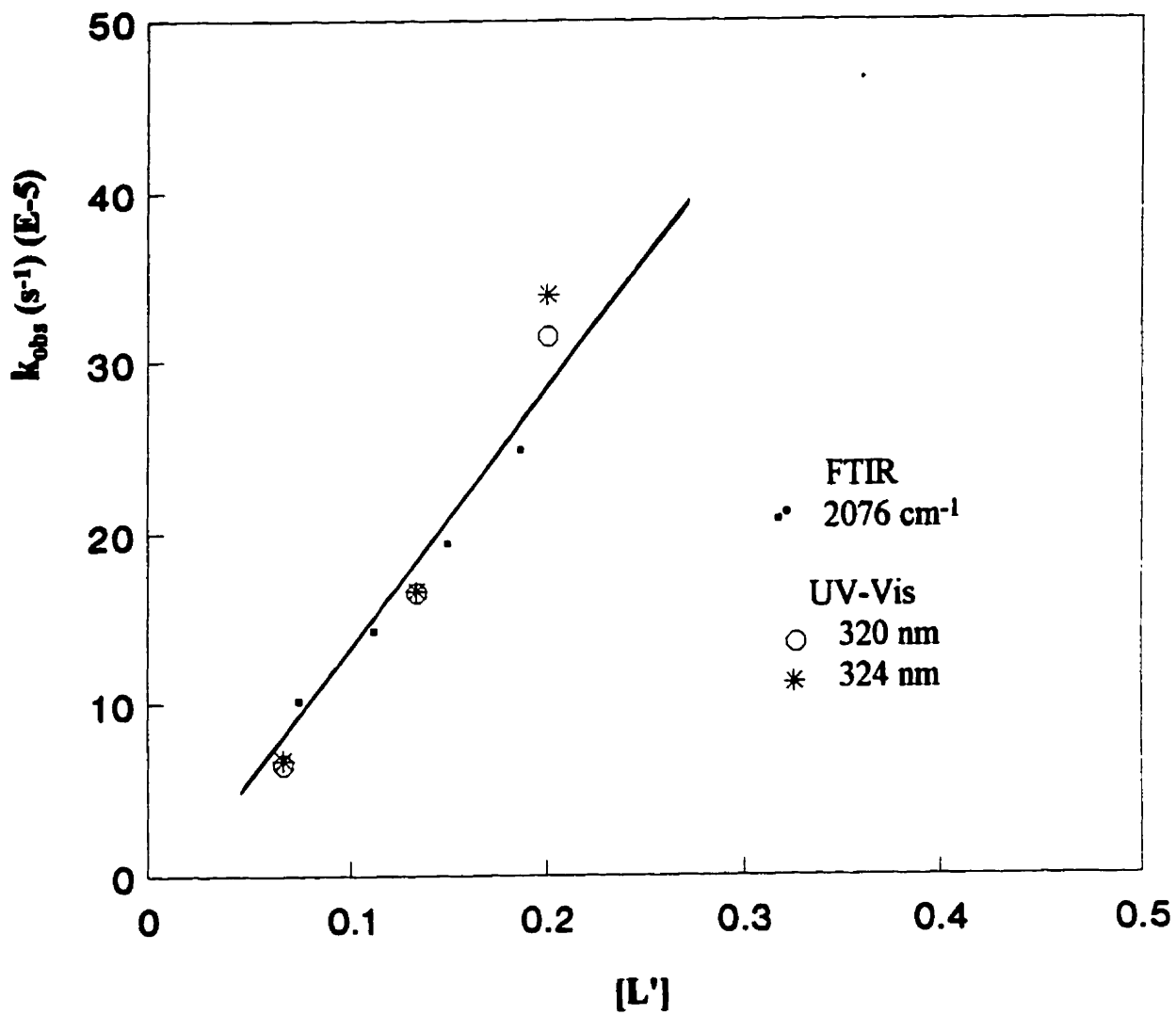
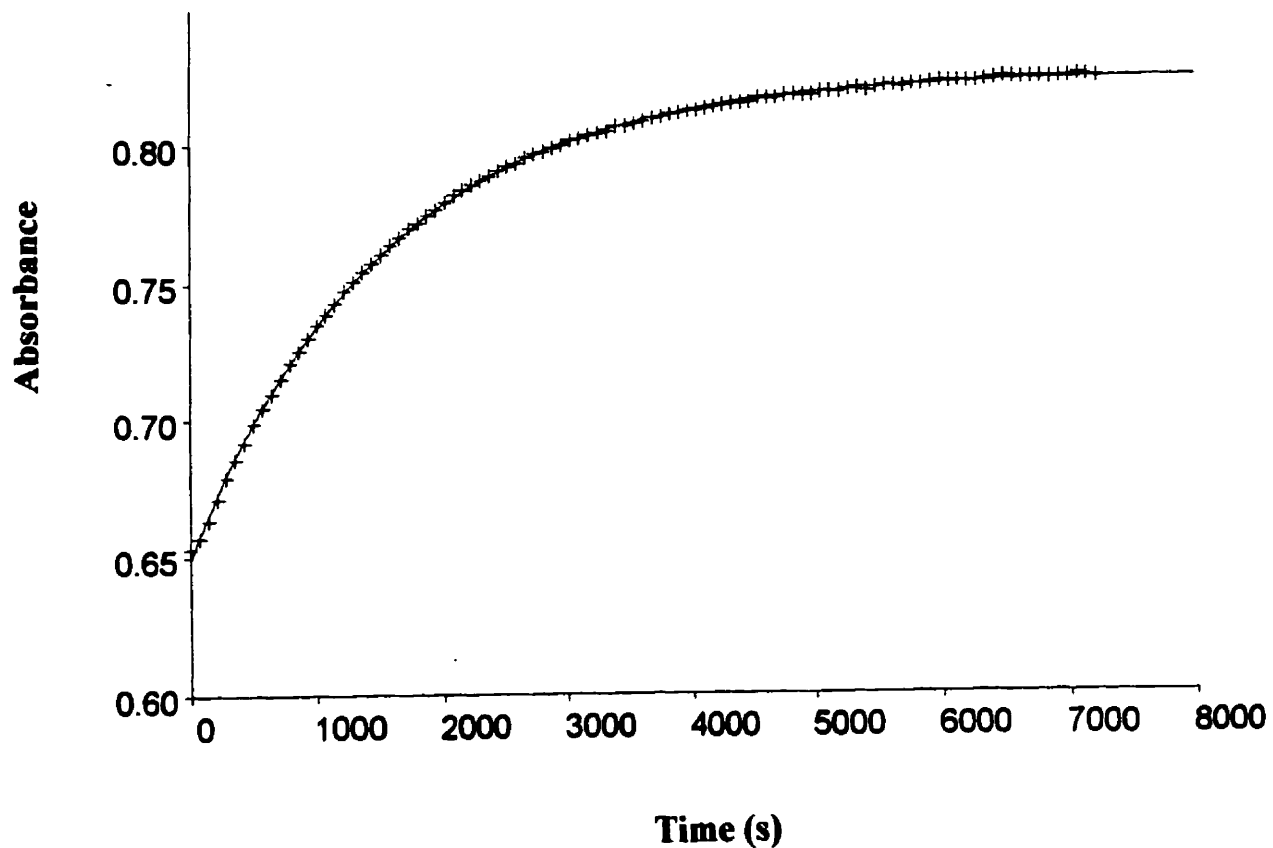
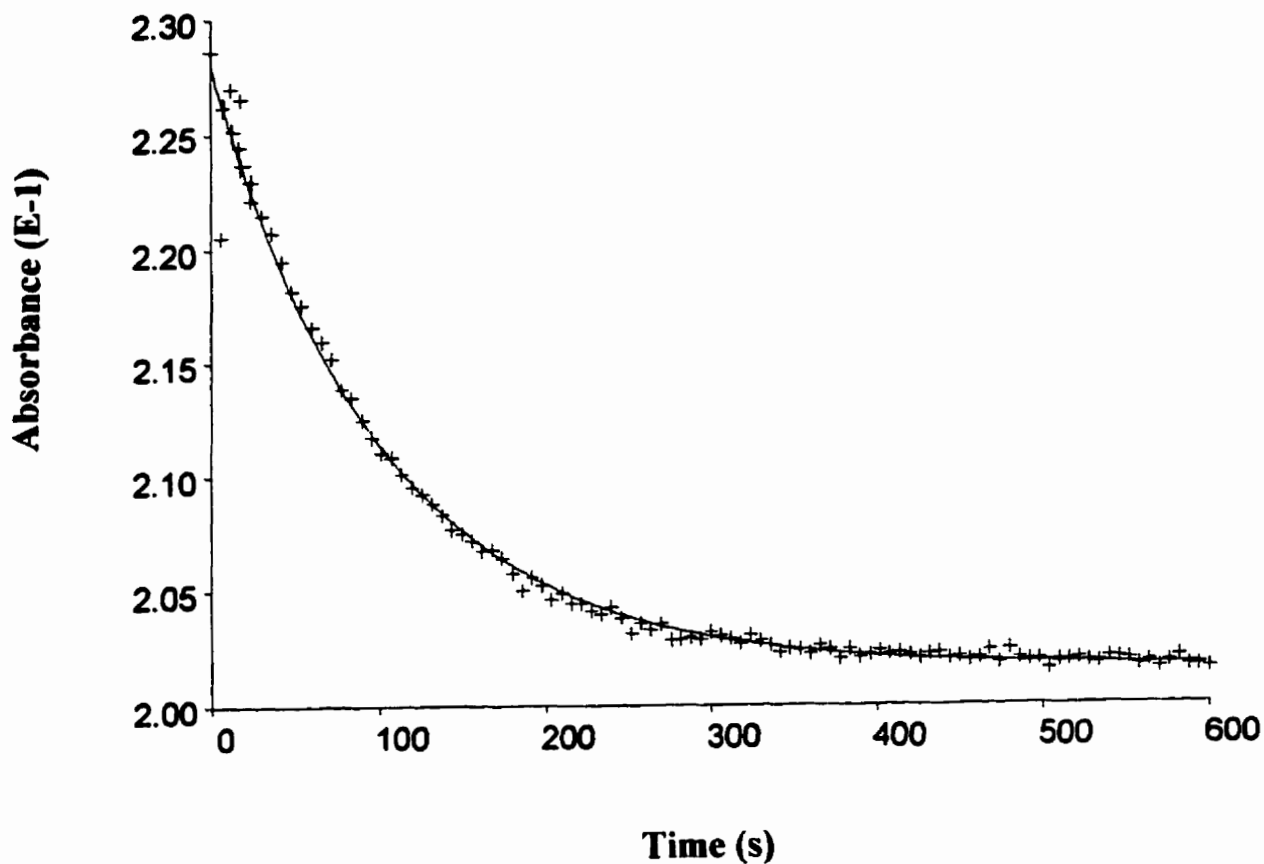


Figure 3.7 Comparison of  $k_{obs}$  values obtained by using different techniques for the reaction of  $Os_6(CO)_{18}$  with  $P(n-Bu)_3$  in toluene at 25.0°C.  $[Complex] = 2 \times 10^{-5} M$  and  $8 \times 10^{-5} M$  for UV and FTIR monitoring, respectively.



**Figure 3.8** Absorbance changes ( $\lambda = 316.0$  nm) vs time for the reaction of  $\text{Os}_6(\text{CO})_{18}$  with  $\text{P}(\text{O-}i\text{-Pr})_3$  in toluene at  $55.0$  °C.  $[\text{Complex}] = 2 \times 10^{-5}$  M,  $[\text{L}'] = 0.4798$  M.



**Figure 3.9** Absorbance changes ( $\lambda = 370.0$  nm) vs time for the reaction of  $\text{Os}_6(\text{CO})_{18}$  with  $\text{PMe}_3$  in toluene at  $15.0^\circ\text{C}$ .  $[\text{Complex}] = 2 \times 10^{-5}$  M,  $[\text{L}'] = 0.6000 \times 10^{-2}$  M.

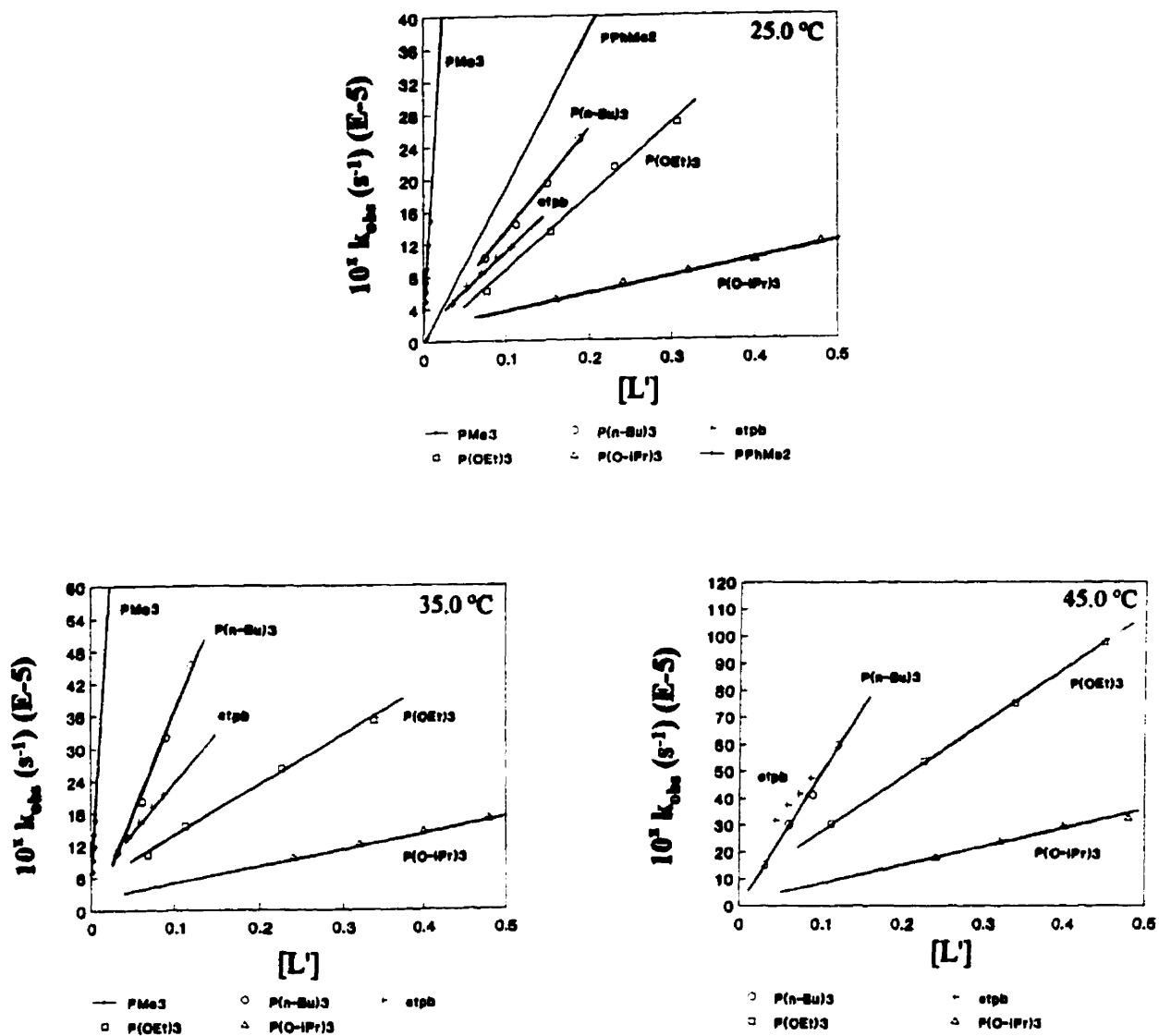


Figure 3.10 Plots of  $k_{\text{obs}}$  vs  $[L']$  for the reactions of  $\text{Os}_6(\text{CO})_{18}$  with nucleophiles  $L'$  in toluene at 25.0°C, 35.0°C, and 45.0°C. When  $L' = \text{PMe}_3$  and  $\text{PPhMe}_2$ ,  $x = -2$ ; for the others  $x = 0$ .

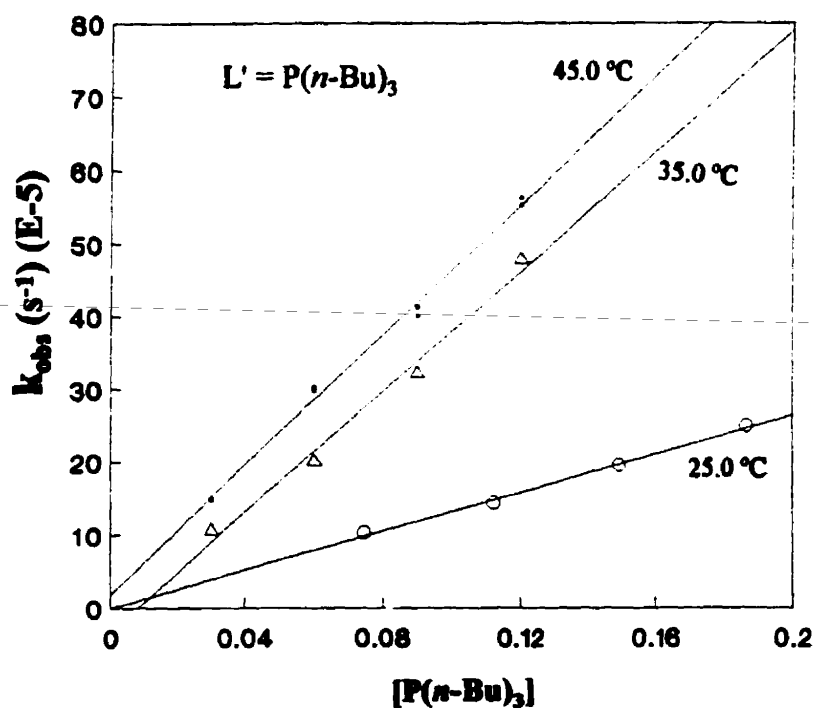
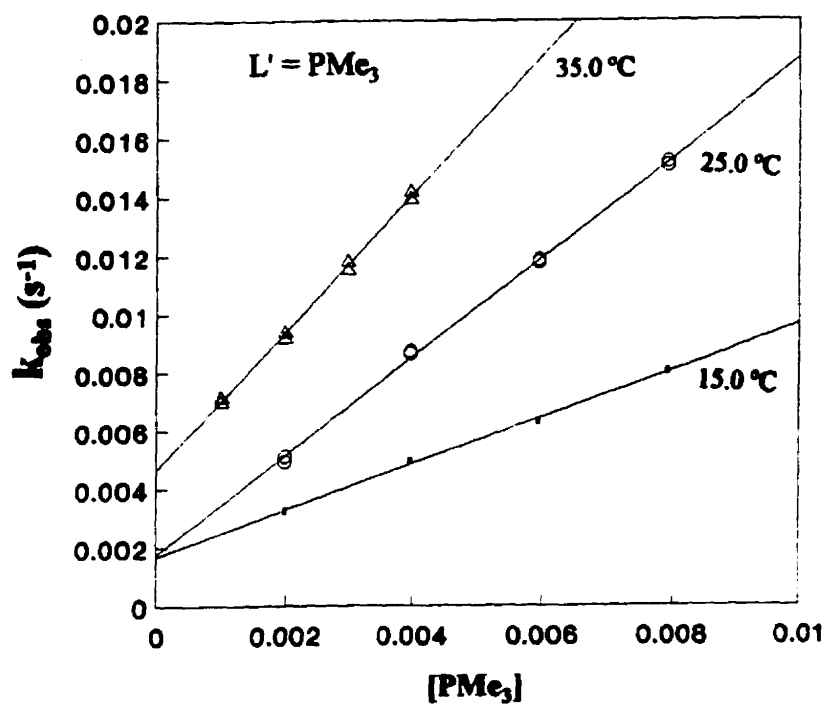


Figure 3.11 Plots of  $k_{\text{obs}}$  vs  $[\text{L}']$  for the reactions of  $\text{Os}_6(\text{CO})_{18}$  with nucleophiles  $\text{PMe}_3$  and  $\text{P}(n\text{-Bu})_3$  in toluene at various temperatures.

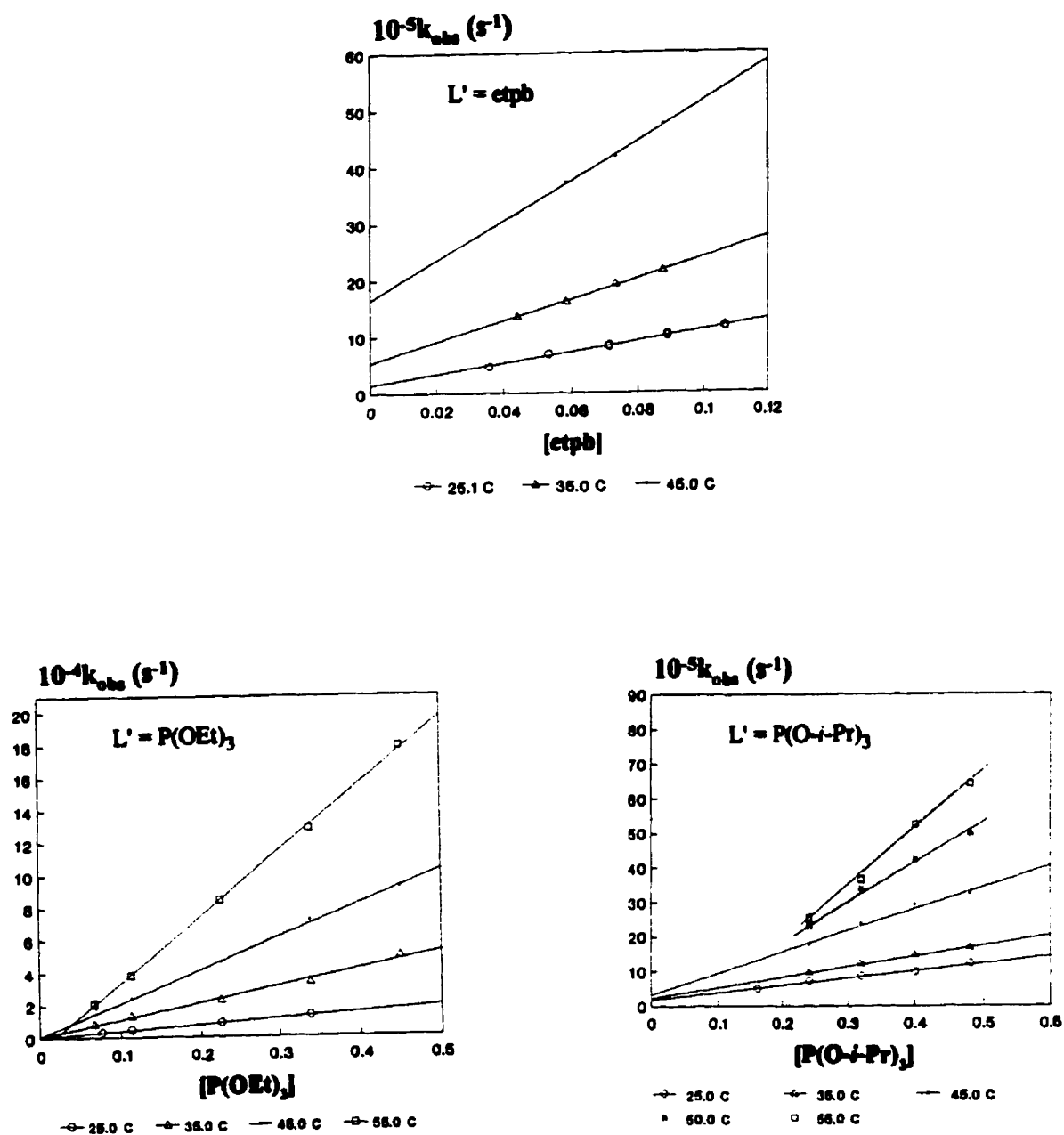


Figure 3.12 Plots of  $k_{\text{obs}}$  vs  $[L']$  for the reactions of  $\text{Os}_6(\text{CO})_{18}$  with nucleophiles  $\text{etpb}$ ,  $\text{P(OEt)}_3$ , and  $\text{P(O-}i\text{-Pr)}_3$  in toluene at various temperatures.

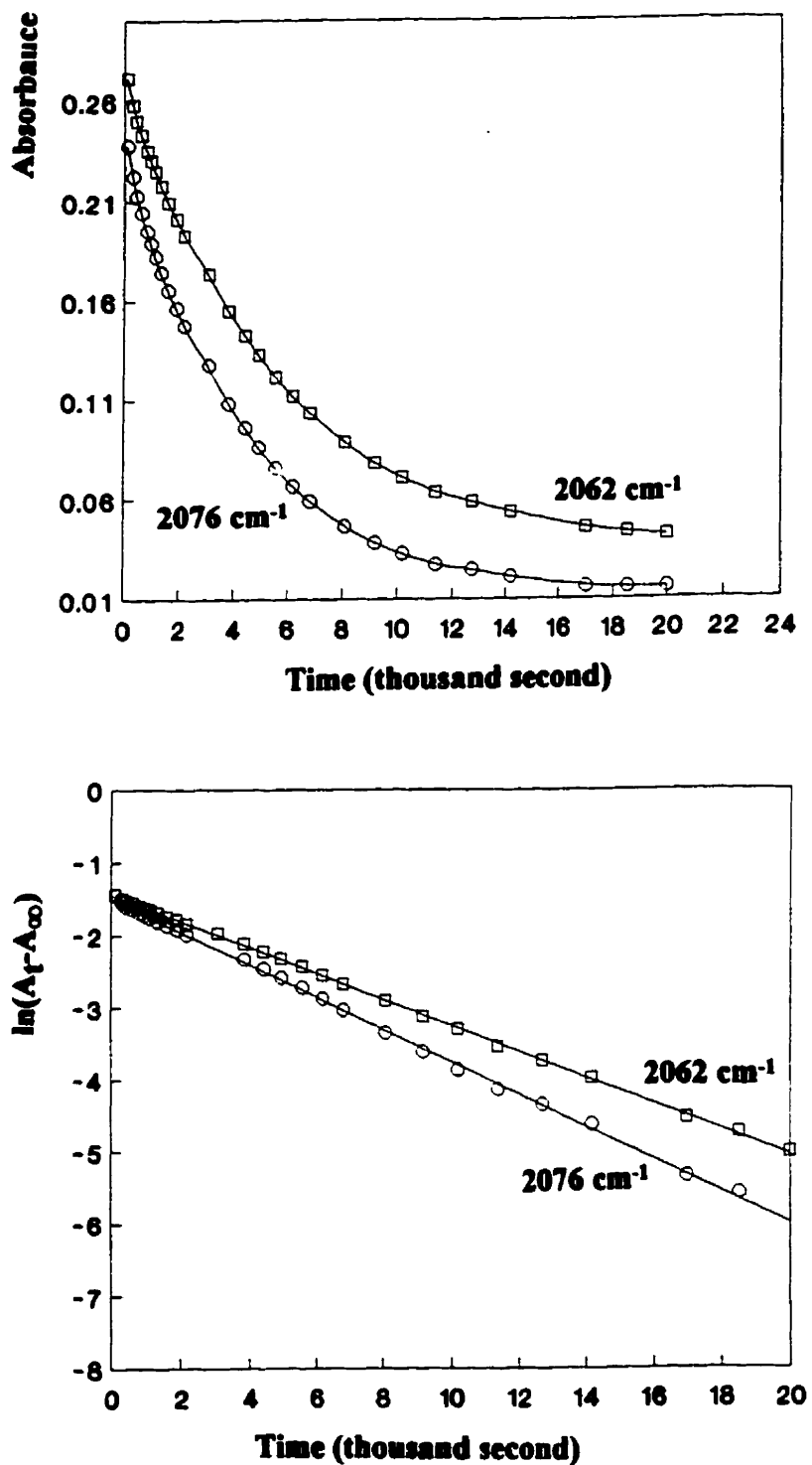


Figure 3.13 Comparison of absorbance changes of two bands for the reaction of  $\text{Os}_6(\text{CO})_{18}$  with  $\text{P}(n\text{-Bu})_3$  in toluene at  $(23.2 \pm 0.1)^\circ\text{C}$ .  $[\text{Complex}] = 8 \times 10^{-5} \text{ M}$ ,  $[\text{L}] = 0.1187 \text{ M}$ .

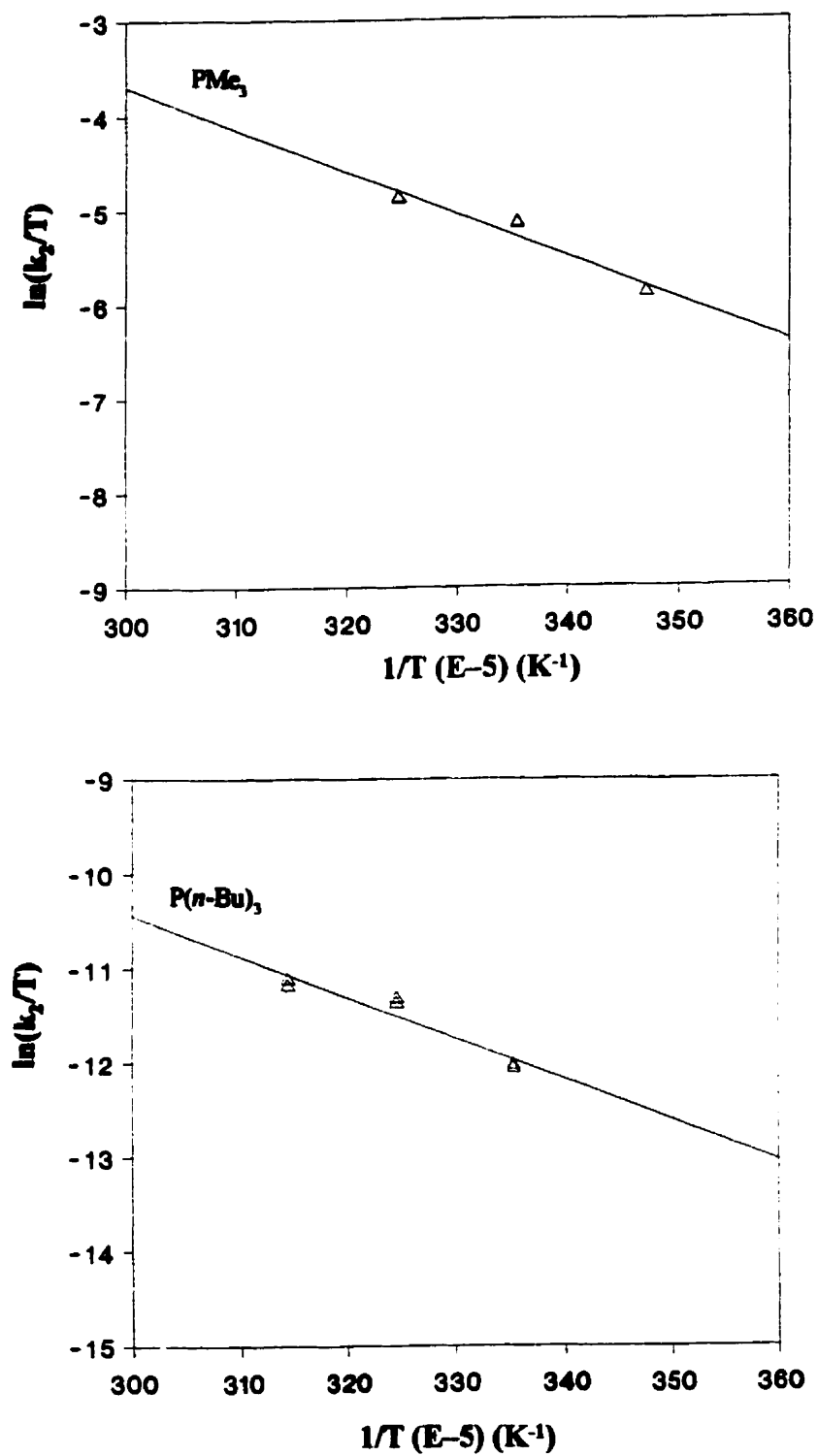


Figure 3.14 Plots of  $\ln(k_2/T)$  vs  $1/T$  for the reactions of  $\text{Os}_6(\text{CO})_{18}$  with nucleophiles  $\text{PMe}_3$  and  $\text{P}(n\text{-Bu})_3$  in toluene.

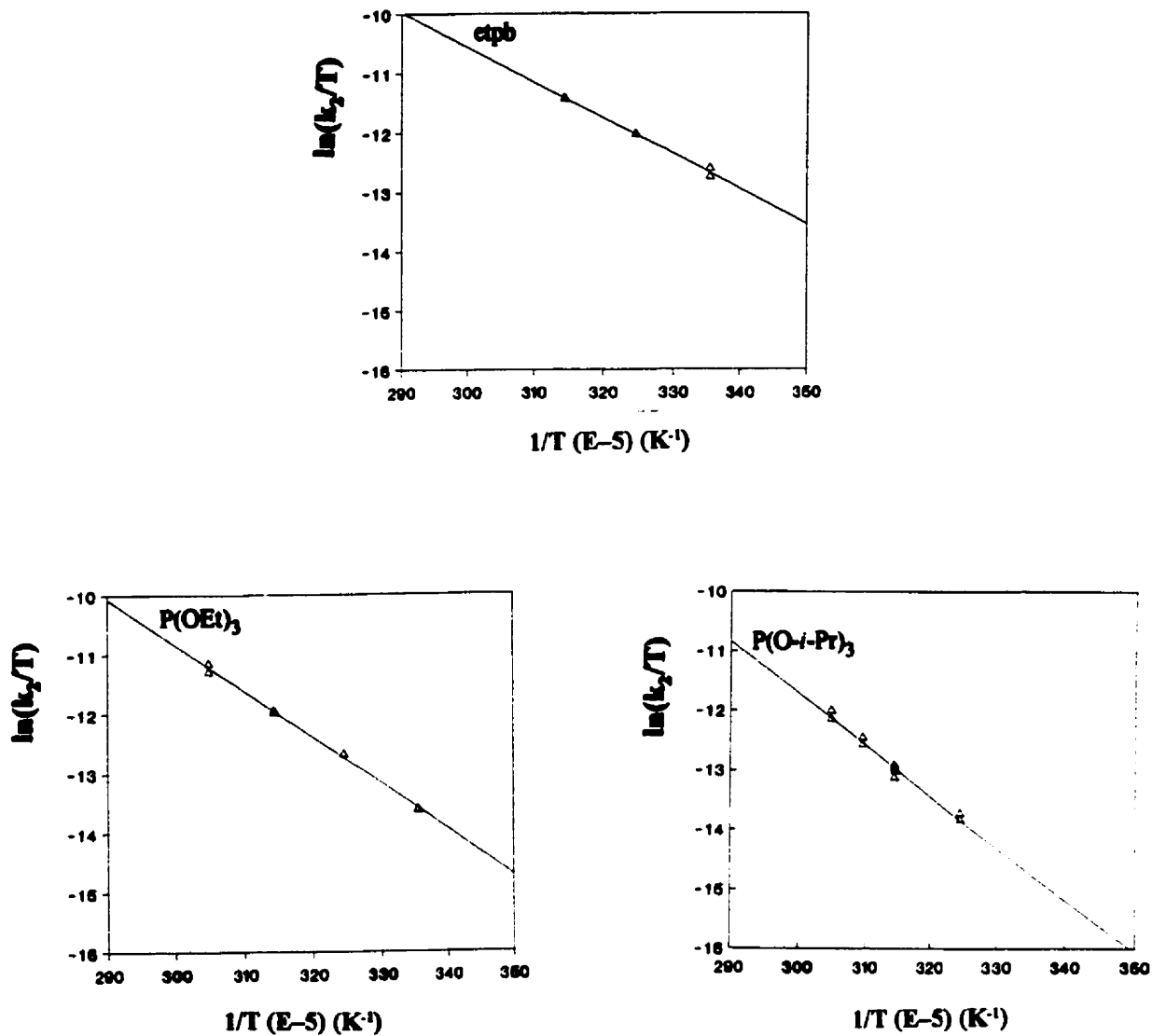
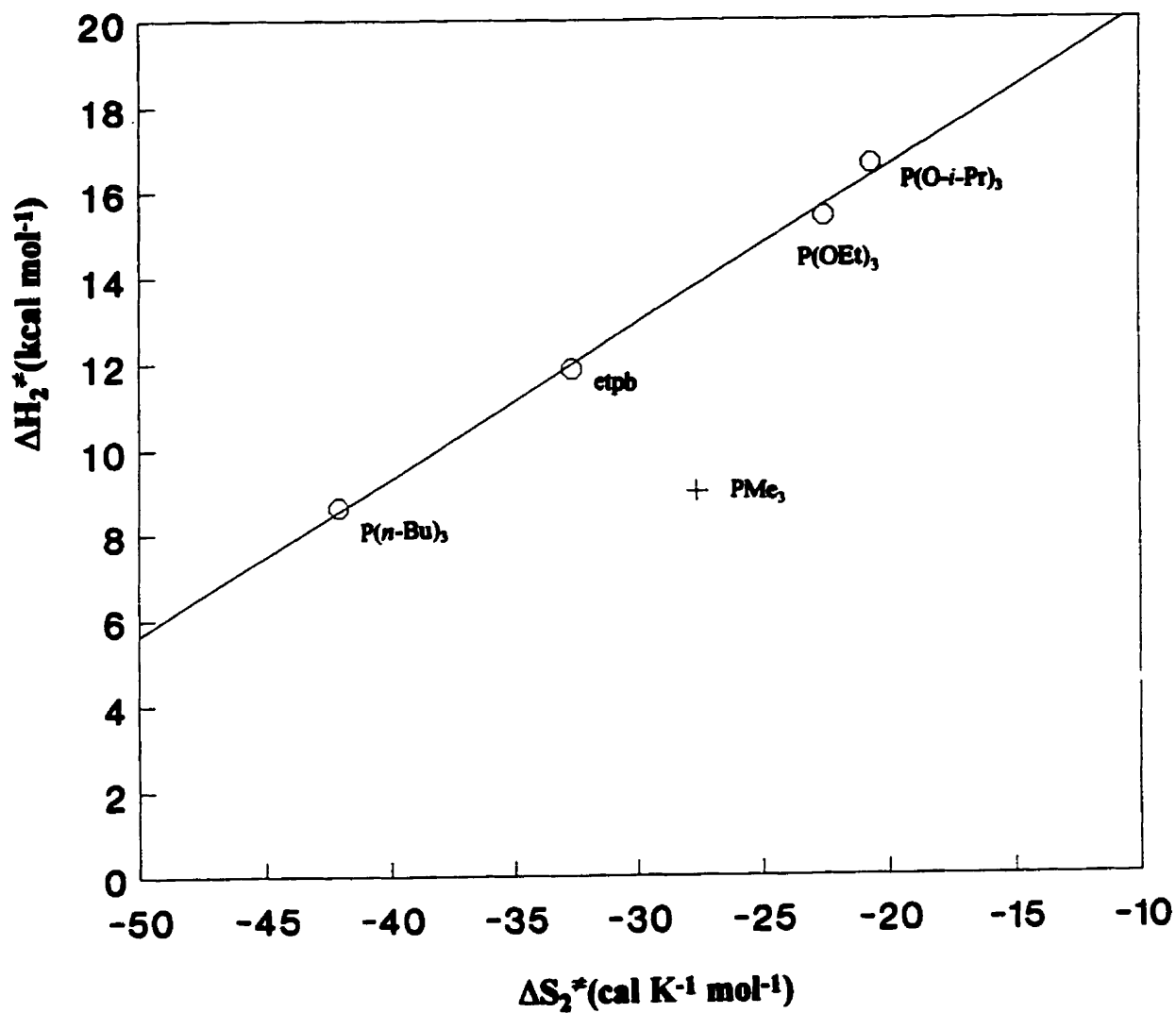
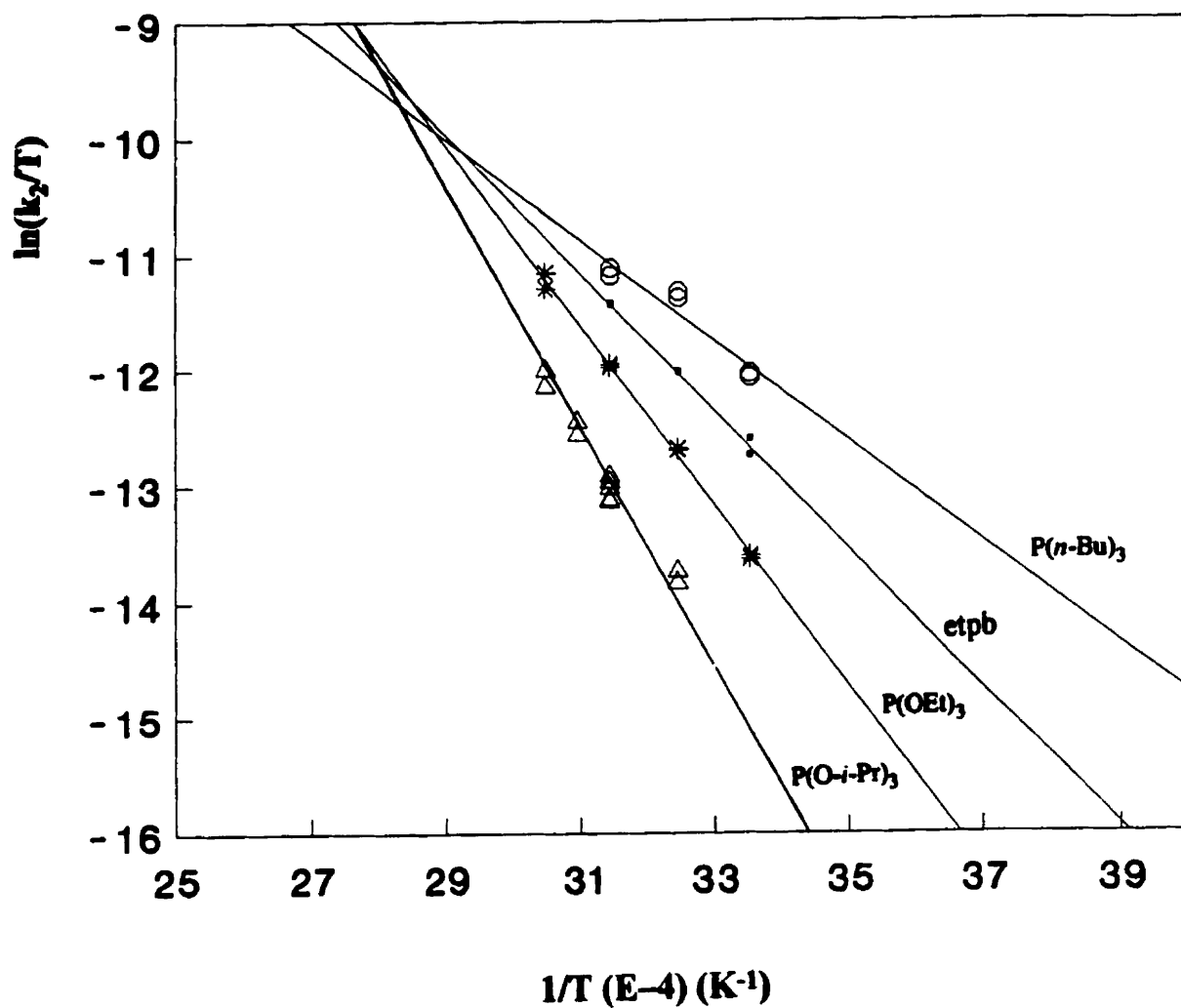


Figure 3.15 Plots of  $\ln(k_2/T)$  vs  $1/T$  for the reactions of  $\text{Os}_6(\text{CO})_{18}$  with nucleophiles etpb,  $\text{P}(\text{OEt})_3$ , and  $\text{P}(\text{O-}i\text{-Pr})_3$  in toluene.



Isokinetic temperature about 89°C

Figure 3.16 Isokinetic relationship,  $\Delta H_2^\ddagger$  vs  $\Delta S_2^\ddagger$ , for the substitution reactions of  $\text{Os}_6(\text{CO})_{18}$  with nucleophiles  $\text{L}'$  in toluene.



Isokinetic temperature around 88 °C

Figure 3.17 Isokinetic relationship,  $\ln(k_2/T)$  vs  $1/T$ , for the substitution reactions of  $Os_6(CO)_{18}$  with nucleophiles  $L'$  in toluene.

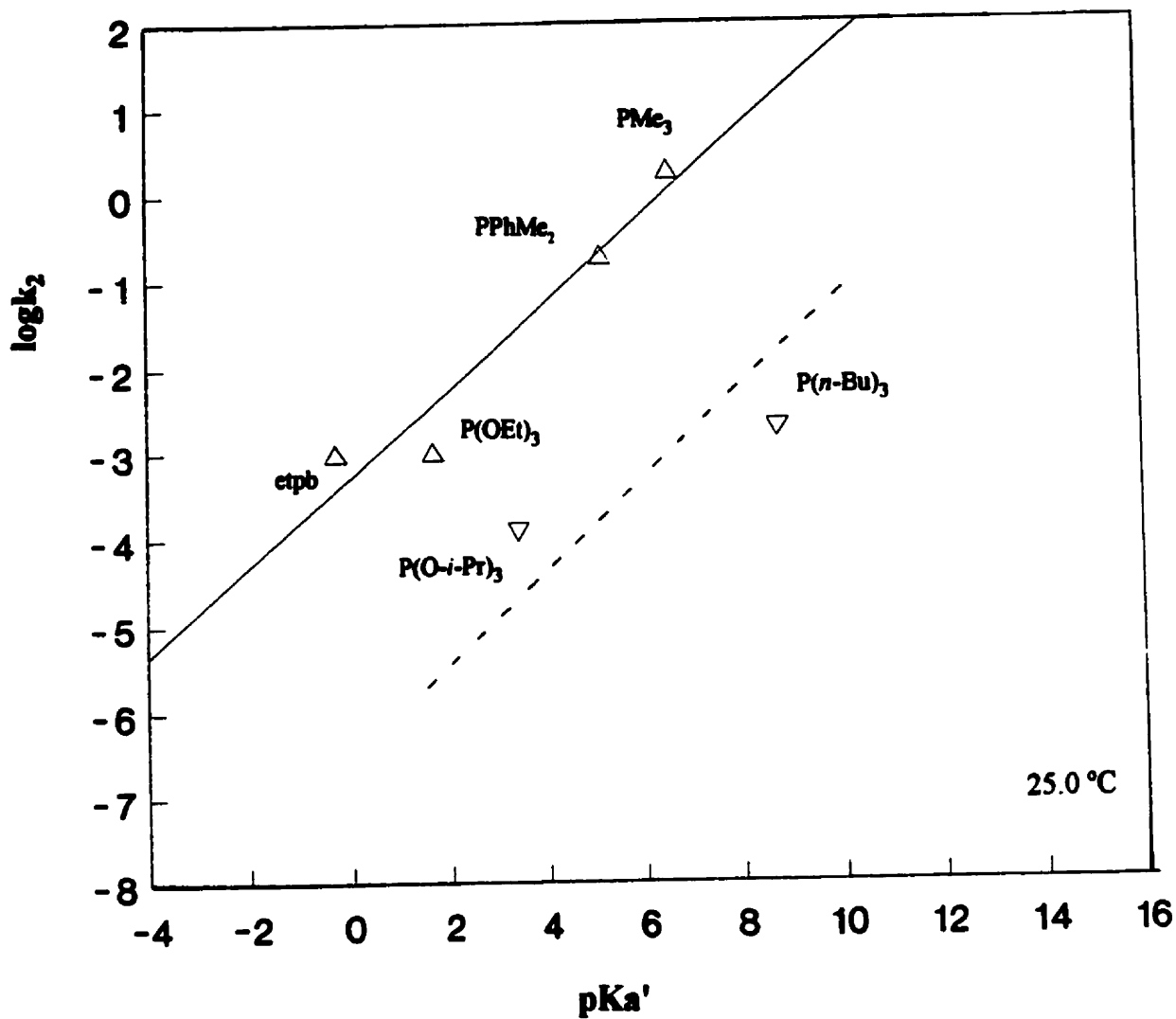


Figure 3.18 Electronic profile for the reactions of  $Os_6(CO)_{18}$  with nucleophiles  $L'$  in toluene at 25.0°C.

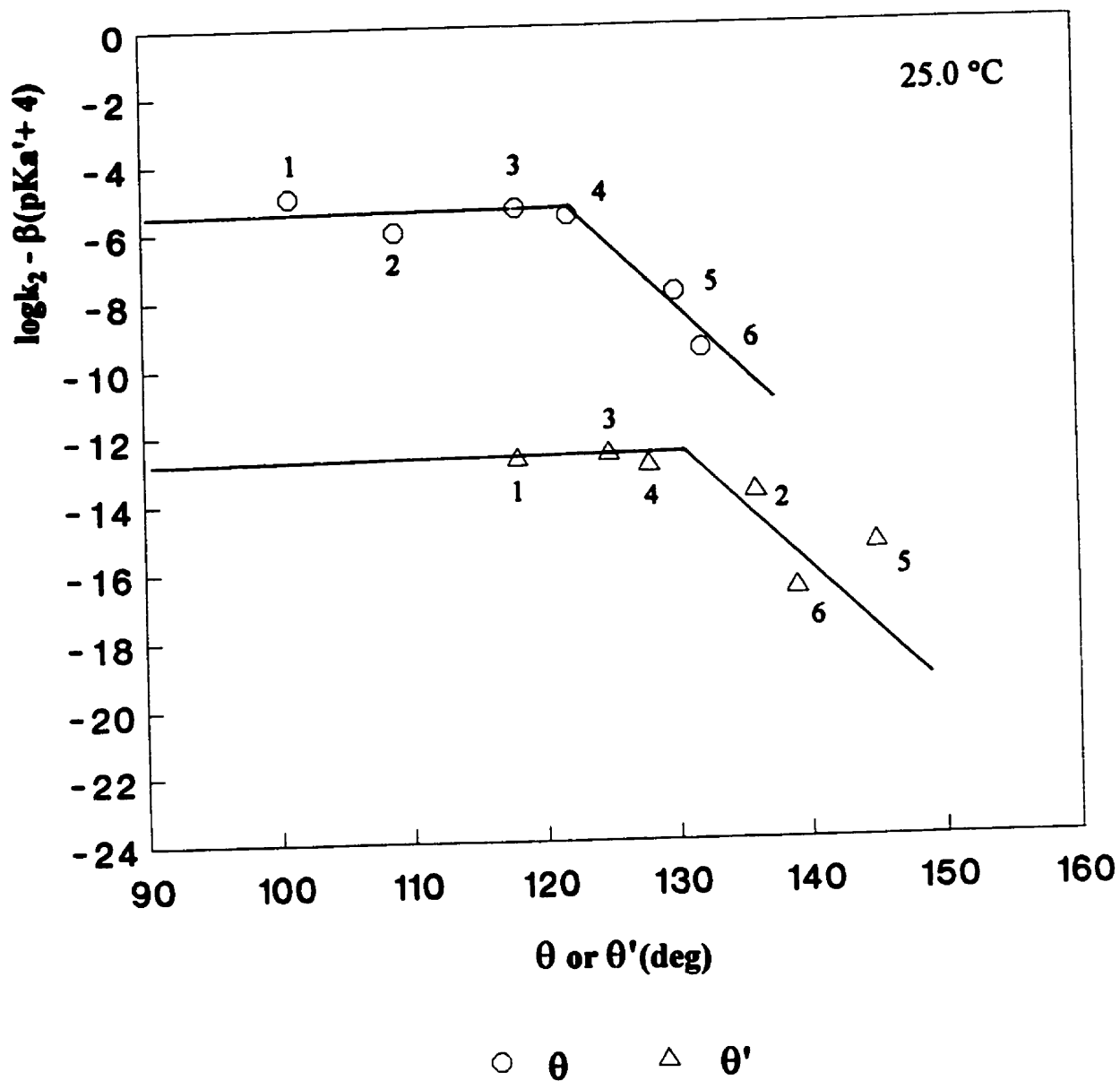
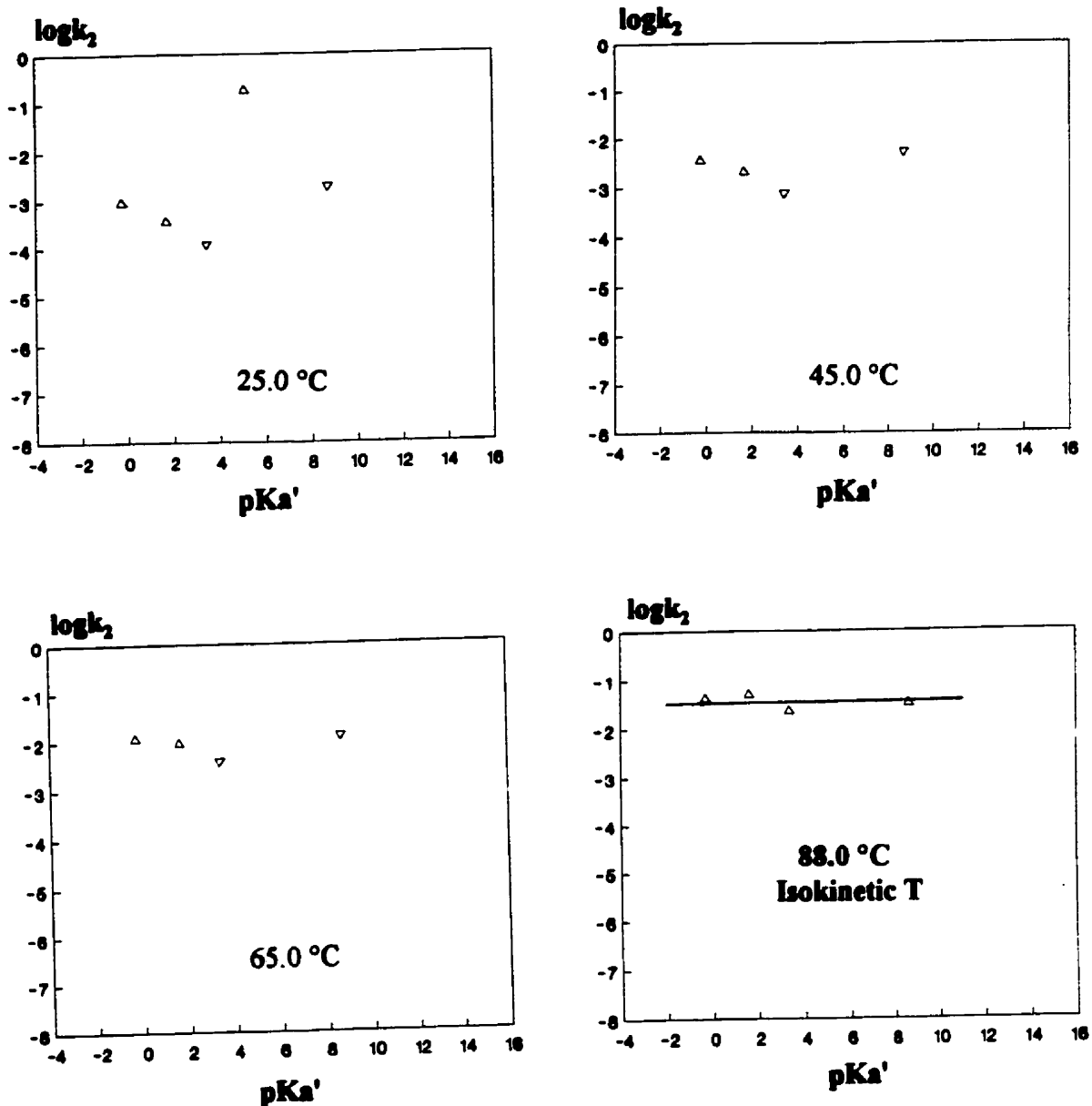


Figure 3.19 Steric profiles for the reactions of  $\text{Os}_6(\text{CO})_{18}$  with nucleophiles  $\text{L}'$  at 25.0°C in toluene.

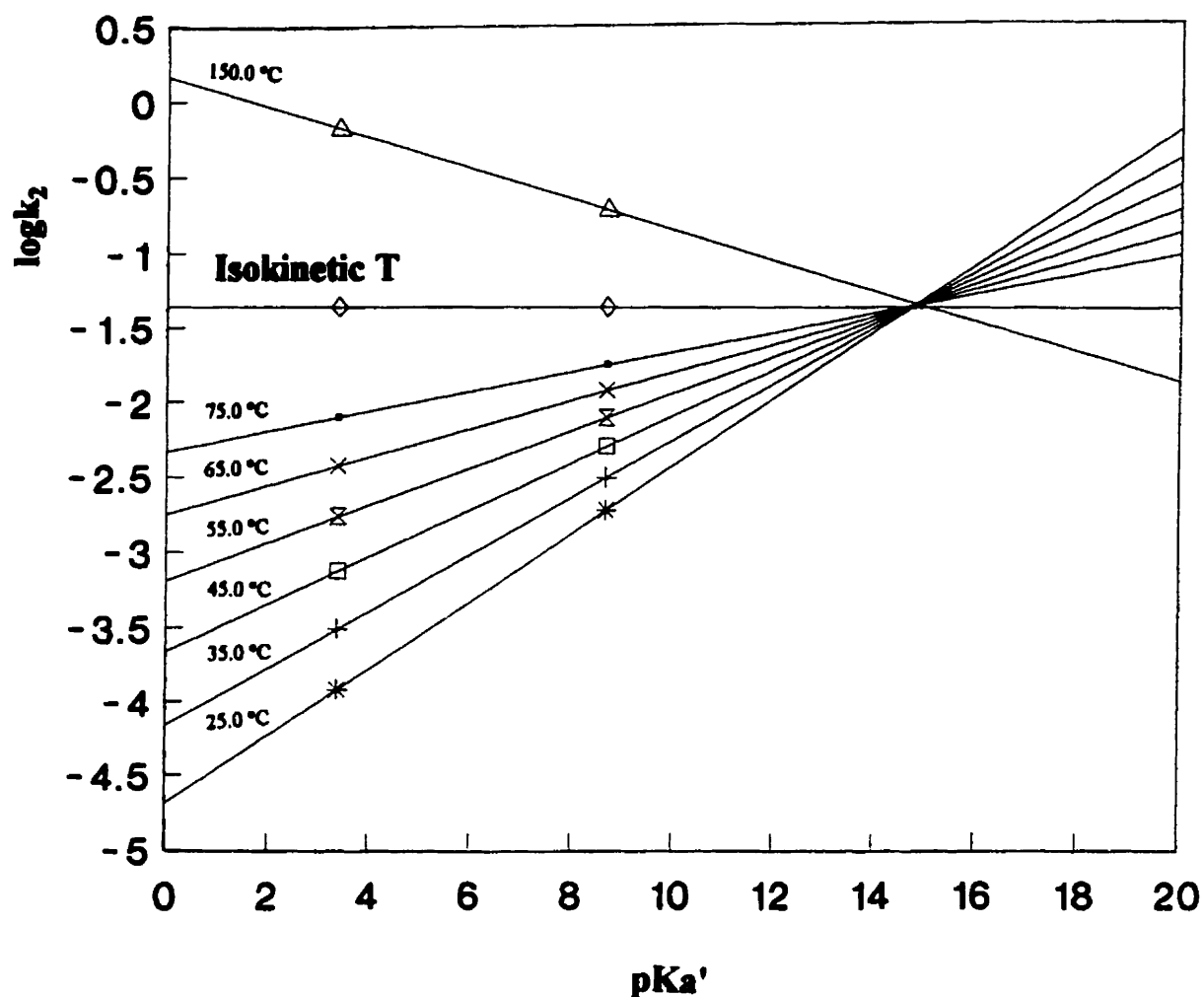
Upper:  $\log k_2^\circ$  vs  $\theta$  ; bottom:  $(\log k_2^\circ - 8)$  vs  $\theta'$

- |                     |                                      |                              |
|---------------------|--------------------------------------|------------------------------|
| 1. <i>ctpb</i>      | 2. $\text{P}(\text{OEt})_3$          | 3. $\text{PMe}_3$            |
| 4. $\text{PPhMe}_2$ | 5. $\text{P}(\text{O-}i\text{Pr})_3$ | 6. $\text{P}(n\text{-Bu})_3$ |



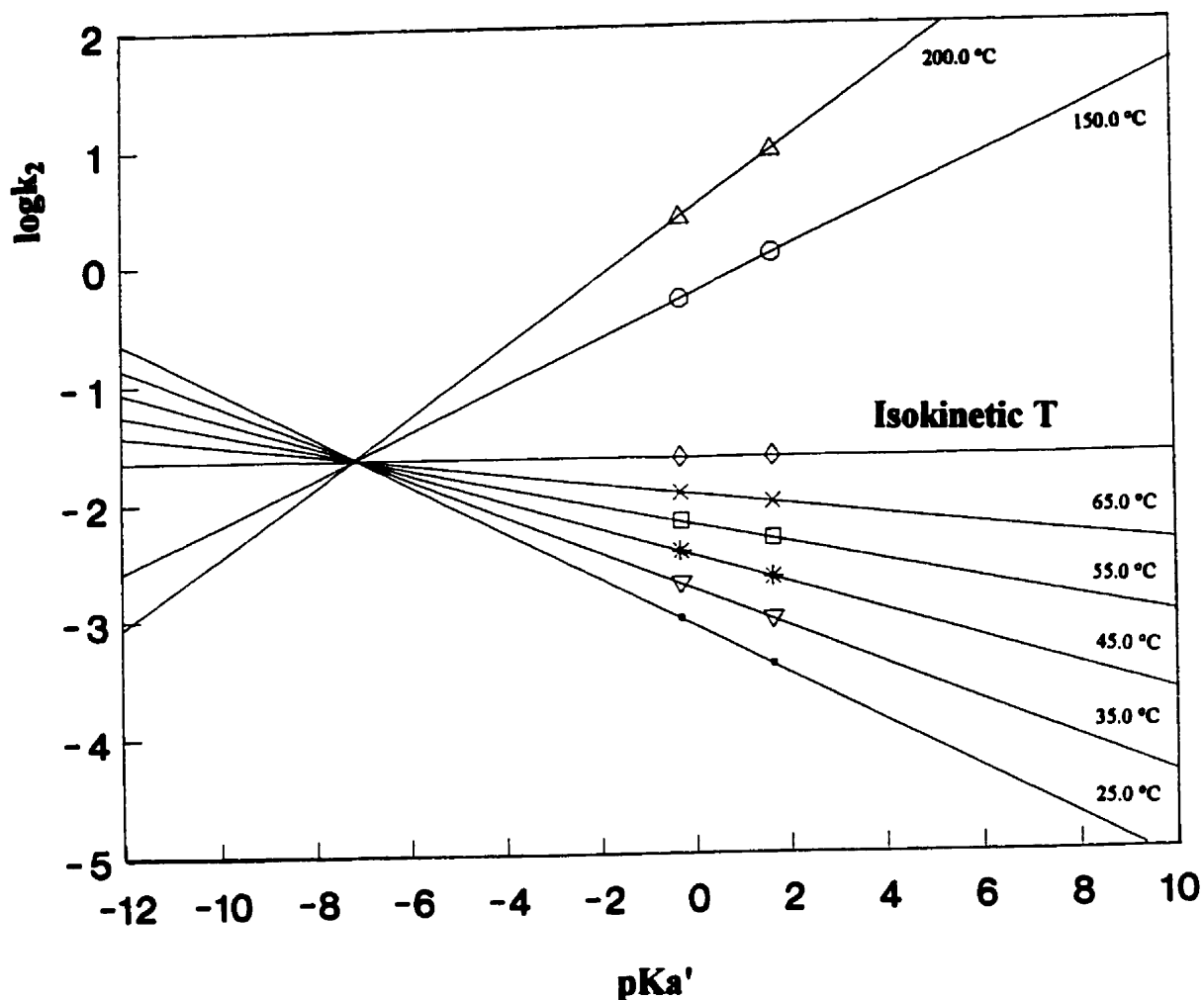
Isokinetic temperature around 88°C

Figure 3.20 A novel IKR,  $\log k_2$  vs  $pK_a'$  for nucleophiles with different  $\sigma$ -basicity and size at the IKT for the reaction series of  $Os_6(CO)_{18}$  with  $L'$  {=  $etpb$ ,  $P(OEt)_3$ , and  $P(O-i-Pr)_3$ , and  $P(n-Bu)_3$ } in toluene.



Isokinetic temperature about 90°C

Figure 3.21(a) A unique IKR,  $\log k_2$  vs  $pK_a'$  for almost isosteric nucleophiles  $P(O-i-Pr)_3$  and  $P(n-Bu)_3$ , which show the same steric effects almost, for the reaction series of  $Os_6(CO)_{18}$  with  $L'$  in toluene at various temperatures. This unique IKR, common point of intersection in the LFER plots at various temperatures, was established for the first time. It also shows an excellent temperature dependence of electronic profiles, and it is therefore a **breakthrough** in providing the first example of the theoretical interconnection between an IKR and LFER. A unique LFER isoparameter  $\xi_{iso}$  — isokinetic  $pK_a'$  — was also established for first time.



Isokinetic temperature about 86°C

Figure 3.21(b) A unique IKR,  $\log k_2$  vs  $pK_a'$  for small nucleophiles with  $\theta < \theta_{th}$ ,  $etpb$  and  $P(OEt)_3$ , which exhibit no steric effects, for the reaction series of  $Os_6(CO)_{18}$  with  $L'$  in toluene at various temperatures.

This unique IKR, common point of intersection in the LFER plots at various temperatures, was established for the first time. It also shows an excellent temperature dependence of electronic profiles, and it is therefore a **breakthrough** in providing the first two examples of the theoretical interconnection between an IKR and LFER. A unique LFER isoparameter  $\xi_{iso}$  — isokinetic  $pK_a'$  — was also established for first time.

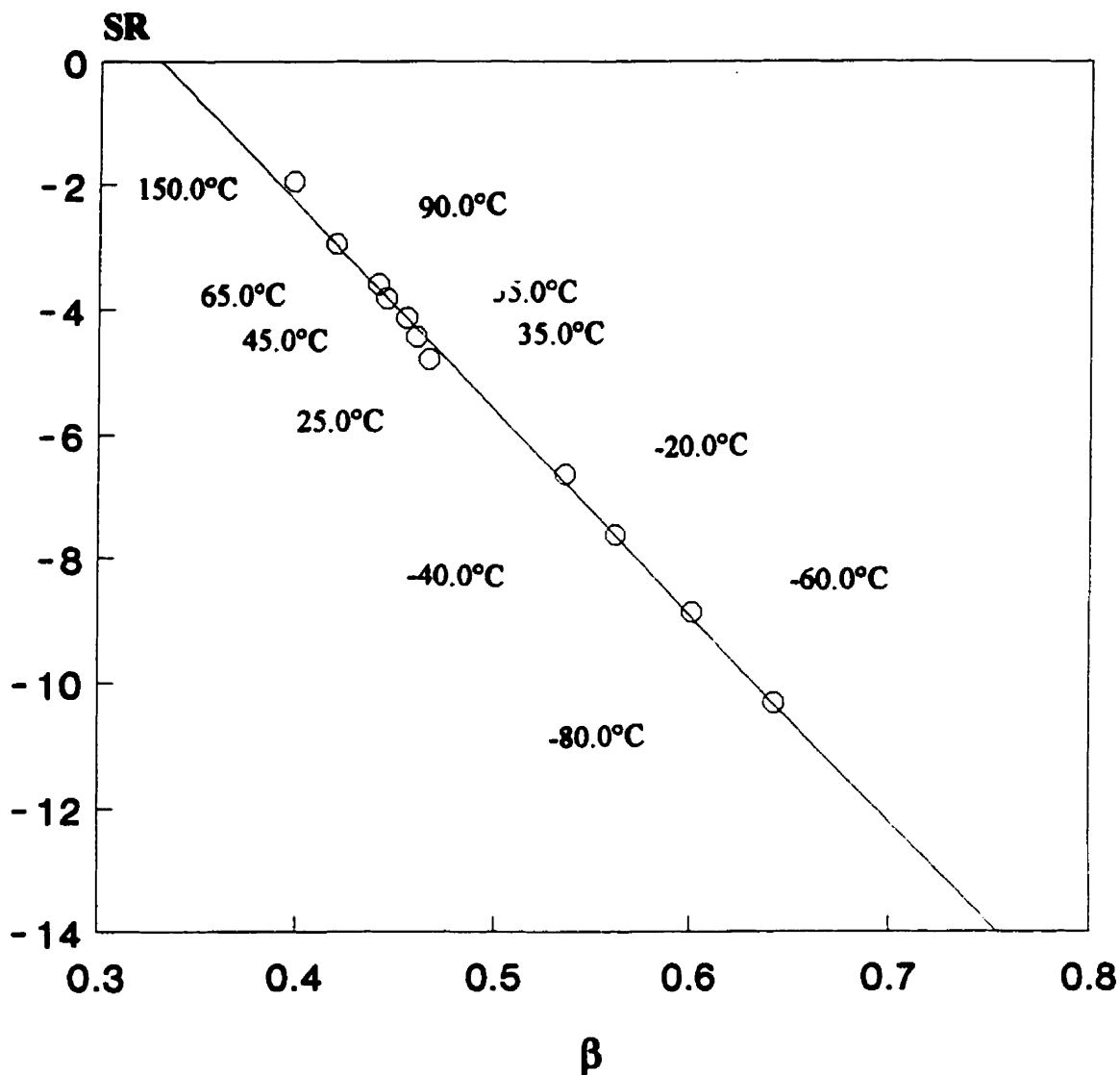
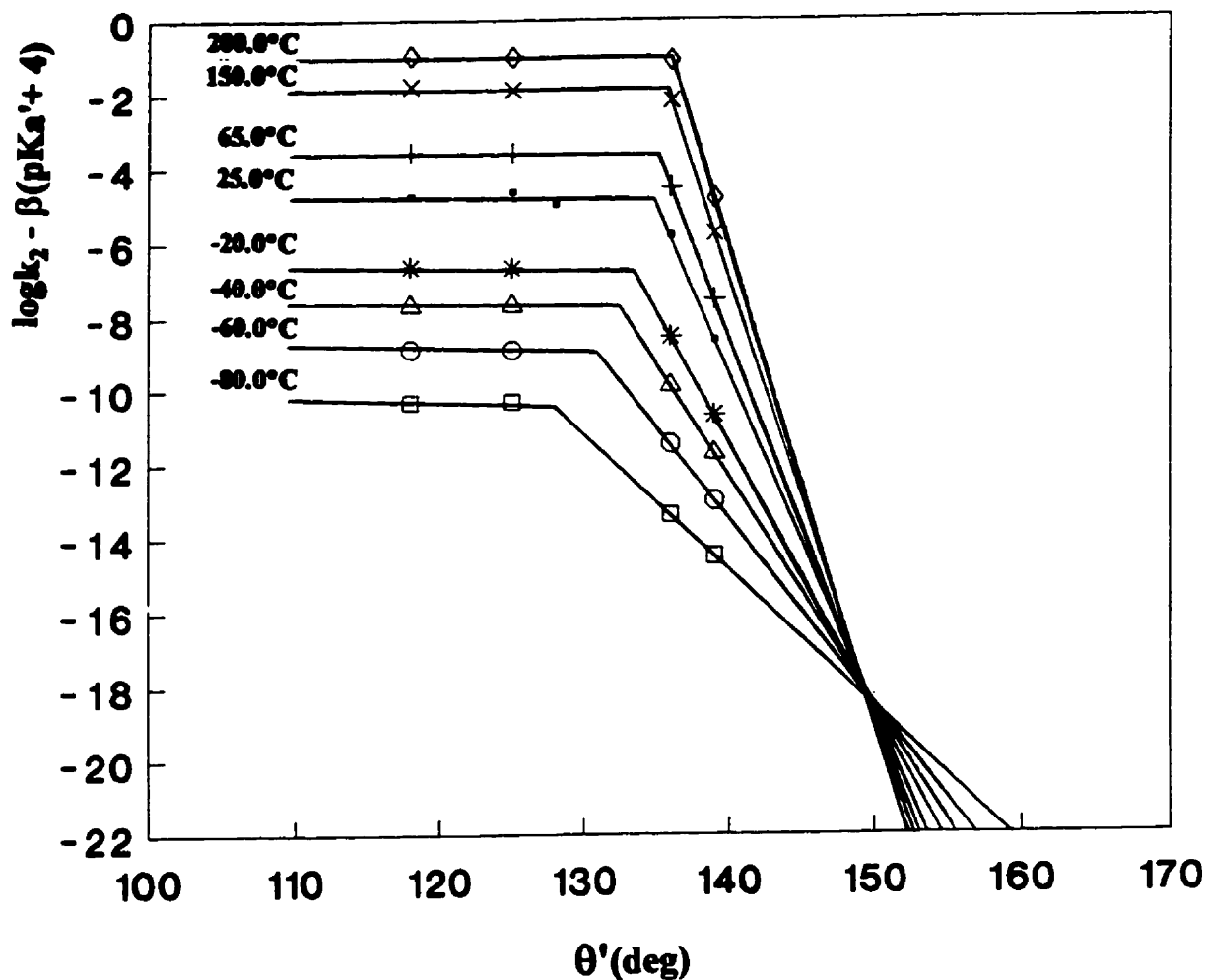


Figure 3.21(c) The correlation of SR with corresponding  $\beta$  value for the reactions of  $\text{Os}_6(\text{CO})_{18}$  with  $L'$  in toluene at various temperatures.  $\theta'$  as a steric parameter for the stereoelectronic analysis.

Least squares analysis shows that the linear relationship is governed by the equation  $\text{SR}_T = 10.9 + (-33.1)\beta_T$  with a correlation coefficient of 0.998.



- When  $T \uparrow$
- SR  $\uparrow$  more reactive
  - $\theta_{th} \uparrow$  later onset of steric effects
  - $\gamma \uparrow$  (more negative) less flexible TSI
  - $\beta \downarrow$  less M...P bond-making in TSI

Figure 3.22(a) A unique LFER isoparameter  $\xi_{iso}$  — isokinetic  $\theta'$  — for the reaction series of  $Os_6(CO)_{18}$  with  $L'$  in toluene at various temperatures was established for the first time.  $L'$  are listed in order from left to right: etpb,  $PMe_3$ ,  $PPhMe_2$ ,  $P(OEt)_3$ , and  $P(n-Bu)_3$ .

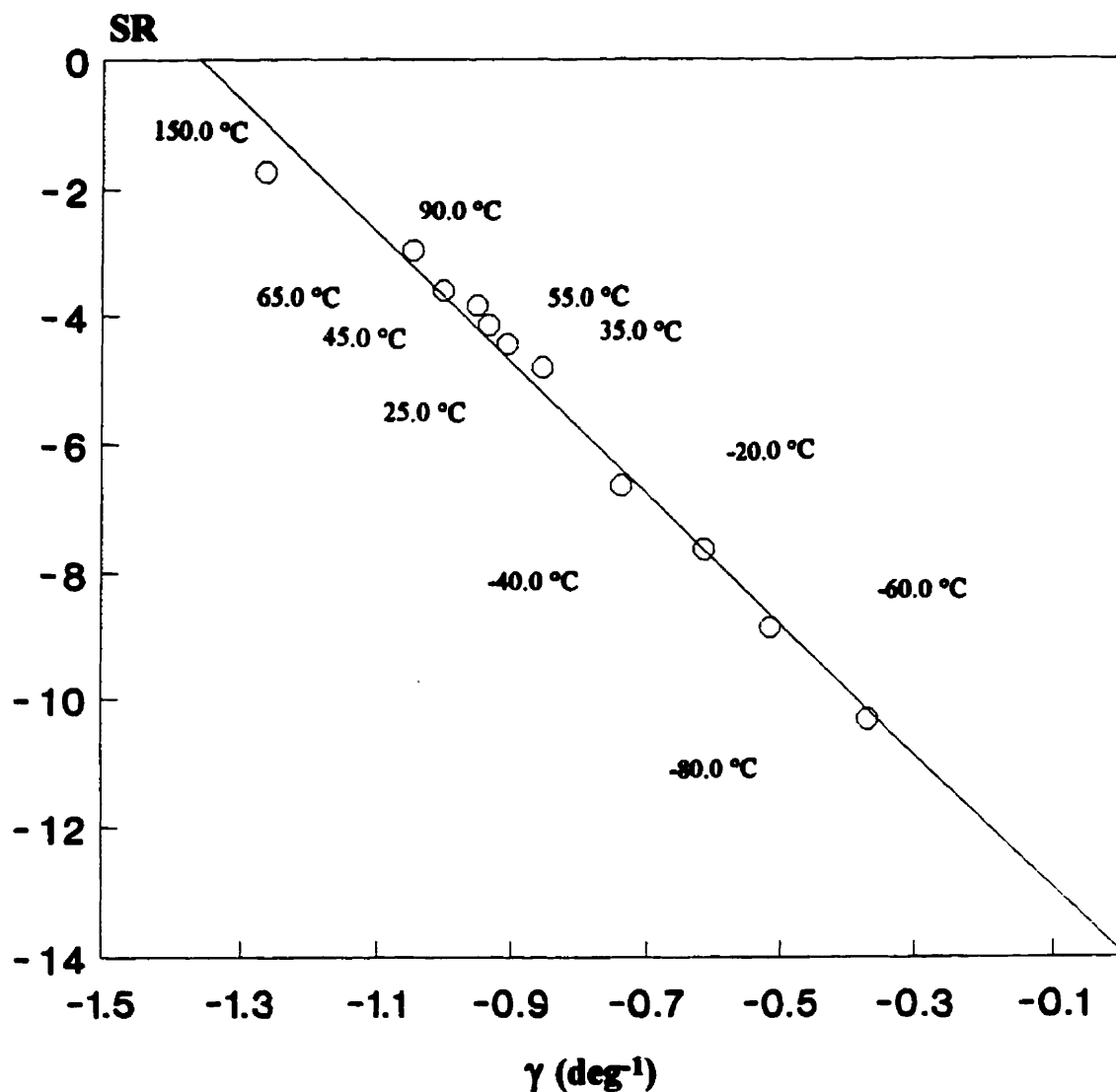


Figure 3.22(b) The correlation of SR with corresponding value of  $\gamma$  for the reaction series of  $\text{Os}_6(\text{CO})_{18}$  with L' in toluene at various temperatures.  $\theta'$  as a steric parameter for the stereoelectronic analysis.

Least squares analysis shows that the linear relationship is governed by the equation  $\text{SR}_T = -13.7 + (-9.7)\gamma_T$  with a correlation coefficient of 0.992.

## CHAPTER 4

### SUMMARY

The kinetic study shows that substitution reactions of these two new clusters,  $\text{Ru}_3(\text{CO})_{11}\text{etpb}$  and  $\text{Ru}_3(\text{CO})_{11}\text{PMe}_3$ , with a variety of P- and As-donor nucleophiles in heptane proceeded through both [L']-dependent and [L']-independent substitution paths,  $k_{\text{obs}} = k_1 + k_2[\text{L}']$ . The rate constants,  $k_1$  and  $k_2$ , were obtained from the dependence of  $k_{\text{obs}}$  on [L'] by a weighted linear least squares analysis in which each value of  $k_{\text{obs}}$  was assumed to have a constant percentage error,  $\sigma(k_{\text{obs}})$ , in a related set of reactions.

The activation parameters,  $\Delta H_1^\ddagger$  and  $\Delta S_1^\ddagger$ , for the [L']-independent path were obtained from an unweighted linear least squares analysis of the dependence of  $\ln(k_{\text{obs}}/T)$  on  $1/T$  according to the Eyring equation,  $\ln(k/T) = 23.76 + \Delta S^\ddagger/R - \Delta H^\ddagger/RT$ . The results for these two new clusters,  $\text{Ru}_3(\text{CO})_{11}\text{etpb}$  and  $\text{Ru}_3(\text{CO})_{11}\text{PMe}_3$ , are excellent in the light of their very small probable errors among the ten clusters  $\text{Ru}_3(\text{CO})_{11}\text{L}$ . When combined with activation parameters for  $\text{Ru}_3(\text{CO})_{12}$  and the other seven  $\text{Ru}_3(\text{CO})_{11}\text{L}$  clusters, the values of  $\Delta H_1^\ddagger$  and  $\Delta S_1^\ddagger$  were found to lie on a fairly good isokinetic plot, the gradient of which leads to an isokinetic temperature of around 116°C. The changes in the activation parameters provide an insight into the nature of  $\text{Ru}_3(\text{CO})_{10}\text{L}$  moieties left after CO dissociation.

For the [L']-independent path, the data for these two new clusters,  $\text{Ru}_3(\text{CO})_{11}\text{PMe}_3$  and  $\text{Ru}_3(\text{CO})_{11}\text{etpb}$ , gave the best fit to the Poë's stereoelectronic equation [1]  $\log k_1 = \alpha_L + \beta_L \delta(^{13}\text{CO}) + \gamma_L \theta$  in

terms of the smallest root mean square deviations (RMSD), 0.07 and 0.02, respectively, among the ten clusters  $\text{Ru}_3(\text{CO})_{11}\text{L}$ . The parameter  $\delta(^{13}\text{CO})$  [2] measures the  $^{13}\text{C}$  chemical shift of  $\text{Ni}(^{13}\text{CO})_3\text{L}$  relative to that in  $\text{Ni}(^{13}\text{CO})_4$ , and is chosen to represent the net electron donor capacity of a substituent L, including  $\pi$ -acidity and  $\sigma$ -basicity of L.  $\theta$  is the Tolman cone angle of each substituent. The parameters  $\delta(^{13}\text{CO})$  and  $\theta$  are characteristic of individual substituents L. The kinetic parameters  $\beta_{\text{L}}$  and  $\gamma_{\text{L}}$  obtained from this analysis for CO dissociation from the ten clusters decrease with increasing temperatures, which is consistent with the fact that the rate constants will become completely independent of the nature of substituents L at the isokinetic temperature.

The  $[\text{L}']$ -dependent paths for these two clusters,  $\text{Ru}_3(\text{CO})_{11}\text{PMe}_3$  and  $\text{Ru}_3(\text{CO})_{11}\text{etpb}$ , correspond to associative substitution without detectable intermediate adducts, even though their possible existence cannot be completely ruled out. It is still possible for such adducts to be formed provided loss of CO from those adducts is faster than their rate of formation. The rate constants  $k_2$  (25.0°C) fit extremely well to the Poë's stereoelectronic equation [3]  $\log k_2 = \alpha + \beta (\text{pKa}' + 4) + \gamma(\theta - \theta_{\text{th}})\lambda$  (RMSD = 0.07 and 0.08;  $R^2 = 0.994$  and 0.98, respectively), where  $\text{pKa}'$  measures the  $\sigma$ -donicity and  $\theta$  the Tolman cone angle of each nucleophile L'. These parameters are characteristic of the individual nucleophiles. The kinetic parameters,  $\alpha$ ,  $\beta$ ,  $\gamma$ , and  $\theta_{\text{th}}$ , were derived from the graphical construction of electronic and steric profiles, which are characteristic of a particular cluster toward nucleophilic attack, then refined by use of a multi-linear regression computer program. The steric threshold,  $\theta_{\text{th}}$ , below which no steric

effects are observed (switching function  $\lambda = 0$ ), is  $123^\circ$  for  $\text{Ru}_3(\text{CO})_{11}\text{PMe}_3$  and  $121^\circ$  for  $\text{Ru}_3(\text{CO})_{11}\text{etpb}$ . When the steric threshold is exceeded, i.e.  $\theta > \theta_{\text{th}}$  ( $\lambda = 1$ ), the steric effect  $\gamma = -0.122 \pm 0.006 \text{ deg}^{-1}$  is found for  $\text{Ru}_3(\text{CO})_{11}\text{PMe}_3$ , and  $\gamma = -0.087 \pm 0.011 \text{ deg}^{-1}$  for  $\text{Ru}_3(\text{CO})_{11}\text{etpb}$ , which implies that further opening of a transition state isomer TSI [3] for  $\text{Ru}_3(\text{CO})_{11}\text{PMe}_3$  is more difficult, and the TSI is more inflexible than that for  $\text{Ru}_3(\text{CO})_{11}\text{etpb}$  although the former creates an open space slightly wider than the latter during approach of a nucleophile. The standard reactivity (defined by the value  $\alpha$ , i.e. the value of  $\log k_2$  for a hypothetical weak and small nucleophile:  $\text{pK}_a' = -4$  and  $\theta < \theta_{\text{th}}$ )  $\text{SR} = -3.08 \pm 0.06$  is obtained for  $\text{Ru}_3(\text{CO})_{11}\text{PMe}_3$  and  $\text{SR} = -4.72 \pm 0.10$  for  $\text{Ru}_3(\text{CO})_{11}\text{etpb}$ , which indicates that the former is much more reactive, i.e. its readiness to create an open space by breaking a M–M bond concurrently with making a  $\text{M}\cdots\text{L}'$  bond during approach of a nucleophile  $\text{L}'$  is a more facile process than that of the latter. The sensitivity of the rates to  $\text{pK}_a'$  of nucleophiles is given by  $\beta = 0.153 \pm 0.021$  for  $\text{Ru}_3(\text{CO})_{11}\text{PMe}_3$ , and  $\beta = 0.176 \pm 0.027$  for  $\text{Ru}_3(\text{CO})_{11}\text{etpb}$ , revealing a slightly lower degree of bond making in the TS of  $\text{Ru}_3(\text{CO})_{11}\text{PMe}_3$ . These parameters provide a quantitative dynamic characterization of the clusters involved.

The substitution reactions of the HNCC  $\text{Os}_6(\text{CO})_{18}$  with P-donor nucleophiles in toluene at various temperatures have been investigated, and they proceed exclusively by an associative mechanism,  $k_{\text{obs}} = a + k_2[\text{L}']$ , where  $a$  is always statistically insignificant or at least small. The site of attachment of a nucleophile in mono-substituted products occurs at a formally electron-deficient metal centre, one of the capping Os atoms with the longest Os–Os distance (2.836 Å) and, therefore,

probably the weakest bond. An intermediate adduct,  $\text{Os}_6(\text{CO})_{18}\text{L}'$ , may be formed during approach of a nucleophile  $\text{L}'$ , and its structure was proposed.

The data obtained for the reaction series of  $\text{Os}_6(\text{CO})_{18}$  with 4  $\text{L}'$  (out of 5) lead to **five types of excellent isokinetic relationships (three are unique)**, which all indicate an IKT about  $88^\circ\text{C}$ :

- I)  $\Delta H_2^\ddagger$  vs  $\Delta S_2^\ddagger$  (conventional)
- II)  $\ln(k_2/T)$  vs  $1/T$  (conventional)
- III)  $\log k_2$  vs  $\text{pKa}'$  for nucleophiles with different  $\sigma$ -basicity and size at the IKT (novel)
- IV)  $\log k_2$  vs  $\text{pKa}'$  for almost isosteric nucleophiles, which show the same steric effects, at various temperatures (unique)
- V)  $\log k_2$  vs  $\text{pKa}'$  for small nucleophiles with  $\theta < \theta_{\text{th}}$ , which exhibit no steric effects, at various temperatures (unique)

The statistical analysis of data on validity of IKR, i.e. the statistical analysis on a common point of intersection of the Eyring plots, also gave exactly the same result, the IKT around  $88^\circ\text{C}$  with a high degree of probability, showing very precise IKR. All the results on IKT, no matter what analysis method was used, are in excellent agreement with one another.

The **novel IKR (III)** clearly illustrated that the rate constants  $\log k_2$  for the reaction series of  $\text{Os}_6(\text{CO})_{18}$  with various nucleophiles except  $\text{PMe}_3$ , no matter what size and  $\sigma$ -basicity they have, eventually become the same when the IKT around  $88^\circ\text{C}$  is reached.

**Unique IKRs (IV) and (V)**, a common point of intersection in the LFER plots at various temperatures, were established for the first time. They also show an excellent temperature dependence of

electronic profiles, and they are therefore **breakthroughs** in providing the first two examples of the theoretical interconnection between an IKR and LFER. Based on these unique IKRs {Figure 3.21(a) and 3.21(b)} in this work, a **definition on IKR** can be given as follows.

$$\frac{\partial \ln k/T(T, \xi)}{\partial(T)} \Big|_{\xi_{\text{iso}}} = \frac{\partial \ln k/T(T, \text{pKa}')}{\partial(T)} \Big|_{\text{pKa}'_{\text{iso}} = 0}$$

The parameter  $\xi$  is not a simple numbering, and it does have **physical meaning**. In this work,  $\xi$  identifies the individual members of the series — the nucleophiles with different  $\sigma$ -basicity and size. When the size of L' is kept constant or  $\theta < \theta_{\text{th}}$ ,  $\xi = \text{pKa}'$ .

When an IKR is found (Figure 3.17), a LFER isoparameter  $\xi_{\text{iso}}$  — isokinetic pKa' in this work {Figure 3.21(a) and 3.21(b)} — appears, and vice versa.

The **unique LFER isoparameters**  $\xi_{\text{iso}}$ , **isokinetic pKa'** and **isokinetic  $\theta'$** , for a series of reactions at various temperatures were **established from both experimental results and theory for the first time**. They are natural outcomes of linear relationships between SR &  $\beta$  and SR &  $\gamma$ , respectively, at various temperatures for the series of reactions. A nucleophile with a pKa' of 14.3 or -7.0, respectively — isokinetic pKa' — will react with the cluster  $\text{Os}_6(\text{CO})_{18}$  with the same value of  $\log k_2$  at various temperatures. A nucleophile with a  $\theta'$  of  $148^\circ$  — isokinetic  $\theta'$  — will react with the cluster  $\text{Os}_6(\text{CO})_{18}$  at the same value of  $\log k_2^\circ$   $\{= \log k_2 - \beta(\text{pKa}' + 4)\}$  at various temperatures.

The kinetic parameters SR,  $\beta$ ,  $\gamma$  and  $\theta_{th}$  for the reactions of  $Os_6(CO)_{18}$  with L' were derived from the electronic and steric profiles, then refined by use of double-linear regression and three-coefficient computer program and  $\theta$  as the steric parameter. The standard reactivity SR shows the lowest value of  $-5.35 \pm 0.30$  (25.0°C) among the HNCCs and LNCCs to date, which implies that opening up of the cluster is a quite slow process during approach of a nucleophile L'. The sensitivity of rates to pKa' of nucleophiles is exceedingly high ( $\beta = 0.514 \pm 0.071$  at 25.0°C) and indicates a remarkably high degree of bond making in the TS. The steric threshold  $\theta_{th}$  ( $= 127^\circ$  at 25.0°) is quite high, showing that the TSI is quite "open" and can accommodate all nucleophiles with various size up to the cone angle of  $127^\circ$  (defined by  $\theta_{th}$ ) without any steric repulsion. When the steric threshold is exceeded, the flexibility of the TS is found to be extremely low as indicated by the value  $\gamma = -0.763 \pm 0.105 \text{ deg}^{-1}$ , which has not been surpassed by any metal carbonyls so far, and implies that the TSI strongly resists further opening and the rate of the reaction will decrease by 83 % for each degree increase in the cone angle of the incoming nucleophile when electronic effects are absent or constant. The criteria for judging the success of the data analyses are explored, and the use of an alternative steric parameter  $\theta'$  ( $= 103.8 + 0.553E_R$ ) [6] is shown to have a negligible effect on the values of SR,  $\beta$ , and  $\theta_{th}$ .  $E_R$  is Brown's ligand repulsion parameter [7], and its values have been rescaled and normalized to  $\theta' = \theta = 145^\circ$  for  $PPh_3$  so that steric effects can be expressed in the same units, whichever steric parameter is used [6].

Two sets of precise values of  $\Delta H_2^\ddagger$  and  $\Delta S_2^\ddagger$  with very nice linearity for reactions of  $\text{Os}_6(\text{CO})_{18}$  with L' were derived from Eyring lines that are either constrained by inclusion of an IKT or not so constrained, and they are in excellent agreement with each other, exhibiting the highly precise IKR again. The small positive values of  $\Delta H_2^\ddagger$  (9 to 17 kcal·mol<sup>-1</sup>), and the large negative values of  $\Delta S_2^\ddagger$  (-21 to -42 cal·K<sup>-1</sup>·mol<sup>-1</sup>) are in line with a straightforward associative reaction mechanism.

## REFERENCES

- [1] L. Chen and A. J. Poë, *Inorg. Chem.*, 28(1989)3641.
- [2] G. Bodner, M. May, and L. McKinney, *Inorg. Chem.*, 19(1980)1951.
- [3] A.J. Poë, D.H. Farrar, and Y. Zheng, *J. Am. Chem. Soc.*, 114(1992)5146.
- [4] C. Couture and D.H. Farrar, *Acta Cryst.*, C42(1986)163.
- [5] W. Linert, *Chem. Soc. Rev.*, (1994)429.
- [6] R.H.E. Hudson and A.J. Poë, *Organometallics*, 14(1995)3238.
- [7] T.L. Brown, *Inorg. Chem.*, 31(1992)1286; T.L. Brown and K.J. Lee, *Coord. Chem. Rev.*, 128(1993)89.

**CHAPTER 5**  
**APPENDICES**

**Table 5.1 Electronic and Steric Parameters for Some P-donor Ligands<sup>a</sup> [1]**

Ligand number	L	$\theta^b$ (deg)	$\chi^c$ ( $\text{cm}^{-1}$ )	pKa <sup>d</sup>	pKa <sup>e</sup>	ER <sup>h</sup>
1	etpb	101	31.20	(1.74)	-0.30	25
2	PF <sub>3</sub>	104	54.7 <sup>f</sup>	(7.84)	5.9	—
3	<b>PPhH<sub>2</sub></b>	106	20.85	(-2.0)	-1.83	—
4	P(OMe) <sub>3</sub>	107	24.10	(2.60)	0.83	52
5	P(OEt) <sub>3</sub>	109	21.60	3.31	1.64	59
6	P(O- <i>n</i> -Bu) <sub>3</sub>	109	20.85	(3.31)	1.64	64
7	P(CH <sub>2</sub> CH <sub>2</sub> CN) <sub>2</sub> H	117	—	0.41	-0.89	—
8	<b>PMe<sub>3</sub></b>	118	8.55	8.65	6.45	39
9	PPh(OMe) <sub>2</sub>	120	19.45	(2.64)	1.48	69
10	PPh(OEt) <sub>2</sub>	121	18.10	(3.1)	1.99	—
11	<b>PPhMe<sub>2</sub></b>	122	10.60	6.50	5.07	44
12	<b>PCl<sub>3</sub></b>	124	48.00	—	-20.1	—
13	<b>PPh<sub>2</sub>H</b>	126	17.35	0.03	0.53	38
14	P(OPh) <sub>3</sub>	128	30.20	-2.0	-2.79	65
15	P(O- <i>i</i> -Pr) <sub>3</sub>	130	19.05	4.08	3.38	74
16	<b>PPhCl<sub>2</sub></b>	131	36.40	—	-12.3	—
17	P(CH <sub>2</sub> CH <sub>2</sub> CN) <sub>3</sub>	132	22.35	1.36	0.76	—

Table 5.1 (continued)

Ligand number	L	$\theta^b$ (deg)	$\chi^c$ ( $\text{cm}^{-1}$ )	pKa <sup>d</sup>	pKa <sup>e</sup>	ER <sup>h</sup>
18	<b>P</b> Et <sub>3</sub>	132	6.30	8.69	7.96	61
19	<b>P</b> ( <i>n</i> -Pr) <sub>3</sub>	132	5.40	8.64	8.57	—
20	<b>P</b> ( <i>n</i> -Bu) <sub>3</sub>	132	5.25	8.43	8.67	64
21	PPh <sub>2</sub> (OMe)	133	16.30	(2.69)	2.09	62
22	PPh <sub>2</sub> (OEt)	133	15.60	(2.91)	2.35	62
23	PPh(OPh) <sub>2</sub>	134	24.10	(-0.42)	-0.91	—
24	P(OCy) <sub>3</sub>	135	18.00	(3.93)	3.46	—
25	<b>P</b> PhEt <sub>2</sub>	136	9.30	6.25	5.94	57
26	<b>P</b> Ph <sub>2</sub> Me	136	12.10	(4.57)	4.06	57
27	<b>P</b> Ph <sub>2</sub> Cl	137	24.65	(-4.1)	-4.39	—
28	PPh <sub>2</sub> (OPh)	139	18.95	(1.15)	0.87	—
29	<b>P</b> Ph <sub>2</sub> Et	140	11.30	(4.9)	4.6	66
30	<b>P</b> Ph <sub>2</sub> ( <i>n</i> -Bu) <sub>3</sub>	140	11.10	(4.6)	4.73	66
31	P(O- <i>o</i> -tol) <sub>3</sub>	141	29.05	-1.83	-2.02	—
32	<b>P</b> ( <i>i</i> -Bu) <sub>3</sub>	143	5.70	7.97	8.36	83
33	<b>P</b> Cy <sub>2</sub> H	143	9.10	4.55	6.08	66
34	<b>P</b> Ph <sub>3</sub>	145	13.25	2.73	3.28	75
35	<b>P</b> ( <i>p</i> -F <sub>3</sub> CC <sub>6</sub> H <sub>4</sub> ) <sub>3</sub>	145	20.2	(-1.39)	-1.39	—
36	<b>P</b> ( <i>p</i> -ClC <sub>6</sub> H <sub>4</sub> ) <sub>3</sub>	145	16.80	1.03	0.87	74
37	<b>P</b> ( <i>p</i> -FC <sub>6</sub> H <sub>4</sub> ) <sub>3</sub>	145	15.70	1.97	1.63	74
38	<b>P</b> ( <i>p</i> -tol) <sub>3</sub>	145	11.50	3.84	4.46	74

Table 5.1 (continued)

Ligand number	L	$\theta^b$ (deg)	$\chi^c$ ( $\text{cm}^{-1}$ )	pKa <sup>d</sup>	pKa <sup>e</sup>	ER <sup>h</sup>
39	<b>P(<i>p</i>-MeOC<sub>6</sub>H<sub>4</sub>)<sub>3</sub></b>	145	10.50	4.57	5.13	76
40	<b>P(<i>p</i>-Me<sub>2</sub>NC<sub>6</sub>H<sub>4</sub>)<sub>3</sub></b>	145	5.25	8.65	8.67	—
41	<b>PPh<sub>2</sub>(<i>i</i>-Pr)</b>	151	10.85	(5.15)	4.90	75
42	<b>P(O-<i>o</i>-PhC<sub>6</sub>H<sub>4</sub>)<sub>3</sub></b>	152	29.15	(-2.0)	-1.68	—
43	<b>PPh<sub>2</sub>(CH<sub>2</sub>Ph)</b>	152	12.30	—	3.92	—
44	<b>PPh<sub>2</sub>Cy<sup>g</sup></b>	153	—	(5.05)	5.6	77
45	<b>P(NMe<sub>2</sub>)<sub>3</sub></b>	157	5.95	—	8.20	—
46	<b>PPh<sub>2</sub>(<i>t</i>-Bu)</b>	157	8.95	—	6.18	97
47	<b>P(<i>i</i>-Pr)<sub>3</sub></b>	160	3.45	(9.7)	9.88	109
48	<b>PPhCy<sub>2</sub><sup>g</sup></b>	162	—	(7.38)	8.3	105
49	<b>P(CH<sub>2</sub>Ph)<sub>3</sub></b>	165	10.35	(4.3)	5.23	—
50	<b>P(<i>m</i>-tol)<sub>3</sub></b>	165	11.1	3.3	4.7	79
51	<b>P(<i>m</i>-ClC<sub>6</sub>H<sub>4</sub>)<sub>3</sub></b>	165	18.40	(1.03)	-0.18	78
52	<b>PCy<sub>3</sub></b>	170	1.40	9.7	11.26	116
53	<b>PPh(<i>t</i>-Bu)<sub>2</sub></b>	170	4.95	—	8.87	124
54	<b>PPh<sub>2</sub>(<i>o</i>-MeOC<sub>6</sub>H<sub>4</sub>)</b>	171	10.30	—	5.27	—
55	<b>P(O-<i>t</i>-Bu)<sub>3</sub></b>	172	12.95	(4.5)	5.75	99
56	<b>P(<i>t</i>-Bu)<sub>3</sub></b>	182	0	11.40	12.20	154
57	<b>P(<i>o</i>-tol)<sub>3</sub></b>	194	10.5	3.08	5.03	113

- a. Ligands characterized by Giering and co-workers [2, 3] as being  $\sigma$  donors only given in bold type; other ligands are  $\pi$ -acids as well as  $\sigma$  donors. No pKa value is available for  $\text{P}(\text{NMe})_3$  and it has been assumed to be only a  $\sigma$  donor.
- b. Tolman cone angles [4].
- c.  $\chi$  values given to two decimal places are from Bartik et al. [5] except those for  $\text{P}(p\text{-F}_3\text{CC}_6\text{H}_4)_3$  and  $\text{P}(p\text{-tol})_3$  which are from Giering and co-workers [3]. Those given to only one decimal place are from Tolman [4].
- d. pKa values in parentheses are estimated by various methods which have been reviewed [6]. Otherwise they are based directly on experimental data for the particular ligands with appropriate extrapolations so that they are valid for equilibria in aqueous solutions [7].
- e. pKa' values for  $\sigma$  donors are calculated from Eq.(5.1) where values of  $\chi$  are available. Otherwise, they and those for  $\pi$ -acid and  $\sigma$ -donor ligands are estimated from Eq.(5.2).
- f. This value was estimated by comparison [6] of the relative  $\sigma$ -donor parameters for  $\text{PEt}_3$ ,  $\text{PF}_3$  and  $\text{PPh}_3$  [8] with the pKa values for  $\text{PEt}_3$  and  $\text{PPh}_3$ .
- g. The pKa values for these ligands were estimated by interpolation between the values for  $\text{PPh}_3$  and  $\text{PCy}_3$ . The pKa' values were obtained from the mean of those found (a) from Eq.(5.2) and the use of the pKa(expt) values, and (b) those found from the interpolated  $\chi$  values and the use of Eq.(5.1).

$$\text{pKa}' = 18.93 - 0.0464 \times 145 - 0.673 \chi \quad (5.1)$$

$$\text{pKa}' = \text{pKa}(\text{expt}) + 0.0464 (\theta - 145) \quad (5.2)$$

- h. Ligand repulsion energies  $E_r$  ( $\text{kcal}\cdot\text{mol}^{-1}$ ) from molecular mechanics calculations on the molecules  $\text{Cr}(\text{CO})_5\text{L}$ , proposed by T.L. Brown [9, 10].

**Table 5.2**  $^{31}\text{P}$  NMR Data for Some P-donor Ligands [11]

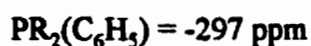
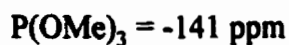
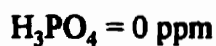
Formula	Chemical shift (ppm) from $\text{H}_3\text{PO}_4^*$				
$\text{P}[(\text{CH}_2)_2\text{CN}]_3$	23	23.4			
$\text{P}(\text{CH}=\text{CH}_2)(\text{C}_6\text{H}_5)_2$	13.8				
$\text{P}(\text{C}_3\text{H}_7)_3$	33				
$\text{P}(\text{C}_4\text{H}_9)_3$	32.3	33	32.6	33.4	32.6
$\text{P}(i\text{-C}_4\text{H}_9)_3$	40				
$\text{P}(\text{C}_5\text{H}_{11})_3$	34				
$\text{P}(\text{C}_6\text{H}_{11})_3$	-7				
$\text{P}(\text{C}_6\text{H}_{17})_3$	31.8				
$\text{P}(\text{C}_8\text{H}_{17})(\text{CH}_2\text{CH}_2\text{CN})_2$	25.3				
$\text{P}(\text{C}_8\text{H}_{17})[\text{C}(\text{O})\text{NH}(\text{C}_6\text{H}_5)]_2$	77				
$\text{P}(\text{C}_6\text{H}_5)_3$	5.9	8	5.88	7	6.6
	5.9	$5.6 \pm 0.2$		5.7	$8.0 \pm 0.5$
$\text{P}(o\text{-C}_6\text{H}_4\text{Cl})_3$	9.2				
$\text{P}(p\text{-C}_6\text{H}_4\text{Cl})_3$	9.2				
$\text{P}(\text{CN})_3$	135.7				
$\text{P}(\text{CF}_3)_2(\text{SCF}_3)$	$-12.8 \pm 0.1$				
$\text{P}(\text{CF}_3)_2(\text{SCH}_3)$	-37.1				
$\text{P}(\text{CF}_3)_3$	$2.6 \pm 0.0$				
$\text{P}(\text{CF}_3)_2\text{CN}$	$40.7 \pm 0.2$				
$\text{P}(\text{CH}_3)_3$	62	61	62		
$\text{P}(\text{CH}_3)_2(\text{C}_2\text{H}_5)$	51	48.5			

Table 5.2 (continued)

Formula	Chemical shift (ppm) from $\text{H}_3\text{PO}_4$ *			
$\text{P}(\text{CH}_3)_2(\text{C}_6\text{H}_5)$	46	47.0		
$\text{P}(\text{CH}_3)(\text{C}_2\text{H}_5)_2$	34	34.0		
$\text{P}(\text{CH}_3)(\text{C}_2\text{H}_5)(\text{C}_6\text{H}_5)$	33.0			
$\text{P}(\text{CH}_3)(\text{C}_6\text{H}_5)_2$	28.0			
$\text{P}(\text{CH}_3)(\text{CN})_2$	81.4			
$\text{P}(\text{CH}_2\text{OH})_3$	31			
$\text{P}(\text{CH}_2\text{CH}_3)_3$	20.4	19	19.1	
$\text{P}(\text{C}_2\text{H}_5)_2(\text{C}_6\text{H}_5)$	16	15.1	16.2	$17.8 \pm 0.5$
	17.0			
$\text{P}(\text{C}_2\text{H}_5)(\text{C}_6\text{H}_5)_2$	12	13.5	12.0	

\* The difference of chemical shift (ppm) between  $\text{H}_3\text{PO}_4$  and  $\text{P}(\text{OMe})_3$  as the references is 141 ppm.

The chemical shift from  $\text{H}_3\text{PO}_4$ :



The chemical shift from  $\text{P}(\text{OMe})_3$ :

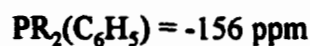
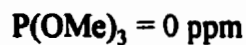
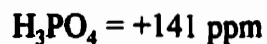


**Table 5.3 Pseudo-First-Order Rate Constants for Reactions of  $\text{Ru}_3(\text{CO})_{11}\text{PMe}_3$  with Nucleophiles  $\text{L}'$  in Heptane  $[\text{Complex}]_0 = 3 \times 10^{-4} \text{ M}$**

T(°C)	[L'](M)	$k_{\text{obs}}(\text{s}^{-1})$	$\sigma(\%)$	Monitored Peak	Run No
<b>L' = AsPh<sub>3</sub></b>					
18.3	0.01580	$(1.50 \pm 0.02) \times 10^{-5}$	1.1	350 nm	1(a)
	0.03160	$(1.51 \pm 0.02) \times 10^{-5}$	1.5	350 nm	1(b)
	0.04740	$(1.40 \pm 0.01) \times 10^{-5}$	0.8	350 nm	1(c)
	0.06320	$(1.59 \pm 0.02) \times 10^{-5}$	1.6	350 nm	1(d)
	0.07900	$(1.55 \pm 0.02) \times 10^{-5}$	1.3	350 nm	1(e)
	0.01580	$(1.54 \pm 0.01) \times 10^{-5}$	0.8	350 nm	2(a)
	0.03160	$(1.57 \pm 0.02) \times 10^{-5}$	1.1	350 nm	2(b)
	0.06320	$(1.64 \pm 0.02) \times 10^{-5}$	1.4	350 nm	2(c)
18.5	0.01580	$(1.50 \pm 0.03) \times 10^{-5}$	1.7	365 nm	3(a)
	0.03160	$(1.72 \pm 0.03) \times 10^{-5}$	1.5	365 nm	3(b)
	0.04740	$(1.75 \pm 0.06) \times 10^{-5}$	3.4	365 nm	3(c)
	0.07900	$(1.72 \pm 0.03) \times 10^{-5}$	2.0	365 nm	3(d)
	0.04740	$(1.92 \pm 0.03) \times 10^{-5}$	1.6	365 nm	4(a)
	0.06320	$(1.80 \pm 0.03) \times 10^{-5}$	1.4	365 nm	4(b)
	0.07900	$(1.69 \pm 0.03) \times 10^{-5}$	2.0	365 nm	4(d)

Table 5.3 (continued)

T(°C)	[L](M)	$k_{\text{obs}}(\text{s}^{-1})$	$\sigma(\%)$	Monitored Peak	Run No
<b>L' = AsPh<sub>3</sub></b>					
32.0	0.01550	$(1.74 \pm 0.04) \times 10^{-4}$	2.2	350 nm	5(a)
	0.03100	$(1.48 \pm 0.02) \times 10^{-4}$	1.5	350 nm	5(b)
	0.04649	$(1.60 \pm 0.01) \times 10^{-4}$	0.5	350 nm	5(c)
	0.01550	$(1.78 \pm 0.04) \times 10^{-4}$	2.1	350 nm	6(a)
	0.06199	$(1.64 \pm 0.02) \times 10^{-4}$	1.2	350 nm	6(b)
	0.07749	$(1.44 \pm 0.01) \times 10^{-4}$	0.9	350 nm	6(c)
32.0	0.01550	$(1.54 \pm 0.03) \times 10^{-4}$	1.9	365 nm	7(a)
	0.03100	$(1.37 \pm 0.02) \times 10^{-4}$	1.3	365 nm	7(b)
	0.04649	$(1.43 \pm 0.01) \times 10^{-4}$	0.7	365 nm	7(c)
	0.01550	$(1.58 \pm 0.03) \times 10^{-4}$	1.8	365 nm	8(a)
	0.06199	$(1.81 \pm 0.02) \times 10^{-4}$	1.2	365 nm	8(b)
	0.07749	$(1.41 \pm 0.01) \times 10^{-4}$	0.7	365 nm	8(c)
	0.01550	$(1.73 \pm 0.02) \times 10^{-4}$	1.2	365 nm	9(a)
	0.06199	$(1.84 \pm 0.02) \times 10^{-4}$	1.3	365 nm	9(b)
41.1	0.01550	$(7.85 \pm 0.08) \times 10^{-4}$	1.0	350 nm	10(a)
	0.06199	$(7.97 \pm 0.12) \times 10^{-4}$	1.4	350 nm	10(b)
	0.07749	$(7.08 \pm 0.08) \times 10^{-4}$	1.2	350 nm	10(c)
	0.06199	$(8.08 \pm 0.12) \times 10^{-4}$	1.4	350 nm	11(a)

Table 5.3 (continued)

T(°C)	[L'](M)	$k_{\text{obs}}(\text{s}^{-1})$	$\sigma(\%)$	Monitored Peak	Run No
<b>L' = AsPh<sub>3</sub></b>					
41.1	0.07749	$(7.15 \pm 0.08) \times 10^{-4}$	1.1	350 nm	11(b)
	0.01550	$(7.30 \pm 0.06) \times 10^{-4}$	0.8	350 nm	12(a)
	0.03100	$(7.51 \pm 0.13) \times 10^{-4}$	1.7	350 nm	12(b)
	0.04649	$(7.61 \pm 0.07) \times 10^{-4}$	0.9	350 nm	12(c)
	0.06199	$(7.50 \pm 0.09) \times 10^{-4}$	1.1	350 nm	12(d)
	0.07749	$(7.25 \pm 0.10) \times 10^{-4}$	1.4	350 nm	12(e)
	0.03100	$(7.82 \pm 0.11) \times 10^{-4}$	1.4	350 nm	13(a)
	0.04649	$(7.41 \pm 0.09) \times 10^{-4}$	1.2	350 nm	13(b)
	0.06199	$(7.50 \pm 0.09) \times 10^{-4}$	1.2	350 nm	13(c)
	0.07749	$(7.24 \pm 0.10) \times 10^{-4}$	1.4	350 nm	13(d)
41.1	0.01550	$(7.58 \pm 0.27) \times 10^{-4}$	3.5	365 nm	14(a)
	0.03089	$(7.44 \pm 0.17) \times 10^{-4}$	2.3	365 nm	14(b)
	0.04649	$(7.69 \pm 0.08) \times 10^{-4}$	1.0	365 nm	14(c)
	0.06199	$(7.36 \pm 0.08) \times 10^{-4}$	1.0	365 nm	14(d)
	0.01550	$(8.09 \pm 0.20) \times 10^{-4}$	2.4	365 nm	15(a)
	0.03100	$(8.25 \pm 0.08) \times 10^{-4}$	0.9	365 nm	15(b)
	0.04649	$(7.52 \pm 0.08) \times 10^{-4}$	1.1	365 nm	15(c)
	0.06199	$(7.30 \pm 0.08) \times 10^{-4}$	1.1	365 nm	15(d)

Table 5.3 (continued)

T(°C)	[L'](M)	$k_{\text{obs}}(\text{s}^{-1})$	$\sigma(\%)$	Monitored Peak	Run No
<b>L' = AsPh<sub>3</sub></b>					
41.1	0.03100	$(6.86 \pm 0.25) \times 10^{-4}$	3.6	365 nm	16(a)
	0.07749	$(6.99 \pm 0.09) \times 10^{-4}$	1.3	365 nm	16(b)
	0.01550	$(9.10 \pm 0.11) \times 10^{-4}$	1.2	365 nm	17(a)
	0.03100	$(8.34 \pm 0.08) \times 10^{-4}$	0.9	365 nm	17(b)
	0.07749	$(7.00 \pm 0.09) \times 10^{-4}$	1.3	365 nm	17(c)
50.4	0.01550	$(2.80 \pm 0.06) \times 10^{-3}$	2.2	365 nm	18(a)
	0.03100	$(2.66 \pm 0.08) \times 10^{-3}$	3.0	365 nm	18(b)
	0.06199	$(2.59 \pm 0.08) \times 10^{-3}$	3.1	365 nm	18(c)
	0.07749	$(2.50 \pm 0.08) \times 10^{-3}$	3.2	365 nm	18(d)
	0.03100	$(2.39 \pm 0.06) \times 10^{-3}$	2.4	365 nm	19(a)
	0.04649	$(2.31 \pm 0.06) \times 10^{-3}$	2.6	365 nm	19(b)
	0.06199	$(2.52 \pm 0.10) \times 10^{-3}$	3.9	365 nm	19(c)
	0.07749	$(2.43 \pm 0.10) \times 10^{-3}$	4.0	365 nm	19(d)
	0.04649	$(2.62 \pm 0.09) \times 10^{-3}$	3.4	365 nm	20(a)
	0.06199	$(2.50 \pm 0.07) \times 10^{-3}$	2.9	365 nm	20(b)
	0.07749	$(2.40 \pm 0.07) \times 10^{-3}$	3.1	365 nm	20(c)

Table 5.3 (continued)

T(°C)	[L'](M)	$k_{\text{obs}}(\text{s}^{-1})$	$\sigma(\%)$	Monitored Peak	Run No
<b>L' = etpb</b>					
40.0	0.02490	$(9.23 \pm 0.20) \times 10^{-4}$	2.2	2042.7 $\text{cm}^{-1}$	21(a)
	0.03113	$(1.01 \pm 0.01) \times 10^{-3}$	1.2	2042.7 $\text{cm}^{-1}$	22(a)
	0.03736	$(1.05 \pm 0.03) \times 10^{-3}$	2.8	2042.7 $\text{cm}^{-1}$	23(a)
	0.04981	$(1.19 \pm 0.03) \times 10^{-3}$	2.7	2042.7 $\text{cm}^{-1}$	24(a)
40.0	0.02490	$(2.63 \pm 0.10) \times 10^{-4}$	4.0	2027.3 $\text{cm}^{-1}$	21(b)
	0.03113	$(2.62 \pm 0.16) \times 10^{-4}$	6.2	2027.3 $\text{cm}^{-1}$	22(b)
	0.03736	$(2.68 \pm 0.14) \times 10^{-4}$	5.4	2027.3 $\text{cm}^{-1}$	23(b)
	0.04981	$2.78 \times 10^{-4}$		2027.3 $\text{cm}^{-1}$	24(b)
40.8	0.01845	$(1.20 \pm 0.05) \times 10^{-4}$	4.4	440 nm	25(a)
	0.03689	$(1.18 \pm 0.08) \times 10^{-4}$	7.0	440 nm	25(b)
	0.05534	$(1.34 \pm 0.05) \times 10^{-4}$	3.8	440 nm	25(c)
	0.07379	$(1.43 \pm 0.07) \times 10^{-4}$	4.8	440 nm	25(d)
	0.09924	$(1.33 \pm 0.06) \times 10^{-4}$	4.7	440 nm	25(e)
40.1	0.01845	$(7.94 \pm 0.30) \times 10^{-5}$	3.8	450 nm	26(a)
	0.03689	$(8.75 \pm 0.24) \times 10^{-5}$	2.7	450 nm	26(b)
	0.05534	$(9.21 \pm 0.25) \times 10^{-5}$	2.7	450 nm	26(c)

Table 5.3 (continued)

T(°C)	[L'](M)	<sup>a</sup> k <sub>obs</sub> (s <sup>-1</sup> )	σ(%)	Monitored Peak	Run No
<b>L' = etpb</b>					
40.1	0.07379	$(9.43 \pm 0.17) \times 10^{-5}$	2.0	450 nm	26(d)
	0.09924	$(9.87 \pm 0.44) \times 10^{-5}$	4.4	450 nm	26(e)
25.0	0.04981	$2.30 \times 10^{-4}$		2043.0 cm <sup>-1</sup>	27(a)
	0.06226	$2.77 \times 10^{-4}$		2043.0 cm <sup>-1</sup>	28(a)
	0.06848	$3.11 \times 10^{-4}$		2043.0 cm <sup>-1</sup>	29(a)
	0.07471	$3.36 \times 10^{-4}$		2043.0 cm <sup>-1</sup>	30(a)
25.0	0.04981	$1.00 \times 10^{-4}$		2027.0 cm <sup>-1</sup>	27(b)
	0.06226	$1.92 \times 10^{-4}$		2027.0 cm <sup>-1</sup>	28(b)
	0.06848	$1.85 \times 10^{-4}$		2027.0 cm <sup>-1</sup>	29(b)
	0.07471	$2.44 \times 10^{-4}$		2027.0 cm <sup>-1</sup>	30(b)
25.0	0.01325	$1.13 \times 10^{-4}$		2042.5 cm <sup>-1</sup>	31(a)
	0.02650	$1.96 \times 10^{-4}$		2042.5 cm <sup>-1</sup>	32(a)
	0.1855	$8.28 \times 10^{-4}$		2042.5 cm <sup>-1</sup>	33(a)
25.0	0.01325	$0.42 \times 10^{-4}$		2027.1 cm <sup>-1</sup>	31(b)
	0.02650	$1.01 \times 10^{-4}$		2027.1 cm <sup>-1</sup>	32(b)
	0.1855	$7.21 \times 10^{-4}$		2027.1 cm <sup>-1</sup>	33(b)

Table 5.3 (continued)

T(°C)	[L'](M)	$k_{\text{obs}}(\text{s}^{-1})$	$\sigma(\%)$	Monitored Peak	Run No
<b>L' = P(OEt)<sub>3</sub></b>					
25.15	0.3656	$(1.86 \pm 0.00) \times 10^{-3}$	0.2	420 nm	34(a)
	0.7311	$(4.00 \pm 0.01) \times 10^{-3}$	0.3	420 nm	34(b)
	0.9139	$(5.13 \pm 0.02) \times 10^{-3}$	0.4	420 nm	34(c)
	1.0966	$(6.31 \pm 0.02) \times 10^{-3}$	0.4	420 nm	35(a)
	0.9139	$(5.14 \pm 0.02) \times 10^{-3}$	0.3	420 nm	35(b)
25.15	0.3656	$(1.88 \pm 0.01) \times 10^{-3}$	0.3	438 nm	36(a)
	0.7311	$(3.97 \pm 0.01) \times 10^{-3}$	0.2	438 nm	36(b)
	0.9139	$(5.25 \pm 0.02) \times 10^{-3}$	0.4	438 nm	36(c)
	0.3656	$(1.89 \pm 0.00) \times 10^{-3}$	0.3	438 nm	37(a)
	1.0966	$(6.46 \pm 0.02) \times 10^{-3}$	0.3	438 nm	37(b)
25.2	0.02340	$(2.00 \pm 0.03) \times 10^{-4}$	1.3	2042.9 cm <sup>-1</sup>	38(a)
	0.09358	$(5.58 \pm 0.16) \times 10^{-4}$	2.9	2042.9 cm <sup>-1</sup>	39(a)
	0.1872	$9.49 \times 10^{-4}$		2042.9 cm <sup>-1</sup>	40(a)
	0.2807	$(15.3 \pm 0.3) \times 10^{-4}$	2.1	2042.9 cm <sup>-1</sup>	41(a)

Table 5.3 (continued)

T(°C)	[L'](M)	$k_{\text{obs}}(\text{s}^{-1})$	$\sigma(\%)$	Monitored Peak	Run No
<b>L' = P(OEt)<sub>3</sub></b>					
25.2	0.02340	$(1.83 \pm 0.07) \times 10^{-4}$	3.7	2014.0 cm <sup>-1</sup>	38(b)
	0.09358	$(5.55 \pm 0.24) \times 10^{-4}$	4.3	2014.0 cm <sup>-1</sup>	39(b)
	0.1872	$(9.34 \pm 0.30) \times 10^{-4}$	3.2	2014.0 cm <sup>-1</sup>	40(b)
	0.2807	$(14.9 \pm 0.4) \times 10^{-4}$	2.8	2014.0 cm <sup>-1</sup>	41(b)
<b>L' = P(OPh)<sub>3</sub></b>					
25.2	0.04724	$(4.16 \pm 0.01) \times 10^{-5}$	0.2	458 nm	42(a)
	0.09447	$(4.79 \pm 0.02) \times 10^{-5}$	0.5	458 nm	42(b)
	0.1889	$(7.83 \pm 0.08) \times 10^{-5}$	1.0	458 nm	42(c)
	0.2362	$(9.29 \pm 0.15) \times 10^{-5}$	1.6	458 nm	42(d)
	0.2834	$(10.5 \pm 0.2) \times 10^{-5}$	2.2	458 nm	42(e)
<b>L' = P(O-<i>i</i>-Pr)<sub>3</sub></b>					
25.15	0.06728	$(1.66 \pm 0.01) \times 10^{-4}$	0.7	438 nm	43(a)
	0.1346	$(2.47 \pm 0.01) \times 10^{-4}$	0.5	438 nm	43(b)
	0.2691	$(4.27 \pm 0.02) \times 10^{-4}$	0.4	438 nm	43(c)

Table 5.3 (continued)

T(°C)	[L'](M)	<sup>a</sup> k <sub>obs</sub> (s <sup>-1</sup> )	σ(%)	Monitored Peak	Run No
<b>L' = P(O-<i>i</i>-Pr)<sub>3</sub></b>					
25.15	0.06728	(1.64±0.01) × 10 <sup>-4</sup>	0.7	438 nm	44(a)
	0.3364	(5.25±0.01) × 10 <sup>-4</sup>	0.3	438 nm	44(b)
	0.4037	(6.31±0.02) × 10 <sup>-4</sup>	0.3	438 nm	44(c)
25.15	0.06728	(1.34±0.01) × 10 <sup>-4</sup>	0.5	418 nm	45(a)
	0.1346	(2.11±0.02) × 10 <sup>-4</sup>	0.7	418 nm	45(b)
	0.2691	(3.88±0.08) × 10 <sup>-4</sup>	2.1	418 nm	45(c)
	0.3364	(4.95±0.02) × 10 <sup>-4</sup>	0.5	418 nm	45(d)
	0.4037	(5.95±0.03) × 10 <sup>-4</sup>	0.5	418 nm	45(e)
25.2	0.2584	(4.24±0.16) × 10 <sup>-4</sup>	3.6	2042.6cm <sup>-1</sup>	46(a)
25.2	0.2584	(3.94±0.23) × 10 <sup>-4</sup>	5.8	2013.0 cm <sup>-1</sup>	46(b)
<b>L' = PPh<sub>2</sub>Et</b>					
25.15	0.05131	(4.61±0.02) × 10 <sup>-5</sup>	0.3	480 nm	47(a)
	0.1026	(4.72±0.03) × 10 <sup>-5</sup>	0.6	480 nm	47(b)

Table 5.3 (continued)

T(°C)	[L'](M)	$^a k_{\text{obs}}(\text{s}^{-1})$	$\sigma(\%)$	Monitored Peak	Run No
<b>L' = PPh<sub>2</sub>Et</b>					
21.15	0.2052	$(4.96 \pm 0.05) \times 10^{-5}$	1.1	480 nm	47(c)
	0.2566	$(5.11 \pm 0.07) \times 10^{-5}$	1.4	480 nm	47(d)
	0.2052	$(4.92 \pm 0.05) \times 10^{-5}$	1.0	480 nm	48(a)
	0.2566	$(5.05 \pm 0.06) \times 10^{-5}$	1.3	480 nm	48(b)
25.2	0.06568	$(9.65 \pm 0.20) \times 10^{-5}$	2.1	2042.6cm <sup>-1</sup>	49(a)
	0.1314	$(1.03 \pm 0.03) \times 10^{-4}$	2.5	2042.6cm <sup>-1</sup>	50(a)
	0.1970	$(1.16 \pm 0.02) \times 10^{-4}$	1.8	2042.6cm <sup>-1</sup>	51(a)
	0.06568	$(9.82 \pm 0.20) \times 10^{-5}$	2.1	2042.6cm <sup>-1</sup>	52(a)
	0.2627	$(1.30 \pm 0.07) \times 10^{-4}$	5.3	2042.6cm <sup>-1</sup>	53(a)
25.2	0.06568	$(5.70 \pm 0.08) \times 10^{-5}$	1.4	2013.6cm <sup>-1</sup>	49(b)
	0.1314	$(5.96 \pm 0.09) \times 10^{-5}$	1.5	2013.6 cm <sup>-1</sup>	50(b)
	0.1970	$(7.87 \pm 0.11) \times 10^{-5}$	1.4	2013.6 cm <sup>-1</sup>	51(b)
	0.2627	$(7.49 \pm 0.14) \times 10^{-5}$	1.9	2013.6 cm <sup>-1</sup>	53(b)

Table 5.3 (continued)

T(°C)	[L'](M)	<sup>a</sup> k <sub>obs</sub> (s <sup>-1</sup> )	σ(%)	Monitored Peak	Run No
<b>L' = PPh<sub>3</sub></b>					
25.15	0.03208	$(5.07 \pm 0.08) \times 10^{-5}$	1.5	486 nm	54(a)
	0.06416	$(5.09 \pm 0.07) \times 10^{-5}$	1.5	486 nm	54(b)
	0.08021	$(5.08 \pm 0.07) \times 10^{-5}$	1.3	486 nm	54(c)
	0.09625	$(5.13 \pm 0.07) \times 10^{-5}$	1.4	486 nm	54(d)
	0.04326	$(5.18 \pm 0.06) \times 10^{-5}$	1.2	486 nm	55(a)
	0.05408	$(5.20 \pm 0.06) \times 10^{-5}$	1.2	486 nm	55(b)
	0.06489	$(5.36 \pm 0.07) \times 10^{-5}$	1.4	486 nm	55(c)
	0.1123	$(5.18 \pm 0.07) \times 10^{-5}$	1.4	486 nm	55(d)
	0.01082	$(5.31 \pm 0.09) \times 10^{-5}$	1.6	486 nm	56(a)
	0.02163	$(5.23 \pm 0.10) \times 10^{-5}$	1.8	486 nm	56(b)
	0.04326	$(5.26 \pm 0.07) \times 10^{-5}$	1.4	486 nm	56(c)
	0.1123	$(5.17 \pm 0.07) \times 10^{-5}$	1.4	486 nm	56(d)

a. k<sub>obs</sub> with uncertainties were obtained by non-linear least squares regression analyses (KORE) of A<sub>t</sub> vs time. k<sub>obs</sub> without uncertainties were obtained by linear least squares analyses of ln|A<sub>t</sub>-A<sub>∞</sub>| vs time.

**Table 5.4 Pseudo-First-Order Rate Constants for Reactions of  $\text{Ru}_3(\text{CO})_{11}\text{etpb}$  with Nucleophiles  $\text{L}'$  in Heptane  $[\text{Complex}]_0 = 2 \times 10^{-4} \text{ M}$**

T(°C)	[L'](M)	$k_{\text{obs}}(\text{s}^{-1})$	$\sigma(\%)$	Monitored Peak	Run No
<b>L' = AsPh<sub>3</sub></b>					
36.2	0.01372	$(2.96 \pm 0.08) \times 10^{-5}$	2.7	365 nm	57(a)
	0.02744	$(2.57 \pm 0.04) \times 10^{-5}$	1.5	365 nm	57(b)
	0.04116	$(2.82 \pm 0.07) \times 10^{-5}$	2.6	365 nm	57(c)
	0.05488	$(2.10 \pm 0.01) \times 10^{-5}$	0.3	365 nm	57(d)
	0.06860	$(2.76 \pm 0.04) \times 10^{-5}$	1.3	365 nm	57(e)
36.2	0.01372	$(2.06 \pm 0.07) \times 10^{-5}$	3.3	435 nm	58(a)
	0.02744	$(3.25 \pm 0.10) \times 10^{-5}$	3.2	435 nm	58(b)
	0.04116	$(2.25 \pm 0.03) \times 10^{-5}$	1.2	435 nm	58(c)
	0.05488	$(2.36 \pm 0.01) \times 10^{-5}$	0.6	435 nm	58(d)
	0.06860	$(3.08 \pm 0.06) \times 10^{-5}$	1.9	435 nm	58(e)
44.9	0.01616	$(9.49 \pm 0.23) \times 10^{-5}$	2.4	315 nm	59(a)
	0.02423	$(8.79 \pm 0.03) \times 10^{-5}$	0.3	315 nm	59(b)
	0.03231	$(9.52 \pm 0.19) \times 10^{-5}$	2.0	315 nm	59(c)
	0.04039	$(9.46 \pm 0.05) \times 10^{-5}$	0.5	315 nm	59(d)

Table 5.4 (continued)

T(°C)	[L'](M)	$k_{\text{obs}}(\text{s}^{-1})$	$\sigma(\%)$	Monitored Peak	Run No
<b>L' = AsPh<sub>3</sub></b>					
44.9	0.01616	$(9.48 \pm 0.70) \times 10^{-5}$	7.4	435 nm	60(a)
	0.02423	$(9.12 \pm 0.03) \times 10^{-5}$	0.3	435 nm	60(b)
	0.03231	$(9.51 \pm 0.15) \times 10^{-5}$	1.5	435 nm	60(c)
	0.04039	$(9.71 \pm 0.05) \times 10^{-5}$	0.6	435 nm	60(d)
44.9	0.01616	$(9.34 \pm 0.08) \times 10^{-5}$	0.8	315 nm	61(a)
	0.02423	$(7.26 \pm 0.07) \times 10^{-5}$	1.0	315 nm	61(b)
	0.03231	$(9.54 \pm 0.07) \times 10^{-5}$	0.7	315 nm	61(c)
	0.05390	$(8.68 \pm 0.15) \times 10^{-5}$	1.7	315 nm	61(d)
	0.06738	$(9.60 \pm 0.22) \times 10^{-5}$	2.3	315 nm	61(e)
45.3	0.01372	$(7.75 \pm 0.08) \times 10^{-5}$	1.0	315 nm	62(a)
	0.02744	$(8.30 \pm 0.06) \times 10^{-5}$	0.7	315 nm	62(b)
	0.04116	$(8.66 \pm 0.06) \times 10^{-5}$	0.7	315 nm	62(c)
	0.05488	$(9.75 \pm 0.06) \times 10^{-5}$	0.6	315 nm	62(d)
	0.06860	$(9.55 \pm 0.13) \times 10^{-5}$	1.3	315 nm	62(e)

Table 5.4 (continued)

T(°C)	[L'](M)	$k_{\text{obs}}(\text{s}^{-1})$	$\sigma(\%)$	Monitored Peak	Run No
<b>L' = AsPh<sub>3</sub></b>					
45.3	0.01372	$(7.89 \pm 0.09) \times 10^{-5}$	1.2	315 nm	63(a)
	0.04116	$(8.65 \pm 0.08) \times 10^{-5}$	0.9	315 nm	63(b)
	0.06860	$(9.49 \pm 0.09) \times 10^{-5}$	0.9	315 nm	63(c)
	0.05488	$(9.84 \pm 0.05) \times 10^{-5}$	0.5	315 nm	64(a)
	0.06860	$(9.51 \pm 0.20) \times 10^{-5}$	2.1	315 nm	64(b)
45.4	0.01372	$(8.74 \pm 0.07) \times 10^{-5}$	0.8	435 nm	65(a)
	0.02744	$(9.26 \pm 0.09) \times 10^{-5}$	1.0	435 nm	65(b)
	0.04166	$(10.3 \pm 0.2) \times 10^{-5}$	1.5	435 nm	65(c)
	0.05488	$(10.5 \pm 0.1) \times 10^{-5}$	1.1	435 nm	65(d)
	0.06860	$(11.0 \pm 0.2) \times 10^{-5}$	1.9	435 nm	65(e)
45.4	0.01372	$(8.65 \pm 0.06) \times 10^{-5}$	0.7	435 nm	66(a)
	0.04166	$(10.6 \pm 0.1) \times 10^{-5}$	1.1	435 nm	66(b)
	0.05488	$(10.7 \pm 0.1) \times 10^{-5}$	0.6	435 nm	66(c)
	0.06860	$(10.6 \pm 0.3) \times 10^{-5}$	2.4	435 nm	66(d)

Table 5.4 (continued)

T(°C)	[L'](M)	<sup>a</sup> k <sub>obs</sub> (s <sup>-1</sup> )	σ(%)	Monitored Peak	Run No
<b>L' = AsPh<sub>3</sub></b>					
45.5	0.01372	$(9.02 \pm 0.08) \times 10^{-5}$	0.9	435 nm	67(a)
	0.02744	$(7.14 \pm 0.25) \times 10^{-5}$	3.5	435 nm	67(b)
	0.04166	$(10.6 \pm 0.1) \times 10^{-5}$	0.9	435 nm	67(c)
	0.05488	$(10.0 \pm 0.1) \times 10^{-5}$	0.7	435 nm	67(d)
	0.06860	$(10.3 \pm 0.1) \times 10^{-5}$	1.0	435 nm	67(e)
54.3	0.008078	$(3.59 \pm 0.05) \times 10^{-4}$	1.5	315 nm	68(a)
	0.01616	$(3.50 \pm 0.01) \times 10^{-4}$	0.4	315 nm	68(b)
	0.02423	$(3.55 \pm 0.06) \times 10^{-4}$	1.8	315 nm	68(c)
	0.03231	$(3.48 \pm 0.02) \times 10^{-4}$	0.6	315 nm	68(d)
54.3	0.008078	$(3.74 \pm 0.17) \times 10^{-4}$	4.6	435 nm	69(a)
	0.01616	$(3.46 \pm 0.02) \times 10^{-4}$	0.5	435 nm	69(b)
	0.02423	$(3.49 \pm 0.04) \times 10^{-4}$	1.2	435 nm	69(c)
	0.03231	$(3.47 \pm 0.02) \times 10^{-4}$	0.5	435 nm	69(d)
54.3	0.008078	$(3.65 \pm 0.05) \times 10^{-4}$	1.4	315 nm	70(a)
	0.01616	$(3.50 \pm 0.01) \times 10^{-4}$	0.4	315 nm	70(b)
	0.02423	$(3.43 \pm 0.06) \times 10^{-4}$	1.6	315 nm	70(c)
	0.03231	$(3.45 \pm 0.02) \times 10^{-4}$	0.6	315 nm	70(d)

Table 5.4 (continued)

T(°C)	[L'](M)	$k_{\text{obs}}(\text{s}^{-1})$	$\sigma(\%)$	Monitored Peak	Run No
<b>L' = AsPh<sub>3</sub></b>					
54.3	0.008078	$(3.88 \pm 0.17) \times 10^{-4}$	4.5	435 nm	71(a)
	0.01616	$(3.50 \pm 0.01) \times 10^{-4}$	0.3	435 nm	71(b)
	0.02423	$(3.43 \pm 0.04) \times 10^{-4}$	1.1	435 nm	71(c)
	0.03231	$(3.46 \pm 0.02) \times 10^{-4}$	0.5	435 nm	71(d)
54.3	0.008078	$(3.32 \pm 0.01) \times 10^{-4}$	0.4	315 nm	72(a)
	0.01616	$(3.25 \pm 0.02) \times 10^{-4}$	0.5	315 nm	72(b)
	0.02423	$(3.33 \pm 0.02) \times 10^{-4}$	0.7	315 nm	72(c)
	0.03231	$(3.32 \pm 0.02) \times 10^{-4}$	0.7	315 nm	72(d)
54.3	0.008078	$(3.35 \pm 0.01) \times 10^{-4}$	0.2	435 nm	73(a)
	0.01616	$(3.29 \pm 0.01) \times 10^{-4}$	0.4	435 nm	73(b)
	0.02423	$(3.36 \pm 0.02) \times 10^{-4}$	0.5	435 nm	73(c)
	0.03231	$(3.33 \pm 0.02) \times 10^{-4}$	0.5	435 nm	73(d)
60.4	0.01348	$(8.14 \pm 0.08) \times 10^{-4}$	1.0	315 nm	74(a)
	0.02695	$(8.18 \pm 0.07) \times 10^{-4}$	0.8	315 nm	74(b)
	0.04043	$(8.34 \pm 0.08) \times 10^{-4}$	0.9	315 nm	74(c)
	0.05390	$(8.24 \pm 0.08) \times 10^{-4}$	0.9	315 nm	75(a)
	0.06738	$(8.09 \pm 0.09) \times 10^{-4}$	1.2	315 nm	75 (b)

Table 5.4 (continued)

T(°C)	[L'](M)	$k_{\text{obs}}(\text{s}^{-1})$	$\sigma(\%)$	Monitored Peak	Run No
<b>L' = AsPh<sub>3</sub></b>					
60.5	0.01348	$(8.50 \pm 0.13) \times 10^{-4}$	1.6	435 nm	76(a)
	0.02695	$(8.60 \pm 0.13) \times 10^{-4}$	1.5	435 nm	76(b)
	0.04043	$(8.58 \pm 0.23) \times 10^{-4}$	2.6	435 nm	76(c)
	0.05390	$(8.54 \pm 0.12) \times 10^{-4}$	1.4	435 nm	77(a)
	0.06860	$(8.36 \pm 0.08) \times 10^{-4}$	0.9	435 nm	77(b)
<b>L' = etpb</b>					
25.05	0.01291	$(6.44 \pm 0.39) \times 10^{-6}$	6.0	2048.5 cm <sup>-1</sup>	78(a)
	0.05165	$(1.29 \pm 0.05) \times 10^{-5}$	6.0	2048.5 cm <sup>-1</sup>	79(b)
	0.07044	$(1.71 \pm 0.10) \times 10^{-5}$	5.7	2048.5 cm <sup>-1</sup>	80(c)
25.05	0.01291	$(4.58 \pm 0.28) \times 10^{-6}$	6.0	2021.6 cm <sup>-1</sup>	78(b)
	0.05165	$(8.13 \pm 0.58) \times 10^{-6}$	7.1	2021.6 cm <sup>-1</sup>	79(b)
	0.07044	$(1.02 \pm 0.09) \times 10^{-5}$	8.4	2021.6 cm <sup>-1</sup>	80(b)
25.1	0.02583	$(1.18 \pm 0.02) \times 10^{-5}$	1.2	2048.5 cm <sup>-1</sup>	81(a)
	0.03874	$(1.31 \pm 0.01) \times 10^{-5}$	0.8	2048.5 cm <sup>-1</sup>	82(a)
	0.06457	$(1.70 \pm 0.01) \times 10^{-5}$	0.8	2048.5 cm <sup>-1</sup>	83(a)

Table 5.4 (continued)

T(°C)	[L'](M)	$^a k_{\text{obs}}(\text{s}^{-1})$	$\sigma(\%)$	Monitored Peak	Run No
<b>L' = etpb</b>					
25.1	0.02583	$(9.38 \pm 0.19) \times 10^{-6}$	2.0	2021.6 cm <sup>-1</sup>	81(b)
	0.03874	$(9.97 \pm 0.11) \times 10^{-6}$	1.1	2021.6 cm <sup>-1</sup>	82(b)
	0.06457	$(1.23 \pm 0.03) \times 10^{-5}$	2.0	2021.6 cm <sup>-1</sup>	83(b)
40.0	0.01115	$(5.07 \pm 0.06) \times 10^{-5}$	1.2	2048.6 cm <sup>-1</sup>	84(a)
	0.02239	$(5.28 \pm 0.02) \times 10^{-5}$	0.4	2048.6 cm <sup>-1</sup>	85(a)
	0.02544	$(5.30 \pm 0.03) \times 10^{-5}$	0.6	2048.6 cm <sup>-1</sup>	86(a)
	0.03093	$(5.71 \pm 0.10) \times 10^{-5}$	1.8	2048.6 cm <sup>-1</sup>	87(a)
	0.04279	$(6.18 \pm 0.08) \times 10^{-5}$	1.3	2048.6 cm <sup>-1</sup>	88(a)
40.0	0.01115	$4.66 \times 10^{-5}$		2021.6 cm <sup>-1</sup>	84(b)
	0.02239	$(4.48 \pm 0.04) \times 10^{-5}$	0.9	2021.6 cm <sup>-1</sup>	85(b)
	0.02544	$(3.98 \pm 0.09) \times 10^{-5}$	2.2	2021.6 cm <sup>-1</sup>	86(b)
	0.03093	$(4.27 \pm 0.07) \times 10^{-5}$	1.6	2021.6 cm <sup>-1</sup>	87(b)
	0.04279	$(4.51 \pm 0.10) \times 10^{-5}$	2.3	2021.6 cm <sup>-1</sup>	88(c)

Table 5.4 (continued)

T(°C)	[L'](M)	<sup>a</sup> k <sub>obs</sub> (s <sup>-1</sup> )	σ(%)	Monitored Peak	Run No
<b>L' = P(OEt)<sub>3</sub></b>					
25.15	0.1146	$(1.83 \pm 0.02) \times 10^{-5}$	0.8	400 nm	89(a)
	0.1638	$(2.53 \pm 0.02) \times 10^{-5}$	0.9	400 nm	89(b)
	0.2456	$(3.80 \pm 0.13) \times 10^{-5}$	3.4	400 nm	89(c)
	0.3275	$(4.93 \pm 0.08) \times 10^{-5}$	1.6	400 nm	89(d)
	0.4094	$(6.23 \pm 0.12) \times 10^{-5}$	1.8	400 nm	89(e)
<b>L' = P(O-<i>i</i>-Pr)<sub>3</sub></b>					
25.2	0.1519	$(1.12 \pm 0.12) \times 10^{-5}$	10	2048.8cm <sup>-1</sup>	90(a)
	0.3038	$(2.22 \pm 0.16) \times 10^{-5}$	7.4	2048.8cm <sup>-1</sup>	91(a)
	0.3914	$(3.14 \pm 0.14) \times 10^{-5}$	4.6	2048.8cm <sup>-1</sup>	92(a)
	0.4557	$(3.37 \pm 0.32) \times 10^{-5}$	9.4	2048.8cm <sup>-1</sup>	93(a)
25.2	0.1519	$(9.87 \pm 1.35) \times 10^{-6}$	14	2019.9cm <sup>-1</sup>	90(b)
	0.3038	$(2.09 \pm 0.18) \times 10^{-5}$	8.5	2019.9cm <sup>-1</sup>	91(b)
	0.3914	$(2.81 \pm 0.14) \times 10^{-5}$	5.2	2019.9cm <sup>-1</sup>	92(b)
	0.4557	$(3.40 \pm 0.20) \times 10^{-5}$	5.8	2019.9cm <sup>-1</sup>	93(b)
	0.4557	$(2.66 \pm 0.27) \times 10^{-5}$	10	2019.9 cm <sup>-1</sup>	94(a)

Table 5.4 (continued)

T(°C)	[L'](M)	$^a k_{\text{obs}}(\text{s}^{-1})$	$\sigma(\%)$	Monitored Peak	Run No
<b>L' = P(O-<i>i</i>-Pr)<sub>3</sub></b>					
25.2	0.1164	$1.4 \times 10^{-5}$		2048.8cm <sup>-1</sup>	95(a)
	0.1519	$1.6 \times 10^{-5}$		2048.8cm <sup>-1</sup>	96(a)
	0.3038	$2.1 \times 10^{-5}$		2048.8cm <sup>-1</sup>	97(a)
	0.3914	$3.0 \times 10^{-5}$		2048.8cm <sup>-1</sup>	98(a)
	0.4557	$3.9 \times 10^{-5}$		2048.8cm <sup>-1</sup>	99(a)
25.2	0.1164	$1.1 \times 10^{-5}$		2019.9cm <sup>-1</sup>	95(b)
	0.1519	$1.6 \times 10^{-5}$		2019.9cm <sup>-1</sup>	96(b)
	0.3038	$2.2 \times 10^{-5}$		2019.9cm <sup>-1</sup>	97(b)
	0.3914	$2.7 \times 10^{-5}$		2019.9cm <sup>-1</sup>	98(b)
	0.4557	$3.6 \times 10^{-5}$		2019.9cm <sup>-1</sup>	99(b)
	0.4557	$2.3 \times 10^{-5}$		2019.9cm <sup>-1</sup>	100(a)
25.15	0.1215	$(6.86 \pm 0.02) \times 10^{-6}$	0.3	400 nm	101(a)
	0.1519	$(8.12 \pm 0.04) \times 10^{-6}$	0.4	400 nm	101(b)
	0.3038	$(1.49 \pm 0.03) \times 10^{-5}$	2.3	400 nm	101(c)
	0.3797	$(1.93 \pm 0.04) \times 10^{-5}$	2.2	400 nm	101(d)
	0.4557	$(2.39 \pm 0.05) \times 10^{-5}$	2.0	400 nm	101(e)

Table 5.4 (continued)

T(°C)	[L](M)	<sup>a</sup> k <sub>obs</sub> (s <sup>-1</sup> )	σ(%)	Monitored Peak	Run No
<b>L' = P(<i>n</i>-Bu)<sub>3</sub></b>					
25.15	0.07354	(2.87±0.01) × 10 <sup>-5</sup>	0.3	400 nm	102(a)
	0.1471	(5.55±0.04) × 10 <sup>-5</sup>	0.8	400 nm	102(b)
	0.2941	(1.10±0.01) × 10 <sup>-4</sup>	1.2	400 nm	102(c)
25.15	0.2941	(1.11±0.01) × 10 <sup>-4</sup>	1.2	400 nm	103(a)
	0.3677	(1.44±0.03) × 10 <sup>-4</sup>	1.8	400 nm	103(b)
	0.4412	(1.80±0.03) × 10 <sup>-4</sup>	1.4	400 nm	103(c)
25.2	0.07828	(4.53±0.26) × 10 <sup>-5</sup>	5.6	2038.6cm <sup>-1</sup>	104(a)
	0.1566	(9.41±0.96) × 10 <sup>-5</sup>	10	2038.6cm <sup>-1</sup>	105(a)
	0.4412	(2.86±0.10) × 10 <sup>-4</sup>	3.6	2038.6cm <sup>-1</sup>	106(a)
25.2	0.07828	(5.97±0.66) × 10 <sup>-5</sup>	11	2047.2cm <sup>-1</sup>	104(b)
	0.1566	(8.92±0.74) × 10 <sup>-5</sup>	8.3	2047.2cm <sup>-1</sup>	105(b)
	0.4412	(2.95±0.11) × 10 <sup>-4</sup>	3.8	2047.2cm <sup>-1</sup>	106(b)

Table 5.4 (continued)

T(°C)	[L'](M)	$k_{\text{obs}}(\text{s}^{-1})$	$\sigma(\%)$	Monitored Peak	Run No
<b>L' = PPh<sub>2</sub>Et</b>					
25.1	0.09649	$(7.74 \pm 0.72) \times 10^{-6}$	9.2	2048.4cm <sup>-1</sup>	107(a)
	0.1930	$(1.06 \pm 0.06) \times 10^{-5}$	5.9	2048.4cm <sup>-1</sup>	108(a)
	0.2414	$(9.64 \pm 0.46) \times 10^{-6}$	4.8	2048.4cm <sup>-1</sup>	109(a)
	0.2895	$(8.64 \pm 0.75) \times 10^{-6}$	8.7	2048.4cm <sup>-1</sup>	110(a)
25.1	0.09649	$(7.99 \pm 0.77) \times 10^{-6}$	9.6	2019.7cm <sup>-1</sup>	107(b)
	0.1930	$(9.95 \pm 0.73) \times 10^{-6}$	7.3	2019.7 cm <sup>-1</sup>	108(b)
	0.2414	$(9.16 \pm 0.46) \times 10^{-6}$	5.0	2019.7 cm <sup>-1</sup>	109(b)
	0.2895	$(9.11 \pm 0.68) \times 10^{-6}$	7.4	2019.7 cm <sup>-1</sup>	110(b)
25.1	0.09649	$(7.74 \pm 0.72) \times 10^{-6}$	9.2	2048.4cm <sup>-1</sup>	111(a)
	0.02895	$(8.64 \pm 0.75) \times 10^{-6}$	8.7	2048.4 cm <sup>-1</sup>	112(a)
25.1	0.09649	$7.791 \times 10^{-6}$		2048.4cm <sup>-1</sup>	111(b)

a.  $k_{\text{obs}}$  with uncertainties were obtained by non-linear least squares regression analyses (KORE) of  $A_t$  vs time.  $k_{\text{obs}}$  without uncertainties were obtained by linear least squares analyses of  $\ln|A_t - A_{\infty}|$  vs time.

**Table 5.5 Pseudo-First-Order Rate Constants for Reactions of  $\text{Os}_6(\text{CO})_{18}$  with Nucleophiles  $\text{L}'$  in Toluene.  $[\text{Complex}] = 8 \times 10^{-5} \text{ M}$  and  $2 \times 10^{-5} \text{ M}$  for FTIR and UV-Vis Monitoring, respectively**

T(°C)	[L'] (M)	$10^4 k_{\text{obs}}(\text{s}^{-1})$	$^a\sigma(\%)$	Band Monitored	Run No.	$^bR$
<b>L' = etpb</b>						
25.1	0.03550	0.469±0.014	3.1	332 nm	1(a)	0.99997
	0.03550	0.528±0.022	4.1	520 nm	1(b)	0.99993
	0.05324	0.688±0.017	2.4	332 nm	2(a)	0.99998
	0.05324	0.745±0.038	5.1	520 nm	2(b)	0.99995
	0.07099	0.845±0.022	2.6	332 nm	3(a)	0.99999
	0.07099	0.825±0.044	5.3	520 nm	3(b)	0.99997
	0.08874	1.02±0.03	2.8	332 nm	4(a)	0.99999
	0.08874	0.992±0.062	6.3	520 nm	4(b)	0.99995
	0.1065	1.15±0.03	2.3	332 nm	5(a)	0.99999
	0.1065	1.17±0.05	4.2	520 nm	5(b)	0.99998
35.0	0.04374	1.36±0.02	1.6	348 nm	6(a)	0.999995
	0.04374	1.51±0.05	3.5	654 nm	6(b)	0.9997
	0.05832	1.62±0.03	1.9	348 nm	7(a)	0.99999
	0.05832	1.80±0.04	2.4	654 nm	7(b)	0.9999

Table 5.5 (continued)

T(°C)	[L'] (M)	$10^4 k_{\text{obs}}(\text{s}^{-1})$	$^a \sigma(\%)$	Band	Run $^b$ R	
				MonitoredNo.		
<b>L' = etpb</b>						
35.0	0.07290	1.92±0.05	2.6	348 nm	8(a)	0.99999
	0.07290	2.07±0.06	2.9	654 nm	8(b)	0.9998
	0.08748	2.16±0.04	2.1	348 nm	9(a)	0.99999
	0.08748	2.31±0.07	3.6	654 nm	9(b)	0.9997
45.0	0.04374	3.18±0.07	2.3	348 nm	10(a)	0.999991
	0.04374	3.79±0.11	3.0	654 nm	10(b)	0.9997
	0.05832	3.73±0.09	2.5	348 nm	11(a)	0.99999
	0.05832	4.33±0.16	3.8	654 nm	11(b)	0.9995
	0.07290	4.17±0.11	2.7	348 nm	12(a)	0.99998
	0.07290	4.78±0.15	3.3	654 nm	12(b)	0.9996
	0.08748	4.74±0.12	2.7	348 nm	13(a)	0.99998
	0.08748	5.32±0.21	4.0	654 nm	13(b)	0.9996
<b>L' = P(OEt)<sub>3</sub></b>						
25.0	0.07650	0.605±0.008	1.4	2075.5 cm <sup>-1</sup>	14(a)	1.000
	0.07650	0.567±0.008	1.4	2038.7cm <sup>-1</sup>	14(b)	1.000

Table 5.5 (continued)

T(°C)	[L'] (M)	$10^4 k_{\text{obs}}(\text{s}^{-1})$	$^a \sigma(\%)$	Band Monitored	Run No.	$^b R$
<b>L' = P(OEt)<sub>3</sub></b>						
25.0	0.1530	1.34±0.02	1.2	2075.5 cm <sup>-1</sup>	15(a)	1.000
	0.1530	1.27±0.02	1.2	2038.7 cm <sup>-1</sup>	15(b)	1.000
	0.2295	2.13±0.04	2.1	2075.5 cm <sup>-1</sup>	16(a)	0.9995
	0.2295	2.30±0.04	1.8	2038.7 cm <sup>-1</sup>	16(b)	0.9997
	0.3060	2.68±0.03	1.0	2075.5 cm <sup>-1</sup>	17(a)	1.00
	0.3060	2.71±0.03	1.0	2038.7 cm <sup>-1</sup>	17(b)	1.00
	0.1125	0.460±0.005	1.1	290 nm	18(a)	0.9999993
	0.1125	0.505±0.005	1.0	334 nm	18(b)	0.999999
	0.2250	0.874±0.017	2.0	290 nm	19(a)	0.999999
	0.2250	0.909±0.008	0.9	334 nm	19(b)	0.9999992
	0.3375	1.29±0.03	2.0	290 nm	20(a)	0.9999993
	0.3375	1.31±0.02	1.1	334 nm	20(b)	0.999999
35.0	0.06750	0.790±0.008	1.0	290 nm	21(a)	0.9999994
	0.06750	1.00±0.01	0.9	334 nm	21(b)	0.9999995
	0.1125	1.30±0.01	1.1	290 nm	22(a)	0.9999994
	0.1125	1.55±0.02	1.3	334 nm	22(b)	0.999999
	0.2250	2.28±0.04	1.8	290 nm	23(a)	0.999999
	0.2250	2.60±0.05	1.8	334 nm	23(b)	0.999997

Table 5.5 (continued)

T(°C)	[L'] (M)	$10^4 k_{\text{obs}}(\text{s}^{-1})$	$^a \sigma(\%)$	Band Monitored	Run No.	$^b R$
<b>L' = P(OEt)<sub>3</sub></b>						
35.0	0.3375	3.31±0.07	2.0	290 nm	24(a)	0.9999992
	0.3375	3.49±0.05	1.4	334 nm	24(b)	0.9999998
45.0	0.1125	2.36±0.03	1.3	290 nm	25(a)	0.9999993
	0.1125	3.03±0.03	0.8	334 nm	25(b)	0.9999997
	0.2250	4.59±0.07	1.4	290 nm	26(a)	0.9999995
	0.2250	5.36±0.06	1.1	334 nm	26(b)	0.9999999
	0.3375	7.13±0.15	2.1	290 nm	27(a)	0.9999994
	0.3375	7.52±0.11	1.5	334 nm	27(b)	0.9999999
	0.4500	9.19±1.18	12	290 nm	28(a)	0.999999
	0.4500	9.76±0.25	2.5	334 nm	28(b)	0.9999997
55.0	0.1125	3.79±0.07	1.9	290 nm	29(a)	0.9999999
	0.1125	4.96±0.14	2.7	334 nm	29(b)	0.9999996
	0.2250	8.43±0.20	2.4	290 nm	30(a)	0.9999999
	0.2250	10.9±0.3	2.4	334 nm	30(b)	0.9999999
	0.3375	12.8±0.4	3.1	290 nm	31(a)	0.9999999
	0.3375	15.3±0.2	1.4	334 nm	31(b)	0.9999999

Table 5.5 (continued)

T(°C)	[L'] (M)	$10^4 k_{\text{obs}}(\text{s}^{-1})$	$^a \sigma(\%)$	Band Monitored	Run No.	$^b R$
<b>L' = P(OEt)<sub>3</sub></b>						
55.0	0.4500	17.9±0.8	4.6	290 nm	32(a)	0.999998
	0.4500	20.5±0.5	2.6	334 nm	32(b)	0.999997
<b>L' = PMe<sub>3</sub></b>						
15.0	$0.1976 \times 10^{-2}$	31.9±0.4	1.3	316 nm	33(a)	0.999998
	$0.1976 \times 10^{-2}$	32.8±0.4	1.2	332 nm	33(b)	0.999998
	0.3953	49.2±0.3	0.8	316 nm	34(a)	0.9999993
	0.3953	49.6±0.4	0.8	332 nm	34(b)	0.9999993
	0.5929	62.2±0.8	1.2	316 nm	35(a)	0.999999
	0.5929	63.4±0.6	1.0	332 nm	35(b)	0.999999
	0.5929	63.4±0.4	0.7	316 nm	36(a)	0.9999995
	0.5929	64.3±0.4	0.7	332 nm	36(b)	0.9999995
	0.7906	79.7±0.5	0.6	316 nm	37(a)	0.9999997
	0.7906	80.6±0.4	0.5	332 nm	37(b)	0.9999997
25.0	0.1976	49.1±0.6	1.3	316 nm	38(a)	0.999998
	0.1976	50.9±0.7	1.3	332 nm	38(b)	0.999998

Table 5.5 (continued)

T(°C)	[L'] (M)	$10^4 k_{\text{obs}}(\text{s}^{-1})$	$^a \sigma(\%)$	Band Monitored	Run No.	$^b R$
<b>L' = PMe<sub>3</sub></b>						
25.0	0.3953	86.8±0.9	1.1	316 nm	39(a)	0.999999
	0.3953	86.3±0.7	0.8	332 nm	39(b)	0.9999993
	0.5929	118±1	0.9	316 nm	40(a)	0.9999994
	0.5929	118±1	0.9	332 nm	40(b)	0.9999992
	0.7906	151±2	1.0	316 nm	41(a)	0.9999994
	0.7906	152±1	0.9	332 nm	41(b)	0.9999995
35.0	0.09882	69.7±0.9	1.3	316 nm	42(a)	0.999999
	0.09882	71.2±0.8	1.2	332 nm	42(b)	0.999998
	0.1976	91.5±1.6	1.8	316 nm	43(a)	0.999998
	0.1976	93.6±1.6	1.7	332 nm	43(b)	0.999997
	0.2965	115±2	1.5	316 nm	44(a)	0.999998
	0.2965	118±2	1.5	332 nm	44(b)	0.999998
	0.3953	139±2	1.8	316 nm	45(a)	0.999998
	0.3953	142±2	1.5	332 nm	45(b)	0.999998
<b>L' = PPhMe<sub>2</sub></b>						
25.0	0.3000	3.47±0.10	3.0	2075.7 cm <sup>-1</sup>	46(a)	0.9999

Table 5.5 (continued)

T(°C)	[L'] (M)	$10^4 k_{\text{obs}}(\text{s}^{-1})$	$^a \sigma(\%)$	Band Monitored	Run No.	$^b R$
<b>L' = PPhMe<sub>2</sub> [12]</b>						
25.0	0.3000	2.65±0.11	4.1	2062.0 cm <sup>-1</sup>	46(b)	0.9999
	0.4000	6.19±0.16	2.5	2075.7 cm <sup>-1</sup>	47(a)	0.9997
	0.4000	4.52±0.14	3.2	2062.0 cm <sup>-1</sup>	47(b)	0.9998
	0.6000	10.3±0.6	5.6	2075.7 cm <sup>-1</sup>	48(a)	0.996
	0.6000	8.58±0.63	7.3	2062.0 cm <sup>-1</sup>	48(b)	0.998
	1.200	19.0±1.2	6.2	2075.7 cm <sup>-1</sup>	49(a)	1.00
	1.200	16.8±1.1	6.5	2062.0 cm <sup>-1</sup>	49(b)	1.00
<b>L' = P(O-<i>i</i>-Pr)<sub>3</sub></b>						
25.0	0.1599	$^c 0.296 \pm 0.016$	5.5	365 nm	50(a)	0.999998
	0.1599	$^c 0.502 \pm 0.024$	4.8	330 nm	50(b)	0.99999
	0.2399	0.625±0.027	4.3	365 nm	51(a)	0.999999
	0.2399	0.710±0.033	4.7	330 nm	51(b)	0.99999
	0.3199	0.841±0.036	4.2	365 nm	52(a)	0.9999993
	0.3199	0.846±0.035	4.2	330 nm	52(b)	0.999991
	0.3998	1.10±0.04	3.5	365 nm	53(a)	0.9999993
	0.3998	0.975±0.030	3.1	330 nm	53(b)	0.999994

Table 5.5 (continued)

T(°C)	[L'] (M)	$10^4 k_{\text{obs}}(\text{s}^{-1})$	$^a \sigma(\%)$	Band Monitored	Run No.	$^b R$
<b>L' = P(O-<i>i</i>-Pr)<sub>3</sub></b>						
25.0	0.4798	1.31±0.04	3.1	365 nm	54(a)	0.9999995
	0.4798	1.20±0.04	3.2	330 nm	54(b)	0.9999994
35.0	0.2399	1.02±0.01	0.7	316 nm	55(a)	0.9999998
	0.2399	0.954±0.006	0.6	334 nm	55(b)	0.9999998
	0.3199	1.31±0.02	1.2	316 nm	56(a)	0.9999992
	0.3199	1.20±0.01	1.0	334 nm	56(b)	0.9999993
	0.3998	1.59±0.02	1.4	316 nm	57(a)	0.999999
	0.3998	1.45±0.02	1.2	334 nm	57(b)	0.999999
	0.4798	1.80±0.02	1.2	316 nm	58(a)	0.999999
	0.4798	1.67±0.02	1.0	334 nm	58(b)	0.9999993
45.0	0.2399	1.83±0.02	1.0	316 nm	59(a)	0.9999995
	0.2399	1.77±0.01	0.7	334 nm	59(b)	0.9999997
	0.3199	2.49±0.01	0.6	316 nm	60(a)	0.9999999
	0.3199	2.37±0.02	0.7	334 nm	60(b)	0.9999998
	0.3998	3.10±0.03	0.9	316 nm	61(a)	0.9999996
	0.3998	2.93±0.02	0.8	334 nm	61(b)	0.9999996

Table 5.5 (continued)

T(°C)	[L'] (M)	$10^4 k_{\text{obs}}(\text{s}^{-1})$	$^a \sigma(\%)$	Band Monitored	Run No.	$^b R$
<b>L' = P(O-<i>i</i>-Pr)<sub>3</sub></b>						
45.0	0.4798	3.44±0.02	0.6	316 nm	62(a)	0.9999998
	0.4798	3.22±0.02	0.6	334 nm	62(b)	0.9999997
50.0	0.2399	2.32±0.05	2.1	316 nm	63(a)	0.999998
	0.2399	2.31±0.04	1.8	334 nm	63(b)	0.999999
	0.3199	3.50±0.04	1.1	316 nm	64(a)	0.9999995
	0.3199	3.36±0.04	1.0	334 nm	64(b)	0.9999995
	0.3998	4.48±0.02	0.5	316 nm	65(a)	0.9999999
	0.3998	4.21±0.02	0.6	334 nm	65(b)	0.9999998
	0.4798	5.25±0.03	0.6	316 nm	66(a)	0.9999998
	0.4798	4.96±0.04	0.8	334 nm	66(b)	0.9999997
55.0	0.2399	2.49±0.05	1.9	316 nm	67(a)	0.999999
	0.2399	2.54±0.04	1.7	334 nm	67(b)	0.999999
	0.3199	3.66±0.08	2.1	316 nm	68(a)	0.999999
	0.3199	3.62±0.07	1.9	334 nm	68(b)	0.999999
	0.3998	5.41±0.08	1.5	316 nm	69(a)	0.9999994
	0.3998	5.22±0.08	1.5	334 nm	69(b)	0.9999993

Table 5.5 (continued)

T(°C)	[L'] (M)	$10^4 k_{\text{obs}}(\text{s}^{-1})$	$^a \sigma(\%)$	Band Monitored	Run No.	$^b R$
<b>L' = P(O-<i>i</i>-Pr)<sub>3</sub></b>						
55.0	0.4798	6.68±0.06	0.9	316 nm	70(a)	0.9999998
	0.4798	6.40±0.04	0.7	334 nm	70(b)	0.9999998
<b>L' = P(<i>n</i>-Bu)<sub>3</sub></b>						
25.0	0.07459	1.02±0.045	4.4	2075.6 cm <sup>-1</sup>	71(a)	0.998
	0.07459	0.611±0.026	4.3	2061.9 cm <sup>-1</sup>	71(b)	1.010
	0.1119	1.43±0.04	2.8	2075.6 cm <sup>-1</sup>	72(a)	0.9997
	0.1119	0.843±0.040	4.7	2061.9 cm <sup>-1</sup>	72(b)	0.9994
	0.1492	1.94±0.12	6.2	2075.6 cm <sup>-1</sup>	73(a)	1.08
	0.1492	1.16±0.07	6.4	2061.9 cm <sup>-1</sup>	73(b)	0.997
	0.1865	2.48±0.06	2.6	2075.6 cm <sup>-1</sup>	74(a)	0.991
	0.1865	1.37±0.03	2.3	2061.9 cm <sup>-1</sup>	74(b)	1.00
	0.06676	0.668±0.011	1.7	324 nm	75(a)	0.999996
	0.06676	0.640±0.011	1.8	320 nm	75(b)	0.999996
	0.1335	1.66±0.05	2.8	324 nm	76(a)	0.999994
	0.1335	1.65±0.05	3.0	320 nm	76(b)	0.999994
	0.2003	3.39±0.12	3.7	324 nm	77(a)	0.999998
	0.2003	3.15±0.10	3.1	320 nm	77(b)	0.999999

Table 5.5 (continued)

T(°C)	[L'] (M)	$10^4 k_{\text{obs}}(\text{s}^{-1})$	$^a \sigma(\%)$	Band Monitored	Run No.	$^b R$
<b>L' = P(<i>n</i>-Bu)<sub>3</sub></b>						
35.0	0.02998	0.959±0.009	0.9	316 nm	78(a)	0.9999993
	0.02998	1.06±0.01	1.2	332 nm	78(b)	0.999999
	0.05997	1.80±0.02	1.1	316 nm	79(a)	0.9999992
	0.05997	2.00±0.03	1.6	332 nm	79(b)	0.999999
	0.08995	3.01±0.04	1.3	316 nm	80(a)	0.9999992
	0.08995	3.20±0.03	1.0	332 nm	80(b)	0.9999992
	0.1199	4.54±0.04	1.0	316 nm	81(a)	0.9999995
	0.1199	4.78±0.04	0.8	332 nm	81(b)	0.9999996
45.0	0.02998	1.47±0.02	1.1	316 nm	82(a)	0.999999
	0.02998	1.48±0.01	0.7	332 nm	82(b)	0.9999994
	0.05997	2.96±0.02	0.8	316 nm	83(a)	0.9999993
	0.05997	3.01±0.02	0.6	332 nm	83(b)	0.9999996
	0.08995	3.99±0.11	2.8	316 nm	84(a)	0.999991
	0.08995	4.12±0.09	2.1	332 nm	84(b)	0.999995
	0.1199	5.52±0.03	0.6	316 nm	85(a)	0.9999996
	0.1199	5.92±0.04	0.6	332 nm	85(b)	0.9999996

a. Percentage error of  $k_{\text{obs}}$  as obtained for individual runs from the KORE programme.

- b. Correlation coefficient.
- c. The data did not agree well because of the following reasons: the reactions lasted about 20 hrs, the time intervals were quite long, and monitored bands were in UV regions (316, 330, and 365 nm), which all caused good data not to be obtained. When  $[L']$  increased or rates of reactions increased, the agreement of two band measurements was getting better (Table 5.5).

**Table 5.6 Eyring Data for Reactions of Os<sub>6</sub>(CO)<sub>18</sub> with Nucleophiles L' in Toluene**

L'	t (°C)	1/T	ln(k <sub>2</sub> /T)
etpb	25.1	3.352892E-03	-12.60469
	25.1	3.352892E-03	-12.74036
	35.0	3.245173E-03	-12.02788
	35.0	3.245173E-03	-12.02102
	45.0	3.143172E-03	-11.42726
	45.0	3.143172E-03	-11.41896
P( <i>n</i> -Bu) <sub>3</sub>	25.1	3.352892E-03	-12.03584
	25.1	3.352892E-03	-12.06919
	35.0	3.245173E-03	-11.37534
	35.0	3.245173E-03	-11.31964
	45.0	3.143172E-03	-11.17983
	45.0	3.143172E-03	-11.11408
P(OEt) <sub>3</sub>	25.0	3.354016E-03	-13.60331
	25.0	3.354016E-03	-13.63197
	35.0	3.245173E-03	-12.69332
	35.0	3.245173E-03	-12.68386
	45.0	3.143172E-03	-11.95275
	45.0	3.143172E-03	-11.97627
	55.0	3.047387E-03	-11.28902

Table 5.6 ( continued )

L'	t (°C)	1/T	ln(k <sub>2</sub> /T)
P(OEt) <sub>3</sub>	55.0	3.047387E-03	-11.15322
P(O- <i>i</i> -Pr) <sub>3</sub>	35.0	3.245173E-03	-13.73119
	35.0	3.245173E-03	-13.83186
	45.0	3.143172E-03	-13.01435
	45.0	3.143172E-03	-13.11524
	45.0	3.143172E-03	-13.12817
	45.0	3.143172E-03	-12.95898
	50.0	3.094538E-03	-12.44672
	50.0	3.094538E-03	-12.55536
	55.0	3.047387E-03	-12.14109
PMe <sub>3</sub>	15.0	3.470415E-03	-5.892298
	15.0	3.470415E-03	-5.891814
	25.0	3.354016E-03	-5.145487
	25.0	3.354016E-03	-5.159863
	35.0	3.245173E-03	-4.887724
	35.0	3.245173E-03	-4.870512

**REFERENCES FOR CHAPTER 5**

- [1] L. Chen, A.J. Poë, *Coord. Chem. Rev.*, 143(1995)265
- [2] M.M. Rahman, H.Y. Liu, K. Eriks, A. Prock and W.P. Giering, *Organometallics*, 8( 1989 )1.
- [3] H.Y. Liu, K. Eriks, A. Prock and W.P. Giering, *Organometallics*, 9( 1990 )1758.
- [4] (a) C.A. Tolman, *J. Am. Chem. Soc.*, 92( 1970 )2953.  
(b) C.A. Tolman, W.C. Seidel and L.W. Glosser, *J. Am. Chem. Soc.*, 96( 1974 )53.  
(c) C.A. Tolman, *Chem. Rev.*, 77( 1977 )313.
- [5] T. Bartik, T. Himmler, H.G. Schulte and K. Seevogel, *J. Organomet. Chem.*, 272( 1984 )29.
- [6] L. Chen, Ph.D. Thesis, University of Toronto, 1991.
- [7] (a) C.A. Streuli, *Anal.Chem.*, 31( 1959 )1652; *Anal. Chem.*, 32(1960)985.  
(b) W.A. Henderson and C.A. Streuli, *J. Am. Chem. Soc.*, 82(1960)5791  
(c) T. Allman and R.G. Goel, *Can.J. Chem.*, 60 ( 1982 ) 716.
- [8] H.R. Jaw and J.I. Zink, *Inorg. Chem.*, 27 ( 1988 ) 3421.
- [9] T.L. Brown *Inorg. Chem.* 31 ( 1992 ) 1286.
- [10] T.L. Brown, and K.J. Lee, *Coord. Chem. Rev.*, 128 ( 1993 ) 89.
- [11] V. Mark, C. Dungan, M. Crutchfield, D.J. Van Wazer, compilation of <sup>31</sup>P NMR Data, Monsanto Company, St. Louis, Missouri, U.S.A.
- [12] A summer student's work.